JOURNAL OF CAVE AND KARST STUDIES

April 2017
Volume 79, Number 1
ISSN 1090-6924
A Publication of the National Speleological Society

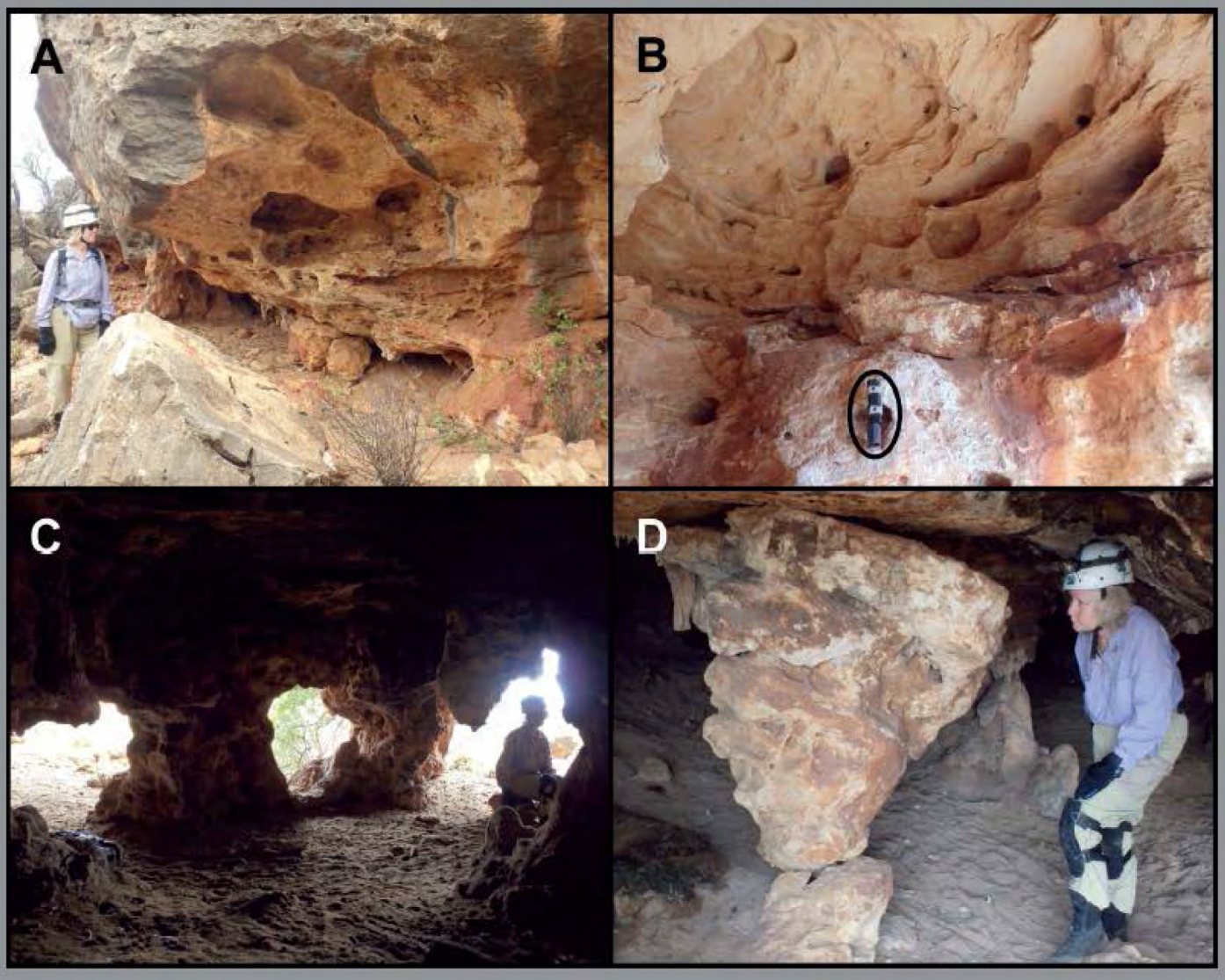

DEDICATED TO THE ADVANCEMENT OF SCIENCE, EDUCATION, AND EXPLORATION

Published By
The National Speleological Society

The *Journal of Cave and Karst Studies* (ISSN 1090-6924, CPM Number #40065056) is a multi-disciplinary, refereed journal published three times a year by the National Speleological Society, 6001 Pulaski Pike NW, Huntsville, AL 35810-4431 USA; Phone (256) 852-1300; Fax (256) 851-9241, email: nss@caves.org; World Wide Web: http://www.caves.org/pub/journal/.
Check the *Journal* website for subscripion rates. Back issues are available from the NSS office.

POSTMASTER: send address changes to the *Journal of Cave and Karst Studies*, 6001 Pulaski Pike NW, Huntsville, AL 35810-4431 USA.

The *Journal of Cave and Karst Studies* is covered by the following ISI Thomson Services Science Citation Index Expanded, ISI Alerting Services, and Current Contents/Physical, Chemical, and Earth Sciences.

Front cover: Photographs from Cape Range Australia flank margin caves. See Mylroie et. al, this issue.

T. Pipan and D.C. Culver – The unity and diversity of the subterranean realm with respect to invertebrate body size. *Journal of Cave and Karst Studies*, v. 79, no. 1, p. 1–9. DOI: 10.4311/2016LSC0119

THE UNITY AND DIVERSITY OF THE SUBTERRANEAN REALM WITH RESPECT TO INVERTEBRATE BODY SIZE

Tanja Pipan[1] and David C. Culver[2]*

Abstract: A variety of subterranean habitats share an absence of light and a dependence on allochthonous productivity, but they differ in many features, including habitat volume. We examined the hypothesis that habitat volume is an important factor in community organization, especially with reference to body size, for a variety of communities for which data were available. We analyzed the results of ten studies that compared body sizes of obligate subterranean dwelling species with respect to habitat. All of the studies confirmed the hypothesis that habitat size was an important determinant of body size. However, surprisingly little information is available on the relationship between body size and habitat size, and only two of the studies reported directly on the size of habitat spaces. Habitat size appears to be an important determinant of body size in subterranean species, but more detailed studies, especially of habitat (pore) size are needed.

Background

Scientists and naturalists have been aware of the subterranean realm and the often bizarre-appearing organisms that inhabit these habitats at least since the discovery, description, and subsequent availability of specimens of the European cave salamander *Proteus anguinus* in the eighteenth and nineteenth centuries (Aljančič et al., 1993; Shaw, 1999). The subterranean fauna, best known from caves, is strongly convergent, with obvious adaptations to subterranean life including elaboration of extra-optic sensory structures and loss of eyes and pigment (Culver et al., 1995). Subterranean habitats themselves are similar to each other in the sense that they share a complete absence of light (Culver and Pipan, 2014), a nearly universal dependence on spatial subsidies of organic carbon and nutrients (Fagan et al., 2007), and a reduction in environmental variability (Covington and Perne, 2015). At the same time, the subterranean environment is diverse, including both karst and other landscapes with caves and landscapes without caves. Racoviţă (1907) emphasized the importance of cracks and crevices in caves, rather than enterable cave passages as primary habitats for the "cave" fauna. A few biologists have even suggested that the entire cave fauna is really a fauna of cracks and crevices (Karaman, 1954). Since Racoviţă's essay, a number of other subterranean habitats, even in regions without caves, have been identified. Perhaps the most prominent non-cave subterranean habitat is the hyporheic, the underflow of rivers and streams (Malard et al., 2000), a habitat with its own unique fauna, including eyeless and depigmented species, that plays a critical role in the health and functioning of streams and rivers (Environmental Agency, 2009). Culver and Pipan (2014) identified a number of other shallow subterranean habitats occurring within a few meters of the surface. These include a variety of terrestrial habitats in the spaces and cracks in rocks, such as covered talus slopes, which are collectively given the name *milieu souterrain superficiel* (MSS) (Juberthie et al., 1980; Ortuño et al., 2013). Although rarely discussed with other subterranean habitats (but see Coiffait, [1958]), soil, especially deep soil, is also an aphotic habitat dependent on allochtonous production, also with a fauna with many eyeless and depigmented species. Still other habitats that harbor troglomorphic fauna, such as miniature perched drainage basins and their associated seepage spring exits (the hypotelminorheic of Meštrov [1962]), shallow calcrete aquifers found in arid regions of Australia (Humphreys, 2001), and termite mounds (Fenolio, 2016), are less well studied. There are also spaces deeper underground, including phreatic aquifers accessed by wells (Malard et al., 1997), deep caves more than 1 km in depth (Sendra and Reboleira, 2012), or mines that have specialized invertebrates (Fišer et al., 2014).

What has been largely neglected are both the unifying features of the subterranean realm beyond the obvious absence of light, and how different subterranean habitats can be quantified and ordered in a way that is important to the biology of the inhabitants. In this paper, we explore a potentially important organizing feature of the wide variety of subterranean habitats—habitat size, or pore volume. Habitat size is potentially a major determinant of maximum body size and shape because the space available, such as the spaces among rocks, can be the same order of magnitude in size as its inhabitants.

The extent to which the size of subterranean organisms is the result of the constraints of pore volume of the habitat may be true in a trivial sense. Fish do not live among sand grains (although they may temporarily bury themselves). There are also trivial ways in which this conjecture is false. No one expects beetles living in a cave passage 1 m in diameter to be smaller than the beetles living in a cave passages 10 m in diameter.

* Corresponding Author: dculver@american.edu
[1] Karst Research Institute at ZRC-SAZU, Titov trg 2, Postojna SI-6230, Slovenia, pipan@zrc-sazu.si
[2] Department of Environmental Science, American University, 4400 Massachusetts Ave. NW, Washington, DC 20016, USA

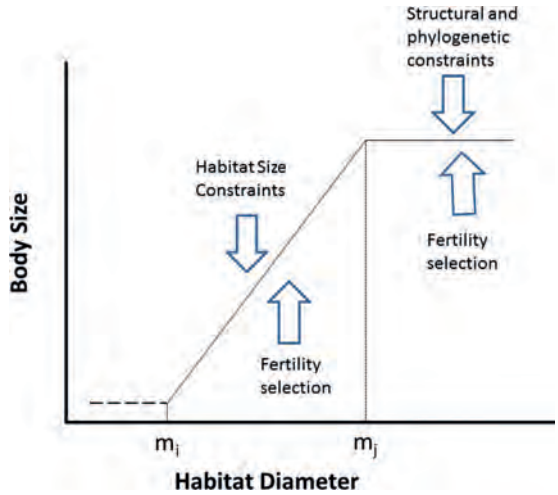

Figure 1. Hypothetical relationship between subterranean habitat diameter (pore size) and body size, with selective forces indicated by arrows. Below a minimum (m_i), there is not sufficient space for animals to occur without burrowing. Above a maximum (m_j), body size is likely constrained by other factors, such as phylogenetic and structural constraints. The relationship need not be linear but is presented as such for simplicity.

What is interesting is the possibility that for a range of habitat sizes, approximately 0.1 mm to 5 cm, size is the result of two opposing sets of forces (Fig. 1). One force is the constraint of habitat size which limits body size, and the opposing forces are those selective forces that tend to increase body size: increased fecundity as a result of increased size (Culver et al, 1995; Fišer et al., 2013), escape from predation (Jones et al., 1992), and storage of nutrients of larger subterranean invertebrates (Hüppop, 2000). Below a minimum pore diameter (m_i in Fig. 1), there is not sufficient space for an organism to survive without moving the particles, and there is a maximum pore diameter (m_j in Fig. 1), above which no organism can be large enough to fill the pore volume.

Body size is a complex factor, subject to many selective pressures, including physiological factors like volume–surface area relationships (Sibley et al, 2012) and demographic factors like size-related fecundity (Kingsolver and Pfennig, 2004). One summary of body size selection is Cope's rule, that body size tends to increase within lineages (e.g., Alroy, 1998, but see Solow and Wang, 2008). The limit on the maximum size m_j is the likely result of phylogenetic and developmental constraints. Our hypothesis is that the range of body sizes between m_i and m_j is determined by the habitat pore diameter, not physiological or ecological constraints.

Finally, we propose a placement of different subterranean habitats along this axis.

METHODS AND MATERIALS

To examine the validity of the habitat size and depth axes, we surveyed the literature for data on the connection between body size and habitat size. We have made this survey as comprehensive as possible, but limited it to comparative studies. We included the following subterranean habitats (see Culver and Pipan [2014] for detailed discussion of habitat types): caves (aquatic and terrestrial), epikarst (aquatic), hyporheic and interstitial aquifers (aquatic), hypotelminorheic and seepage springs (aquatic), soil, and intermediate-size terrestrial subterranean habitats including the *milieu souterrain superficiel* (MSS) of Juberthie et al. (1980) and talus slopes.

For the connection between body size and habitat size, we consulted the publications listed in Table 1. Pore sizes were estimated by Culver and Pipan (2014), and in some cases, pore dimensions were given by the authors of the papers listed in Table 1.

Ideally, it would be possible to combine these studies into a meta-analysis (Borenstein et al., 2009), but the studies listed in Table 1 do not share enough in common, including statistical testing. Some analyze size without measurement of habitat size; some compare species among habitats; and a few compare body sizes and habitat sizes within a habitat type. For this reason, we can only provide a narrative, and not a statistical test.

Table 1. Literature consulted for relationship between habitat and body size.

Reference	Subject
Arnedo et al. (2007)	Body sizes of *Dysdera* spiders in cave, surface, and MSS habitats
Coineau (2000)	Within and between habitat comparison of body sizes of aquatic interstitial crustaceans
Culver and Ehlinger (1980)	Body sizes and gravel sizes of *Caecidotea* isopods in cave streams
Culver et al. (2009)	Among habitat comparisons of copepod body sizes in epikarst and caves
Culver et al. (2010)	Among habitat comparisons of *Stygobromus* amphipod sizes
de Bovée et al. (1995)	Within habitat comparisons of body sizes of aquatic interstitial crustaceans
Ducarme et al. (2004)	Comparison of body sizes of mites in soil and caves
Růžička (1998)	Body sizes of *Theonoe minutissima* spiders in talus slopes and surface habitats
Trontelj et al. (2012)	Among habitat comparison of *Niphargus*amphipod sizes

Table 2. Characteristics of *Caecidotea* isopod and gravel size distributions in four West Virginia cave streams. Data from Culver and Ehlinger (1980).

Isopod and Gravel Sizes	Linwood Cave, Pocahontas Co.	Harman Cave, Randolph Co.	Bowden Cave, Randolph Co.	Glady Cave, Randolph Co.
C. holsingeri size with standard errors (in mm)	5.7 ± 0.2	2.8 ± 0.2	2.5 ± 0.1	3.6 ± 0.1
C. camula size with standard errors (in mm)	absent	absent	8.2 ± 0.4	7.0 ± 0.4
Body size distribution	Unimodal, narrow size range, intermediate in size	Unimodal, narrow size range, small in size	Bimodal, broad size range	Broadly unimodal, skewed to smaller sizes
Median gravel size with interquartile range (in mm diameter)	11.9 (5.9 – 19.1)	5.6 (2.4 – 10.3)	11.9 (1.4 – 19.1)	8.7 (2.4 – 19.1)
Gravel distribution	Uniform for small gravel	Unimodal, skewed to small sizes	Strongly bimodal	Weakly bimodal

Results

Arnedo et al. (2007) analyzed body sizes in *Dysdera* spiders from lava tubes, MSS, and surface habitats in the Canary Islands, with pore diameters (not directly measured) largest in surface habitats and smallest in lava tubes. Phylogeny of Canary Island *Dysdera* is shown in Figure 2. When phylogenetic effects are taken into account and sister species are compared, a pattern of correlation between habitat and body size emerges. There are two MSS specialists, *Dysdera madai* and *D. esquiveli*. *Dysdera madai* is smaller (2.50 mm carapace length) than its sister species *D. iguanensis* (3.12 mm), primarily a surface dweller, but sometimes in MSS. *D. esquiveli* is the same size (2.21 mm) as a sister lava-tube species (*D. hernandezi*, 2.18 mm) but smaller than the ancestral surface species, *D. brevisetae* (3.60 mm). As far as lava-tube species, all six of the species except for *D. hernandezi* are larger, and in one case the same size, as their surface sister species. All in all, MSS species are smaller than surface dwellers while lava-tube species are larger, except for *D. hernandezi*.

Coineau (2000) noted that there were major size differences, more than an order of magnitude, between interstitial crustaceans and cave crustaceans. This is especially apparent in amphipods in the family Ingolfiellidae, where cave species range in size from 12 to 28 mm and species in interstitial sands reach only 1 mm. She noted a strong correlation between particle size and size of a variety of crustaceans within interstitial habitats, with crustaceans reaching 1 to 3 mm long in sandy gravels, while those in sands are less than 1 mm long, although she did not quantify this relationship.

Culver and Ehlinger (1980) investigated the size distributions of both the *Caecidotea* isopods and the stream gravels they inhabit (Table 2). Size distribution of *C. holsingeri* and *C. cannula* paralleled that of the stream gravels. In the two caves with bimodal distribution of gravel sizes, both species occurred, and in the two caves with unimodal distributions of gravel sizes, only one species occurred (Table 2). When gravels were small, isopod sizes tended to be small. A remarkable feature of the system was the size plasticity of *C. holsingeri*, where adults ranged in size from 2.5 to 5.7 mm. Culver and Ehlinger (1980) suggest that part of the reason for the match of gravel and body size is that washout rates from gravels, a source of mortality, is minimized when the size of isopods and gravels are matched. Fertility selection then presumably maximizes size within this constraint.

Culver et al. (2009) investigated possible differences in body sizes of different ecological groups of copepods—stygobionts known only from epikarst, stygobionts known from other subterranean habitats as well, and stygophiles, species known from surface habitats as well—found in drip waters (epikarst) of six Slovenian caves. The pore size of the epikarst habitat is small (Fairchild and Baker, 2012), for example a soda straw formation through which epikarst water exits has an outside diameter of approximately 5 mm (Curl, 1972). Culver et al. (2009) hypothesized that epikarst

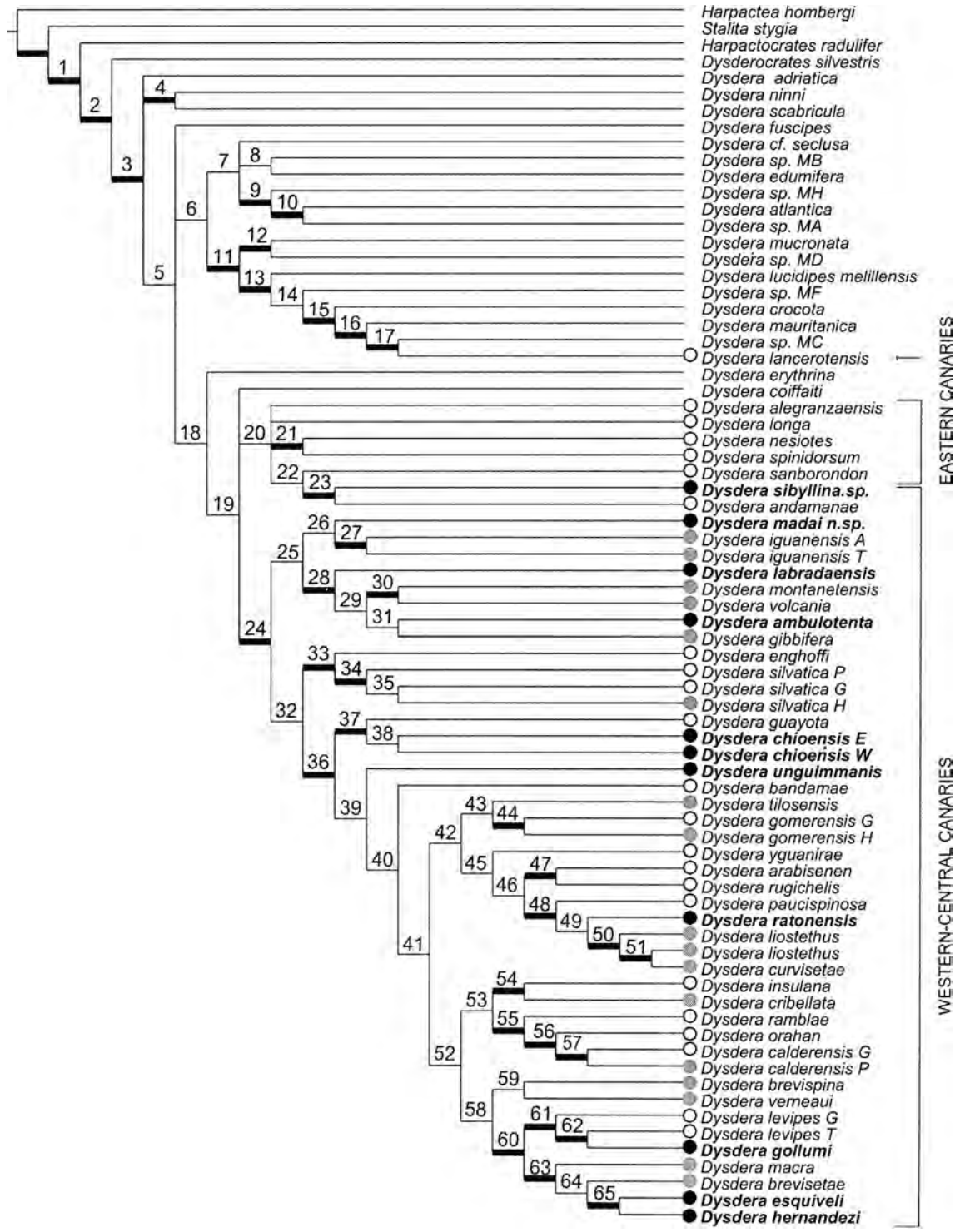

Figure 2. Strict consensus tree of the five most parsimonious trees for the spider genus *Dysdera* from the Canary Islands. Thick branches denote clades recovered under all alignment parameter cost combinations. Black dots identify troglobionts, white dots refer to endemic Canarian species exclusively reported from epigean localities, and gray dots show epigean species also collected in subterranean habitats. From Arnedo et al. (2007).

Table 3. Analysis of copepod size in relation to ecological classification, for all copepod sizes known from Slovenian caves. For HSD (honestly significant difference) groups, those not connected by the same letter are significantly different. For ANOVA, $F_{2,52} = 7.58$, $p < 0.002$. From Culver et al. (2009).

Group	n	Mean (mm)	S.E.	Tukey-Kramer HSD group
Epikarst stygobionts	4	0.495	0.061	a
Other stygobionts	25	0.652	0.045	b
Stygophiles	26	0.93	0.071	b

specialists would be smaller than more generalist species because of pore-size constraints, and in fact, they did find that stygobionts in epikarst were smaller than other species living in epikarst (Table 3).

Culver et al. (2010) looked for correlations between habitat size and body size for the amphipod genus *Stygobromus*. They found that median body sizes for *Stygobromus* in the four habitats ranged from 9 mm in cave streams to 5.4 mm in epikarst (Fig. 3). Hypotelminorheic and phreatic species were intermediate in size. This is in accord with the relative pore size of the habitat, with the possible exception of phreatic habitats, about which we know little, but are likely variable in pore size. The variability of body sizes within a habitat probably is the result not only of pore size differences but competition among species as well. Additionally, there may be a tradeoff between size and shape, such that large amphipods may be narrower. However, Culver et al. (2010) found no differences in shape, as measured by relative antennal size, for different-size habitats.

In a study in Morocco, de Bovée et al. (1995) examined the relationship between amphipods and isopods and granulometry of sediments in two rivers in the High Atlas mountains. They noted that silt in the sediment usually excluded amphipods and isopods (see Fig. 1), and both isopod and amphipod species typically were found in gravels as opposed to clay and sand. They suggest that the amphipod and isopod species may be further subdivided in the habitat by finer differences in sediment size, but they present no direct evidence on this point.

Ducarme et al. (2004) compared body sizes of mites in deep soil and caves in Belgium. The largest cave species was *Veigaia paradoxa* (1065 µm), and the largest deep-soil species was *Leptogamasus suecicus* (610 µm, Table 4). In all seven families with both deep soil and caves representatives, all the cave species within a family were larger than all the deep soil species within a family. The maximum size is likely set in part by phylogenetic constraints.

Růžička (1998) compared body lengths of the spider *Theonoe minutissima* in peat bogs and talus slopes, the latter being a shallow subterranean habitat. The subterranean populations in talus slopes were larger than the surface dwelling populations in peat bogs by about 10 percent.

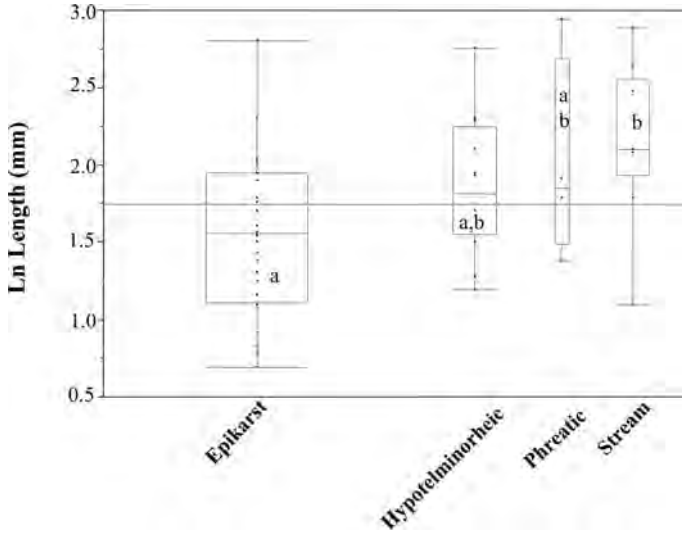

Figure 3. Box and whiskers plots of ln female body length of species of the amphipod genus *Stygobromus* for epikarst, hypotelminorheic, cave streams, and phreatic habitats in North America. The overall mean is represented by the line across the entire figure. Boxes contain 50 percent of the data points; the line across each box is the group median; the whiskers show minimum and maximum values. The widths of the rectangles are proportional to sample size. Dots are individual data points. Plots with the same letter (a or b) do not differ according to the Tukey-Cramer HSD test. From Culver et al. (2010).

Presumably, pore sizes are larger in talus with its many rocks than in peat bogs, largely composed of fine sediments.

Trontelj et al. (2012) also found that the body size of *Niphargus* amphipods from species-rich cave communities of the Dinaric karst of central and southeastern Europe was correlated with pore size. They compared species from four habitats within or directly connected to caves, epikarst, cave interstitial, phreatic, and cave stream. Small-pore interstitial and epikarst was represented by the ecomorph they called small pore. Large-pore phreatic and cave streams were represented by four ecomorphs, cave stream, cave lake, lake giants, and daddy-longlegs (Fig. 4). The four large-pore ecomorphs were also distinguished by different shapes in their figure. As in Culver et al.'s (2010) study, phreatic species were somewhat enigmatic, represented by three distinct ecomorphs.

Discussion

Overall, there is a match between habitat size and organism size, as predicted (Fig. 1), and there seems to be a tradeoff between environmental constraints (in terms of pore size) and the benefits (in terms of reproductive fitness) of being large. However, the data available for analysis are not entirely satisfactory. In particular, relatively little attention has been

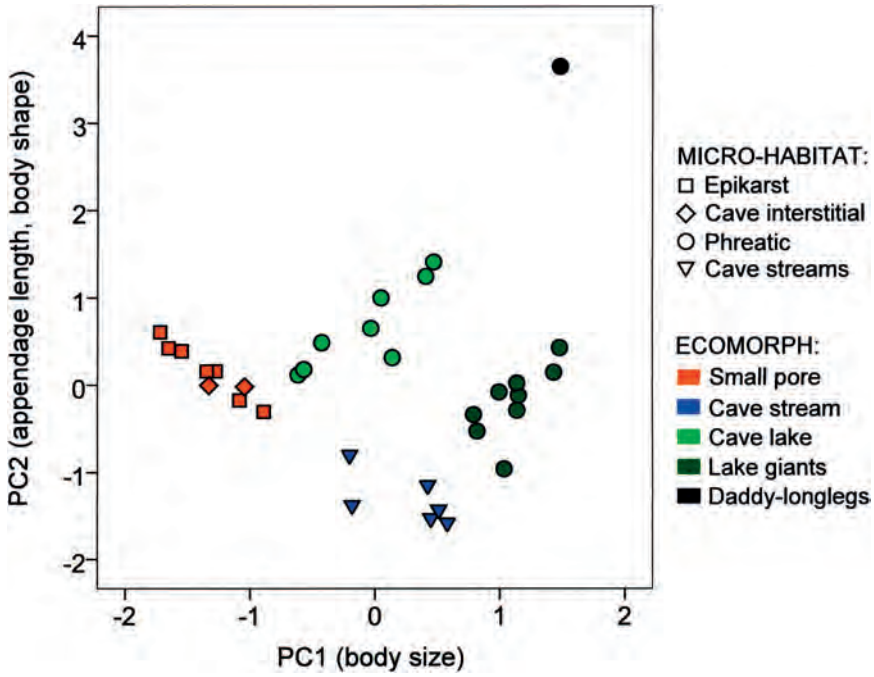

Figure 4. Principal Components Analysis on morphometric traits (mean values) of 33 *Niphargus* species and populations from seven cave communities in the Dinaric karst. The first two axes (PC1 and PC2) together explain 97.5 percent of the total variation. The first principal component is body length only, and accounts for 72.4 percent of the total variation. Cave microhabitats (symbols) and proposed ecomorphs (colors) are only partly in agreement. There is no morphological distinction between inhabitants of the epikarst and the cave interstitial, and there are three distinct morphological groups within the phreatic habitat. From Trontelj et al. (2012).

Table 4. Average body size (in µm) for deep soil and cave mite indicator species in Belgium. Adapted from Ducarme et al. (2004).

	Deep Soil		Caves	
Family	Species	Body Length	Species	Body Length
Rhodacaridae				
	Rhodacarellus apophyseus	366	*Rhodacarus aequalis*	588
			Rhodacarus agrestis	645
Parasitidae				
	Leptogamasus suecicus	610	*Vulgarogamasus* sp.	1053
Veigaiidae				
	Veigaia exigua	491	*Veigaia paradoxa*	1065
Eupodidae				
	Claveupodes sp.	227	*Benoinyssus ereynetoides*	285
	Cocceupodes sp.	281		
Rhagidiidae				
	Shibala longisensilla	583	*Poecilophysis spelaea*	1033
	Hammenia macrostella	309		
Tydaeoidae				
	Tydaeolus sp.	154	*Riccarodoellinae* sp.	465
	Coccotydaeolus sp.	154		
	Sellnickochthonius facoti	148	*Liochthonius leptaleus*	197
			Liochthonius propinquus	180
			Liochthonius strenzkei	220

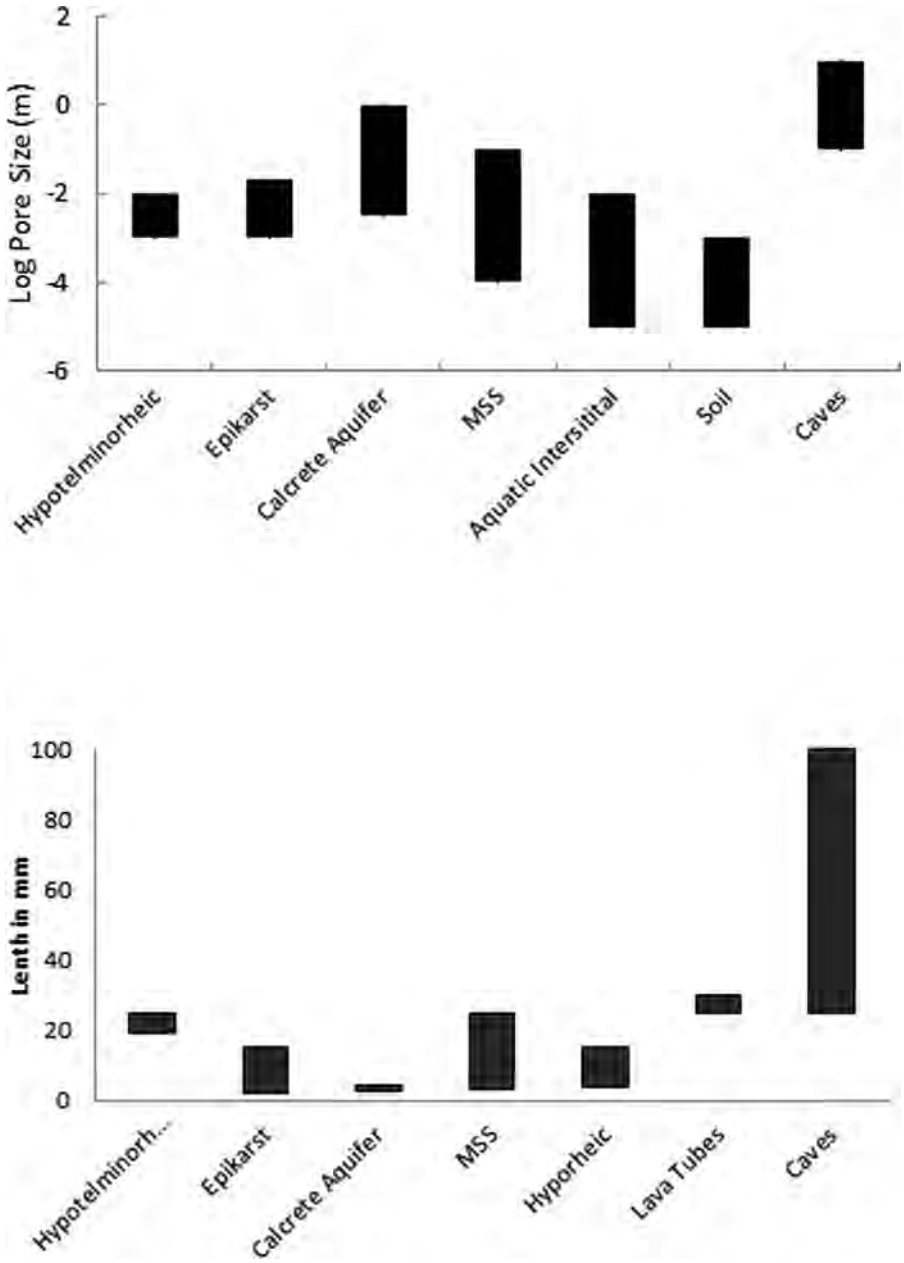

Figure 5. Histograms of body lengths of inhabitants and log of pore size for different subterranean habitats.

paid to the actual pore size of subterranean habitats, the exceptions being Culver and Ehlinger (1980) and de Bovée et al. (1995). Pore size can be determined from particle size as well, at least for uniformly sized particles. For example, a sphere with a diameter of 0.828 *r* can be inserted into a uniformly packed volume of sediments of radius *r*. Culver and Pipan (2014) provided some general estimates of pore size for different subterranean habitats, and overall the sizes of organisms in these habitats seem to match pore size (Fig. 5).

Only two of the studies explicitly took into account phylogenetic effects (Arnedo et al., 2007; Trontelj et al, 2012), although most other studies limited comparisons to within genera or families. The studies did encompass a wide variety of taxonomic groups, including both aquatic (Amphipoda, Copepoda, Isopoda) and terrestrial (Araneae, Acari) and encompassed a number of different subterranean habitats, including caves, lava tubes, interstitial habitats, talus slopes, epikarst, and *milieu souterrain superficiel*.

Body length itself is but one measure of the habitat dimensions needed by an organism. In an elegant study of some *Niphargus* amphipods, Delić et al. (2016) showed that both water velocity and the presence of competitors had a major effect on relative lengths of antennae and pereopods, but a small effect on body size. Overall thinning and

elongation of the body can occur as well, and it is carried to an extreme in some deep-soil mites such as *Gordialycus tuzetae,* which is nearly 3 mm long and only 0.05 mm wide (Thibaud and Coineau, 1998). Differences in overall shape of organisms are approximated by Principal Components Analysis as well as other multivariate analyses. Such analyses are likely to be informative in the present context (e.g., Trontelj et al., 2012. Given the fundamental connection between habitat size and organism size, it is curious that this connection is less well studied than the effect of competition on body size (Vergnon et al., 2013). Their study illustrates this very clearly; the ratio of body sizes of dytisicid beetles in calcrete aquifers (1.3:1) is that predicted by the theory of limiting similarity (MacArthur and Levins, 1967). But the overall sizes of the beetles vary from aquifer to aquifer, possibly the result of different pore sizes in different habitats, but there is no data on granulometry of these habitats.

In addition to habitat (pore) size, several other parameters are likely to be useful in ordinating subterranean communities. Communities in different subterranean habitats, such as caves, talus slopes, and soil, differ in species richness and in the frequency of troglomorphy among the resident species (see Pipan and Culver, 2012; Culver and Pipan, 2015). Subterranean habitats themselves vary along several important parameters, including percent organic matter and connectivity to the surface (Culver and Pipan, 2014), and water velocity (Delić et al., 2016). These habitats and their associated communities can be ordered along an axis of depth, a proxy for amount of organic matter and connection to surface habitats, and species richness of communities, as well as the degree of specialization of the component species, can then be compared to depth. Together with pore size, depth is likely to prove to be an important organizing principle for the variety of subterranean communities. While clearly not a substitute for the naming and description of different subterranean habitats, it is a way to consider the unity of subterranean habitats.

Conclusions

The role of habitat size in determining body size is far from trivial. For a range of habitat sizes, the size of the invertebrates occupying the habitat seems to approach some maximum for that habitat, unless there are competing species that further affect body size. The reasons that body size is maximized within the constraints of habitat size are likely twofold. First, larger subterranean animals have larger eggs and higher fecundity (Fišer et al., 2013), resulting in natural selection in favor of increased body size (Jones et al., 1992). Second, the absence of large predators reduces or eliminates the selective pressure toward smaller body size caused by predation. In cases where body size does not appear to be maximized, interspecific competition has been strongly implicated (Trontelj et al., 2012; Vergnon et al., 2013).

Acknowledgements

This project was supported by funds from funds from Slovenian Research Agency (BI-US/15-16-077) and the Mellon Fund of the College of Arts and Sciences, American University. Cene Fišer and Daniel Fong read an earlier version of this paper and made a number of useful suggestions.

References

Aljančič, M., Bulog, B., Kranjc, A., Josipovič, D., Sket, B., and Skoberne, P., 1993, Proteus: the Mysterious Ruler of the Karst Darkness: Ljubljana, Slovenia, Vitrum, 75 p.

Alroy, J., 1998, Cope's rule and the dynamics of body mass evolution in North American fossil mammals: Science, v. 280, p. 731–734. https://doi.org/10.1126/science.280.5364.731.

Arnedo, M.A., Oromí, P., Múrria, C., Macías-Hernández, N., and Ribera, C., 2007, The dark side of an island radiation: systematics and evolution of troglobitic spiders of the genus *Dysdera* Latreille (Araneae, Dysderidae) in the Canary Islands: Invertebrate Systematics, v. 21, p. 623–660. https://doi.org/10.1071/IS07015.

Borenstein, M., Hedges, L.V., Higgins, J.P.T., and Rathski, A.R., 2009, Introduction to Meta-Analysis: West Sussex, U.K., John Wiley and Sons, 420 p.

Coiffait, H., 1958, Les coléoptères du sol: Vie et Milieu Supplement, v. 7, 204 p.

Coineau, N., 2000, Adaptations to interstitial groundwater life, *in* Wilkens, H., Culver, D.C., and Humphreys, W.H., eds., Subterranean Ecosystems: Amsterdam, The Netherlands, Elsevier, p. 189–206.

Covington, M.D., and Perne, M., 2015, Consider a cylindrical cave: a physicist's view of cave and karst science: Acta Carsologica, v. 44, p. 363–380. doi:10.3986/ac.v44i3.1925.

Culver, D.C., and Ehlinger, T.J., 1980, The effects of microhabitat size and competitor size on two cave isopods: Brimleyana, v. 4, p. 103–113.

Culver, D.C., Holsinger, J.R., Christman, M.C., and Pipan, T., 2010, Morphological differences among eyeless amphipods in the genus *Stygobromus* dwelling in different subterranean habitats: Journal of Crustacean Biology, v. 30, p. 68–74. https://doi.org/10.1651/09-3156.1.

Culver, D.C., Kane, T.C., and Fong, D.W., 2005, Adaptation and Natural Selection in Caves. The Evolution of *Gammarus minus:* Cambridge, Mass., Harvard University Press, 223 p.

Culver, D.C., Pipan, T., and Schneider, K., 2009, Vicariance, dispersal and scale in the aquatic subterranean fauna of karst regions: Freshwater Biology, v. 54, p. 918–929. https://doi.org/10.1111/j.1365-2427.2007.01856.x.

Culver, D.C., and Pipan, T., 2009, Biology of Caves and Other Subterranean Habitats: Oxford, England, Oxford University Press, Biology of Habitats Series, 254 p.

Culver, D.C., and Pipan, T., 2014, Shallow Subterranean Habitats. Ecology, Evolution, and Conservation: Oxford, England, Oxford University Press, Biology of Habitats Series, 258 p.

Culver, D.C., and Pipan, T., 2015, Shifting paradigms in the evolution of cave life: Acta Carsologica, v. 44, p. 415–425. https://doi.org/10.3986/ac.v44i3.1688.

Curl, R.L., 1972, Minimum diameter stalactites: Bulletin of the National Speleological Society, v. 34, p. 129–136.

de Bovée, F., Yacoubi-Khebiza, M., Coineau, N., and Boutin, C., 1995, Influence du substrat sur la réparition des Crustacés interstitiels du Haut-Atlas occidental: Internationale Revue der Gesamten Hydrobiologie und Hydrographie, v. 80, p. 453–468. https://doi.org/10.1002/iroh.19950800310.

Delić, T., Trontelj, P., Zakšek, V., and Fišer, C., 2016, Biotic and abiotic determinants of appendage evolution in a cave amphipod: Journal of Zoology, v. 299, p. 42-50.

Ducarme, X., Wauthy, G., André, H.M., and Lebrun, P., 2004, Survey of mites in caves and deep soil and evolution of mites in these habitats: Canadian Journal of Zoology, v. 82, p. 841–850. https://doi.org/10.1139/z04-053.

Environmental Agency 2009. The Hyporheic Handbook: Bristol, England, Environmental Agency, science report SC050070, 264 p.

Fagan, W.F, Lutscher, F., and Schneider, K., 2007, Population and community consequences of spatial subsidies derived from central-place foraging: American Naturalist, v. 170, p. 902–915. https://doi.org/10.1086/522836.

Fairchild, I.J., and Baker, A., 2012, Speleothem Science. From Process to Past Environments: Chichester, England, Wiley-Blackwell, 432 p.

Fenolio, D., 2016, Life in the Dark. Illuminating Biodiversity in the Shadowy Haunts of Planet Earth: Baltimore, Maryland, Johns Hopkins University Press, 317 p.

Fišer, C., Pipan, T., and Culver, D.C., 2014, The vertical extent of groundwater metazoans: an ecological and evolutionary perspective: Bioscience, v. 64, p. 971-979. https://doi.org/10.1093/biosci/biu148.

Fišer, C., Zagmajster, M., and Zakšek, V., 2013, Coevolution of life history traits and morphology in female subterranean amphipods: Oikos, v. 122, p. 770–778. https://doi.org/10.1111/j.1600-0706.2012.20644.x.

Humphreys, W.F., 2001, Groundwater calcrete aquifers in the Australian arid zone: the context to an unfolding plethora of stygal biodiversity: Records of the Western Australian Museum, Supplement, no. 64, p. 63–83.

Hüppop, K., 2000, How do cave animals cope with the food scarcity in caves?, *in* Wilkens, H., Culver, D.C., and Humphreys, W.H., eds., Subterranean Ecosystems. Amsterdam, The Netherlands, Elsevier, p. 159–188.

Jones, R., Culver, D.C., and Kane, T.C., 1992, Are parallel morphologies of cave organisms the result of similar selection pressures?: Evolution, v. 46, p. 353–365. https://doi.org/10.2307/2409856.

Juberthie, C., Delay, B., and Bouillon, M., 1980, Sur l'existence d'un milieu souterrain superficiel en zone non calcaire: Compte Rendus de l'Académie des Sciences de Paris, v. 290, p. 49–52.

Karaman, S.L., 1954, Über unsere unterirdische fauna: Acta Musei Macedonica Scientiarum Naturalium, v. 1, p. 195–216.

Kingsolver, J.G., and Pfennig, D.W., 2004, Individual-level selection as a cause of Cope's rule of phyletic size increase: Evolution, v. 58, p. 1608–1612. https://doi.org/10.1111/j.0014-3820.2004.tb01740.x.

MacArthur, R.H., and Levins, R., 1967, The limiting similarity, convergence, and divergence of coexisting species: American Naturalist, v. 101, p. 377–383.

Malard, F., Ward, J.V., and Robinson, C.T., 2000, An expanded perspective of the hyporheic zone: Verhaltlungen der Internationalen Vereinigung für Theoretische und Angewandte Limnologie, v. 27, p. 431–437.

Meštrov, M., 1962, Un nouveau milieu aquatique souterrain: le biotope hypotelminorhéique: Compte Rendus Academie des Sciences, Paris, v. 254, p. 2677–2679.

Ortuño, V.M., Gilgado, J.D., Jiménez-Valverde, A., Sendra, A., Pérez-Suárez, G., and Herrero-Borgoñón, J.J., 2013, The "alluvial mesovoid shallow substratum", a new subterranean habitat: PLOS ONE, v.8, art. 76311, 16 p. https://doi.org/10.1371/journal.pone.0076311.

Pipan, T., and Culver, D.C., 2012, Convergence and divergence in the subterranean realm: a reassessment: Biological Journal of the Linnean Society, v. 107, p. 1–14. https://doi.org/10.1111/j.1095-8312.2012.01964.x.

Racoviţă, E.G., 1907, Essai sur les problèmes biospéologiques: Archives de Zoologie Expérimentale et Générale, v. 6, p. 371–488.

Růžička, V., 1998, The subterranean forms of *Lepthyphantes imporbulus, Theonoe minutissima* and *Theridion bellicosum* (Araneae: Linyphiidae, Theridiidae), *in* Selden, P.A., ed., Edinburgh, Scotland: Proceedings of the 17th European Colloquium of Arachnology, Edinburgh 1997: British Arachnological Society, p. 101–105.

Sendra, A, and Reboleira, A.S.A.S., 2012, The world's deepest subterranean community: Krubera-Voronja Cave (West Caucasus): International Journal of Speleology, v. 41, p. 221–230. https://doi.org/10.5038/1827-806X.41.2.9.

Shaw, T.R. 1999. *Proteus* for sale and for science in the 19th century: Acta Carsologica, v. 28, p. 229–285.

Sibley, R.M., Brown, J.H., and Kodric-Brown, A., eds., 2012, Metabolic Ecology: a Scaling Approach: New York, New York, Wiley-Blackwell, 365 p.

Solow, A.R., and Wang, S.C., 2008, Some problems with assessing Cope's rule: Evolution, v. 62, p. 2092–2096. https://doi.org/10.1111/j.1558-5646.2008.00410.x.

Thibaud, J.M., and Coineau, Y., 1998, Nouvelles stations pour le genre *Gordialycus* (Acarien: Nematalycidae): Biogeographica, v. 74, p. 91–94.

Trontelj, P., Blejec, A., and Fišer, C., 2012, Ecomorphological convergence in cave communities: Evolution, v. 66, p.3852–3865. https://doi.org/10.1111/j.1558-5646.2012.01734.x.

Vergnon, R., Leijs, R., van Nes, E.H., and Scheffer, M., 2013, Repeated parallel evolution reveals limiting similarity in subterranean diving beetles: American Naturalist, v. 182, p. 67–75. https://doi.org/10.1086/670589.

S. Popović, G. Subakov Simić, M. Stupar, N. Unković, O. Krunić, N. Savić, and M. Ljaljević Grbić – Cave biofilms: characterization of phototrophic cyanobacteria and algae and chemotrophic fungi from three caves in Serbia. *Journal of Cave and Karst Studies*, v. 79, no. 1, p. 10–23. DOI: 10.4311/2016MB0124

CAVE BIOFILMS: CHARACTERIZATION OF PHOTOTROPHIC CYANOBACTERIA AND ALGAE AND CHEMOTROPHIC FUNGI FROM THREE CAVES IN SERBIA

Slađana Popović[1]*, Gordana Subakov Simić[2], Miloš Stupar[2], Nikola Unković[2], Olivera Krunić[3], Nevena Savić[3], and Milica Ljaljević Grbić[2]

Abstract: Cyanobacteria, algae (Chlorophyta and Bacillariophyta), and fungi were identified from biofilm samples from three caves in western Serbia: Ribnička, Hadži Prodanova, and Rćanska. Temperature, light intensity, and relative humidity varied from 16.9 °C to 24.9 °C, 61% to 87%, and 215 Lux to 4400 Lux, respectively. In general, the highest number of documented taxa belonged to Cyanobacteria, with chroococcalean taxa prevailing and *Gloeocapsa* species as the most diverse. A large percentage of observed fungi were Ascomycetes or Zygomycetes, while the only representative of Basidiomycetes was *Rhizoctonia* s. lat. However, a redundancy analysis revealed that different taxonomic groups were dominant at different localities: cyanobacteria and fungi in Ribnička and Hadži Prodanova, and Chlorophyta and Bacillariophyta in Rćanska. The statistical analysis showed that relative humidity is an important physical parameter influencing the development of various microbial communities in different caves. Cyanobacteria were mostly found in places with lower relative humidity, while Chlorophyta and Bacillariophyta were found in places with higher humidity. The documented physical parameters did not have a significant impact on the distribution of fungi. Measured chlorophyll-a content was highest on horizontal surfaces, where the highest content of organic/inorganic matter were also recorded. The highest water content was observed in biofilm samples from which many cyanobacteria taxa were identified.

Introduction

The territory of Serbia is one of the curiosities of the world in terms of the complexity of the geological composition, both related to the number and diversity of lithologic and stratigraphic units, as well as in terms of tectonic structure. The geological heterogeneity of the territory is largely a consequence of magmatic activity accompanied by intense movements of the earth's crust during the Cretaceous and Tertiary Alpine tectonics. In a small area of 88,000 km^2, the six major geotectonic regions (Inner Dinarides, Šumadijsko-Kopaonička Zone, Serbian-Macedonian Mass, Carpatho-Balkan Mountains, Moesian Platform, and the Pannonian Basin) (Dimitrijević, 1974), can be distinguished, along with dozens of lower-order geotectonic areas or units. Carpatho Balkanids and Inner Dinarides of western Serbia are regions where the terrain is built of carbonate sediments with very distinctive karst forms, both on the surface and underground (Filipović et al., 2005). The underground karst forms are characterized by a large number and great diversity of caves and caverns, of which many are protected due to their scientific and cultural relevance and importance.

Caves are not only unique natural monuments in terms of geological structure and complexity, but also represent a unique habitat for a large number of organisms such as viruses, bacteria, fungi, lichen, algae, protozoa, plants and animals (Falasco et al., 2014). Phototrophic microorganisms can easily be found at cave entrances illuminated by direct or indirect sunlight and as lampenflora in areas near artificial lights, usually associated with various heterotrophic microorganisms, predominantly bacteria and fungi, also common in the inner, non-illuminated parts of the cave (Mulec and Kosi, 2008; Czerwik-Marcinkowska, 2013). Various colorations on speleothems, precipitates, corrosion residues, structural changes, and biofilms represent evidence of a microbial community (Ogórek et al., 2016).

Little is known about the microbiota of Serbian caves (Popović et al., 2015), unlike many other European countries: Spain (Martinez and Asencio, 2010; Roldán and Hernández-Mariné, 2009; Urzì et al., 2010; Busquets et al., 2014), France (Borderie et al., 2011, 2014; Bastian and Alabouvette, 2009), Italy (Cennamo et al., 2012; Giordano et al., 2000), Poland (Czerwik-Marcinkowska and Mrozińska, 2009, 2011; Czerwik-Marcinkowska, 2013; Ogórek et al., 2013; Pusz et al., 2014), Slovenia (Klemenčić and Vrhovšek, 2005; Mulec and Kosi, 2008; Mulec et al., 2008, 2012), Greece (Lamprinou et al., 2009, 2012, 2014; Pantazidou and Roussomoustakaki, 2005), Czech Republic (Poulíčková and Hašler, 2007), Turkey (Selvi and Altuner, 2007), and Russia (Mazina and Maximov, 2011). We investigated cyanobacterial, algal, and fungal

* Corresponding Author: spopovic.bio@gmail.com
[1] University of Belgrade, Scientific Institution, Institute of Chemistry, Technology and Metallurgy, Department of Ecology and Technoeconomics, 11000 Belgrade, Serbia
[2] University of Belgrade, Faculty of Biology, 11000 Belgrade, Serbia
[3] University of Belgrade, Faculty of Mining and Geology, 11000 Belgrade Serbia

diversity in three karst caves in Serbia and related diversity to the environmental factors of light, temperature, and relative humidity and how these factors contribute to colonization by microorganisms.

Materials and Methods

Sampling Sites and Sampling Procedure

Ribnička Cave (RIB) (Fig. 1a) is situated in the northwestern part of Serbia, in the valley of the river Ribnica, south of Mionica (44°12′20.27″N, 20°5′32.59″E). The gorge through which Ribnica River flows is constructed of Lower and Upper Cretaceous and Lower Triassic limestone. The cave entrance is 25 m wide and 12 m high and only 1 m above the riverbed, and the total length of the cave is 127 m. From the main chamber, several short galleries diverge (Đurović, 1998). Because of the dimensions of the cave entrance and the main hall, the microclimate of the cave is heavily influenced by seasonal and daily fluctuations of outside climatic factors, primarily temperature.

Hadži Prodanova Cave (HP) (Fig. 1b) is located in the upper part of the Rašćanska River, 7 km from Ivanjica (43°37′38.78″N, 20°14′25.30″E), in fissured Triassic limestones. This cave is a spacious form of underground karst topography and consists of an entrance channel, the central hall, and radiating lateral canals, with a total length of about 420 m. The cave entrance is narrow and tall, about 5 to 6 m high and approximately 2 m wide at the beginning, then slightly narrows and continues to the spacious central hall. The cave is very dry, and only dripping water makes it hydrologically active (Đurović, 1998).

The Ršanska Caves (RC) are located on the left side of the Ršanska River, in the Dragačevo territory (43°44′2.70″N, 20°14′29.37″E), and these partly explored underground karst forms consist of Velika, Suva, and Slepa Caves and Bezdan Pit, which are composed of mostly massive Upper Cretaceous limestone, with the total length of the canals being about 750 m. The upper part of Velika Cave, with a total length of about 380 m (Fig. 1c), has a cascading elevation, while the lower part is composed of three levels of galleries, the main canyon with a cascading rocky floor, the hydrologically active level that ends in a siphon, and a dry, hydrologically inactive level (Đurović, 1998). The sampling was conducted at the entrance of lower part of Velika Cave. This entrance is approximately 13 m wide and 17 m high. Since the investigated caves are still not open for tourists, there are no anthropogenic activities that may have affected the cave's ecosystems.

For algological and mycological analyses, seven sampling sites were chosen in Ribnička, while five sampling sites were selected in Hadži Prodanova and Ršanska. The locations of each sampling site near the cave entrance are shown in Fig. 1. All samples, with the exception of samples from sampling sites RC2 and RIB6, were collected from the cave walls where variously colored biofilms were formed. Sampling site RC2 was located on the horizontal surface of a large stone in the middle of the cave on which the mud deposits were observed, while sampling site RIB6 was on the cave floor.

Light intensity, temperature, and relative humidity were measured using the DMV 1300 Luxmeter, Velleman, Belgium and Temperature Humidity Meter, Extech, USA. These parameters were measured three times at each sampling site, and for each parameter, the mean values and standard errors were calculated.

Algological and Mycological Analyses

Samples for algological analyses were taken directly from the stone substrata using a non-destructive, adhesive-tape method (Gaylarde and Gaylarde, 1998; Urzì and de Leo, 2001) and by scraping the biofilm with a flame-sterilized scalpel. Afterward, the samples were stored in labeled sterile polyethylene bags and transported on ice until laboratory processing. The part of the scraped material was mixed with a drop of glycerol, and it and the adhesive strips were directly observed using the light microscope Zeiss Axio-Imager M.1 with software AxioVision 4.8. Algae and cyanobacteria were identified using the appropriate literature: John et al. (2003), Komárek and Anagnostidis (1998; 2005), Komárek (2013), Komárek and Fott (1983), Krieger and Gerloff (1962), Hofmann et al. (2013), and Starmach (1972).

For mycological analysis, five samples were collected from each of the sampling sites by swabbing the stone surfaces with sterile cotton swabs. After sampling, swabs were put in sterile polyethylene bags until laboratory processing. In laboratory conditions, swab samples were diluted in 10 mL sterile, deionized water and shaken steadily for 10 minutes. Aliquots of 1 mL prepared suspension were inoculated onto dichloran 18% glycerol agar (DG18) and malt extract agar (MEA), both with antibiotics added to suppress bacterial growth. Chloramphenicol in the concentration of 0.1 g L^{-1} was added to DG18 medium, while streptomycin (500 mg L^{-1}) was added to MEA (Samson et al., 2010). Procedures were done in triplicate. The inoculated plates were then incubated in dark conditions for seven days at 25 °C (Memmert Incubator UE500). Pure cultures of each isolate were obtained via single conidial transfer of primary isolates to the following nutrient media: Creatine sucrose agar (CREA), Czapek Yeast extract agar (CYA), DG18, Dichloran Rose Bengal Chloramphenicol agar (DRYES), MEA, Oatmeal agar (OA), and Potato Carrot Agar (PCA). After an incubation period of seven days, fungi were identified based on colony macromorphology and microscopic features of fungal reproductive structures using a stereomicroscope (Stemi DV4, Zeiss) and light microscope (Carl Zeiss Axio Imager M.1 with software AxioVision 4.8). Fungal isolates were identified to the species or genus level using the following dichotomous keys: Bensch et al. (2012), Ellis (1971), Ellis and Ellis (1997), García et al. (2006), Rapper and Fennel (1965), Samson et al. (2010), Samson and Varga (2007), Watanabe (2010), and Woudenberg et al. (2013).

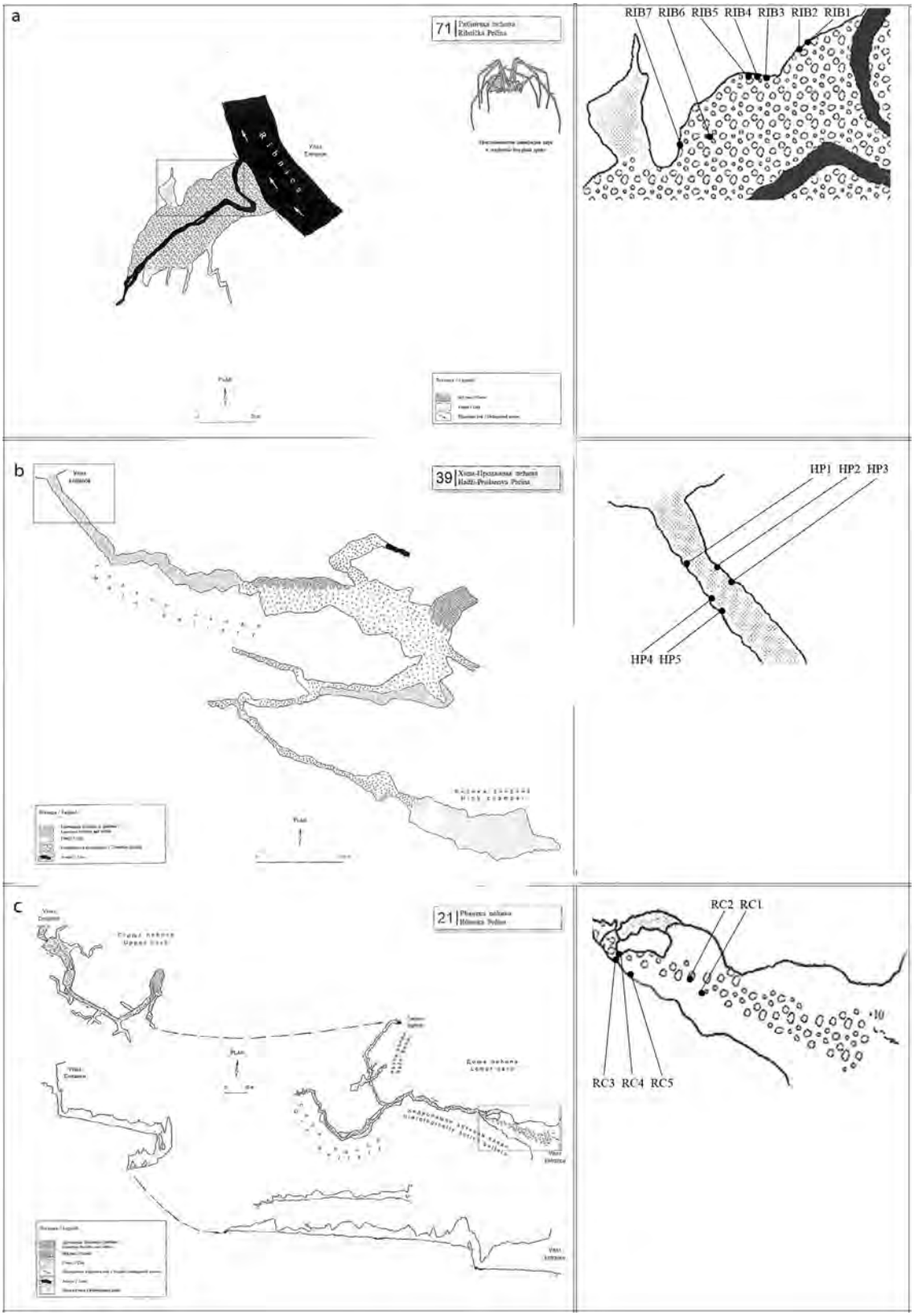

Figure 1. Maps of the three investigated caves with sampling sites near the entrance of each cave: a-Ribnička (RIB1–RIB7), b-Hadži Prodanova (HP1–HP5), and c-Rćanka Caves (RC1–RC5). The sampling sites had the following distances from the cave entrances: RIB1, 8 m; RIB2, 9 m; RIB3, 13 m; RIB4, 13.5 m; RIB5, 14 m; RIB6, 22 m; RIB7, 26 m; HP1, 5 m; HP2, 6 m; HP3, 7 m;, HP4, 7 m; HP5, 8 m; RC1, 22 m; RC2, 24 m; RC3, 34 m; RC4, 34 m; RC5, 30 m.

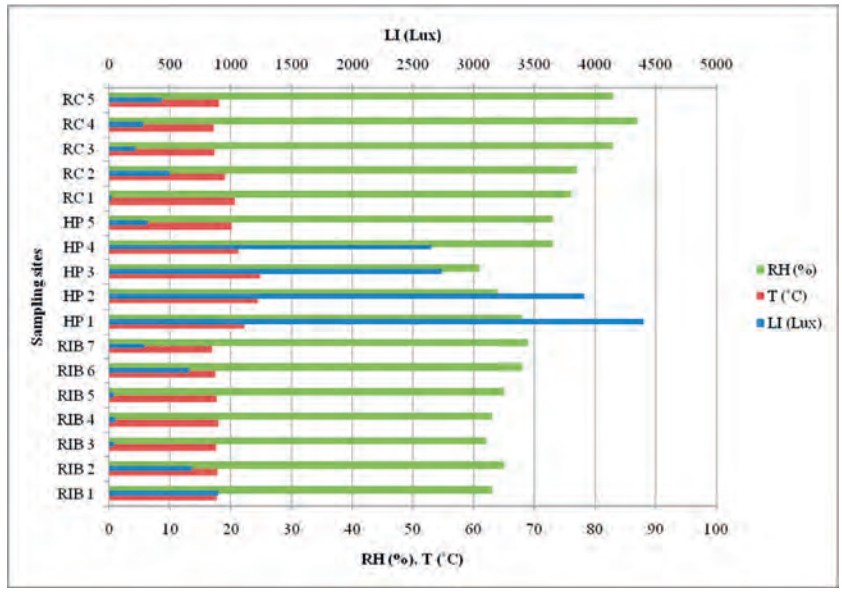

Figure 2. Measured physical parameters: light intensity (LI in Lux), temperature (T in °C), and relative humidity (RH %) at sampling sites from Ribnička (RIB1–RIB7), Hadži Prodanova (HP1–HP5), and Rćanska (RC1–RC5) caves.

Determination of Chlorophyll-a, and Biofilm Content

A round metal matrix covering a surface of 3.14 cm^2 was used to mark the surface on stone substrata from which the two biofilm samples were scraped for chlorophyll-a extraction and determination of the water content and content of inorganic/organic matter in biofilm samples.

Stone surfaces on which the metal matrix was applied were smooth and had minor imperfections. Scraped samples were kept in sterile polyethylene bags, and upon the arrival in the laboratory, samples were immediately prepared for the chlorophyll-a extraction. The biofilm samples were weighted and boiled in 20 mL of 100% ethanol. After homogenization, the samples were filtered, and the absorbance of the filtrate was measured before and after acidification at 665 nm and 750 nm on the spectrophotometer (Cecil CE 2501). The chlorophyll-a content was determined using the formula described in the study by Popović et al. (2015), and was expressed as μg Chl-a cm^{-2}.

Samples for the determination of the water content were kept in a sealed container to avoid water evaporation until their arrival at the laboratory. The water content and organic/inorganic matter in the biofilm samples expressed in percent and mg cm^{-2} were determined based on the difference in sample weight before and after drying at 105 °C and ashing at 550 °C The difference in biofilm weight between fresh samples and those dried at 105 °C gave the water content of the biofilm, while the difference between the weights at 105 °C and 550 °C was organic matter. The residue remaining at 550 °C was the inorganic part of the biofilm.

Statistical Analysis

Two redundancy analyses were performed using the program CANOCO for Windows, Version 5.0 (Ter Braak and Šmilauer, 2012). The first RDA analysis was performed to examine the potential effects of measured environmental variables on cyanobacterial, algal, and fungal community with the cave used as a supplementary variable. For project data, presence/absence of all recorded taxa was used as a measure. Then each taxon was assigned to a taxonomic group (Cyanobacteria, Chlorophyta, Bacillariophyta, or fungi). In further analysis, we used these groups instead of individual taxa. The measured environmental variables temperature, relative humidity, and light intensity were submitted to the interactive forward selection, in which the statistical significance of each variable was tested by the Monte Carlo permutation test at a cutoff point of P=0.05. RDA with the option 'center and standardize' was used. The main goal was to show if some groups are influenced by any of the measured environmental factors. The second RDA analysis, with cave as an explanatory variable, was performed to demonstrate the preference of microorganism groups for a certain cave, as well as the proportion of documented taxa found in every cave.

Results

Light intensity varied from the lowest value of 21.5 Lux, measured at sampling site RC1, to the highest value of 4400 Lux, measured at sampling site HP1. The highest temperature was measured at HP3 (24.9 °C) and the lowest at RIB7 (16.9 °C). The lowest relative humidity was measured at HP3 (61%), and the highest at RC4 (87%) (Fig. 2). The highest

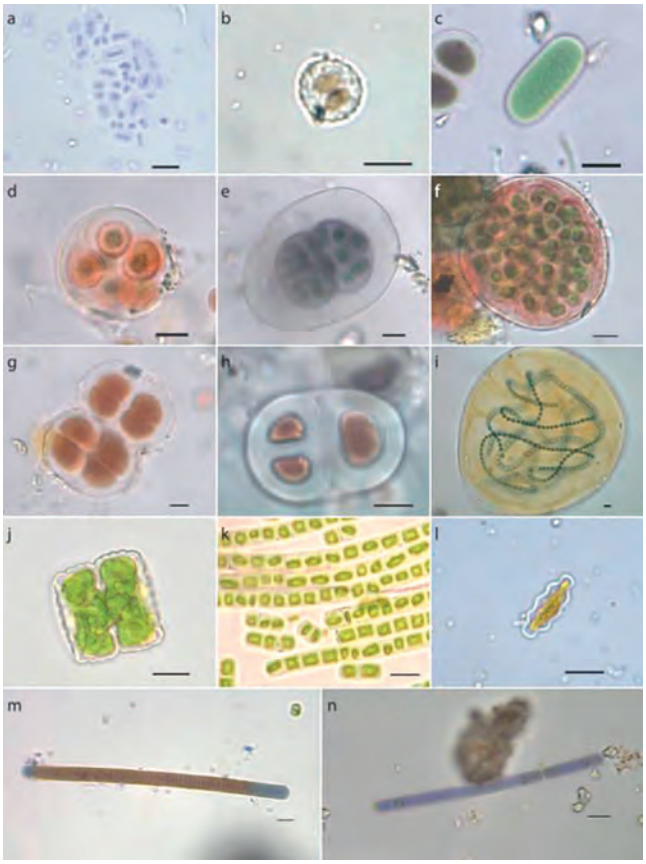

Figure 3. Micrographs of some documented cyanobacteria and algae in biofilm samples from Ribnička (a - *Aphanothece caldariorum*; b - *Asterocapsa* sp.; c - *Cyanothece aeruginosa*; d - *Gloeocapsa sanguinea*; e - *Gloeocapsa alpina*; h - *Chroococcus ercegovicii*), from Hadži Prodanova (f - *Gloeocapsa novacekii*; g - *Chroococcus* sp.; i - *Nostoc commune*; m - *Oscillatoria sancta*), and from Rćanska (j - *Cosmarium rectangulum*; k - *Klebsormidium flaccidum*; l - *Luticola nivalis*; n - *Phormidium* sp.) caves. Scale bars 10 µm.

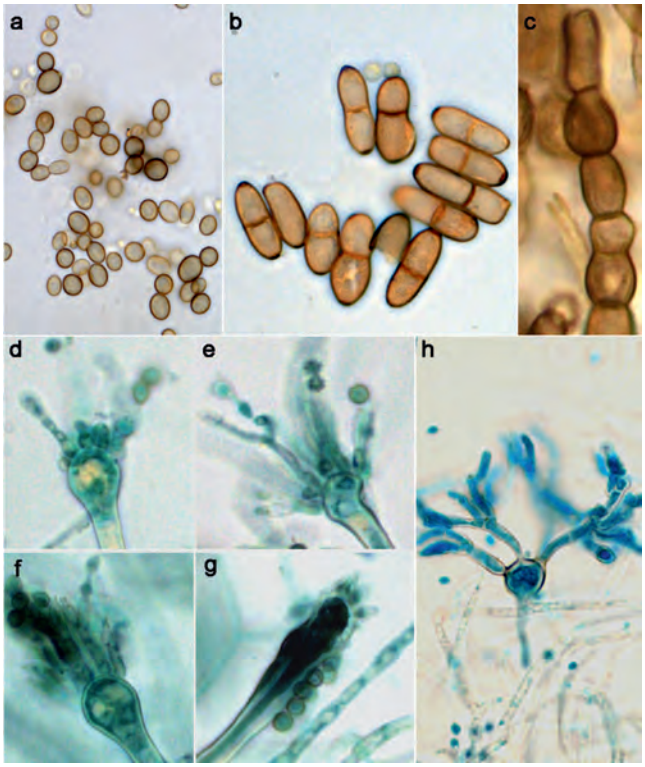

Figure 4. Culturable fungi (seven days, malt extract agar) from Hadži Prodanova, Rćanska, and Ribnička caves: a. black yeast cells; b. didimospores of *Cladosporium*-like dematiaceous Hyphomycetes; c. unbranched chain of microcolonial fungi meristematic cells; d–g. aberant conidiogenus apparatus in *Aspergillus* sect. *Nidulantes* culture; h. microciclic conidiation in *Penicillium* sp. culture.

values of light intensity and temperature were measured in Hadži Prodanova. Measured relative-humidity values were obviously lowest in Ribnička, where cyanobacteria prevailed, and some sampling sites in Hadži Prodanova. The differences in the measured physical parameters were easily visible when the data from all localities were compared, but there were no significant differences among the sampling sites in any one cave, except for light intensity.

The two methods of biofilm sampling for cyanobacterial and algological analyses, non-destructive adhesive tape and scraping the biofilm with flame-sterilized scalpels, were found to support each other and contributed to a more detailed identification of taxa in biofilm. During the survey in the investigated caves, Cyanobacteria (Table 1) and algae (Chlorophyta and Bacillariophyta) (Table 2) were documented. The highest number of documented taxa belonged to Cyanobacteria, with chroococcalean taxa prevailing and species of the genus *Gloeocapsa* being the most diverse. Oscillatoriales and Nostocales were present to a lesser extent. Most of the cyanobacteria that were documented in these three caves were aerophytic taxa, while Chlorophyta and Bacillariophyta had aerophytic and freshwater representatives. Some of the documented taxa are shown in Figure 3. Many cyanobacterial and algal taxa were documented only in one of the caves. *Aphanothece saxicola, Desmococcus olivaceus*, *Hantzschia amphioxys* and *Nitzschia* sp. were documented in all three, while *Aphanocapsa muscicola, Chroococcus* sp., *Chroococcus turgidus, Gloeocapsa biformis, Gloeocapsa reicheldtii, Gloeocapsa violascea, Leptolyngbya foveolarum, Oscillatoria sancta, Nostoc commune, Trochiscia granulata* and *Luticola nivalis* were found in two caves.

In all investigated samples, 27 different fungal morphotypes, including filamentous fungi, yeasts (Fig. 4a), and microcolonial fungi (Fig. 4c) were isolated. A list of identified fungi is presented in Table 3. The majority of documented fungi were Ascomycetes or Zygomycetes. However, the plant pathogen *Rhizoctonia* s. l. (teleomorph: *Thanatephorus* sp.) was the only member of Basidiomycetes documented in this study; it was isolated from walls of Hadži Prodanova. Microcolonial fungi,

Table 1. Cyanobacterial taxa from Ribnička (RIB1–RIB7), Hadži Prodanova (HP1–HP5) and Rćanska (RC1–RC5) caves (+ indicates sampling sites where specific taxa were documented).

Cyanobacterial Taxa	RIB1	RIB2	RIB3	RIB4	RIB5	RIB6	RIB7	HP1	HP2	HP3	HP4	HP5	RC1	RC2	RC3	RC4	RC5
Chroococcales																	
Aphanocapsa fusco lutea Hansgirg					+												
Aphanocapsa muscicola (Meneghini) Wille	+									+							
Aphanocapsa parietina (Nägeli ex Kützing) Nägeli								+		+	+						
Aphanocapsa rivularis (Carmichael) Rabenhorst								+	+	+	+						
Aphanocapsa Nägeli sp. 1	+					+	+										
Aphanocapsa Nägeli sp. 2														+	+	+	+
Asterocapsa H.-J. Chu sp.	+						+										
Aphanothece caldariorum P.G.Richter			+	+													
Aphanothece saxicola Nägeli							+		+	+				+			
Aphanothece Nägeli sp.	+					+											
Chroococcidiopsis kashayi Friedmann											+	+					
Chroococcidiopsis Geitler sp.													+		+		+
Chroococcus ercegovicii Komárek & Anagnostidis	+		+	+		+	+										
Chroococcus Nägeli sp.	+						+	+		+							
Chroococcus turgidus (Kützing) Nägeli	+																+
Cyanothece aeruginosa (Nägeli) Komárek	+						+										
Eucapsis F.E.Clements & H.L.Shantz sp.														+		+	
Gloeocapsa aeruginosa Kützing			+														
Gloeocapsa alpina Nägeli	+						+										
Gloeocapsa atrata Kützing										+							
Gloeocapsa biformis Ercegovic	+								+	+	+						
Gloeocapsa compacta Ercegovic										+							
Gloeocapsa fusco lutea Kirchner	+																
Gloeocapsa haematodes (Kützing) Kützing				+													
Gloeocapsa novacekii Komárek & Anagnotidis										+	+						
Gloeocapsa reicheltii P.G.Richter							+			+	+						
Gloeocapsa rupestris Kützing	+						+										
Gloeocapsa sanguinea (C.Agardh) Kützing	+						+										
Gloeocapsa violascea Kützing	+						+			+							
Gloeocapsa Kützing spp.							+				+						
Gloeothece rupestris (Lyngbye) Bornet							+										
Microcrocis P.G.Richter sp.						+											
Pseudocapsa dubia Ercegovic		+								+	+						
Oscillatoriales																	
Leptolyngbya foveolarom (Gomont) Anagnostidis & Komárek										+				+	+	+	

Table 1. Continued.

Cyanobacterial Taxa	RIB1	RIB2	RIB3	RIB4	RIB5	RIB6	RIB7	HP1	HP2	HP3	HP4	HP5	RC1	RC2	RC3	RC4	RC5
Leptolyngbya Anagnostidis & Komárek spp.						+			+								
Oscillatoria sancta Kützing ex Gomont										+						+	
Phormidium Kützing ex Gomont sp.														+		+	+
Phormidium ambiguum Gomont									+								
Phormidium interruptum Kützing ex Forti									+								
Symploca muscorum Gomont ex Gomont														+			
Nostocales																	
Nostoc commune Vaucher ex Bornet & Flahault							+			+							
Scytonema C.Agardh ex É.Bornet & C.Flahault sp. 1							+										
Scytonema C.Agardh ex É.Bornet & C.Flahault sp. 2									+								
Scytonema C.Agardh ex É.Bornet & C.Flahault sp. 3										+							

well-known as rock-inhabiting fungi, were frequently encountered in all studied caves (Isola et al., 2016).

During laboratory cultivation, microscopic analyses revealed the presence of atypical fungal structures, such as aberrant conidial apparatus in *Aspergillus* sp. sect. *Nidulantes* (Fig. 4d, g) and microcyclic conidiation in one *Penicillium* isolate (Fig. 4h).

Interactive forward selection revealed that relative humidity was the only measured environmental variable that was statistically significant (Fig. 5A). The redundancy analysis including humidity as an explanatory variable and Cyanobacteria, Chlorophyta, Bacillariophyta, and fungi as response data showed that relative humidity was positively correlated with the first RDA axis ($r = 0.7067$), which explained 23.99% of the total variance in our data. Thus, the first axis represented the variation in cyanobacterial, algal, and fungal assemblage explainable by the humidity variable, and the second vertical axis represented a part of residual variation that was not explained by that variable, which suggested that there might also have been other environmental factors influencing the distribution of these groups of microorganisms. Still, the effect of humidity was significant, as confirmed by the result of the Monte Carlo permutation test ($F = 4.6$, $p = 0.0075$). Bacillariophyta and Chlorophyta showed positive correlations with the first RDA axis, which showed that most preferred places are those with higher levels of air humidity. On the other hand, cyanobacteria showed a negative correlation with the first RDA axis, as they were mostly found in places with lower humidity. Fungi showed a slightly negative, almost nonexistent correlation with the first RDA axis, but a highly positive correlation with the second RDA axis, meaning that other factors affected the appearance and development of fungi in a certain locality. Cyanobacteria also showed a correlation with the second axis, but it was negative.

The second redundancy analysis (Fig. 5B) showed that the caves were separated along the first axis, as were taxonomic groups. Cyanobacteria and fungi were placed on the left side of the ordination diagram (they were mostly found in Hadži Prodanova and Ribnička), while Chlorophyta and Bacillariophyta were placed on the right side of the ordination diagram (mostly found in Rćanska). In addition, each group is represented as a pie symbol, in which the proportion of documented taxa found in every cave can be seen. Cyanobacterial taxa, with the most numerous being from the order Chroococcales, were predominant in Ribnička and Hadži Prodanova, while in Rćanska smaller number of taxa were recorded. The fungi showed the same pattern. On the other hand, Chlorophyta and Bacillariophyta were mostly documented in samples from Rćanska.

The lowest values of chlorophyll-a content, expressed as μg Chl-a cm^{-2}, were documented at sampling sites RIB2 and RIB5, where few cyanobacterial and algal taxa were found. Two sampling sites that were on a horizontal substrate (RIB6 and RC2) had the highest concentrations of chlorophyll-a (Fig. 6). The content of organic matter expressed as mg cm^{-2} was also the highest at RIB6 and RC2, and the highest content of

Table 2. Algal taxa (Chlorophyta and Bacillariophyta) from Ribnička (RIB1–RIB7), Hadži Prodanova (HP1–HP5) and Ŕćanska (RC1–RC5) caves (+ indicates sampling sites where specific taxa were documented).

Algal Taxa	RIB1	RIB2	RIB3	RIB4	RIB5	RIB6	RIB7	HP1	HP2	HP3	HP4	HP5	RC1	RC2	RC3	RC4	RC5
Chlorophyta																	
Apatococcus F.Brand sp.													+				
Coccomyxa Schmidle sp.								+									
Cosmarium parvulum var excavatum Insam & Krieger														+			+
Cosmarium rectangulum Reinsch														+		+	
Desmococcus olivaceus (Persoon ex Acharius) J.R.Laundon		+	+		+	+		+	+		+				+	+	+
Klebsormidium flaccidum (Kützing) P.C.Silva, K.R.Mattox & W.H.Blackwell														+	+	+	+
Klebsormidium subtile (Kützing) Tracanna ex G.Tell														+		+	
Pediastrum simplex var echinulatum Wittrock															+		
Stichococcus bacillaris Nägeli																+	
Trochicia granulata (Reinsch) Hansgirg								+	+	+					+	+	
Bacillariophyta																	
Hantzschia amphyoxis (Ehrenberg) Grunow						+		+		+							+
Luticola nivalis (Ehrenberg) D.G.Mann								+							+		+
Navicula Bory de Saint-Vincent spp.														+	+	+	+
Nitzschia linearis W.Smith														+			
Nitzschia Hassall spp.						+		+						+	+	+	+

Table 3. Identified culturable fungi in biofilm samples from Ribnička (RIB1–RIB7), Hadži Prodanova (HP1–HP5) and Rćanska (RC1–RC5) caves and methods that are used for their identification.

Fungal Isolates	Source of Isolation	Identification Method
Alternaria spp. and *Alternaria* like genera (3 morphotypes)		
Alternaria Nees sp. 1 sect. *Alternata*	HP1	PCA, DRYES, DG18 (Woudenberg et al., 2015)
Alternaria Nees sp. 2 sect. *Alternata*	RIB7	PCA, DRYES, DG18 (Woudenberg et al., 2015)
Aspergillus spp. (6 morphotypes)		
Aspergillus P. Micheli sp. 1. sect. *Usti*	HP3	CYA, MEA, DG18 (Rapper and Fennel, 1965; Samson and Varga, 2007)
Aspergillus P. Micheli sp. 2. sect. *Nidulantes*	HP2, HP3, HP4	CYA, MEA, DG18 (Rapper and Fennel, 1965; Samson and Varga, 2007)
Aspergillus P. Micheli sp. 3. sect. *Nigri*	RIB7, HP1, HP3, HP4, RC5	CYA, MEA, DG18 (Rapper and Fennel, 1965; Samson and Varga, 2007)
Aspergillus P. Micheli sp. 4. sect. *Clavati*	HP4, HP5	CYA, MEA, DG18 (Rapper and Fennel, 1965; Samson and Varga, 2007)
Aspergillus P. Micheli sp. 5. sect. *Terei*	HP1, HP5	CYA, MEA, DG18 (Rapper and Fennel, 1965; Samson and Varga, 2007)
Aspergillus P. Micheli sp. 6. sect. *Circummdati*	HP4	CYA, MEA, DG18 (Rapper and Fennel, 1965; Samson and Varga, 2007)
Cladosporium spp. and *Cladosporium* like genera (4 morphotypes)		
Cladosporium cladosporioides (Fresen.) G.A. de Vries s. lat	RIB2, RIB6, RIB7, HP1, HP5, RC2	MEA, DG18, DRYES (Bensch et al., 2012)
Cladosporium sphaerospermum Penz. s. lat	RC3	MEA, DG18, DRYES (Bensch et al., 2012)
Cladosporium Link spp.	RIB1, RIB6, RC2, HP3	MEA, DG18, DRYES (Bensch et al., 2012)
Other Hyphomycetes		
Aureobasidium pullulans (de Bary) G. Arnaud	RIB2, RIB5, HP3, RC3	MEA, OA, DG18 (Samson et al., 2010)
Botrytis cinerea Pers.	RIB1, RIB2	MEA, OA, DG18 (Samson et al., 2010)
Epicoccum nigrum Link.	RIB1, RIB5, RIB7, HP1, HP2, HP5	MEA, OA, DG18 (Samson et al., 2010)
Paecilomyces variotii Bainier	HP5, RC3	MEA, OA, DG18 (Samson et al., 2010)
Humicola Traaen sp.	RC2, RC3, RC4	MEA, OA, DG18 (Watanabe, 2010)
Penicillium Link spp. (3 morphotypes)	HP4, HP5, RIB1, RIB4, RIB5, RIB6, RIB7, HP3, HP4, RC1, RC4	CYA, MEA, CREA (Pitt, 1979; Samson et al., 2010)
Periconia bysoides Pers.	HP3	MEA, OA (Ellis, 1971; Ellis and Ellis, 1997)
Zygomycetes (3 morphotypes)		
Mucor Micheli: Fr. spp.	RC3, RC4	MEA, OA, DG18 (Samson et al., 2010)
Rhizopus stolonifer (Ehrenb.) Vuill.	HP4, HP5	MEA, OA, DG18 (Samson et al., 2010)
Basidiomycetes		
Rhizoctonia DC. s. lat	HP2	MEA, OA (García et al., 2006)

Note: Nutrient media: CYA = Czapek Yeast extract agar; CREA - Creatine sucrose agar; DG18 = Dichloran 18% Glycerol agar; DG18 = Dichloran Rose Bengal Chloramphenicol agar; MEA = Malt extract agar; OA = Oatmeal agar; PCA = Potato Carrot Agar.

inorganic matter was found at RC2 and RIB1. The water content was high at RC2, RIB3, RIB6, and RC4. In general, the highest biomass was observed at RIB6 and RC2. The lowest values of all three biofilm parameters were recorded at RIB5, HP4, and RC3. The table depicting the measured biofilm parameters in percentages was included to display the relationship of every measured component in each biofilm sample (Table 4). The water was the main biofilm constituent at RIB3, RIB7, HP3 and RC4.

DISCUSSION

Cyanobacteria and algae (with green algae and diatoms as the most important (Falasco et al., 2014)), are the most

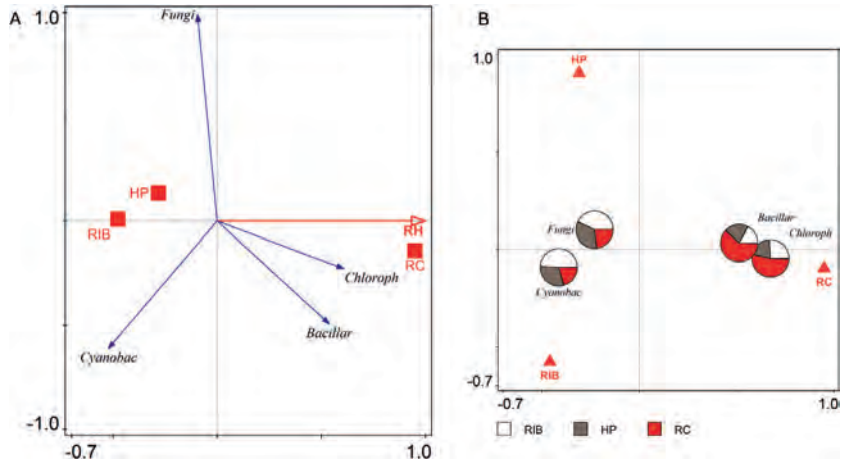

Figure 5. A - Redundancy analysis biplot ordination on the basis of the measured environmental variable relative humidity and cyanobacterial, algal (Chlorophyta and Bacillariophyta), and fungal community with cave as a supplementary variable. B - Redundancy-analysis biplot ordination of cyanobacteria, algae (Chlorophyta and Bacillariophyta), and fungi with locality as an explanatory variable. Each group was represented as a pie symbol, in which the proportion of documented taxa found in every cave can be seen. Caves: Ribnička RIB, Hadži Prodanova HP, and Rćanska RC.

common phototrophic constituents of cave ecosystems (Mulec et al., 2008). Cyanobacteria and green algae are considered the pioneer colonizers of many exposed surfaces, followed by various heterotroph such as bacteria and fungi. These organisms play an important role in biofilm genesis (Falasco et al., 2014). Cyanobacteria prevail compared to other microorganisms (Czerwik-Marcinkowska, 2013; Mulec et al., 2008; Selvi and Altuner, 2007; Mulec and Kosi, 2008; Mazina and Maximov, 2011), especially in cave entrances (Mulec and Kosi, 2008). Most of the documented cyanobac-

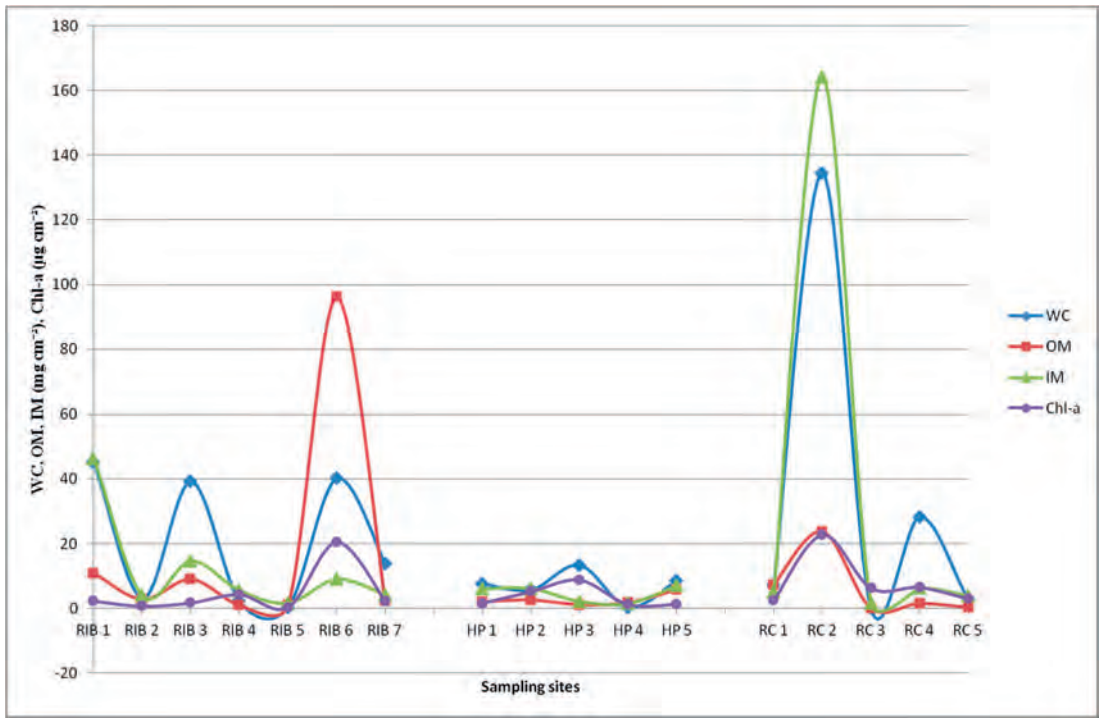

Figure 6. Chlorophyll-a content (Chl-a) expressed as µg cm^{-2} water content (WC) and content of organic/inorganic matter (OM/IM) expressed as mg cm^{-2} determined in biofilm samples from Ribnička (RIB1–RIB7), Hadži Prodanova (HP1–HP5), and Rćanska (RC1–RC5) caves.

Table 4. Water content (WC) and content of organic/inorganic matter (OM/IM), represented as percentages, determined in biofilm samples from Ribnička (RIB1–RIB7), Hadži Prodanova (HP1–HP5) and Rćanska (RC1–RC5) caves.

Biofilm Content	RIB1	RIB2	RIB3	RIB4	RIB5	RIB6	RIB7	HP1	HP2	HP3	HP4	HP5	RC1	RC2	RC3	RC4	RC5
WC	44.2	32.3	62.4	25.9	11.1	27.6	68.3	49.0	40.0	80.8	9.1	40.3	36.1	41.7	2.0	78.8	40.9
OM	10.6	27.7	14.3	10.7	33.3	66.2	11.3	12.9	17.6	6.7	50.0	27.0	37.5	7.4	2.0	4.1	4.1
IM	45.2	40.0	23.3	63.3	55.6	6.2	20.5	38.2	42.4	12.5	40.9	32.7	26.4	50.9	96.0	17.2	55.0

teria from the caves we investigated were typical aerophytic taxa. Coccoid forms of cyanobacteria were the most common, followed by Oscillatoriales and then Nostocales (Lamprinou et al., 2009, 2012, 2014; Martinez and Asencio, 2010; Pantazidou and Roussomoustakaki, 2005). Most coccoid cyanobacteria produce thick mucilaginous sheaths by which they attach to the substrates to help further colonization by other microorganisms. However, Oscillatoriales, which are usually less present, can form hormogonia that help them colonize new sites in the caves (Pantazidou and Roussomoustakaki, 2005). The most common genus found during this survey, *Gloeocapsa*, has been reported in various habitats with many different ecological characteristics, indicating its tolerance to a wide range of environmental conditions (Cennamo et al., 2012). Chlorophyta and Bacillariophyta are usually found together with cyanobacteria (Czerwik-Marcinkowska, 2013; Lamprinou et al., 2012; Cennamo et al., 2012; Selvi and Altuner, 2007; Mazina and Maximov, 2011; Klemenčić and Vrhovšek, 2005). Among green algae, unicellular forms tend to dominate (Roldán and Hernández-Mariné, 2009). These groups are represented by both aerophytic and freshwater taxa. In addition, aquatic taxa of Bacillariophyta can be present, but they usually show some morphological modifications (Falasco et al., 2014).

Even though cyanobacteria prevail in general, they are not always predominant; in our case, Cyanobacteria, Chlorophyta and Bacillariophyta were not equally distributed.

The temperature and relative humidity did not show large differences among the sampling sites in one cave due to the sampling sites' proximity to each other, but light intensity showed differences among all three examined caves; even small differences can have an immense impact on the ecosystem. The light intensity depended on factors like the distance from the entrance, exposure of the sampling site, rock depressions, and the presence of bigger cavities. Light intensity and other factors are also affected by the size and orientation of the cave entrance, as well as by the presence or absence of vegetation in front of the entrance. The highest temperature was usually measured at sampling sites that were closest to the cave entrance or at the entrance. The highest measured values of temperature and light intensity were recorded in Hadži Prodanova, which was probably due to the specific shape of the narrow and tall entrance facing south, allowing more light to reach cave walls. The highest humidity values were mostly measured at sampling sites that were farthest from the cave entrances, at places that were well shaded, and, as was the case with Rćanska, at sampling sites where running and dripping water was present. Furthermore, sampling sites in Rćanska were farther from the entrance and more isolated from external conditions compared to the other two investigated localities.

The constrained analysis of measured ecological parameters showed that only relative humidity was statistically significant. The highest humidity values were documented in Rćanska, where most of Chlorophyta and Bacillariophyta were recorded. On the contrary, the lowest humidity was documented in Ribnička and Hadži Prodanova, where Cyanobacteria were dominant. This suggests that humidity is likely an important factor in the development of specific communities in a given location. The presence of periodically available water in forms such as rain, dew, or condensation is important for the microbial colonization of rock surfaces (Whitton, 2012). However, cyanobacteria are known to produce extracellular polymeric substances (polysaccharides, proteins, lipids, and nucleic acids) that, aside from having many beneficial roles such as chelating toxic substances, serving as a nutrient reservoir, regulating calcification processes, and protecting from UV radiation, can also retain water, which is of great importance (Whitton, 2012; Falasco et al., 2014). For that reason, many cyanobacteria are very desiccation-tolerant and are able to inhabit places that are more arid compared to many other algal groups (Poulíčková and Hašler, 2007).

Chlorophyta and Bacillariophyta were recorded mainly in places with higher humidity. They dominated the entrance walls of Rćanska, especially at sampling sites RC2, 3, and 4. As mentioned, sampling site 2 was located on a horizontal plane, where mud and water accumulated. Sites 3 and 4 were characterized by the presence of dripping water, where algae from the genus *Klebsormidium* were mostly present. *Desmococcus olivaceus*, one of the most common aerophytic algae (Rindi, 2007), was one of the most frequently found algal taxa in this cave. On the other hand, Bacillariophyta were unequally distributed in all three caves. In Ribnička, they were documented only on the cave floor, inhabiting accumulated soil and mud (sampling site RIB 6). In Hadži Prodanova, most of the diatoms were found at the sampling site with highest illumination (HP1) while, in Rćanska they were present in association with Chlorophyta at the sampling site where mosses were present (RC5). The appearance of diatoms and changes in their composition were related to humidity fluctuations. In general, surfaces that are illuminated, wet, and

characterized by the presence of mosses are richer in diatoms. *Luticola nivalis* and *Hantzschia amphioxys* are typical aerophilous diatoms that can be found in the majority of caves, and they can be considered cosmopolitan taxa. *Hantzschia amphioxys*, common as an epiphytic diatom, usually occurs on mosses (Falasco et al., 2014).

Aerophytic cyanobacteria and algae are significantly influenced by temperature, light, and moisture conditions (Poulíčková and Hašler, 2007), but many other factors such as the input of nutrients, type and physicochemical substrate properties (pH, rock substance, porosity), cave morphology (size, location, dimension, orientation), and water availability affect the composition of the microbial communities and can explain the variation in species composition (Czerwik-Marcinkowska, 2013; Lamprinou et al., 2012; Pantazidou and Roussomoustakaki, 2005). The importance of the substrate can be seen from the fact that the calcareous, alkaline nature of the substrate favors the proliferation of cyanobacteria where the light is adequate (Pantazidou and Roussomoustakaki, 2005).

At both sampling sites with the highest content of chlorophyll-a, a thick green biofilm containing densely packed cells of cyanobacteria and algae was present. Biofilm at RIB6 was mostly made of densely entangled *Leptolyngbya* sp. According to Knott et al. (2004), horizontal surfaces collect more algae than do vertical surfaces. Certain parts of biofilms from cave walls can be washed with water that periodically flows over the rocks, or it can just "fall off" from time to time. In addition, these sampling sites contained the highest amount of organic matter. Sampling sites RIB7 and HP3, which had the highest water content expressed as a percentage, also had the highest number of cyanobacterial taxa, for which extracellular polymeric substances are responsible for retaining water. The sampling site RC4 also had a high water content percent because of the presence of seeping water. The correlation between chlorophyll-a content and light intensity was not observed ($r = –0.061$).

Fungal spores and hyphal fragments are introduced into caves through the air and water flow (Hsu and Agoramoorthy, 2001). Likewise, trogloxenes, animals that live within caves but periodically come out to feed, are known carriers of plant and animal remains, organic debris, and fungal propagules. The majority of fungi isolated and identified in this survey are frequently cited as plant and leaf-litter inhabitants (members of genera *Alternaria, Aspergillus, Botrytis, Cladosporium, Epicoccum*, and *Periconia*), while fungi, represented by species of genera *Humicola, Mucor, Paecilomyces, Penicillium, Rhizopus*, and *Rhizoctonia*, are typical soil colonizers (Dix and Webster, 1995). Hence the majority of identified fungi can be considered transients in cave habitats (Vanderwolf et al., 2013). On the other hand, yeast-like micro-colonial fungi in the form of torulose, branched hyphae and meristematic cells, documented via microscopic analyses of cultured fungi in all studied caves, are nowadays recognized as typical rock-inhabiting fungi (Ruibal et al., 2009). So this phylogenetically diverse group of melanized ascomycetes can be thought of as an autochthonous or residential fungal community in caves.

The establishment of fungal communities in cave habitats is mostly dependent on the availability of nutrients. The highest number of culturable fungi were isolated from the sampling sites where very developed biofilms were observed and high biomass was documented, such as RIB1. On the other hand, our recorded micro-environmental conditions of temperature, light intensity, and relative humidity were shown to not influence the distribution of fungi at sampling sites. However, Sterling and Lewis (1998) reported that these micro-environmental conditions were critical for the secondary release of spore and fungal growth within the caves and heavily influenced differences in fungal communities inside and outside of caves.

During the microscopic analyses of fungal isolates, the presence of atypical structures, such as the aberrant conidiogenus apparatus in *Aspergillus* sp. sect. *Nidulantes* and microcycle conidiation in one *Penicillium* culture, was observed. Microcycle conidiation, the phenomena of the direct production of conidia from asexual spores without hyphal growth, bypassing the somatic phase in the normal fungal life cycle, has been described in a broad range of fungi, including the genera *Acremonium*, *Aspergillus*, *Cercospora*, *Neurospora*, *Paecilomyces*, *Penicillium* and *Trichoderma* (Hanlin, 1994). Presumably, morphological variances typical of microcycle conidiation and aberrant conidiophore formation are a key mechanism for survival and proliferation of mold spores of the aforementioned genera in adverse environmental conditions (Lapaire and Dunkle, 2003). Furthermore, microcycle conidiation encompasses a normal phase in the life cycle of several fungal groups, among which are rust and smut fungi, as well as other plant (e.g., Taphrinales and Calvicipitales) and insect pathogens (Entomophthorales).

Conclusions

Cyanobacteria, algae (Chlorophyta and Bacillariophyta), and fungi were examined from biofilm samples taken from the entrances of Ribnička, Hadži Prodanova, and Rćanska caves. Cyanobacteria, with chroococcalean taxa prevailing and *Gloeocapsa* species as the most diverse, had the highest number of documented taxa. The majority of identified fungi were Ascomycetes or Zygomycetes, with *Rhizoctonia* s. l. as the only representative of Basidiomycetes. Physical parameters temperature and relative humidity did not show such big differences among sampling sites as did light intensity, which was dependent on the distance from the entrance and rock position. According to redundancy analysis and interactive forward selection that were performed on all measured environmental parameters, only relative humidity was a physical parameter that was statistically significant, meaning that it is likely an important factor influencing the development of microbial communities at different localities. Most of

Bacillariophyta and Chlorophyta were found at places with higher relative humidity, while many cyanobacteria were found in places where lower air humidity was measured. Measured physical parameters did not have a significant influence on the distribution of fungi. The second redundancy analysis that was performed confirmed that different taxonomic groups were dominant at different caves, cyanobacteria and fungi in Ribnička and Hadži Prodanova and Chlorophyta and Bacillariophyta in Rćanska cave. Chlorophyll-a content did not show correlation with light intensity. It was highest on a horizontal surfaces where the highest content of organic and inorganic matter were recorded. Higher water content in biofilm was found in samples from which many cyanobacterial taxa were identified.

It is known that many microorganisms from biofilms, through various known mechanisms of biodeterioration, can cause substantial damage to the stone surfaces. The exploration of their diversity, especially of phototrophic components, represents a contribution to the flora of Serbia, and is also the basis for further research that will include more experimental studies in terms of the conservation of these protected sites.

ACKNOWLEDGEMENTS

This research was supported by the Ministry of Science and Technological Development, Republic of Serbia, Projects No. 176018 and No 176020 and Ministry of Agriculture and Environmental Protection of Republic of Serbia.

REFERENCES

Bastian, F., and Alabouvette, C., 2009, Lights and shadows on the conservation of a rock art cave: the case of Lascaux Cave: International Journal of Speleology, v. 38, no. 1, p. 55–60. https://doi.org/10.5038/1827-806X.38.1.6.

Bensch, K., Braun, U., Groenewald, J.Z., and Crous, P.W., 2012, The genus *Cladosporium*: Studies in Mycology, v. 72, 401 p. https://doi.org/10.1016/S0166-0616(14)60069-5.

Borderie, F., Laurence, A.-S., Naoufal, R., Faisl, B., Geneviève, O., Dominique, R., and Badr, A.-S., 2011, UV-C irradiation as a tool to eradicate algae in caves: International Biodeterioration and Biodegradation, v. 65, p. 579–584. https://doi.org/10.1016/j.ibiod.2011.02.005.

Borderie, F., Tête, N., Cailhol, D., Alaoui Sehmer, L., Bousta, F., Rieffel, D., Aleya, L., and Alaoui Sossé, B., 2014, Factors driving epilithic algal colonization in show caves and new insight into combating biofilm development with UV-C treatment: Science of the Total Environment, v. 484, p. 43–52. https://doi.org/10.1016/j.scitotenv.2014.03.043.

Busquets, A., Fornós, J.J., Zafra, F., Lalucat, J. and Merino, A., 2014, Microbial communities in a coastal cave: Cova des Pas de Vallgornera (Mallorca, Western Mediterranean): International Journal of Speleology, v. 43, no. 2, p. 205–216. https://doi.org/10.5038/1827-806X.43.2.8.

Cennamo, P., Marzano, C., Ciniglia, C., Pinto, G., Cappelletti, P., Caputo, P., and Pollio, A., 2012, A survey of the algal flora of anthropogenic caves of Campi Flegrei (Naples, Italy) archeological district: Journal of Cave and Karst Studies, v. 74, no. 3, p. 243–250. https://doi.org/10.4311/2011JCKS0194.

Czerwik-Marcinkowska, J., 2013, Observations on aerophytic cyanobacteria and algae from ten caves in the Ojców national park: Acta Agrobotanica, v. 66, no. 1, p. 39–52. https://doi.org/10.5586/aa.2013.005.

Czerwik-Marcinkowska, J., and Mrozińska, T., 2009, Epilithic algae from caves of the Krakowsko-Częstochowska upland (Southern Poland): Acta Societatis Botanicorum Poloniae, v. 78, no. 4, p. 301–309. https://doi.org/10.5586/asbp.2009.040.

Czerwik-Marcinkowska, J., and Mrozińska, T., 2011, Algae and cyanobacteria in caves of the Polish Jura: Polish Botanical Journal, v. 56, no. 2, p. 203–243.

Dimitrijević, M., 1974, The Dinarides: A model based on the new global tectonics, *in* Jankovic, S., ed., Metallogeny and Concepts of the Geotectonic Development of Yugoslavia: Belgrade, Faculty of Mining and Geology, Department of Economic Geology, p. 141–178.

Dix, N.J., and Webster, J., 1995, Fungal Ecology: London, Chapman and Hall, 549 p.

Đurović, P., ed., 1998, Speleološki atlas Srbije, posebno izdanje br. 52: Beograd, Geografski institut „Jovan Cvijić" SANU, Zavod za zaštitu prirode Srbije, Geografski fakultet u Beogradu, Biološki fakultet Univerziteta u Beogradu, 290 p. (Speleological Atlas of Serbia: Belgrade, Jovan Cvijic Geographical Institute, Serbian Academy of Sciences and Arts special issue 52, 290 p.)

Ellis, M.B., 1971, Dematiaceous Hyphomycetes: Kew, Surrey, England, Commonwealth Mycological Institute, 608 p.

Ellis, M.B., and Ellis, J.P., 1997, Microfungi on Land Plants, an Identification Handbook second edition: Slough, England, The Richmond Publishing Co. Ltd, 868 p.

Falasco, E., Ector, L., Isaia, M., Wetzel, C.E., Hoffmann, L. and Bona, F., 2014, Diatom flora in subterranean ecosystems: a review: International Journal of Speleology, v. 43, no. 3, p. 231–251. https://doi.org/10.5038/1827-806X.43.3.1.

Filipović, B., Krunić, O. and Lazić, M., 2005, Regionalna hidrogeologija Srbije: Beograd, Rudarsko geološki fakultet Univerziteta u Beogradu, 401 p.

García, V.G., Onco, M P., and Susan, V.R., 2006, Review. Biology and systematics of the form genus *Rhizoctonia*: Spanish Journal of Agricultural Research, v. 4, no. 1, p. 55–79. https://doi.org/10.5424/sjar/2006041-178.

Gaylarde, P.M., and Gaylarde, C.C., 1998, A rapid method for the detection of algae and cyanobacteria on the external surfaces of buildings, *in* Gaylarde, C.C., Barbosa, T.C.P., and Gabilan, N.H., eds., Proceedings of the Third Latin American Biodegradation and Biodeterioration Symposium: The British Phycological Society, paper 37.

Giordano, M., Mobili, F., Pezzoni, V., Hein, M.K., and Davis, J.S., 2000, Photosynthesis in the caves of Frasassi (Italy): Phycologia, v. 39, p. 384–389. https://doi.org/10.2216/i0031-8884-39-5-384.1.

Hanlin, R.T., 1994, Microcycle conidiation–a review: Mycoscience, v. 35, p. 113–123. https://doi.org/10.1007/BF02268539.

Hsu, M.J., and Agoramoorthy, G., 2001, Occurrence and diversity of thermophilous soil microfungi in forest and cave ecosystems of Taiwan: Fungal Diversity, v. 7, p. 27–33.

Hofmann, G., Werum, M., and Lange-Bertalot, H., 2013, Diatomeen im Süßwasser – Benthos von Mitteleuropa. Bestimmungsflora Kieselalgen für die ökologische Praxis: Königstein, Koeltz Scientific Books. 908.

Isola, D., Zucconi, L., Onofri, S., Caneva, G., de Hoog, G. S., and Selbmann, L., 2016, Extremotolerant rock inhabiting black fungi from Italian monumental site: Fungal Diversity, v. 76, no. 1, p. 75–96. https://doi.org/10.1007/s13225-015-0342-9.

John, D.M., Whitton, B.A., and Brook, A.J., eds., 2003, The Freshwater Algal Flora of the British Isles: an Identification Guide to Freshwater and Terrestrial Algae: UK, Cambridge University Press. 702 p.

Klemenčič, A.K., and Vrhovšek, D., 2005, Algal flora of Krška Jama Cave, Slovenia: Acta Musei Nationalis Pragae, Series B, Historia Naturalis, v. 61, no. 1–2, p. 77–80.

Knott, N.A., Underwood, A.J., Chapman, M.G. and Glasby, T.M., 2004, Epibiota on vertical and on horizontal surfaces on natural reefs and on artificial structures: Journal of the Marine Biological Association of the United Kingdom, v. 84, p. 1117–1130. https://doi.org/10.1017/S0025315404010550h.

Komárek, J., 2013, Süßwasserflora von Mitteleuropa, Bd 19/3: Cyanoprokaryota 3: Heterocystous genera: Heidelberg, Springer Spektrum, 1130 p.

Komárek, J., and Anagnostidis, K., 1998, Cyanoprokaryota 1. Teil/1st Part: Chroococcales, *in* Ettl, H., Gärtner, G., Heynig, H., and Mollenhauer, D., eds., Süßwasserflora von Mitteleuropa 19/1: Jena-Stuttgart-Lübeck-Ulm, Gustav Fischer, 548 p.

Komárek, J., and Anagnostidis, K., 2005, Cyanoprokaryota 2. Teil: Oscillatoriales, *in* Ettl, H., Gärtner, G., Heynig, H., and Mollenhauer, D., eds., Süßwasser flora von Mitteleuropa, 19/2: Berlin, Spektrum Akademischer Verlag, 759 p.

Komárek, J., and Fott, B., 1983, Chlorophyceae (Grünalgen). Ordnung: Chlorococcales. Das Phytoplankton dês Süßwassers, Systematik und Biologie, *in* Elster, H.J., and Ohle, W., eds., Die Binnengewässer XVI, 7 (1): Stuttgart, Germany, Schweizerbart'sche Verlagsbuchhandlung, 1044 p.

Krieger, W., and Gerloff, J., 1962, Die Gattung Cosmarium: Weinheim, Verlag von J. Cramer. 410 p.

Lamprinou, V., Danielidis, D.B., Economou-Amilli, A., and Pantazidou, A., 2012, Distribution survey of Cyanobacteria in three Greek caves of Peloponnese: International Journal of Speleology, v. 41, no. 2, p. 267–272. https://doi.org/10.5038/1827-806X.41.2.12.

Lamprinou, V., Danielidis, D.B., Pantazidou, A., Oikonomou, A., and Economou-Amilli, A., 2014, The show cave of Diros vs. wild caves of Peloponnese, Greece – distribution patterns of Cyanobacteria: International Journal of Speleology, v. 43, no. 3, p. 335–342. https://doi.org/10.5038/1827-806X.43.3.10.

Lamprinou, V., Pantazidou, A., Papadogiannaki, G., Radea, C., and Economou-Amilli, A., 2009, Cyanobacteria and associated invertebrates in Leontari Cave, Attica (Greece): Fottea, v. 9, no. 1, p. 155–164. https://doi.org/10.5507/fot.2009.014.

Lapaire, C.L., and Dunkle, L.D., 2003, Microcycle conidiation in *Cercospora zeaemaydis*: Phytopathology, v. 93, p. 193–199. https://doi.org/10.1094/PHYTO.2003.93.2.193.

Martínez, A., and Asencio, A.D., 2010, Distribution of cyanobacteria at the Gelada Cave (Spain) by physical parameters: Journal of Cave and Karst Studies, v. 72, no. 1, p. 11–20. https://doi.org/10.4311/jcks2009lsc0082.

Mazina, S.E., and Maximov, V.N., 2011, Photosynthetic organism communities of the Akhshtyrskaya Excursion Cave: Moscow University Biological Sciences Bulletin, v. 66, no. 1, p. 37–41. https://doi.org/10.3103/S009639251101007X.

Mulec, J., and Kosi, G., 2008, Algae in the aerophytic habitat of Račiške ponikve cave (Slovenia): Natura Sloveniae, v. 10, no. 1, p. 39–49.

Mulec, J., Kosi, G., and Vrhovšek, D., 2008, Characterization of cave aerophytic algal communities and effects of irradiance levels on production of pigments: Journal of Cave and Karst Studies, v. 70, no. 1, p. 3–12.

Mulec, J., Kryštůfek, V., and Chroňáková, A., 2012, Comparative microbial sampling from eutrophic caves in Slovenia and Slovakia using RIDA®COUNT test kits: International Journal of Speleology, v. 41, no. 1, p. 1–8. https://doi.org/10.5038/1827-806X.41.1.1.

Ogórek, R., Lejman, A., and Matkowski, K., 2013, Fungi isolated from Niedźwiedzia Cave in Kletno (Lower Silesia, Poland): International Journal of Speleology, v. 42, no. 2, p. 161–166. https://doi.org/10.5038/1827-806X.42.2.9.

Ogórek, R., Dyląg, M., Kozak, B., Višňovská, Z., Tančinová, D., and Lejman, A., 2016, Fungi isolated and quantified from bat guano and air in Harmanecká and Driny Caves (Slovakia): Journal of Cave and Karst Studies, v. 78, no. 1, p. 41–49. https://doi.org/10.4311/2015MB0108.

Pantazidou, A., and Roussomoustakaki, M., 2005, Biodiversity and ecology of cyanobacteria in a variety of hypogean ecosystems (Greece): Proceedings of the 14th International Congress of Speleology, vol. 2: Athens, Hellenic Speleological Society, paper P-29, p. 624–627.

Popović, S., Subakov Simić, G., Stupar, M., Unković, N., Predojević, D., Jovanović, J., and Ljaljević Grbić, M., 2015, Cyanobacteria, algae and microfungi present in biofilm from Božana Cave (Serbia): International Journal of Speleology, v. 44, no. 2, p. 141–149. https://doi.org/10.5038/1827-806X.44.2.4.

Poulíčková, A., and Hašler, P., 2007, Aerophytic diatoms from caves in central Moravia (Czech Republic): Preslia, v. 79, p. 185–204.

Pusz, W., Ogórek, R., Uklańska-Pusz, C.M., and Zagożdżon, P., 2014, Speleomycological research in underground Osówka complex in Sowie Mountains (Lower Silesia, Poland): International Journal of Speleology, v. 43, no. 1, p. 27–34. https://doi.org/10.5038/1827-806X.43.1.3.

Raper, K.B., and Fennell, D.I., 1965, The Genus *Aspergillus*: Baltimore, The Williams and Wilkins Company, 686 p.

Rindi, F., 2007, Diversity, distribution and ecology of green algae and cyanobacteria in urban habitats, *in* Seckbach, J., ed., Algae and Cyanobacteria in Extreme Environments: Dordrecht, Springer, p. 621–638. https://doi.org/10.1007/978-1-4020-6112-7_34.

Roldán, M., and Hernández-Mariné, M., 2009, Exploring the secrets of the three-dimensional architecture of phototrophic biofilms in caves: International Journal of Speleology, v. 38, p. 41–53. https://doi.org/10.5038/1827-806X.38.1.5.

Ruibal, C., Gueidan, C., Selbmann, L., Gorbushina, A.A., Crous, P.W., Groenewald, J.Z., Muggia, L., Grube, M., Isola, D., Schoch, C.L., Staley, J.T., Lutzoni, F., and De Hoog, G.S., 2009, Phylogeny of rock-inhabiting fungi related to *Dothideomycetes*: Studies in Mycology, v. 64, p. 123–133. https://doi.org/10.3114/sim.2009.64.06.

Samson, R.A., Houbraken, J., Thrane, U., Frisvad, J.C., and Andersen, B., 2010, Food and Indoor Fungi: The Netherlands, CBS-KNAW Fungal Biodiversity Centre Utrecht, 390 p.

Samson, R.A., and Varga, J., 2007, *Aspergillus* Systematics in the Genomic Era: Utrecht, The Netherlands, Fungal Biodiversity Centre, Studies in Mycology 59, 206 p.

Selvi, B., and Altuner, Z., 2007, Algae of Ballıca Cave (Tokat-Turkey): International Journal of Natural and Engineering Sciences, v. 1, no. 3, p. 99–103.

Starmach, K., 1972, Chlorophyta III. Zielenice nitkowate: Ulotrichales, Ulvales, Prasiolales, Sphaeropleales, Cladophorales, Trentepohliales, Sipholales, Dichotomosiphonales: Warszawa and Krakow, Panstwowe Wyadwnictwo Naukowe, series Flora slodkowodna Polski 10, 750 p.

Sterling, D.A., and Lewis, R.D., 1998, Pollen and fungal spores indoor and outdoor of mobile homes: Annals of Allergy, Asthma and Immunology, v. 80, p. 279–285. https://doi.org/10.1016/S1081-1206(10)62971-7.

Ter Braak, C.J.F., and Šmilauer, P., 2012, Canoco Reference Manual and User's Guide: Software for Ordination, version 5.0: Ithaca, USA, Microcomputer Power, 496 p.

Urzi, C., and de Leo, F., 2001, Sampling with adhesive tape strips: an easy and rapid method to monitor microbial colonization on monument surfaces: Journal of Microbiological Methods, v. 44, p. 1–11. https://doi.org/10.1016/S0167-7012(00)00227-X.

Urzì, C., de Leo, F., Bruno, L., and Albertano, P., 2010, Microbial diversity in paleolithic Caves: a study Case on the Phototrophic Biofilms of the Cave of Bats (Zuheros, Spain): Microbial Ecology, v. 60, p. 116–129. https://doi.org/10.1007/s00248-010-9710-x.

Vanderwolf, K.J., Malloch, D., McAlpine, D.F., and Forbes, G.J., 2013, A world review of fungi, yeasts, and slime molds in caves: International Journal of Speleology, v. 42, no. 1, p. 77–96. https://doi.org/10.5038/1827-806X.42.1.9.

Watanabe, T., 2010, Pictorial Atlas of Soil and Seed Fungi: Morphologies of Cultured Fungi and Key to Species, third edition: Boca Raton, Florida, US, CRC press, 426 p.

Whitton, B.A., ed., 2012, Ecology of Cyanobacteria II, Their Diversity in Space and Time: London, UK, Springer, 760 p.

Woudenberg, J.H.C., Groenewald, J.Z., Binder, M., and Crous, P.W., 2013, *Alternaria* redefined: Studies in Mycology, v. 75, p. 171–212. https://doi.org/10.3114/sim0015.

K.D. Webster, L. Rosales Lagarde, P.E. Sauer, A. Schimmelmann, J.T. Lennon, and P.J. Boston – Isotopic evidence for the migration of thermogenic methane into a sulfidic cave, Cueva de Villa Luz, Tabasco, Mexico. *Journal of Cave and Karst Studies*, v. 79, no. 1, p. 24–34. DOI: 10.4311/2016ES0125

ISOTOPIC EVIDENCE FOR THE MIGRATION OF THERMOGENIC METHANE INTO A SULFIDIC CAVE, CUEVA DE VILLA LUZ, TABASCO, MEXICO

Kevin D. Webster[1]*, Laura Rosales Lagarde[2], Peter E. Sauer[5], Arndt Schimmelmann[5], Jay T. Lennon[3], Penelope J. Boston[4]

Abstract: Methane (CH_4) is an economic resource and a greenhouse gas, but its migration through rocks is not immediately associated with speleogenesis. Sulfuric-acid speleogenesis is a cave-forming mechanism that has produced a variety of economically important oil fields and aquifers, and is theorized to be related to the oxidation of CH_4 and hydrocarbons. Despite hypotheses that the oxidation of CH_4 may provide a basis for the generation of sulfides during sulfuric-acid speleogenesis, evidence from active systems has not yet been obtained. In this study, we address how CH_4 influences the development of sulfidic cave systems by sampling the CH_4, H_2S, and CO_2 concentrations, as well as $\delta^{13}C_{CH_4}$, $\delta^{2}H_{CH_4}$, and $\delta^{13}C_{CO_2}$ values, in a cave currently forming by sulfuric-acid speleogenesis, Cueva de Villa Luz. CH_4, H_2S, and CO_2 concentrations were highest directly above springs in the cave, showing that all three gases enter by means of the spring water. The $\delta^{13}C_{CH_4}$ and $\delta^{2}H_{CH_4}$ in the air of CVL ranged from –47.92 ± 0.15 to –35.47 ± 0.12 ‰ (VPDB) and –117 to –83 ‰ (VSMOW), respectively. Keeling plots suggest that CH_4 with $\delta^{13}C_{CH_4} = -24 \pm 3$ ‰ and $\delta^{2}H_{CH_4} = -40 \pm 50$ ‰ was outgassing from spring water. This stable-isotope signature does not fall within traditional published $\delta^{13}C_{CH_4}$ versus $\delta^{2}H_{CH_4}$ fields. Our data suggest that the CH_4 entering Cueva de Villa Luz is the remnant of a larger thermogenic CH_4 flux that is incompletely oxidized in the subsurface as it travels to Cueva de Villa Luz. Our data support links between the processes forming Cueva de Villa Luz and the proposed mechanisms for other caves associated with sulfuric acid.

Introduction

The migration of subsurface methane (CH_4) through rock units toward the earth's surface creates natural gas deposits, contributes to the atmospheric CH_4 burden, and supports microbial communities, but is rarely thought to alter the encountered rock units. However, CH_4 and other hydrocarbons may enhance the porosity and permeability of limestones by fostering sulfuric-acid speleogenesis (Davis, 1980; Egemeier, 1981; Kirkland and Evans, 1976; Hill, 1990, 1995). As CH_4-rich fluids migrate within the subsurface and interact with evaporites, such as anhydrite or gypsum, they obtain sulfate (SO_4^{2-}) that may react with CH_4 to form hydrogen sulfide (H_2S):

$$Ca^{2+} + 2SO_4^{2-} + 2CH_4 + 2H^{+} \rightarrow 2H_2S + CaCO_3 + 3H_2O + CO_2 \quad (1)$$

The introduction of sulfide to oxygen in near-surface environments results in the formation of sulfuric acid (H_2SO_4), a strong acid capable of rapidly dissolving limestone.

With some of the world's largest hydrocarbon deposits and aquifers hosted in sulfuric-acid dissolution-influenced limestones (Hill, 1995), a better understanding of how these caves form is important for finding new oil fields and drinking water. The suggestion that sulfuric-acid speleogenesis is associated with hydrocarbons originated from studies of Lower Kane Cave in Wyoming (Davis, 1980; Egemeier, 1981). Later, the morphologies and mineral assemblages of caves in the Guadalupe Mountains spurred hypotheses that these caves formed through sulfuric-acid speleogenesis (Hill, 1990, 1995; Peryt et al., 2012). The negative $\delta^{34}S$ values of hydrogen sulfide from springs and sulfide minerals in the caves suggested that microorganisms were responsible for the generation of the sulfides. Additionally, $\delta^{13}C_{CO_2}$ values from carbonates in these and other settings suggested that CH_4 and hydrocarbons were oxidized in tandem with SO_4^{2-} reduction. Although the migration of CH_4 is hypothesized to be important for the formation of sulfidic caves, to our knowledge no studies of these caves have measured CH_4 concentrations in multiple locations from their entrances to their interiors, nor have measurements of both $\delta^{13}C_{CH_4}$ and $\delta^{2}H_{CH_4}$ values been made in a cave currently undergoing sulfuric-acid speleogenesis.

* Corresponding author: kevdwebs@indiana.edu
[1] Department of Ecology and Evolution, University of Arizona, 1041 E Lowell St., Tuscan, Az. 85719, USA
[2] Department of Earth and Atmospheric Sciences, Indiana University, 1001 E 10th St., Bloomington, IN 47405, USA
[3] Department of Physical and Life Sciences, Nevada State College, School of Liberal Arts and Sciences, 1021 Paradise Hills Drive, Ste. 246, Henderson, NV 89002, USA
[4] Department of Biology, Indiana University, 1001 E 3rd St., Bloomington, IN 47405, USA
[5] NASA Astrobiology Institute, NASA Ames Research Center, Moffett Field, CA 94035

Stable-isotope ratios of carbon and hydrogen in CH_4 provide a tool for understanding the origins and reactions of CH_4 in the environment. For example, atmospheric CH_4 has $\delta^{13}C_{CH_4}$ and $\delta^{2}H_{CH_4}$ values that are roughly –47.5 ‰ (VPDB) and –100 ‰ (VSMOW), respectively (Thom et al., 1993). Thermogenic CH_4, which forms from the breakdown of organic matter by heat, has $\delta^{13}C_{CH_4}$ and $\delta^{2}H_{CH_4}$ values that generally range from –56 to –20 ‰ and from –300 to –70 ‰, respectively (Schoell, 1988; Whiticar, 1999). The original $\delta^{13}C_{CH_4}$ and $\delta^{2}H_{CH_4}$ values are altered during both biotic and abiotic CH_4 oxidation; the former causes an increase of 8.5 ‰ in $\delta^{2}H_{CH_4}$ for each ‰ increase in $\delta^{13}C_{CH_4}$ (Feisthauer et al., 2011). Thermochemical sulfate reduction, a form of abiotic methane oxidation, shows $\delta^{13}C_{CH_4}$ and $\delta^{2}H_{CH_4}$ values of roughly –30 and –120 ‰ respectively (Liu et al., 2014). Furthermore, the mixing of CH_4 from different sources can create CH_4 with unusual isotopic ratios. For example, the Homorod mud volcano of Romania exhibits variations in $\delta^{2}H_{CH_4}$ values from –25 to +30 ‰ that result from mixing between microbially produced CH_4 and CH_4 with a $\delta^{2}H_{CH_4}$ of +124 ‰ generated from incomplete abiotic oxidation (Etiope et al., 2011).

CH_4 has been measured from only two caves undergoing sulfuric-acid speleogenesis. The caves showed different characteristics. In Movile Cave in Romania, the CH_4 in an isolated pocket of air between the cave's roof and a water body had a concentration of 10,000 ppmv and a $\delta^{13}C_{CH_4}$ value of –60 ‰, indicating the presence of microbially generated CH_4 (Sarbu et al., 1996; Hutchens et al., 2004). CH_4 concentrations in Frasassi Cave in Italy ranged from 1.9 to 2.2 ppmv at a single collection site (Jones et al., 2012), although isotopic compositions were not reported. The current CH_4 data set from sulfidic caves must be augmented in order to rigorously test current theories about hydrocarbon-driven sulfuric-acid speleogenesis.

We tested the hypothesis that hydrocarbons are fundamental in sulfuric-acid speleogenesis in the active Cueva de Villa Luz (CVL) system by measuring CH_4, H_2S, and CO_2 concentrations and $\delta^{13}C_{CH_4}$, $\delta^{2}H_{CH_4}$, and $\delta^{13}C_{CO_2}$ values. If CH_4 oxidation is responsible for the generation of H_2S in sulfidic caves, then abundances of CH_4, H_2S, and CO_2 should be correlated in cave air as the gases follow the same pathway into the cave unless there are additional destruction or production mechanisms along the way. Additionally, the $\delta^{13}C_{CH_4}$ and $\delta^{2}H_{CH_4}$ values should show signs of oxidation, and $\delta^{13}C_{CO_2}$ values should be relatable to oxidized CH_4. This study presents the first observations of CH_4 concentrations along gradients from cave entrance to interior and of the stable-isotope ratios of hydrogen in CH_4 in the air of an actively forming sulfidic cave.

Geological Setting

Regional Geological Setting

CVL is a shallow cave, has several natural openings, and is located in the Sierra de Chiapas 2 km south of Tapijulapa, Tabasco, Mexico. It is hosted within a carbonate shelf of the middle Cretaceous Sierra Madre Formation (Rosales Lagarde et al., 2006; Fig. 1). The sedimentary record of the region spans from the Jurassic to the Tertiary and includes hydrocarbon formation (Aguilar Rodríguez, 2007; Clara Valdéz et al., 2009). Regional hydrocarbons, such as oils located about 50 km north of CVL, are presumably derived from Cretaceous marine limestones (Guzman-Vega and Mello, 1999).

Several potential sources of hydrogen sulfide (H_2S) are present in the CVL region. Possible sources of H_2S for CVL include the volcano El Chichón located 50 km west of CVL; petroleum basins located 50 km north of CVL such as the Macuspana and the Comalcalco basins; petroleum deposits within the Sierra de Chiapas; and economic sulfide deposits 25 km west of CVL (Pantoja-Alor, 1989; Hose et al., 2000; Rosales Lagarde et al., 2006, 2014; Fig. 1). However, sulfur-isotope ratios of dissolved sulfide in the H_2S-rich brackish springs of CVL range from –24 to –6 ‰ Vienna Canyon Diablo Troilite (VCDT) and indicate that biological sulfate reduction of anhydrite-derived sulfate is the main mechanism producing the hydrogen sulfide in the groundwater column feeding the cave (Rosales Lagarde, 2013).

The regional tectonic history includes periods of extension and compression resulting in large scale faulting, fracturing, and folding (Meneses-Rocha, 2001; Alcàntara García et al., 2004; García Palomo et al., 2006). The main passage of CVL follows the strike of east-northeast bedding planes of Cretaceous limestone. This limestone is folded into a northwest plunging anticline and cut by a thrust fault (Rosales Lagarde, 2013; Fig. 1). Faulting and fracturing seem to facilitate the upward migration of deeper fluids. Additionally, hydrocarbon seeps in the region are common (Aguilar Rodríguez, 2007; PEMEX, personal communication).

Geomorphology and Geochemistry of Cueva de Villa Luz

The cave's main entrance and twenty-four skylights connect the air of CVL with the atmosphere (Fig. 2) (Hose and Pisarowicz, 1999). CVL is a weakly hydrothermal system and has a slightly elevated mean annual cave-air temperature of 28 °C compared to the regional mean annual atmospheric temperature of 27 °C. Sulfide-rich springs release H_2S into the cave air, where it ranges in concentration from 1 to 40 ppmv depending on location (Hose and Pisarowicz, 1999). CVL is known to experience strong H_2S and carbon monoxide outgassing events when the H_2S concentration may increase from < 12 ppmv to > 240 ppmv in less than 3 minutes (Kleina, and Hose, pers. comm.; Boston, unpub. results). The cause of these outgassing events is unknown.

CVL's twenty-six known internal springs broadly fall into two categories: (i) springs with < 4.3 mg L^{-1} dissolved O_2 and < 0.1 mg L^{-1} dissolved H_2S and (ii) springs with < 0.1 mg L^{-1} dissolved O_2 and 300 to 500 mg L^{-1} dissolved H_2S (Hose et al., 2000). Non-sulfidic springs have a higher temperature than

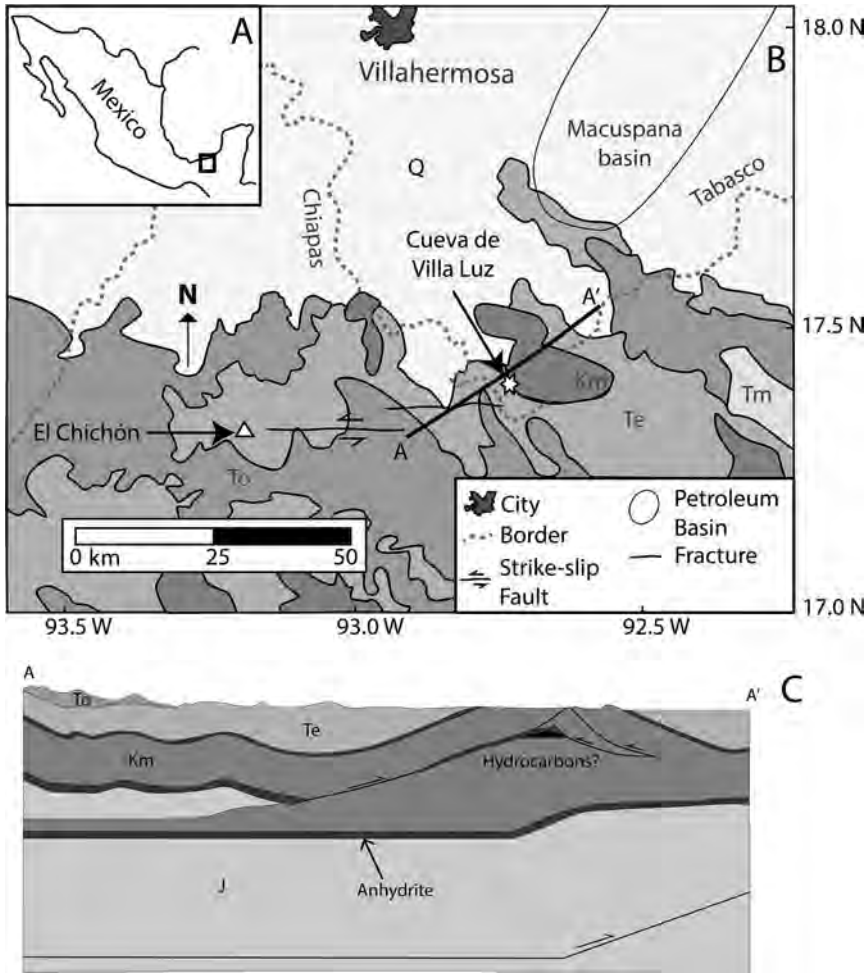

Figure 1. The regional setting of the study area showing A) the location of the study area in Mexico and B) geological features and units that may be influencing the CH_4 concentrations in Cueva de Villa Luz. Q: Quaternary sediments; Te: Eocene units; To: Oligocene units; Tm: Miocene units; Km: Cretaceous units; J: Jurassic units. C) A cross-section from A to A′ showing lithological units in the region. This map has been redrawn from Alcàntara García et al. (2004) and the U.S. Geological Survey World Energy Assessment Team (2000).

those with sulfide (Rosales Lagarde, 2013). All springs are brackish, and the water chemistry is influenced by dissolution of limestone, dolomite, halite, and gypsum (Rosales Lagarde et al., 2014; Hose et al., 2000, Spilde et al., 2004).

Methods

Air Sampling

The geochemistry of cave air is affected by atmospheric conditions, which may dominate near entrances or skylights, and internal cave processes, which may dominate the chemistry in cave interiors (Peyraube et al., 2016). We sampled air in CVL using *in-situ* and discrete techniques. We used *in-situ* sampling to measure H_2S concentrations and obtained discrete air samples in 1 L Tedlar bags for later analysis of CH_4 and CO_2. We selected sampling locations based on their proximity to springs and entrances and measured the distances from each sampling location to the nearest entrance or spring based on the map of Hose and Pisarowicz (1999). Samples were defined as "near a spring" if they were obtained < 2 m from a spring and samples were defined as "near an entrance" if they were < 10 m from an entrance.

We measured H_2S concentrations with a GasBadge Pro H_2S instrument (Industrial Scientific, Pasadena, Texas) and a Ventis MX4 device (Industrial Scientific, Pasadena, Texas) from nine locations in CVL (Fig. 2) (Table 1). We measured H_2S concentrations at several elevations above the stream to assess the extent to which exsolution of H_2S from spring waters altered the concentration of H_2S in cave air. When data were measured with both the GasBadge and the Ventis (Table 1), we took the average of the H_2S concentrations (average difference, Ventis − Gasbage = –2 ppmv). At locations 1 through 12 we obtained discrete air samples in the cave, and we also obtained a discrete air sample from the local atmosphere 20 m from the main entrance of CVL using

Table 1. H_2S concentrations in Cueva de Villa Luz. Dates are listed as mm/dd/yyyy.

Site	Name	Date Collected	Closest Entrance (m)	Closest Spring (m)	[H_2S] 20 cm (ppmv)	[H_2S] 20 cm e (2SD)[a]	[H_2S] 50 cm (ppmv)	[H_2S] 50 cm e (2SD)[a]	[H_2S] 100 cm (ppmv)	[H_2S] 100 cm e (2SD)[a]	[H_2S] 150 cm (ppmv)	[H_2S] 150 cm e (2SD)[a]
Site 4	Midway Springs	12/19/2013	9	0	7	4	3	5	5.1	0.9	4.85	0.15
Site 5	RBCSG[b]	12/16/2013	23	27	11.6	1.0	6.2[c]	1.0	4.3[d]	1.0e[e]	...	...
Site 7	Slot Spring 2	12/16/2013	23	0	23.05	0.05	13.8	1.2	7.6	1.8	6.9	0.9
Site 9	Behind Spring	12/16/2013	15	0	11.8	0.6	8.7	0.4	9.5	0.5	5.1	0.6
Site 13	OPP[e]	12/16/2013	14	3	5.9	0.6	8[c]	5[c]	8	2	6.6	1.5
Site 14	Sala Grande 1	12/16/2013	20	6	1.5	1.1	2.5	1.3	1.5	1.1	2.9	0.9
Site 15	Sala Grande 2	12/16/2013	20	13	3.6	0.7	4.2	0.4	3	0.8	2.9	1.0
Site 16	Sala Grande 3	12/16/2013	25	16	2.4	1.0	1.9	0.8	1.2	1.2	1.1	1.1
Site 17	BYR[f]	12/16/2013	24	25	...	...	2.7	1.0	0.9	0.8	0.9	0.8

[a] SD = Standard Deviation.
[b] Room Before the Crawl to Sala Grande.
[c] Sample was obtained at 40 cm above the spring.
[d] Sample was obtained at 60 cm above the spring.
[e] Outside of Perched Pool.

Figure 2. A simplified map of Cueva de Villa Luz in Mexico redrawn from Hose and Pisarowicz (1999). A cross-section of the cave's main passage is shown from A to B. Numerous skylights and springs are present in the cave. Arrows indicate air sample locations. Discrete air samples were obtained from sites 1 to 12.

standard air-sampling techniques (Fig. 2) (Webster et al., 2016). All discrete cave-air samples from locations near springs were obtained 30 cm above the springs.

Laboratory Analyses

We measured CH_4 and CO_2 concentrations from discrete samples with a Varian 450 gas chromatograph (GC) (see Webster et al., 2016). CH_4 and CO_2 calibration curves for concentration and uncertainty estimates were calculated following the methods of Webster et al. (2016).

We measured the $\delta^{13}C_{CH_4}$, $\delta^{2}H_{CH_4}$ and $\delta^{13}C_{CO_2}$ values to help determine the sources of CH_4 and CO_2 entering CVL. $\delta^{13}C_{CH_4}$, $\delta^{2}H_{CH_4}$ and $\delta^{13}C_{CO_2}$ values were measured on a Thermo Finnigan Delta Plus XP isotope-ratio mass-spectrometer (IRMS). $\delta^{13}C_{CH_4}$ and $\delta^{2}H_{CH_4}$ values were measured in continuous-flow mode using a gas chromatography-oxidation/pyrolysis-IRMS (GC-ox/pyr-IRMS) interface following previously published methods (Miller et al., 2002; Webster et al., 2016). $\delta^{13}C_{CO_2}$ was measured with a Thermo Finnigan GasBench II inlet connected to the IRMS.

Raw $^{13}C/^{12}C$ and $^{2}H/H$ isotope ratios measured by the mass spectrometer were converted to conventional δ-values using two-point calibrations. The in-house CH_4 reference materials were calibrated against international measurement standards NBS 19, LSVEC, VSMOW, and SLAP. Reference materials had $\delta^{13}C_{CH_4}$ values of –38.25 ± 0.06 and –58.64 ± 0.15 ‰ and $\delta^{2}H_{CH_4}$ values of –41 ± 3 and –160 ± 4 ‰, respectively. Analytical uncertainties of the $\delta^{13}C_{CH_4}$ and $\delta^{2}H_{CH_4}$ values of the CH_4 reference materials ranged from ± 0.07 to ± 0.15 ‰ (2 SD), and ± 8 to ± 12 ‰ (2 SD), respectively, depending on the day of measurement, and these were assigned to data from air samples that were measured on the same day.

Raw $^{13}C/^{12}C$ ratios of CO_2 were converted to $\delta^{13}C_{CO_2}$ values on the VPDB scale using a single standard with

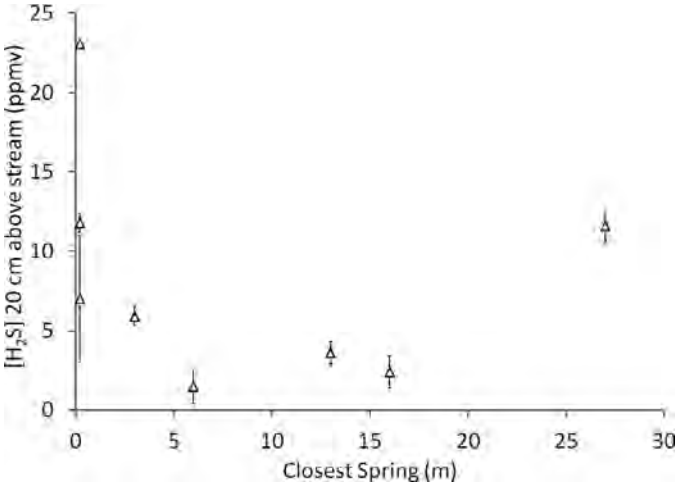

Figure 3. H_2S concentration in air 20 cm above the cave stream versus distance to the nearest spring in Cueva de Villa Luz. The elevated H_2S concentration at a distance of 28 m from a spring may be related to turbulent water entering from an adjacent room.

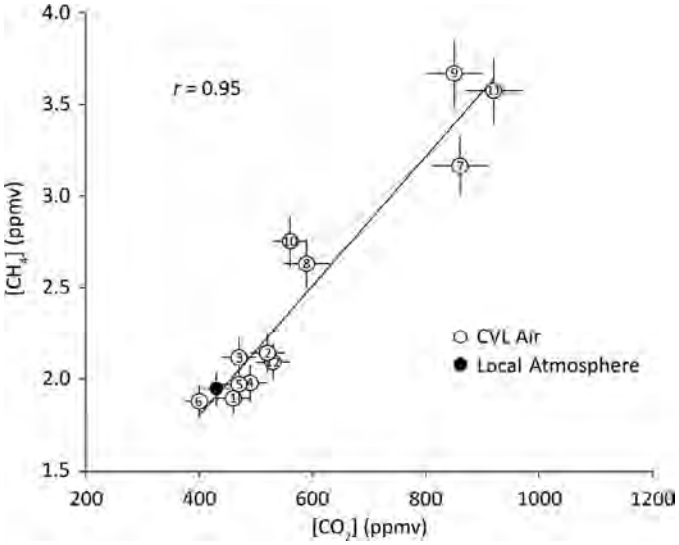

Figure 4. CH_4 versus CO_2 concentrations in Cueva de Villa Luz (CVL) showing a strong positive correlation ($r = 0.95$, $n = 12$, $p < 0.01$). Open circles represent CVL air samples, whereas the black circle represents the open atmosphere outside of the cave.

$\delta^{13}C_{CO_2} = -12.0 \pm 0.2$ ‰. Samples and standards were measured ten times. Sample uncertainties were assessed using the methods of Webster et al. (2016).

Quantitative Analyses

Relationships between CH_4, CO_2, and H_2S concentrations and their distances to a spring were assessed through two-sample *t*-tests assuming unequal variance. Additionally, correlations between CH_4 and CO_2 concentrations in the air of CVL were examined through regression analysis. The isotopic composition of the source of CH_4 from cave springs was assessed using Keeling plots, as described in Thom et al. (1993). This approach assumes that gas samples represent varying mixtures of two gas end-members with contrasting CH_4 concentrations and isotopic compositions. The $\delta^{13}C_{CH_4}$ and $\delta^2H_{CH_4}$ values of CH_4 entering from springs were determined by the *y*-intercepts of linear regression analyses of $\delta^{13}C_{CH_4}$ and $\delta^2H_{CH_4}$ values of air samples versus $[CH_4]^{-1}$ of the same samples (where $[CH_4]$ is the concentration of CH_4 in ppmv). Keeling plots were also used to determine the potential $\delta^{13}C_{CO_2}$ end member value of CO_2 in CVL air following the methods of Rey et al. (2012).

Results

H_2S concentrations in the air of CVL ranged from 0.9 ± 0.8 to 23.05 ± 0.05 ppmv (Table 1) and were highest closest to springs (two-sample *t*-test unequal variance, $t_{14} = 3.02$, $p = 0.005$; Fig. 3). CH_4 concentrations ranged from 1.88 ± 0.10 ppmv to 3.67 ± 0.18 ppmv ($n = 12$), and CO_2 concentrations ranged from 400 ± 20 ppmv to 920 ± 50 ppmv ($n = 12$; Fig. 4; Table 2). The concentrations of CH_4 and CO_2 in the local atmosphere were 1.96 ± 0.10 ppmv and 430 ± 20 ppmv, respectively. CH_4 and CO_2 concentrations were positively correlated in the atmosphere of CVL ($r = 0.95$, $n = 12$, $p < 0.01$; Fig. 4). CH_4 and CO_2 concentrations were higher at locations close to springs than at other locations (CH_4: two-sample *t*-test unequal variance, t_5 stat = 3.57, $p = 0.008$; CO_2: two-sample *t*-test unequal variance, t_6 stat = 3.05, $p = 0.01$; Fig. 5A). CH_4 and CO_2 concentrations were not related to the distance from an entrance (CH_4: two-sample *t*-test unequal variance, t_5 stat = –1.16, $p = 0.15$; CO_2: two-sample *t*-test unequal variance, t_3 *stat* = –0.75, $p = 0.25$; Fig. 5B).

$\delta^{13}C_{CO_2}$ values ranged from –12.0 ± 0.2 to –8.7 ± 0.4 ‰ (Table 3). Air samples near cave entrances showed the lowest concentrations of CO_2 and had $\delta^{13}C_{CO_2}$ values around –9.6 to –9.4 ‰. The $\delta^{13}C$ of atmospheric CO_2, –10.8 ± 0.6 ‰, did not match the $\delta^{13}C_{CO_2}$ values of other samples with near atmospheric CO_2 concentrations, nor samples of atmospheric CO_2 from other studies (Peyraube et al., 2013; Fernandez-Cortes et al., 2015), and was excluded from further analyses. As CO_2 concentrations increased, their $\delta^{13}C_{CO_2}$ values diverged from the $\delta^{13}C_{CO_2}$ of low-CO_2 samples (Table 3). The slope of $\delta^{13}C_{CO_2}$ data in a Keeling plot was not different from zero ($r^2 = 0.23$, $n = 12$, $p = 0.11$).

The relationships between CH_4 concentration and $\delta^{13}C_{CH_4}$ and $\delta^2H_{CH_4}$ values in CVL air fit a two end-member mixing model in Keeling plots (Fig. 6). $\delta^{13}C_{CH_4}$ ranged from –47.92 ± 0.15 to –35.47 ± 0.12 ‰ and was linearly related to the inverse CH_4 concentration ($\delta^{13}C_{CH_4} = [-45 \pm 7] \times [CH_4]^{-1} + [-24 \pm 3]$, $r^2 = 0.98$, $n = 9$, $p < 0.01$; Fig. 6A). $\delta^2H_{CH_4}$ ranged from –117 ± 9 to –65 ± 12 ‰ and was linearly related to the inverse CH_4 concentration ($\delta^2H_{CH_4} = [-140 \pm 80] \times$

Table 2. Sample collection dates and measurement dates for the concentrations of CH_4 and CO_2. Dates are listed as mm/dd/yyyy.

		CH_4 concentration			CO_2 Concentration		
Site	Collection Date	Analysis Date	Conc. (ppmv)	e (2SD)[a]	Analysis Date	Conc. (ppmv)	e (2SD)[a]
Site 1	12/17/2013	12/31/2013	1.89	0.09	12/31/2013	460	30
Site 2	12/17/2013	12/31/2013	2.14	0.11	12/31/2013	520	30
Site 3	12/17/2013	12/31/2013	2.12	0.11	12/31/2013	470	30
Site 3	12/17/2013	12/31/2013	2.03	0.10	12/31/2013	450	30
Site 4	12/17/2013	12/31/2013	1.98	0.10	12/31/2013	490	30
Site 5	12/16/2013	12/31/2013	1.97	0.10	12/31/2013	470	30
Site 6	12/16/2013	12/31/2013	1.88	0.09	12/31/2013	400	20
Site 7	12/16/2013	12/31/2013	3.16	0.16	12/31/2013	860	50
Site 7	12/16/2013	12/31/2013	3.03	0.15	12/31/2013	860	50
Site 8	12/16/2013	12/31/2013	2.63	0.13	12/31/2013	590	40
Site 8	12/16/2013	12/31/2013	2.33	0.12	12/31/2013	570	30
Site 9	12/16/2013	12/31/2013	3.67	0.18	12/31/2013	850	50
Site 10	12/16/2013	12/31/2013	2.74	0.14	12/31/2013	560	30
Site 11	12/17/2013	12/31/2013	3.58	0.18	12/31/2013	920	50
Site 12	12/17/2013	12/31/2013	2.09	0.10	12/31/2013	530	30
Outside Cave	12/17/2013	12/31/2013	1.96	0.10	12/31/2013	430	30

[a] SD = Standard deviation.

$[CH_4]^{-1} + [-40 \pm 50]$, $r^2 = 0.62$, $n = 8$, $p = 0.02$; Fig. 6B). Air samples from locations nearest to entrances define one end-member of CH_4 entering the cave with a $\delta^{13}C_{CH_4}$ of -47.6 ± 0.8 ‰ and a $\delta^2H_{CH_4}$ of -112 ± 14 ‰. Samples obtained near springs suggest a second source of CH_4 entering CVL with a $\delta^{13}C_{CH_4}$ of -24 ± 3 ‰ and a $\delta^2H_{CH_4}$ of -40 ± 50 ‰ (Figs. 6, 7).

Discussion

Hydrogen Sulfide, Methane, and Carbon Dioxide Enter CVL from Springs

The observed concentrations in CVL of H_2S, CH_4, and CO_2, and the stable-isotope compositions of CH_4 and CO_2 result from a combination of airflow through the cave,

Table 3. Sample stable isotopic compositions of CH_4 and CO_2. Dates are listed as mm/dd/yyyy.

		$\delta^{13}C_{CH_4}$			$\delta^2H_{CH_4}$			$\delta^{13}C_{CO_2}$		
Site	Collection Date	Analysis Dates	‰ (VPDB)	e (2SD)[a]	Analysis Dates	‰ (VSMOW)	e (2SD)[a]	Analysis Date	‰ (VPDB)	e (2SD)[a]
Site 1	12/17/2013	4/9/2014	-47.26	0.12	LSV[b]	…	…	1/9/2014	-9.4	0.2
Site 2	12/17/2013	4/3/2014	-45.71	0.15	3/18/2014	-96	10	1/9/2014	-10	0.2
Site 3	12/17/2013	4/3/2014	-46.51	0.15	3/19/2014	-97	12	1/9/2014	-9.6	0.3
Site 4	12/17/2013	SL[c]	…	…	LSV[b]	…	…	1/9/2014	-9.6	0.3
Site 5	12/16/2013	4/4/2014	-45.73	0.07	3/18/2014	-116	10	1/9/2014	-9.6	0.7
Site 6	12/16/2013	4/3/2014	-47.92	0.15	3/21/2014	-117	9	1/9/2014	-9.5	0.3
Site 7	12/16/2013	4/9/2014	-38.28	0.12	3/18/2014	-104	10	1/9/2014	-12	0.2
Site 8	12/16/2013	4/3/2014	-42.45	0.15	3/19/2014	-87	12	1/9/2014	-10.6	0.2
Site 9	12/16/2013	4/9/2014	-35.47	0.12	3/19/2014	-65	12	1/9/2014	-10.4	0.2
Site 9	12/16/2013	10/9/2014	-39	3	…	…	…	…	…	…
Site 10	12/16/2013	4/3/2014	-40.63	0.15	3/21/2014	-83	8	1/9/2014	-9.7	0.3
Site 11	12/17/2013	SL[c]	…	…	LSV[b]	…	…	1/9/2014	-9.1	0.3
Site 12	12/17/2013	SL[c]	…	…	LSV[b]	…	…	1/9/2014	-8.7	0.4
Outside Cave	12/17/2013	4/3/2014	-47.34	0.15	3/18/2014	-107	10	1/9/2014	-10.8[d]	0.6[d]

[a] SD = Standard deviation.
[b] Sample was not measured due to low sample volume (LSV = low sample volume).
[c] The sample had leaked at the time of measurement (SL = sample leakage).
[d] This measurement did not agree with other measurements of low CO_2 concentration air.

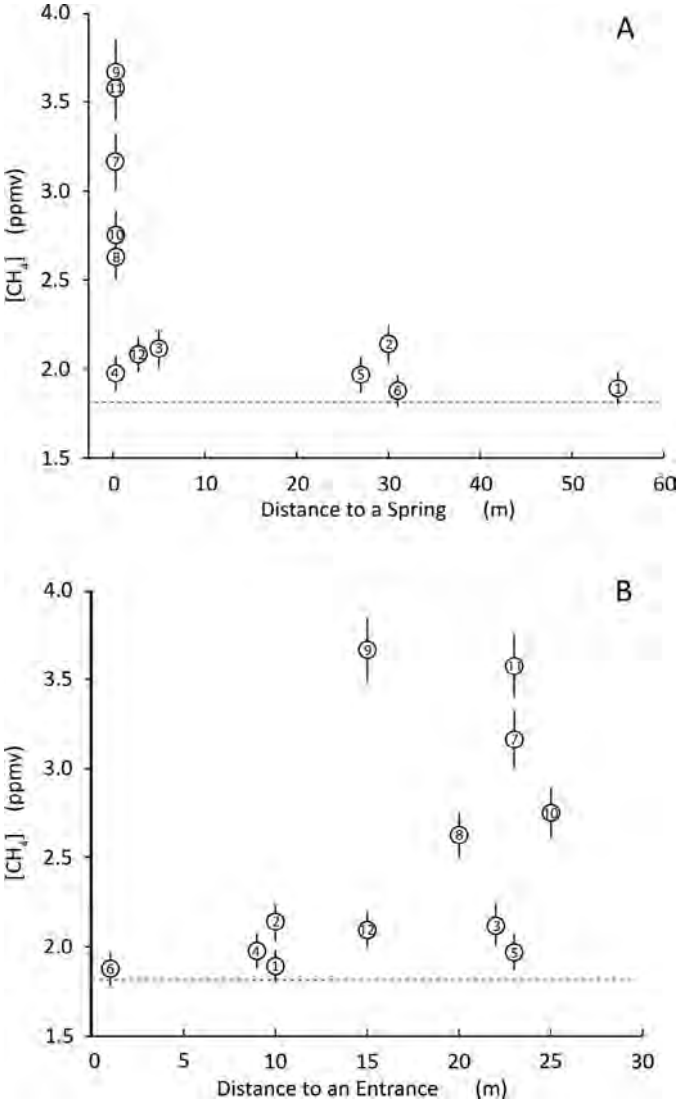

Figure 5. A) CH_4 concentrations in cave air at different distances from springs. B) CH_4 concentrations in cave air at different distances from an entrance. Dashed lines indicate the global atmospheric average CH_4 concentration (Adushkin and Kudryavtsev, 2013).

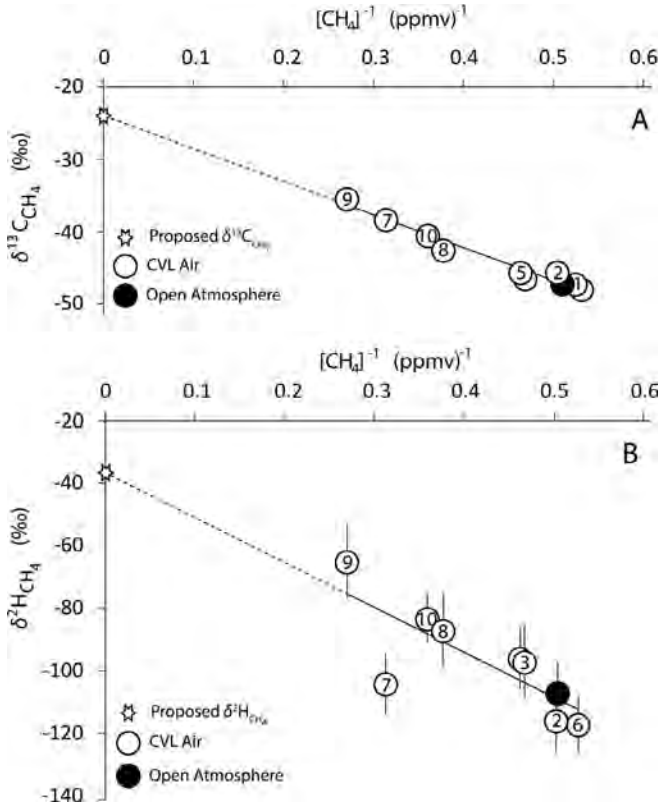

Figure 6. Keeling plot of $\delta^{13}C_{CH_4}$ from cave air (A, $\delta^{13}C_{CH_4} = [-45 \pm 7] \times [CH_4]^{-1} + [-24 \pm 3]$, $r^2 = 0.98$, $n = 9$, $p < 0.01$) and $\delta^2H_{CH_4}$ (B, $\delta^2H_{CH_4} = [-140 \pm 80] \times [CH_4]^{-1} + [-40 \pm 50]$, $r^2 = 0.62$, $n = 8$, $p = 0.02$. The error bars are smaller than the data points in A. The star marks the y-intercept that indicates the $\delta^{13}C_{CH_4}$ and $\delta^2H_{CH_4}$ of the dissolved CH_4 in the spring water. The open circles represent Cueva de Villa Luz air samples, and black circles represent the outside atmosphere as measured during the study.

biogeochemical processes operating within the cave, and biogeochemical processes in the waters that feed the cave springs. The temperature of the open atmosphere at the time of sampling was lower than the temperature inside CVL, and cool air was felt entering from the skylights. This type of airflow should result in cave air composition near skylights that resembles the open atmosphere, as was observed in CVL at the time of sampling. Additionally, high rates of atmospheric exchange are indicated by roughly atmospheric CH_4 and CO_2 concentrations at sample sites that were neither close to an entrance nor immediately adjacent to springs.

Elevated CH_4 and CO_2 concentrations at springs imply that CH_4 and CO_2 are exsolving from spring water (Fig. 4). The only site located close to a spring that did not show elevated CH_4 and CO_2 concentrations was Midway Spring (Site 4), which is located 9 m from a skylight (Fig. 4). Elevated CH_4 concentrations in cave air near springs have not been reported from other caves. The CH_4 concentrations in CVL that were not located by springs (1.9 to 2.2 ppmv) are more similar to those measured in the sulfidic Frasassi Cave system (1.9 to 2.2 ppmv) in Italy (Jones et al., 2012) than they are to the sulfidic Movile Cave (10,000 ppmv) in Romania (Hutchens et al., 2004). This difference may be due to the lack of atmospheric connectivity at the site in Movile Cave, which is mostly water-filled. We did not observe CH_4 concentrations below 1.5 ppmv, as have been observed in many epigenic, non-sulfidic caves in Gibraltar, Australia, the United States, and Spain (Mattey et al., 2013; Fernandez-Cortes et al., 2015; McDonough et al., 2016; Webster et al., 2016; Lennon et al., 2016). Our results demonstrate that if *in-situ* CH_4 oxidation processes were operating in CVL, they were not strong enough to react all of the CH_4 in the collected samples. We can therefore

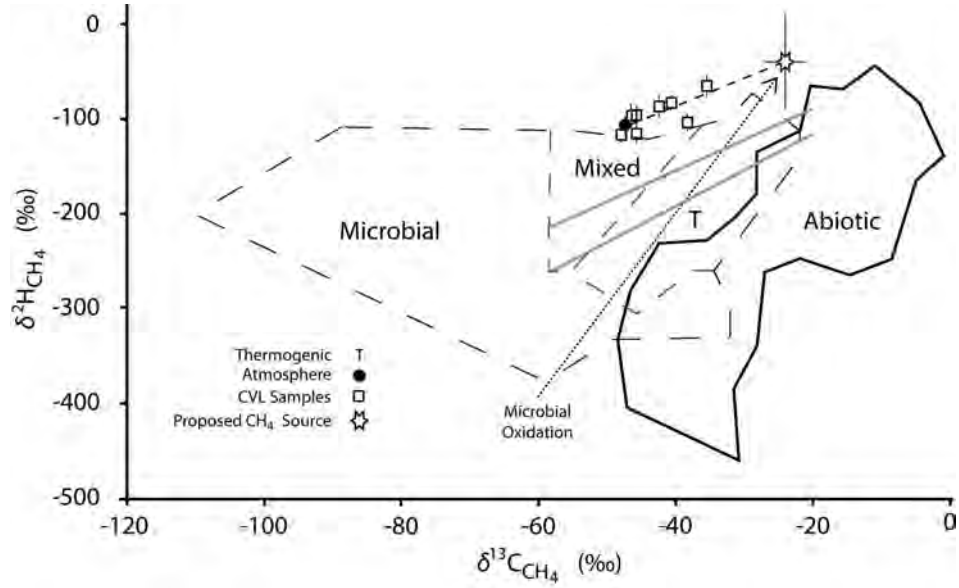

Figure 7. Isotopic characteristics of methane in air samples from Cueva de Villa Luz (CVL) plotted on published occurrence envelopes for microbial, thermogenic (T), and abiotic methanes (Etiope and Sherwood Lollar, 2013). Solid grey lines represent observed isotopic boundaries of methane from terrestrial and marine source rocks (Schoell, 1980). Data from CVL air samples (squares) plot along a bidirectional mixing line between an atmospheric source of CH_4 and a methane entering CVL with a stable isotopic signature of $\delta^{13}C_{CH_4} = -24 \pm 3$ ‰, $\delta^2H_{CH_4} = -40 \pm 50$ ‰.

conclude that two most likely processes affecting CH_4 in CVL are atmospheric circulation and spring-water outgassing.

Stable Isotopic Composition and Sources of Methane

The CH_4 concentrations and values of $\delta^{13}C_{CH_4}$ and $\delta^2H_{CH_4}$ observed in CVL are consistent with mixing between an atmospheric CH_4 source and a CH_4 source entering from the springs. The lowest concentrations of CH_4 in the air of CVL were measured at locations that were both close to entrances and far from springs. The $\delta^{13}C_{CH_4}$ and $\delta^2H_{CH_4}$ values from these locations plot near the respective values of atmospheric CH_4 (Figs. 6, 7). The concentrations and isotopic composition of CH_4 from the local atmosphere and cave locations near skylights agree with other measurements of atmospheric CH_4 (Mikaloff Fletcher et al., 2004). The CH_4 concentrations in CVL suggest that a secondary source of CH_4 with a $\delta^{13}C_{CH_4}$ of –24 ± 3 ‰ and a $\delta^2H_{CH_4}$ of –40 ± 50 ‰ enters CVL dissolved in spring water. CH_4 with this stable isotopic composition does not closely match known isotopic compositions generated by primary biotic or abiotic processes, and is driven largely by relatively positive $\delta^2H_{CH_4}$ values (Fig. 7).

The origin of the CH_4 entering CVL at springs can be constrained in three ways, by comparing the CH_4 isotopically to other CH_4 sources in the region, by taking into account the regional thermal history, and by compensating for shifts in CH_4 isotopic composition caused by oxidation. A possible explanation for $\delta^{13}C_{CH_4}$ values in cave air is that the CH_4 entering CVL from the springs has an original isotopic composition with a $\delta^{13}C_{CH_4}$ value of –24 ± 3 ‰ and a $\delta^2H_{CH_4}$ value of –40 ± 50 ‰, based on the Keeling analysis. However, this $\delta^{13}C_{CH_4}$ of CH_4 from CVL spring water is incompatible with CH_4 from neighboring sedimentary basins, which have $\delta^{13}C_{CH_4}$ values of –32 to –70 ‰ in the Macuspana Basin; –38 to –45 ‰ in the Papaloapan Basin; –39 to –55 ‰ in the Cuichapa Basin; and –40 to –52 ‰ in the Reforma Basin (Clara Valdés et al., 2009). The most similar $\delta^{13}C_{CH_4}$ value from a regional natural gas well is about –32 ‰ from the Macuspana Basin (Talukdar et al., 2002; Clara Valdés et al., 2009). Additionally, the proposed $\delta^2H_{CH_4}$ value of CH_4 entering CVL from springs is very positive compared to values from the literature (Schoell, 1980; Etiope et al., 2011; Etiope and Sherwood Lollar et al., 2013). The evidence implies that a parental CH_4 with the proposed $\delta^{13}C_{CH_4}$ and $\delta^2H_{CH_4}$ values is unlikely, and supports the idea that CH_4 entering CVL in springs is the remnant of a larger CH_4 flux at depth that has been mostly oxidized to CO_2 on the way to the cave.

The thermal history of the CVL region provides a way to help determine whether abiotic or biotic oxidation is most likely to have altered the CH_4 entering CVL, because the temperature ranges at which they occur do not overlap. The minimum temperature for the onset of abiotic CH_4 oxidation has been estimated to range from 100 to 140 °C, whereas microbial CH_4 oxidation (methanotrophy) generally takes place from 0 to 80 °C (Machel, 1998, 2001; Worden et al., 1995; Holler et al., 2011). Vitrinite reflectance (R_o) data from source rocks in the region range from 0.5 to 0.8 % (Guzman-Vega and Mello, 1999) and correspond to maximum

subsurface temperatures of 60 to 90 °C (Bjørlykke, 1989). Additionally, modern water temperatures from oil wells in the region (30 to about 60 °C) and dissolved silica geothermometers from ground water in the region do not suggest that volcanic heat flow is affecting groundwater temperature (Nencetti et al., 2005). These observations suggest that methanotrophy is responsible for consuming CH_4 in the subsurface before entering CVL.

Correcting for the expected isotopic shifts associated with partial methanotrophic loss of CH_4 can hindcast the original isotopic composition and reveal the origin of CH_4 entering CVL. Microbial oxidation imparts an increase of about 8.5 ‰ in the $\delta^2H_{CH_4}$ value for every increase of 1 ‰ in the $\delta^{13}C_{CH_4}$ value (Feisthauer et al., 2011). If methanotrophy is assumed to be occurring in the subsurface, then the original stable isotopic composition of the CH_4 entering CVL is hindcast to match a thermogenic source (Fig. 7).

Possible Electron Acceptors for Methane Oxidation

The co-occurrence of CH_4 and H_2S supports our claim that sulfate is the most likely electron acceptor, but what about other potential acceptors? Alternative electron acceptors such as O_2, and nitrate (NO_3^-) are known to be metabolically coupled to CH_4 oxidation in other environments (Hu et al., 2011; Mattey et al., 2013). However, O_2 and NO_3^- concentrations in the anoxic springs of CVL were below detection in previous studies, where the concentration of each was < 0.1 mg L^{-1} (Hose et al., 2000; Rosales Lagarde et al., 2014). Addionally, organoclastic sulfate reduction competes with anaerobic CH_4 oxidation only when organic matter is abundant ($\sim$ 1 % by sediment weight) (Malinverno and Pohlman 2011; Pohlman et al., 2013), and the organic carbon concentration in CVL spring water is comparatively low, ranging from 0.5 to 3.5 mg L^{-1} (Rosales Lagarde, 2013).

Stable Isotopic Composition and Sources of Carbon Dioxide

The $\delta^{13}C_{CO_2}$ values near springs suggest that oxidized CH_4 is not the primary contributor to dissolved CO_2 in the spring water. The lowest CO_2 concentration in CVL (Site 6, 1 m from an entrance) had a $\delta^{13}C_{CO_2}$ value of -9.5 ± 0.3 ‰ which matches known atmospheric CO_2 concentrations (400 ± 20 ppmv) and $\delta^{13}C_{CO_2}$ values (–10 ‰) (Peyraube et al., 2013; Fernandez-Cortes et al., 2015). The two highest CO_2 concentrations in CVL at Site 11 (Sulfur Spring) and Site 7 (Slot Spring) were associated with the second-most-positive $\delta^{13}C_{CO_2}$ value of -9.1 ± 0.3 ‰ at Site 11 and the most negative $\delta^{13}C_{CO_2}$ value of -12.0 ± 0.2 ‰ at Site 7. Processes that may cause diverging $\delta^{13}C_{CO_2}$ values of CO_2 near springs include the oxidation of CH_4 and other organic compounds, which are typically ^{13}C-depleted, and the dissolution of marine carbonates, like those that host CVL, that have $\delta^{13}C$ values from 1 to 4 ‰ (Keith and Weber, 1964; Knauth and Kennedy, 2009). $\delta^{13}C_{CO_2}$ values of the air above these springs are similar to the $\delta^{13}C$ values of –9 to –12 ‰ for dissolved CO_2 measured in sulfidic springs 45 km northwest of CVL (Nencetti et al. 2005). The similarity of $\delta^{13}C_{CO_2}$ ranges from both areas demonstrate that processes causing diverging $\delta^{13}C_{CO_2}$ values at high CO_2 concentrations are regional rather than specific to CVL.

Comparison With Other Sulfidic Cave Systems

Our proposed model of CH_4 migration into CVL from petroleum basins not only provides sufficient CH_4, but also agrees with proposed pathways of sulfur migration into CVL (Rosales Lagarde et al., 2014). The entrance of thermogenic CH_4 into CVL also agrees with observations of CH_4 and longer-chain hydrocarbons emanating from "Group II" springs of the Sierra de Chiapas region northwest of CVL (Nencetti et al., 2005). The CH_4/ethane molecular ratios from these springs generally match the CH_4/ethane ratios from petroleum basins when the ratios from springs are corrected for the differential solubility of CH_4 and ethane in water (Clara Valdés et al., 2009; Dai et al., 2014). More broadly, a thermogenic source of CH_4 suggests that the processes forming CVL are analogous to those that are thought to have formed Lower Kane Cave and the caves of the Guadalupe Mountains (Kirkland and Evans, 1976; Davis, 1980; Hill, 1995).

Conclusions

High CH_4, H_2S, and CO_2 concentrations occur in cave air near springs in CVL, demonstrating that the three gases entered in solution via spring water. The poor match of the proposed stable isotopic signature of CH_4 entering CVL from springs ($\delta^{13}C_{CH_4} = -24 \pm 3$ ‰, $\delta^2H_{CH_4} = -40 \pm 50$ ‰) with known $\delta^{13}C_{CH_4}$ values from other studied systems and the thermal history of the region implies that the CH_4 is of a secondary origin, with subterranean anaerobic methanotrophy as the most likely explanation. If methanotrophy is altering the CH_4 as it traveled to CVL, the original source of the CH_4 is mathematically predicted to have a thermogenic origin. The incomplete oxidation of CH_4 in the presence of sulfate appears to be generating the H_2S that enters CVL with spring water. This evidence for CH_4 migrating from regional petroleum basins while being oxidized in the presence of sulfates connects the geochemical processes that are forming CVL to other caves, like those of the Guadalupe Mountains and Lower Kane Cave, whose origins have been attributed to sulfuric acid speleogenesis.

Acknowledgements

The authors thank the National Geographic Society Expeditions Council for support (Grant #EC0644-13 to PJB) as well as the authorities and inhabitants of the Tacotalpa municipality and the town of Tapijulapa. This material is

based upon work supported by the U.S. Department of Energy, Office of Science, Office of Basic Energy Sciences, Chemical Sciences, Geosciences, and Biosciences Division under Award Number DE-SC0006978. This study forms part of the collaboration between the Universidad Juárez Autónoma de Tabasco and the New Mexico Institute of Mining and Technology. M.N. Spilde and D.E. Northup aided in discussions on previous work carried out in CVL. P.L. Griffin provided helpful insight during many discussions about stable isotope fractionation. T.V. Royer made analytical gas chromatography available. C. Gassaway edited a version of this manuscript. The comments of anonymous reviewers improved the quality of this manuscript.

References Cited

Adushkin, V.V., and Kudryavtsev, V.P., 2013, Estimating the global flux of methane into the atmosphere and its seasonal variations: Izvestiya, Atmospheric and Oceanic Physics, v. 49, no. 2, p. 128–136. https://doi.org/10.1134/S0001433813020023.

Aguilar Rodríguez, A., 2007, Presencia de hidrocarburos en el municipio de Tacotalpa, Tabasco: Horizonte Eploratorio, v. July-September 2007, p. 5–9.

Alcàntara García, J.R., Ham Wong, J.M., Medina Flores, U., Hernàndez Peñaloza, J.J., de la Cruz Rivera, V.M., Peña Ramirez, H., Namson, J., and Spaw, J.M., 2004, Identification and evaluation of plays in the Simojovel Project, southeastern Mexico: American Association of Petroleum Geologists International Conference October 24-27, 2004, Cancun, Mexico. abstract a90217, 6 p.

Bjørlykke, K., 1989, Sedimentology and Petroleum Geology. Berlin Heidelberg, Springer-Verlag, 363 p.

Clara Valdés, M.d.L., Villanueva Rodríguez, L., and Caballero García, E., 2009, Geochemical integration and interpretation of source rocks, oils, and natural gases in southeastern Mexico: *in* Bartolini, C., and Román Ramos, J.R., eds., Petroleum Systems in the Southern Gulf of Mexico: AAPG Memoir, v. 90, p. 337–368. https://doi.org/10.1306/13191091M903337.

Dai, JinXing, Ni, YunYan, Hu, GuoYi, Huang, ShiPeng, Liao, FengRong, Yu, Cong, Gong, DeYu, and Wu, Wei, 2014, Stable carbon and hydrogen isotopes of gases from the large tight gas fields in China: Science China Earth Sciences, v. 57, no. 1, 88–103. https://doi.org/10.1007/s11430-013-4701-7.

Davis, D.G., 1980, Cave development in the Guadalupe Mountains: a critical review of recent hypotheses: NSS Bulletin, v. 42, no. 3, p. 42–48.

Egemeier, S.J., 1981, Cavern development by thermal waters: National Speleological Society Bulletin, v. 43, p. 31–51.

Etiope, G., Baciu, C.L., and Schoell, M., 2011, Extreme methane deuterium, nitrogen and helium enrichment in natural gas from the Homorod seep (Romania): Chemical Geology, v. 280, p. 89–96. https://doi.org/10.1016/j.chemgeo.2010.10.019.

Etiope, G., and Sherwood Lollar, B., 2013, Abiotic methane on earth: Reviews of Geophysics, v. 51, no. 2, p. 276–299. https://doi.org/10.1002/rog.20011.

Feisthauer, S., Vogt, C., Modrzynski, J., Szlenkier, M., Krüger, M., Siegert, M., and Richnow, H.-H., 2011, Different types of methane monooxygenases produce similar carbon and hydrogen isotope fraction patterns during methane oxidation: Geochimica et Cosmochimica Acta, v. 75, no. 5, p. 1173–1184. https://doi.org/10.1016/j.gca.2010.12.006.

Fernandez-Cortes, A., Cuezva, S., Alvarez-Gallego, M., Garcia-Anton, E., Pla, C., Benavente, D., Jurado, V., Saiz-Jimenez, C., and Sanchez-Moral, S., 2015, Subterranean atmospheres may act as daily methane sinks: Nature Communications, v. 6, no. 7003. https://doi.org/10.1038/ncomms8003.

García-Palomo, A., Macías, J.L., Arce, J.L., Mora, J.C., Hughes, S., Saucedo, R., Espíndola, J.M., Escobar, R., and Layer, P., 2006, Geological evolution of the Tacaná Volcanic Complex, México-Guatemala: *in* Rose, W.I., Bluth, G.J.S., Carr, M.J., Ewert, J.W., patino, L.C., and Vallance, J.W., eds., Volcanic Hazards in Central America, Geological Society of America Special Paper 412, p. 39–57. https://doi.org/10.1130/2006.2412(03).

Guzman-Vega, M.A., and Mello, M.R., 1999, Origin of oil in the Sureste Basin, Mexico: AAPG Bulletin, v. 83, no. 7, p. 1068–1095.

Hill, C.A., 1990, Sulfuric acid speleogenesis of Carlsbad Cavern and its relationship to hydrocarbons, Delaware Basin, New Mexico and Texas: AAPG Bulletin, v. 74, no. 11, p. 1685–1694.

Hill, C.A., 1995, Sulfur redox reactions: Hydrocarbons, native sulfur, Mississippi Valley-type deposits, and sulfuric acid karst in the Delaware Basin, New Mexico and Texas: Environmental Geology, v. 25, p. 16–23. https://doi.org/10.1007/BF01061826.

Holler, T., Widdel, F., Knittel, K., Amann, R., Kellermann, M.Y., Hinrichs, K.-U., Teske, A., Boetius, A., and Wegener, G., 2011, Thermophilic anaerobic oxidation of methane by marine microbial consortia: The ISME Journal, v. 5, p. 1946–1956. https://doi.org/10.1038/ismej.2011.77.

Hose, L.D., Palmer, A.N., Palmer, M.V., Northup, D.E., Boston, P.J., and DuChene H.R., 2000, Microbiology and geochemistry in a hydrogen-sulphide-rich karst environment: Chemical Geology, v. 169, p. 399–423. https://doi.org/10.1016/S0009-2541(00)00217-5.

Hose, L.D., and Pisarowicz, J.A., 1999, Cueva de Villa Luz, Tabasco, Mexico: reconnaissance study of an active sulfur spring cave and ecosystem: Journal of Cave and Karst Studies, v. 61, no. 1, p. 13–21.

Hu, Shihu, Zeng, R.J., Keller, J., Lant, P.A., and Yuan, Zhiguo, 2011, Effect of nitrate and nitrite on the selection of microorganisms in the denitrifying aerobic methane oxidation process: Environmental Microbiology Reports, v. 3, no. 3, p. 315–319. https://doi.org/10.1111/j.1758-2229.2010.00227.x.

Hutchens, E., Radajewski, S., Dumont, M.G., McDonald, I.R., and Murrell, J.C., 2004, Analysis of methanotrophic bacteria in Movile Cave by stable isotope probing: Environmental Microbiology, v. 6, no. 2, p. 111–120. https://doi.org/10.1046/j.1462-2920.2003.00543.x.

Jones, D.S., Albrecht, H.L., Dawson K.S., Schaperdoth, I., Freeman, K.H., Pi, Yundan, Pearson, A., and Macalady, J.L., 2012, Community genomic analysis of an extremely acidophilic sulfur oxidizing biofilm: The ISME Journal, v. 6, p. 158–170. https://doi.org/10.1038/ismej.2011.75.

Keith, M.L., and Weber, J.N., 1964, Carbon and oxygen isotope composition of selected limestones and fossils: Geochimica et Cosmochimica Acta, v. 28, p. 1787–1816. https://doi.org/10.1016/0016-7037(64)90022-5.

Kirkland, D.W., and Evans, R., 1976, Origin of limestone buttes, gypsum plain, Culberson County, Texas: AAPG Bulletin, v. 60, no. 11, p. 2005–2018.

Knauth, L.P., and Kennedy, M.J., 2009, The late Precambrian greening of the earth: Nature, v. 460, p. 728–732. https://doi.org/10.1038/nature08213.

Lennon, J.T., Nguyễn-Thùy, D., Phạm, T.M., Drobniak, A., Tạ, P.H., Phạm, N.Đ., Streil, T., Webster, K.D., and Schimmelmann, A., 2016, Microbial contributions to subterranean methane sinks: Geobiology. https://doi.org/10.1111/gbi.12214.

Liu, Q.Y., Worden, R.H., Jin, Z.J., Liu, W.H., Li, J., Gao, B., Zhang, D.W., Hu, A.P., and Yang, C., 2014, Thermochemical sulphate reduction (TSR) versus maturation and their effects on hydrogen stable isotopes of very dry alkane gases: Geochimica et Cosmochimica Acta, v. 137, p. 208–220. https://doi.org/10.1016/j.gca.2014.03.013.

Machel, H.G., 1998, Gas souring by thermochemical sulfate reduction at 140 degrees C: Discussion: AAPG Bulletin, v. 82, no. 10, p. 1870–1873.

Machel, H.G., 2001, Bacterial and thermochemical sulfate reduction in diagenetic settings – old and new insights: Sedimentary Geology, v. 140, p. 143–175. https://doi.org/10.1016/S0037-0738(00)00176-7.

Malinverno, A., and Pohlman, J.W., 2011, Modeling sulfate reduction in methane hydrate-bearing continental margin sediments: Does a sulfate sulfate-methane transition require anaerobic oxidation of methane?: Geochemistry, Geophysics, Geosystems, v. 12, no. Q07006. https://doi.org/10.1029/2011GC003501.

Mattey, D.P., Fisher, R., Atkinson, T.C., Latin, J.-P., Durrell, R., Ainsworth, M., Lowry, D., and Fairchild, I.J., 2013, Methane in underground air in Gibraltar Karst: Earth and Planetary Science Letters, v. 374, p. 71–80. https://doi.org/10.1016/j.epsl.2013.05.011.

McDonough, L.K., Iverach, C.P., Beckman, S., Manfield, M., Rau, G.C., Baker, A., and Kelly, B.F.J., 2016, Spatial variability of cave-air carbon dioxide and methane concentrations and isotopic compositions in a semi-arid karst environment: Environmental Earth Sciences, v. 75, no. 700. https://doi.org/10.1007/s12665-016-5497-5.

Meneses-Rocha, J.J., 2001, Tectonic evolution of the Ixtapa Graben, an example of a strike-slip basin of Southeastern Mexico: implications for regional petroleum systems, *in* Bartolini, C., Buffler, R.T., and Cantú-Chapa, A., eds., The Western Gulf of Mexico Basin: Tectonics Sedimentary Basins and Petroleum Systems: AAPG Memoir, v. 75, p. 183–216.

Mikaloff Fletcher, S.E., Tans, P.P., Bruhwiler, L.M., Miller, J.B., and Heimann, M., 2004, CH_4 sources estimated from atmospheric observations

of CH_4 and its $^{13}C/^{12}C$ isotopic ratios: 1. Inverse modeling of source processes: Global Biogeochemical Cycles, v. 18 (GB4004). https://doi.org/10.1029/2004GB002223.

Miller, J.B., Mack, K.A., Dissly, R., White, J.W.C., Dlugokencky, E.J., and Tans, P.P., 2002, Development of analytical methods and measurements of $^{13}C/^{12}C$ in atmospheric CH_4 from the NOAA Climate Monitoring and Diagnostics Laboratory Global Air Sampling Network: Journal of Geophysical Research, v. 107, no. D13, p. ACH 11-1–ACH 11-15. https://doi.org/10.1029/2001JD000630.

Nencetti, A., Tassi, F., Vaselli, O., Macías, J.L., Magro, G., Capaccioni, B., Minissale, A., and Mora, J.C., 2005, Chemical and isotopic study of thermal springs and gas discharges from Sierra de Chiapas, Mexico: Geofísica Internacional, v. 44, no. 1, p. 39–48.

Pantoja-Alor, J., 1989, Informe geológico minero de la Mina de Sta. Fe, Chis, *in* Salas, G.P., ed., Geologia Económica de Mexico, p. 413–420.

Peryt, T.M., Durakiewicz, T., Peryt, D., and Pobrezhsky, A., 2012, Carbon and oxygen isotopic composition of the Middle Miocene Badenian gypsum-associated limestones of West Ukraine, Geologica Acta, v. 10, no. 4, p. 319–332. https://doi.org/10.1344/105.000001753.

Peyraube, N., Lastennet, R., Denis, A., and Malaurent, P., 2013, Estimation of epikarst air P_{CO_2} using measurements of water $\delta^{13}C_{TDIC,}$ cave air P_{CO_2} and $\delta^{13}C_{CO_2}$: Geochimica et Cosmochimica Acta, v. 118, p. 1–17. https://doi.org/10.1016/j.gca.2013.03.046.

Peyraube, N., Lastennent, R., Denila, J., Villanueva, J.D., Houillon, N., Malaurent, P., and Denis, A., 2016, Effect of diurnal and seasonal temperature variation on Cussac cave ventilation using CO_2 assessment: Theoretical and Applied Climatology 2016. 14 p. https://doi.org/10.1007/s00704-016-1824-8.

Pohlman, J.W., Riedel, M., Bauer, J.E., Canuel, E.A., Paull, C.K., Lapham, L., Grabowski, K.S., Coffin, R.B., and Spence, G.D., 2013, Anaerobic methane oxidation in low-organic content methane seeps: Geochimica et Cosmochimica Acta, v. 108, p. 184–201. https://doi.org/10.1016/j.gca.2013.01.022.

Rey, A., Etiope, G., Belelli-Marchesini, L., Papale, D., and Valentini, R., 2012, Geological carbon sources may confound ecosystem carbon balance estimates: Evidence from a semi-arid steppe in the southeast of Spain. Journal of Geophysical Research Biogeosciences 117 (G03034), https://doi.org/10.1029/2012JG001991.

Rosales Lagarde, L., 2013, Sulfidic Karst Springs and Speleogenesis in the Sierra de Chiapas. Austin, Association for Mexican Cave Studies bulletin 24, 79 p.

Rosales Lagarde, L., Boston, P.J., Campbell, A.R., Hose, L.D., Axen, G., and Stafford, K.W., 2014, Hydrogeology of northern Sierra de Chiapas, Mexico: a conceptual model based on a geochemical characterization of sulfide-rich karst brackish springs: Hydrogeology Journal, v. 22, no. 6, p. 1447–1467. https://doi.org/10.1007/s10040-014-1135-z.

Rosales Lagarde, L., Boston, P.J., Campbell, A., and Stafford, K.W., 2006, Possible structural connection between Chichón Volcano and the sulfur-rich springs of Villa Luz Cave (a.k.a. Cueva de las Sardinas), Southern Mexico, *in* Ramón Espinasa-Pereña and John Pint, eds., Proceedings of the X, XI, and XII International Symposia on Vulcanospeleology. Austin, Association for Mexican Cave Studies bulletin 19, p. 177–184.

Sarbu, S.M., Kane, T.C., and Kinkle, B.K., 1996, A chemoautotrophically based cave ecosystem: Science, v. 272, no. 5270, p. 1953–1955. https://doi.org/10.1126/science.272.5270.1953.

Schoell, M., 1980, The hydrogen and carbon isotopic composition of methane from natural gasses of various origins: Geochimica et Cosmochimica Acta, v. 44, no. 5, p. 649–661. https://doi.org/10.1016/0016-7037(80)90155-6.

Schoell, M., 1988, Multiple origins of methane in the Earth, *in* Schoell, M., ed., Origins of Methane in the Earth: Chemical Geology, v. 71, p. 1–10. https://doi.org/10.1016/0009-2541(88)90101-5.

Spilde, M.N., Fischer, T.P., Northup, D.E., Turin, H.J., and Boston, P.J., 2004, Water, gas, and phylogenetic analyses from sulfur springs in Cueva de Villa Luz, Tabasco, Mexico (abst.): Geological Society of America Abstracts with Programs, v. 3, no. 5, paper 106-11.

Talukdar, S.C., Guevara, E.H., Jones, R.H., Galindo, A., Romero, M.A., Wawrzyniec, T.F., Villanueva, L., Khaled, F., Ambrose, W.A., Jennette, D.C., Dunlap, D.B., Meneses-Rocha, J.J., Sánchez-Barreda, L., and Lugo, J.E., 2002., Hydrocarbon source and charge in the Neogene in the Macuspana and Veracruz Basins, Mexico: Gulf Coast Association of Geological Societies Transactions, v. 52, p. 925–934.

Thom, M., Bösinger R., Schmidt, M., and Levin, I., 1993, The regional budget of atmospheric methane of a highly populated area: Chemosphere, v. 26, p. 143–160. https://doi.org/10.1016/0045-6535(93)90418-5.

U.S. Geological Survey World Energy Assessment Team, 2000, U.S. Geological Survey World Petroleum Assessment 2000: U.S. Geological Survey Digital Data Series DDS, 60, 4 CDROMs.

Webster, K.D., Mirza, A., Deli, J.M., Sauer, P.E., and Schimmelmann, A., 2016. Consumption of atmospheric methane in a limestone cave in Indiana, USA: Chemical Geology, v. 443, p. 1–9. https://doi.org/10.1016/j.chemgeo.2016.09.020.

Whiticar, M.J., 1999, Carbon and hydrogen isotope systematics of bacterial formation and oxidation of methane: Chemical Geology, v. 161, p. 291–314. https://doi.org/10.1016/S0009-2541(99)00092-3.

Worden, R.H., Smalley, P.C., and Oxtoby, N.H., 1995, Gas sourcing by thermochemical sulfate reduction at 140 °C: AAPG Bulletin, v. 79, no. 6, p. 854–863.

J. Mylroie, J. Mylroie, W. Humphreys, D. Brooks, and G. Middleton – Flank margin cave development and tectonic uplift, Cape Range, Australia. *Journal of Cave and Karst Studies*, v. 79, no. 1, p. 35–47. DOI: 10.4311/2015ES0142

FLANK MARGIN CAVE DEVELOPMENT AND TECTONIC UPLIFT, CAPE RANGE, AUSTRALIA

John Mylroie[1], Joan Mylroie[1], William Humphreys[2], Darren Brooks[3], and Greg Middleton[4]

Abstract: Cape Range, Australia, on the northwest coast of the continent at 21° S, 113° E, is a north-northeast-striking anticlinal ridge 315 m high, 130 km long, and 32 km wide extending into the sea and consisting of Miocene carbonate rocks with a series of coastal terraces of Pliocene and Quaternary carbonates and siliciclastic dunes. Inland escarpments, representing former sea cliffs, and deep valleys cutting the limbs of the anticlinal ridge host many cave entrances at a variety of elevations. The lowest unit, the Mandu Formation, a chalky and marly limestone, contains many tafoni (pseudokarst) caves with simple, single-chamber plans and widths up to 15 m or more and height up to 10 m. The higher, purer Miocene limestones and the younger Pliocene and Pleistocene coastal terrace limestones host numerous flank margin caves from 300 m elevation in the Miocene rocks to sea level in the Quaternary rocks. These caves have entrances up to 30 m wide and heights of 6 m, with single-chamber caves being common, but complex caves are also present. Some caves are entered by small entrances that lead to large phreatic chambers, which eliminates both sea cave and tafoni as possible explanations. The close association of these caves with sea cliffs and incised valleys argues against a deep hypogene origin, which would leave a cave pattern unrelated to the surface configuration. Miocene uplift tapered off into the Pliocene. The flank margin caves in the paleo sea cliffs represent the outcome of the interplay of tectonic activity and glacioeustasy over a 300 m vertical range, with lowstands causing valley incision, while highstands raised the fresh-water lens and allowed cave development in the valley walls. Cave development began with the first tectonic-driven subaerial exposure in the Miocene and continued through to the last Pleistocene interglacial.

Introduction

A May 2014 expedition to Cape Range at North West Cape of Australia was conducted to look into what the flank margin caves of Cape Range could reveal about the timing of the uplift of the range and the interaction of that uplift with eustatic sea-level change in the Miocene. These results could be informative about the earliest time for cave generation and put an upper time limit on the colonization of Cape Range caves by troglobitic organisms. The research could also assist in other questions about karst development in an active tectonic setting on a continental margin. This expedition was a reconnaissance designed to provide an overview of cave configuration and setting at Cape Range, with a goal of determining what speleogenetic hypotheses can be constructed for later testing. The interpretations presented here are therefore preliminary and speculative. Much more field data are necessary to derive solid conclusions, and the ideas expressed here will help guide future work.

The Cape Range peninsula, or North West Cape, is located along the northwestern coast of Western Australia, from south latitude 21° 45′ southward to 22° 30′ and from east longitude 113° 30′ to 114° 15′, the largest inhabitation being the town of Exmouth (Fig. 1). Cape Range is bounded by Australia's longest fringing reef, the Ningaloo Reef. The range is constructed of Miocene to Quaternary sedimentary rocks, primarily limestones that have been compressed by tectonics into an anticlinal ridge that forms the axis of the peninsula, striking north-northeast. Cape Range was the location of the first producing oil well discovery, in 1953, in Western Australia, with a further 36 wells being drilled there up through 1995 (Collins et al., 2006). The interest of the petroleum industry in this region has helped produce a series of geological studies (e.g., Crostella, 1996), while more recently tourism has focused interest on biological and ecological studies (e.g., Humphreys, 1993).

Cape Range has a range of monthly average temperatures from 17 to 27 °C, with a maximum temperature of 45 °C frequently occurring in January (Collins et al., 2006). Rainfall is approximately 300 mm annually, and some of the rainfall occurs as single events from cyclones and mid-latitude depressions; but evaporation is 1700 to 3050 mm annually, creating a severe water deficit (Collins et al., 2006). Just prior to this expedition, a catastrophic rainfall event caused major flooding in the area, with destruction of roads, buildings, and bridges.

[1] Department of Geosciences, Mississippi State University, Mississippi State, MS 39762 USA mylroie@geosci.msstate.edu
[2] Western Australian Museum, Collections & Research, Welshpool, WA 6106, Australia; Australian Centre for Evolutionary Biology and Biodiversity, and School of Biological Sciences, the University of Adelaide, SA 5005, Australia; School of Animal Biology, University of Western Australia, 35 Stirling Highway, Crawley, WA 6009, Australia
[3] PO Box 710, Exmouth, WA 6707, Australia
[4] PO Box 269, Sandy Bay, Tasmania 7006, Australia

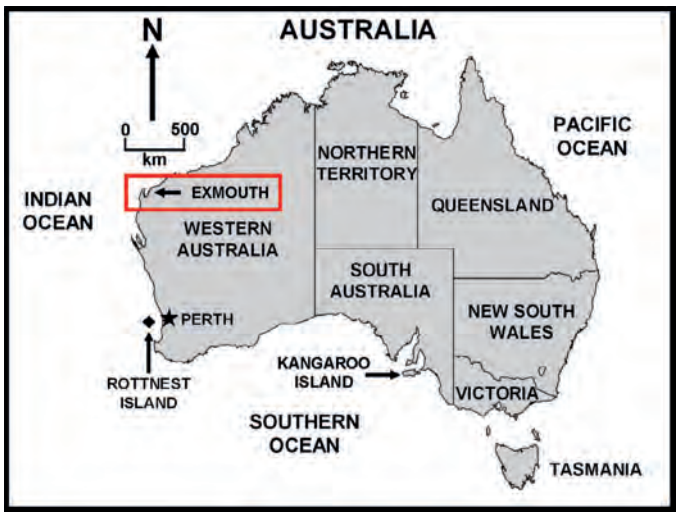

Figure 1. Map of Australia with the location of the Cape Range highlighted.

The Geology of Cape Range

Cape Range and Exmouth Gulf to the east are part of the larger Carnavon Basin, where post-Eocene faulting has resulted in compression and folding of basin sediments (Collins et al., 2006), forming anticlinal ridges and domes separated by synformal lowlands. The Cape Range anticline that forms North West Cape is 130 km long and 32 km wide, with a maximum elevation of 315 m (Whitney and Hengesh, 2015). The ridge is greatly dissected by stream valleys (Fig. 2), which creates significant local relief given the proximity of sea level. The Cape Range anticline is separated from the adjacent Rough Range anticline to the southeast by the Bundegi and Patterson-Learmouth faults (Van de Graaff et al., 1976).

The northward drift of the Australian continent since the Middle Eocene resulted in the deposition of carbonate units in the Cape Range area beginning in the Oligocene, with folding initiated in the Miocene as carbonate deposition continued (Allen, 1993). The geologic section of interest (Fig. 3) follows that of Allen (1993), with late Oligocene to early Miocene limestones resting unconformably on earlier units not exposed at Cape Range. In Cape Range, the lowest exposed unit is the Miocene Mandu Calcarenite (also known as the Mandu Limestone or the Mandu Formation), a chalky to marly calcarenite, calcisiltite, and calcilutite with moderate amounts of quartz and up to 25 % clays, 280 m thick, and deposited in water about 120 m deep (Chaproniere, 1975). The overlying Tulki Limestone is a coarse-grained calcarenitic, muddy foraminiferal packstone, and mud-free grainstone almost 100 m thick, deposited in shallow waters about 12 m in depth (Chaproniere, 1975). The Trealla Limestone overlies the Tulki Limestone, but the actual contact may be difficult to distinguish unless the faunal assemblages are examined; it is 20 m thick (Collins et al., 2006). The unit is most clearly expressed on the east side of Cape Range, whereas on the west side it interfingers with the Pilgramunna Formation, a quartz-rich bioclasitc grainstone 25 m thick (Chaproniere, 1975) that may have formed as a lagoonal barrier to the west (Collins et al., 2006). The final Miocene unit is the Vlaming Sandstone, 65 m thick, a well-sorted calcarenite with significant quartz content (Collins et al., 2006). The Vlaming is restricted to the west side of the range.

Marine-carbonate deposition on the axis of the Cape Range anticline had ceased by the Late Miocene, when uplift created subaerial exposure (Collins et al., 2006), and the subsequent Plio-Pleistocene depositional processes in this area were dominated by eolian sands, both calcitic and quartzose. The margins of the Cape Range anticline accumulated fringing lagoonal deposits, as continued uplift created terraces separated by escarpments (Fig. 4). These terraces are overlain by the Exmouth Sand, a fine- to medium-grained calcarenite with a basal coarse-grained to pebbly quartzose calcarenite and with local coral boundstones unconformable on the terrace below (Collins, et al., 2006). This sequence is interpreted to be a transition from sublittoral to eolian depositional environments, with the Muiron Member and Milyering Member of the Exmouth Sandstone occupying the top and penultimate terraces, respectively (Van de Graaff et al., 1976). The lower two terraces are occupied by the Jurabi (higher) and Tantabiddi (lower) Members of the Bundera Calcarenite and contain extensive coralgal reef deposits (Collins et al., 2006). The Jurabi Member is dominated by coralgal boundstone considered late Pliocene based on the occasional shark's tooth (Wyroll, et al., 1993); the Tantabiddi Member contains lagoonal carbonate gravels and sands and is late Pleistocene (MIS 5e) based on a U/Th age of 132–127 ka (Collins et al, 2006). Whitney and Hengesh (2015) provide a compilation of Western Australia U/Th dates from late Pleistocene fossil reefs and provide an age range of 130–117 ka with a mean age of 123.5 ± 6.5 ka. The Bundera Calcarenite underlies most of the coastal plain that fringes Cape Range. It consists primarily of calcarenite to calcirudite with coralgal reef deposits. The Mowbowra Conglomerate Member of the Bundera Calcarenite is a limestone pebble conglomerate (locally a fanglomerate) that contains minor coralgal reef deposits and well-sorted calcarenite. It forms an extensive veneer over the lower terraces and hosts unusual karren (Fig. 5), indicating that surficial denudation by karst processes has lowered the land surface. Whitney and Hengesh (2015) indicate that tectonic movement is still active at Cape Range, with both uplift and subsidence occurring, with respective ranges of 0.049 ± 0.030 mm yr^{-1} for uplift locations and –0.013 ± 0.034 mm yr^{-1} for subsidence locations. As they assumed no karst denudation, which would place the dated corals at a higher elevation than measured today when first emergent, these estimates are therefore a minimum value. While denudation rates for uplifted MIS 5e coral terraces on Guam have been measured at 0.064 mm yr^{-1} (Miklavič et al., 2012), Guam is a moist tropical island. Cape

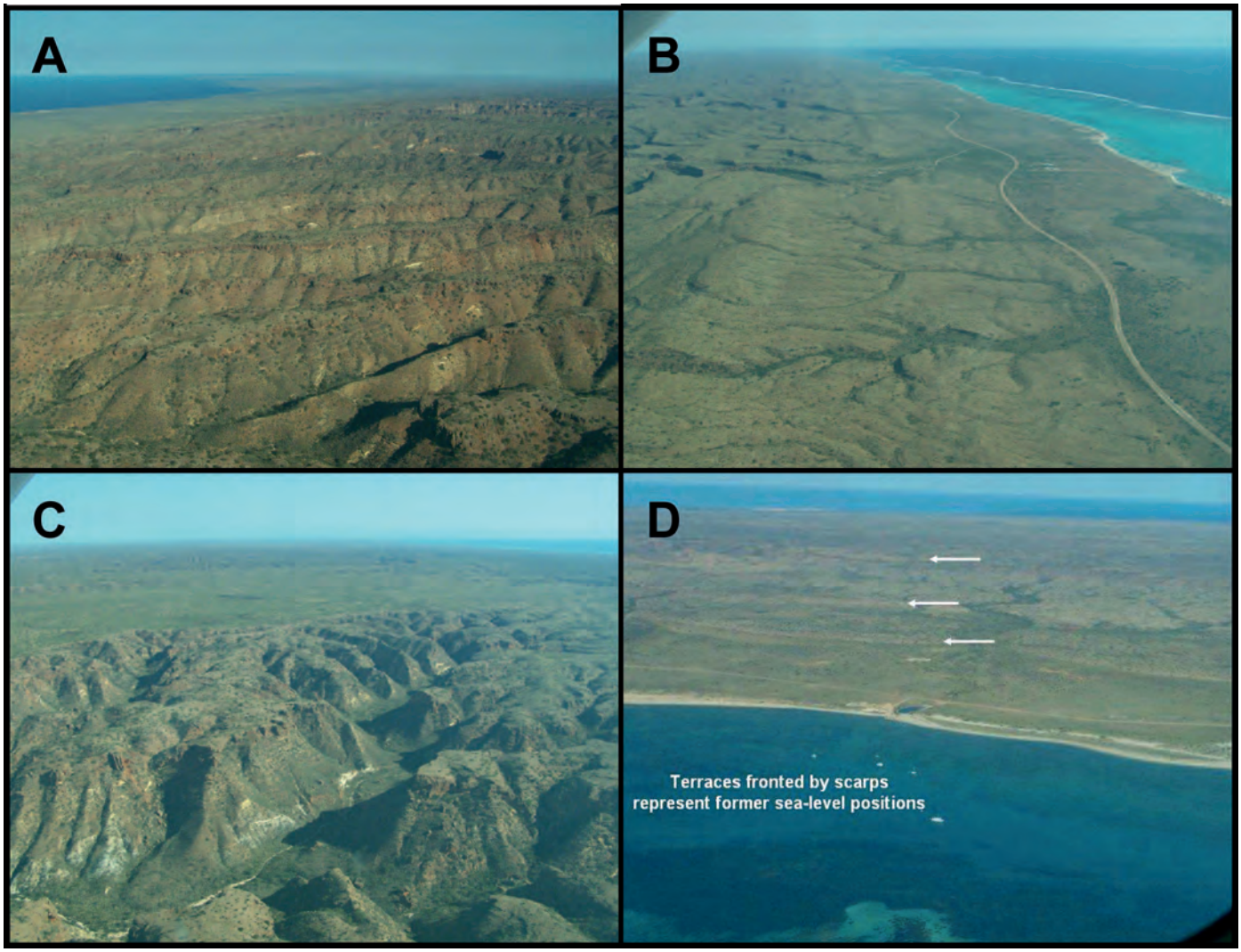

Figure 2. Low-altitude aerial photographs of the Cape-Range peninsula. A. Looking south along the east coast of the range, with the gentle anticline rising to the crest at the right side of the image. B. Looking south along the west coast of the range, with the gentle anticline rising to the crest at the left side of the image; note also the terraces. C. Closer image of the deep stream-valley incisions into the anticline. D. View eastward across the peninsula, with terraces and their associated scarps indicated by white arrows.

Range is an arid environment with a negative water budget, so denudation rates would be expected to be much less.

The Cave Question

The existence of epigenic stream caves in Cape Range is well established, and caves with lengths of multiple kilometers and depths over 100 m exist (e.g., Brooks, 2009; Fig. 6). However, these caves are quite cryptic, with vertical entrances commonly not in agreement with current landscape topography. Most obvious to the casual observer are the many cave entrances in the cliffs fronting the sea on the east and west sides of the peninsula and within the walls of valleys and gorges that drain the anticlinal ridge that forms Cape Range (Fig. 7). These caves appear to be of two types (Fig. 8), tafoni, pseudokarst caves formed by wind and subaerial weathering (Owen, 2013), and flank margin caves, formed in a discharging fresh-water lens (Mylroie, 2013). Superficially, both cave types look similar, having entrances that are usually wider than they are high and being a single, open chamber. However, tafoni usually have a maximum interior width that is little more than the entrance width and rarely have more than a single, simple chamber (Waterstrat et al., 2010; Owen 2013). Their configuration reflects their origin from the outside in by surficial processes. The existing caves could also be sea or littoral caves, formed by wave action against a rocky shore. Sea caves are also formed by an outside in mechanism similar to that forming tafoni. As a result, the entrance width and maximum width tend to be similar, and the interior

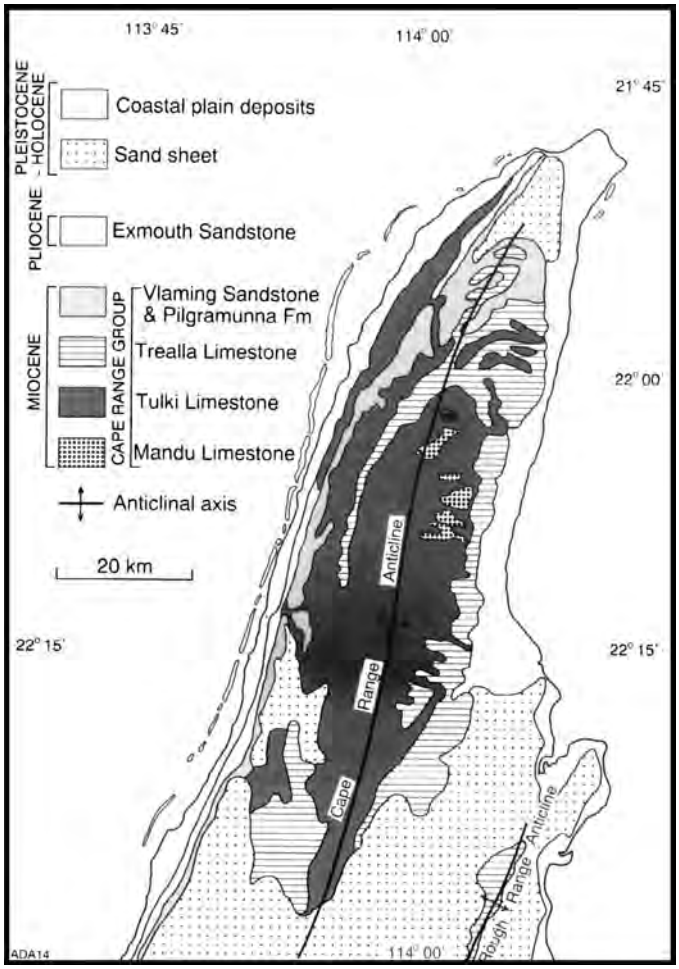

Figure 3. Geologic map of the Cape Range, showing the Miocene carbonate units and the anticline that forms the range. From Allen (1993).

morphology is simple compared to true karst caves, lacking dissolutional cusps, thin bedrock pillars and partitions, and complex passage connections. Waterstrat et al., (2010) discuss in detail the criteria for separating sea caves and tafoni from flank margin caves. Sea caves are tied to the exterior of the rock mass they form in, derived from the interplay of wave dynamics, tidal activity, and the rock's mechanical characteristics. As a result, once uplifted, sea caves are more vulnerable to removal by surface erosion than are flank margin caves, which are initially not exposed. It is unlikely that the caves of the narrow interior gorges are sea caves, as wave energy dynamics in such an enclosed water body most likely would not produce the necessary mechanical erosion forces required for sea-cave development.

Flank margin caves commonly have more elaborate chamber patterns and can be a series of chambers, only one of which may connect to the outside (Fig. 9). Entrances can be very small, leading to chambers with elaborate phreatic sculpturing, including wall pockets and cusps, bedrock pendants and arches, and oval side passages called *rimouts* (Fig. 10). Because flank margin caves form in the discharging margin of the fresh-water lens, under the flank of the enclosing landmass (hence the name), they are very vulnerable to breaching by surficial erosion processes. This mechanism also means that the caves form from the inside out. As scarp or slope retreat occurs, the caves are first tangentially intersected to form a small entrance. As scarp and slope retreat continue, the entire outer wall of the cave may be removed, creating a chamber with an entrance width close to that of the maximum chamber width. Such a large entrance allows external weathering processes to influence the cave interior. In this manner, flank margin caves can decay into apparent tafoni by this overprinting action, confusing the observer as to the true origin of the cave. In active coastal regions, breaching of flank margin caves by marine processes can also lead to overprinting to produce a hybrid cave (*sensu* Kambesis and Machel, 2013). A fractal analysis of cave types (Kambesis et al., 2015a) has demonstrated that caves of epigene, hypogene, flank margin, tafoni, and littoral origin can be separated from each other by analysis of their fractal dimension and lacunarity as provided by cave maps.

In the Cape Range, the tafoni appear to be lithologically biased, being formed mostly in the Miocene Mandu Formation, a marl that underlies purer limestones higher in the section. Those upper limestones, primarily the Tulki Limestone across the range and, above it, the Pilmagrunna Limestone on the west side and the Trealla Limestone on the east side, host what appear to be primarily flank margin caves and only a few tafoni. The Mandu Formation also appears to host a few flank margin caves (e.g., Fig. 7D); its marly characteristics make it an aquitard, and springs are perched on its upper contact with the Tulki Limestone. Dissolution caves of indeterminate origin also underlie the coastal plain on both sides of the Cape Range, some developed in Quaternary limestones.

Flank margin caves are found on the cliffs of the incised valleys and in the cliffs that front each of the coastal terraces (Fig. 2). From top to bottom, the caves are found fronting the Muiron Terrace, the Milyering Terrace, the Jurabi Terrace, and the Tantabiddi Terrace (Fig. 4).

Flank Margin Cave Origin in Cape Range

The morphology of the dissolution caves in the paleo sea cliffs and gorge walls of Cape Range indicates that most are undoubtedly phreatic in origin. They are almost certainly not epigene caves, having no conduit-flow pattern, wall scallops, or fluvial sediments and lacking a clear higher-elevation input to lower-elevation output plan. This exclusion of an epigene origin leaves two possibilities. First, the caves could be classic hypogene caves formed at depth by aggressive fluids in a laminar-flow system and now uplifted and breached by surface processes. Or they could be flank margin caves, and a fresh-water lens laminar-flow discharge produced the caves, formed when sea level was at the elevations where the caves are now

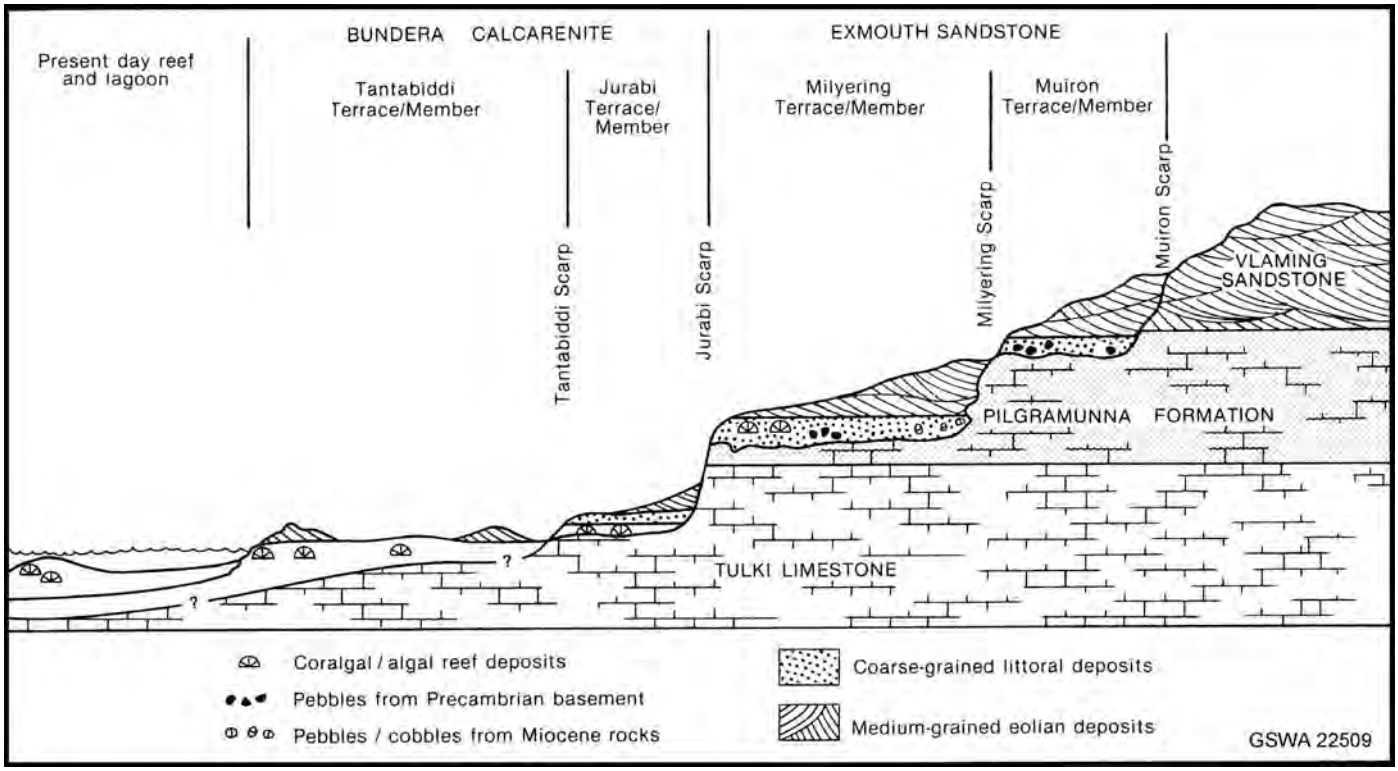

Figure 4. Depiction of the terraces and scarps on the west side of Cape Range, with Quaternary units stacked on terraces cut into the Miocene limestones. Vertical range displayed is approximately 110 m. From Van de Graaff et al. (1976).

found or perhaps at lower elevations from which they have been uplifted to their present position.

If the caves are hypogene in origin, their current expression on the cliffs and gorge walls is an accident of random intersection by surficial processes. If they are flank margin in origin, tied to the flank of the land, then the cave distribution should be controlled by the orientation of that flank, be it a paleo sea cliff fronting a coastal terrace or a gorge wall. The field work of the expedition indicates that the caves exist in a pattern that reflects the cliffed environment in which they are found. The long axis of the cave is almost always parallel to the cliff in which they are located (a few exceptions do exist, such as Adit Cave). Hypogene caves should follow a regional joint trend and be independent of the sea-cliff and gorge-axis directions, except to the degree to which jointing controls those features. Hypogene caves should have their long axis either at random or along the regional joint set. The caves in the cliffs do not show any secondary indicators of hypogene development, such as residual native sulfur, gypsum, or calcite spar wall coatings.

If one eliminates pseudokarst tafoni and sea caves and also eliminates epigene and hypogene caves, only flank margin caves remain. The observed caves contain all the features associated with flank margin caves. The Cape Range flank margin caves are not as individually extensive as those found in other well-known flank margin cave settings, such as the Bahamas (Mylroie and Mylroie, 2009a) or Isla de Mona (Frank et al., 1996). Cave chambers in the Cape Range can be large, 30 m or more long in the cliff-parallel axis and 15 m or more deep into the cliff, with ceiling heights up to 6 m, but the caves are usually not complex chamber associations with numerous passage interconnections. Large but simple flank margin cave patterns are associated with limited lens stability time, meaning that as the caves were forming, sea level changed and the cave is either abandoned if sea level dropped or flooded by non-speleogenetic marine water if sea level rose. This type of flank margin cave development is observed in the Mariana Islands (Jenson, et al., 2006), Barbados (Kambesis and Machel, 2013), Curaçao (Kambesis et al., 2015b), Kangaroo Island, Australia (Mylroie and Mylroie, 2009b), and in Mallorca island (Mylroie, et al., 2015), areas with active tectonics. Flank margin cave development as a result of tectonic influence on a passive continental coast has been presented for the Naracoorte karst area in Southeastern Australia (White and Webb, 2015).

The flank margin caves in Cape Range with the greatest degree of passage complexity are found at lower elevations, in what appear to be paleo coastal positions. There are two explanations. One is that the sea level was stable for longer periods of time at the lower elevations and the increase in lens-stability time allowed a longer duration for flank margin caves to mature. This longer stability time would be consistent with a decreasing tectonic uplift rate, given that uplift is believed to have been completed by the Pliocene (Wyrwoll, et

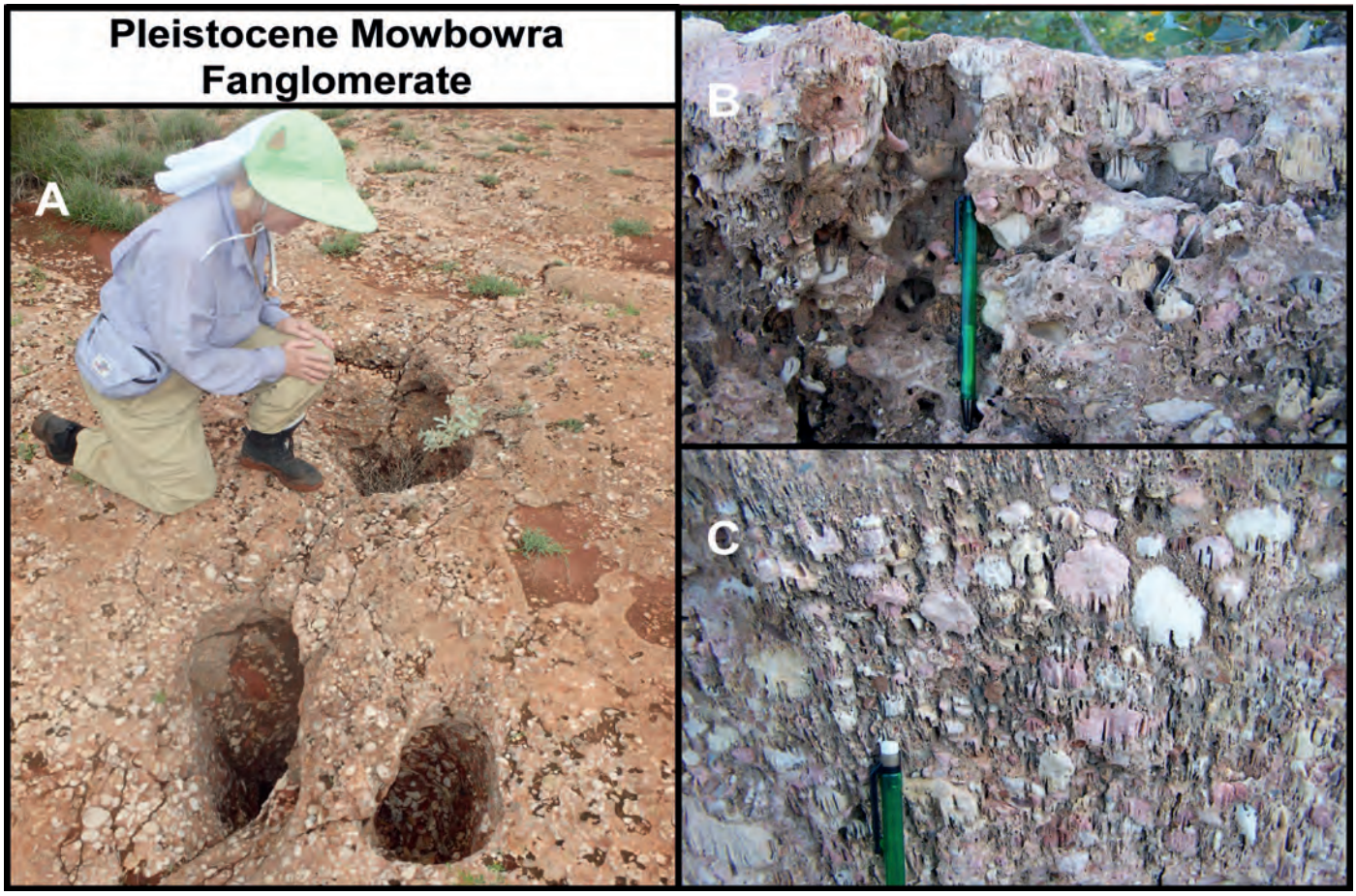

Figure 5. Karren in the Pleistocene Mowbowra Fanglomerate, east side of the Cape Range. Both the clasts and matrix are dominated by carbonates. A. Dissolution holes that cut through both clasts and matrix. B. Vertical ledge showing the variety of clasts (pencil 14 cm long for scale). C. Close-up of the unusual dissolution pattern produced in the carbonate clasts (pencil as in B for scale). The amount of dissolution shown is an indication that karst denudation has been significant, even in relatively young Pleistocene deposits.

al., 1993), or if it has continued (Whitney and Hengesh, 2015) it has done so at a slow rate. The second explanation is that the high-level caves in the gorges are older, more degraded by surficial erosion, and have lost some of their original length and complexity; in their original state they would have been similar to the lower elevation paleo sea cliff caves. The observed configuration of the higher-elevation caves would, however, indicate that the main chambers observed today are the original chambers and that there has been little loss of cave complexity. If correct, this observation indicates that lens-stability time varied, being shorter for older, high-elevation caves and longer for younger, low-elevation caves, consistent with a declining tectonic uplift rate.

Flank Margin Cave Genesis and Cape Range Geologic History

Accepting for the moment that the observed caves in the purer limestones (i.e., excluding the Mandu Formation) are flank margin caves, then what is the scenario that would allow their development on both the paleo sea cliffs and gorge walls? The paleo sea-cliff position is easy to explain. As the limestones of Cape Range were exposed subaerially, meteoric catchment and establishment of a fresh-water lens could occur. Once the lens was established, it discharged to the sea, and flank margin caves could form. As uplift continued or sea level fell eustatically, the initial suite of flank margin caves would be abandoned, and new ones would form at a lower level within the limestones. This model works well to explain flank margin caves on tectonically uplifted islands around the world, such as Barbados, Curaçao, Guam, and Mallorca, as noted earlier.

The situation for flank margin caves found in the gorge walls deep into the interior of Cape Range is more problematic. Recently, a model to explain gullies on Barbados, *bokas* on Curaçao, and *calas* on Mallorca, all cliffed rectilinear re-entrants in coastal limestones, has been developed (Mylroie, 2013). The basic model argues that if

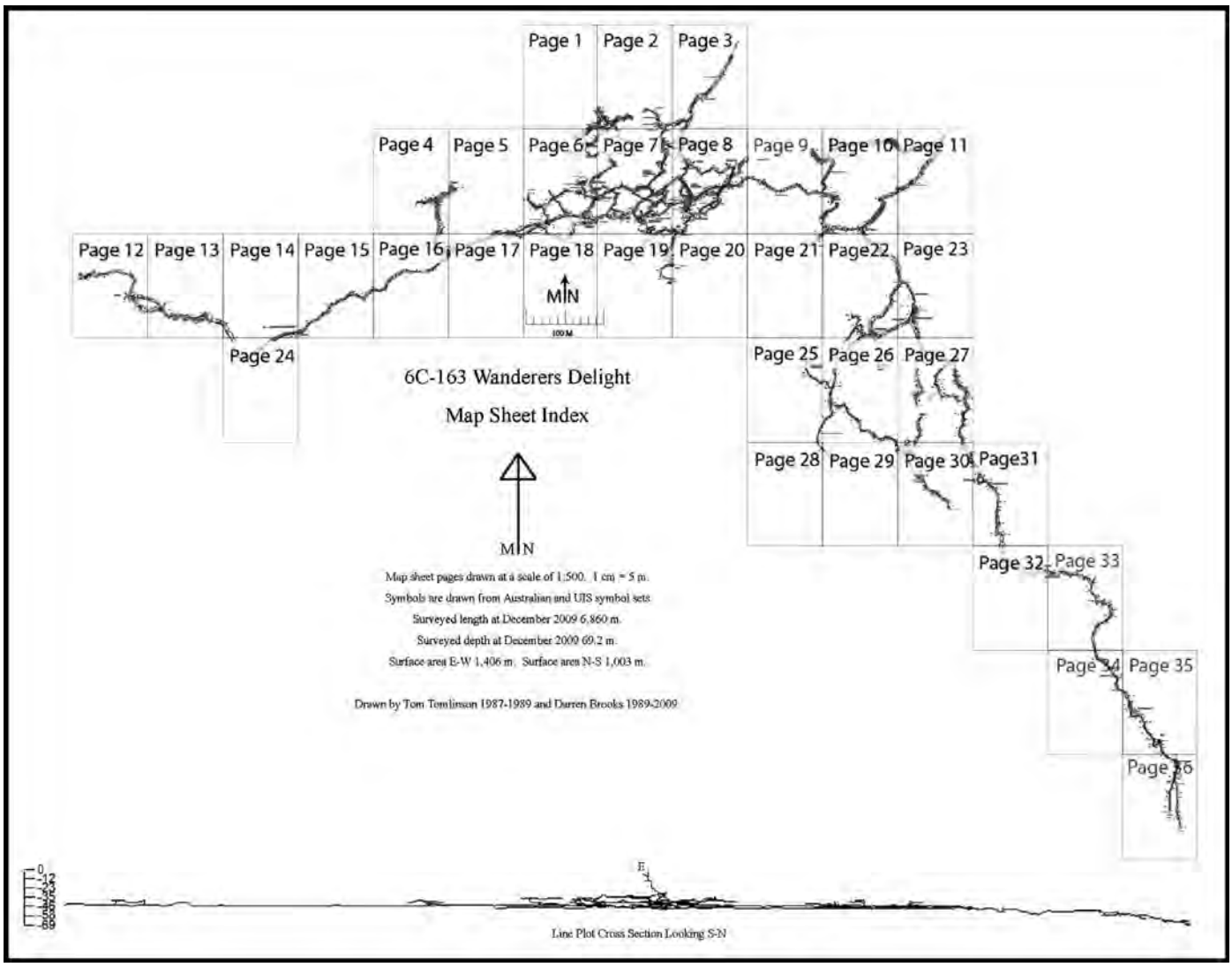

Figure 6. Map of Wanderers Delight, an epigenic stream cave 6.86 km long and 69 m deep. From Brooks (2009).

there is a sea-level fall on a carbonate coast, inland overland flow will cut valleys into the coastal limestones. If sea level rises, these valleys become invaded by marine water, and the valley walls become sites for flank margin cave development. The islands listed above all share a history of tectonic uplift associated with glacioeustasy. This condition guarantees that coastal valleys will be cut and later invaded by marine water. Applying this model to the Cape Range indicates that initial uplift would produce a subaerial landmass, allowing development of a fresh-water lens, but also allowing for surface flow and valley incision. Continued uplift would allow deeper valley incision. A subsequent eustatic sea-level rise would flood those valleys and create the fresh-water lens discharge necessary for flank margin cave development in those valley walls. Because uplift is episodic but continuous over the long term and Miocene glacioeustasy (Fig. 11) was an overprint on that uplift, the stability period of the fresh-water lens could be expected to be short, so that caves of high complexity did not have time to develop. On Barbados, the presence of dense calcite vadose speleothems such as stalactites, stalagmites, and flowstone on the walls of gullies was initially interpreted to indicate that the gullies themselves were collapsed epigenic stream caves (Kambesis and Machel, 2013). However, the width of some of those gullies was too great to have supported such a cave passage. The speleothems have since been interpreted as having grown in the caves after the marine invasion and been exposed in the gully walls by relatively minor wall retreat. (Kambesis and Machel, 2013). The deep, wide gorges of the Cape Range are far too large to have been a single cave-stream passage, and speleothems present are commonly associated with flank margin caves in the gorge walls. Figure 12 presents a model of valley invasion by marine waters, subsequent flank margin cave formation, and cave degradation.

One of the hallmarks of flank margin cave development is the presence of a series of chambers, all at a single elevation.

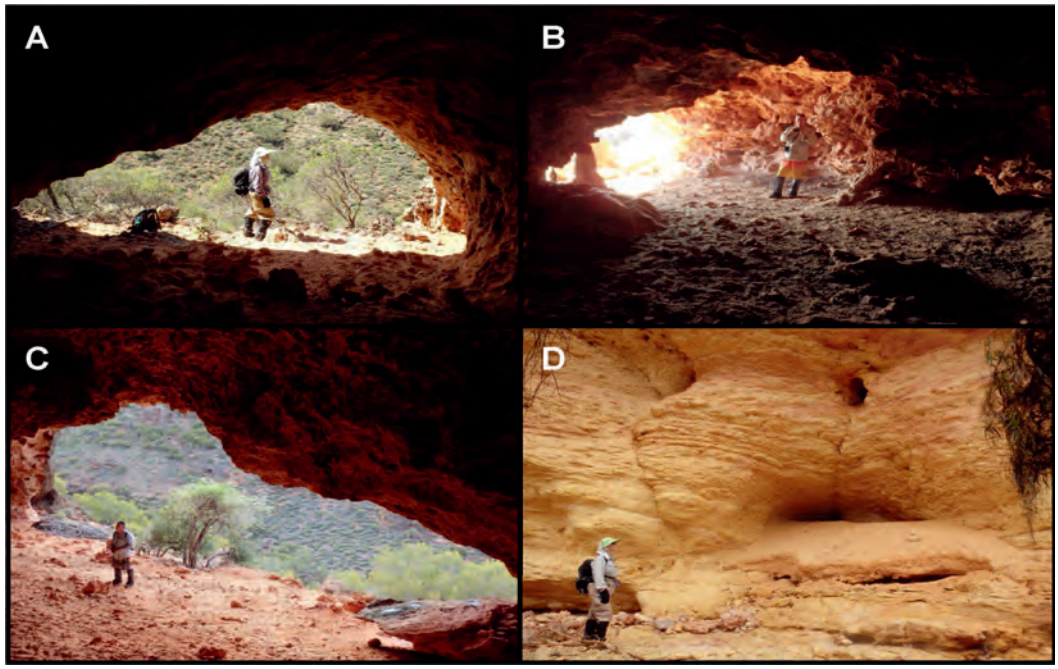

Figure 7. Flank margin caves of the Cape Range. A–C. Typical flank margin caves with entrances high on the valley wall in the Tulki Limestone. D. Small dissolution caves, much modified by tafoni processes, Mandu Formation. Note that the dissolution passages occupy joints, consistent with the Mandu Formation's aquitard character.

This line of caves has been called beads-on-a-string, and it reflects the sea level, and hence lens position, at the time of cave development (Mylroie, 2013). Such lines of flank margin caves are commonly found as multiple horizons on tectonically active islands, each line representing a sea-level position. At Cape Range, the caves are commonly a series of chambers along a common line, but in many places that line appears to be tilted. This tilt may follow the dip of the beds at 3 to 8 degrees on the west side of Cape Range, and 3 to 6 degrees on the east side (Whitney and Hengesh, 2015). This situation could indicate cave development prior to continued folding of the anticline, and an original straight line of caves could now be bent as a result of the subsequent folding and uplift. Alternatively, cave development could be favored at a specific stratigraphic horizon, perhaps a bed of higher rock solubility, and as dropping sea level "slid" down the limb of the anticline, caves were developed in the same bed at progressively lower elevations. Finally, valley incision could have progressed into the distal portions of the anticlinal limbs as uplift continued, and when the valley was invaded to a

Figure 8. Flank margin cave, at X, in the Tulki Limestone. Shallower, broader openings below the flank margin cave are tafoni developed in the Mandu Formation.

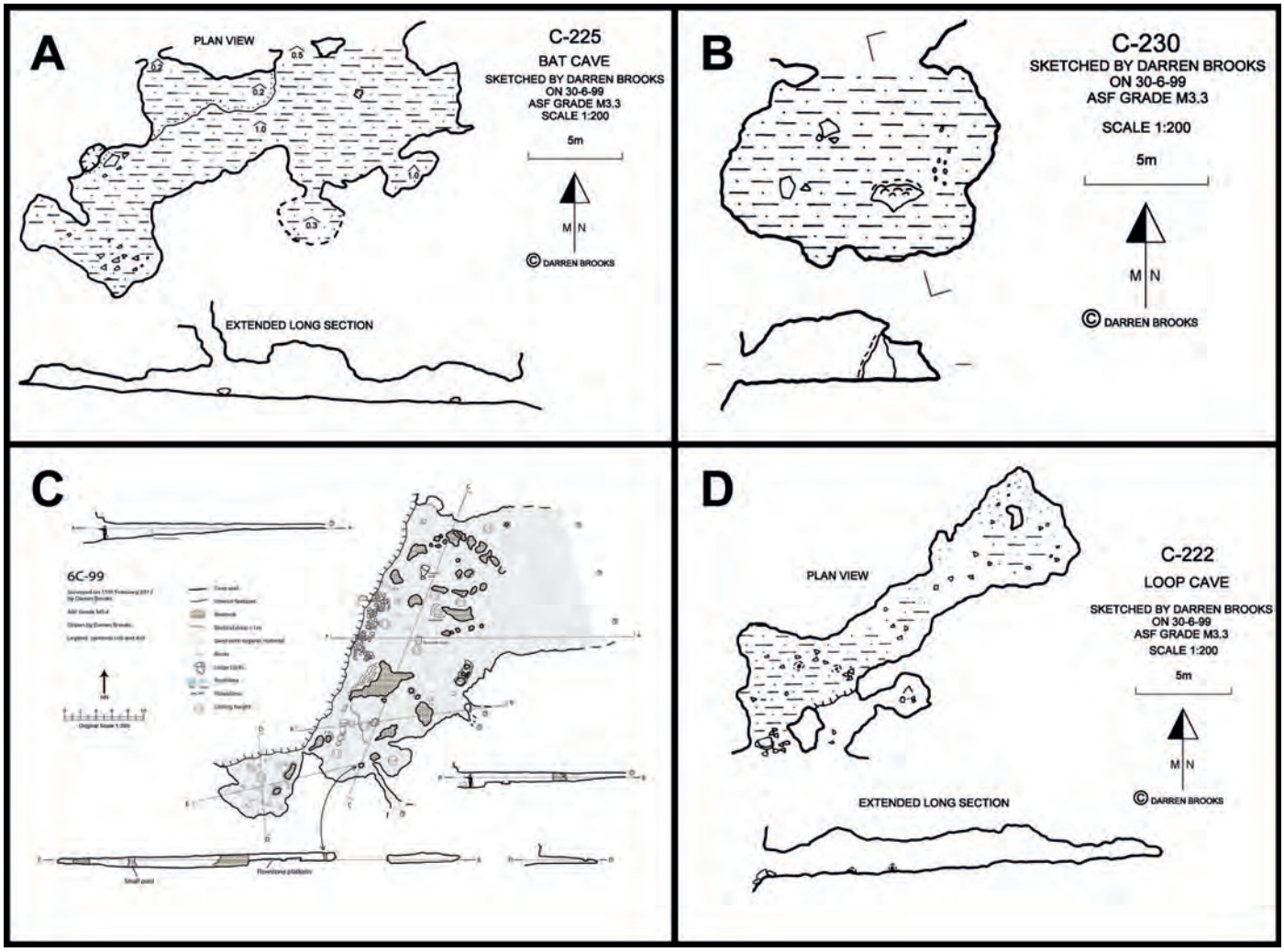

Figure 9. Maps of four flank margin caves in the Cape Range. A. Flank margin cave with multiple entrances and some chamber complexity. B. Simple flank margin cave with one entrance. C. Complex flank margin cave with numerous bedrock pillars subdividing the chambers. D. Flank margin cave with two small entrances leading into large chambers.

small degree during each sea level rise, it did so progressively farther away from the anticlinal axis, displacing cave development to only that portion of the valley that was flooded.

An important question regarding the model of marine water invading incised valleys during a transgression is: Where are the marine deposits that should be associated with that transgression? While one could expect to see fossil corals attached to valley walls, the amount of cliff and slope retreat necessary to expose the existing flank margin caves to the degree seen today would have removed any coastal or bioerosion notches, sea caves or fossil deposits, and similar features associated with a cliffed rocky coast (Waterstrat et al., 2010). It is possible that some of the fossil corals found in the Mowbowra Conglomerate are material representing corals deposited on, and then erosionally removed from, the paleo-cliff line after a drop in sea level.

Testing Flank Margin Cave Development

The determination of how, and perhaps more importantly when, the flank margin caves of the Cape Range formed requires detailed data collection and analysis. A representative sample of the caves need to be mapped. That mapping has to establish cave elevation, long-axis orientation, and long-axis inclination. The cave map subsequently needs to be analyzed to create entrance width to maximum width ratios (EW/MW), and area to perimeter (A/P) ratios. From these results the data set can be compared to those from tafoni to demonstrate that both cave types exist; A versus P is especially good at this determination (see Waterstrat et al., 2010). The long axis orientation data can be analyzed to see if the long axis faithfully follows the valley wall's orientation and can also be compared to the regional joint sets' orientations to see if there is any correlation. As gorge-wall orientation will be influenced by preexisting joint sets, differentiating cave orientation

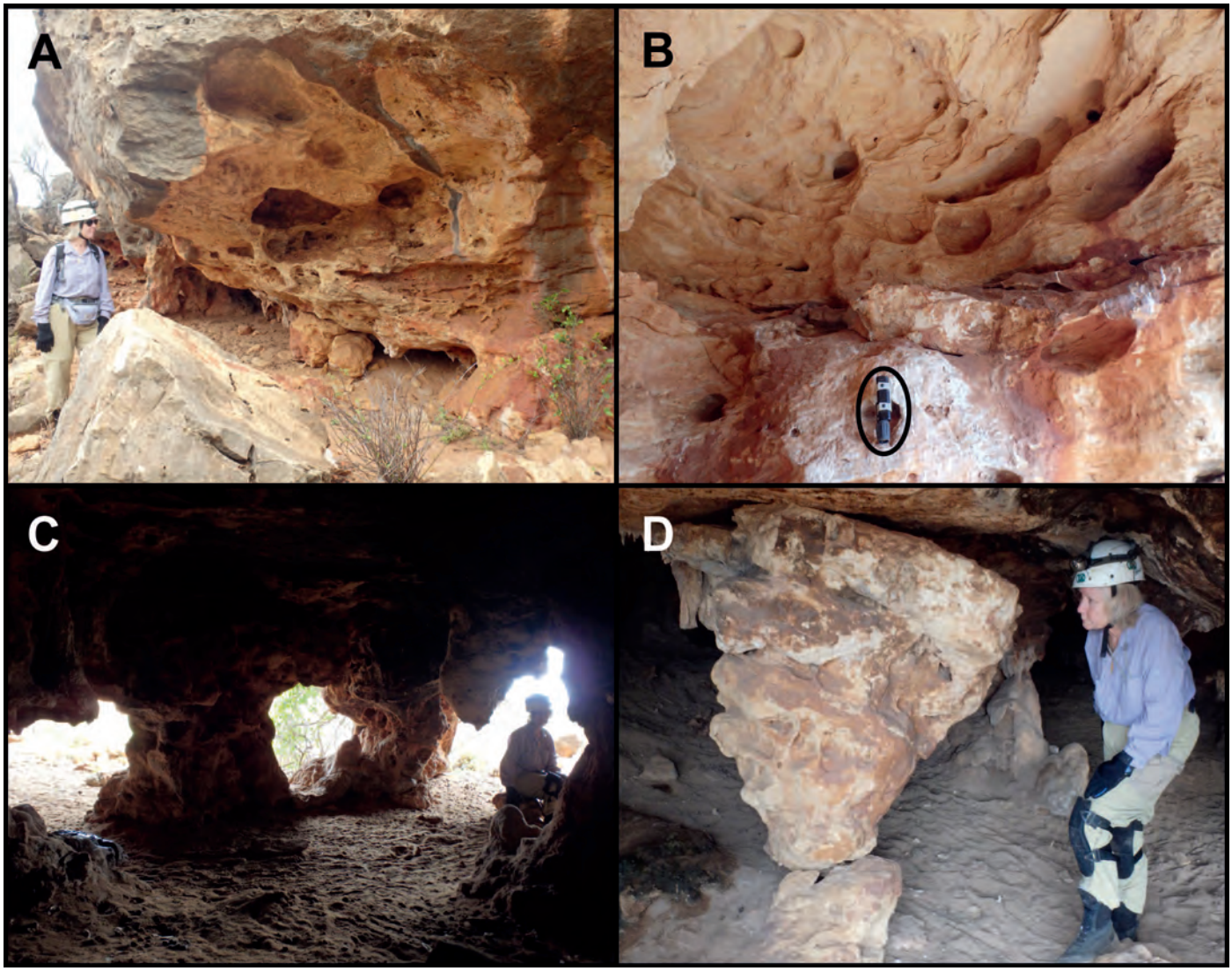

Figure 10. Speleogens in Cape Range flank margin caves. A and B. Dissolution pockets and rimouts (flashlight in circle in B 15 cm long for scale). C. Remnant bedrock pillars. D. Remnant bedrock pillar slowly disarticulating from the roof and floor. It is known as the Tornado.

produced by flow along joints in the hypogene condition from more recent flank margin caves produced by joint-controlled cliff orientation may be difficult. The cave elevation data will help determine if there is any correlation between true horizontality and position on the anticlinal limbs. The cave inclination data can detect whether the caves follow the bedding or cross it; if the caves cross bedding, it is an indicator of horizontal control independent of bedding, such as control by the fresh-water lens margin. In many places there are definite horizons of cave development on the walls of the gorges. The site-specific vertical separation of these horizons needs to be determined. If there is always a set difference in vertical separation between two cave horizons, then they probably formed as horizontal lines of caves. Any elevation disparities between widely spaced sites would then be due to later folding.

Summary

The caves on the paleo sea cliffs on the east and west sides of the Cape Range and the caves found in the deep gorges draining the range are flank margin caves when the caves are located in the Tulki or overlying limestones. The Mandu Formation contains primarily tafoni. The younger Pliocene and Pleistocene terrace limestones also host numerous flank margin caves. The flank margin caves at high elevations are very old, concurrent with the uplift and initial Miocene subaerial exposure of the Cape Range. As rapid uplift is thought to have ended in the Pliocene, even the lower-elevation flank margin caves in the gorges are likely Late Miocene in age, but those in the Jurabi Terrace are Pliocene in age, and those in the Tantabiddi Terrace are late Pleistocene in age. Cave development continued as the Quaternary carbon-

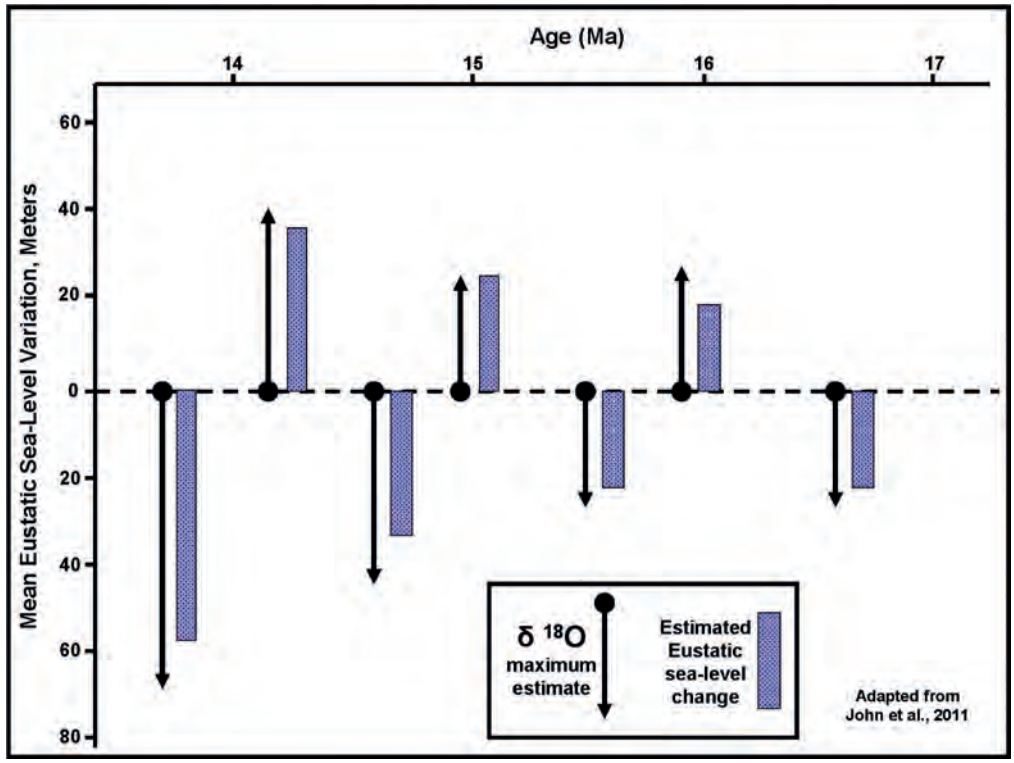

Figure 11. Australian Miocene eustatic sea-level curve adapted from John et al. (2011). The rising sea level was more than sufficient to flood valleys in the Cape Range during uplift in the Miocene.

ates were deposited and subjected to glacioeustasy and slower rates of tectonic movement.

The flank margin caves in the Cape Range gorges and valleys developed as a result of a complex interplay between tectonic uplift and Miocene glacioeustasy. Some of the caves may have developed while folding was still occurring, and their original speleogenetic position altered as a result. Following the Pliocene, cave development position was solely controlled by the high-amplitude, short-wavelength glacioeustasy of the Pleistocene with a minor tectonic overprint.

Acknowledgements

The authors thank two anonymous reviewers for comments that improved the manuscript. We also thank Mississippi State University for the sabbatical granted to John Mylroie and Exxon Mobil for logistical support. Field work was funded by the Western Australian Museum.

References

Allen, A.D., 1993, Outline of the geology and hydrogeology of Cape Range, Carnarvon Basin, Western Australia, *in* Humphreys, W. F., ed., The biogeography of Cape Range, Western Australia: Records of the Western Australian Museum, Supplement No. 45, p. 25–38.

Brooks, D., 2009, The Longest Crawl. A chronological history, and description, of Wanderers Delight 6C-163: The Western Caver, v. 49, p.74–128.

Chaproniere, G.C.H. ., 1975, Palaeoecology of Oligo-Miocene larger Foraminiferida, Australia. Alcheringa, v. 1, p. 37–58. doi:10.1080/03115517508619479.

Collins, L.B., Shu, Z.R., McNamara, K.J., and Wood, D., 2006, Evolution of the Tertiary to Quaternary carbonates of the Cape Range region and Ningaloo Reef. Northwest Australia. Excursion Guide for the INQUA Conference, Exmouth, Australia: Curtin University of Technology, 72 p.

Crostella, A., 1996, Hydrocarbon potential of the North West Cape area, Carnarvon Basin: PESA Journal, no. 24, p 15–34.

Humphreys, W.F., ed., 1993, The Biogeography of Cape Range, Western Australia. Records of the Western Australian Museum, Supplement No. 45, 258 p.

Jenson, J.W., Keel, T.M., Mylroie, J.R., Mylroie, J.E., Stafford, K.W. Taborosi, D., and Wexel, C., 2006, Karst of the Mariana Islands: The interaction of tectonics, glacioeustasy and fresh-water/sea-water mixing in island carbonates: Geological Society of America Special Paper 404, p. 129-138.

John, C.M., Karner, G.D., Browning, E., Leckie, R.M., Matero, Z., Carson, B., and Lowery, C., 2011, Timing and magnitude of Miocene eustasy from the mixed siliciclastic stratigraphic record of the northeastern Australian margin: Earth and Planetary Science Letters, v. 304, p. 455–467. https://doi.org/10.1016/j.epsl.2011.02.013.

Kambesis, P.N., and Machel, H.G., 2013, Caves and karst of Barbados, *in* Lace, M.J., and Mylroie, J.E., eds., Coastal Karst Landforms: Dordrecht, Springer, Coastal Research Library 5, p.227–244. https://doi.org/ doi:10.1007/978-94-007-5016-6 10.

Kambesis, P.N., Larson, E.B., and Mylroie, J.E., 2015a, Morphometric analysis of cave patterns using fractal indices, *in* Feinberg, J., Gao, Yongli, and Alexander, E.C., Jr., eds., Caves and Karst Across Time: Geological Society of America Special Paper 516, p. 67–86. https://doi.org/10.1130/2015.2516(06).

Kambesis, P.N., Mylroie, J.R., Mylroie, J.E., Larson, E.B., Owen-Nagel, A.M., and Sumrall, J.B., 2015b, Influence of karst denudation on the northwest coast of Curaçao, *in* Glumac, B. and Savarese, M., eds., Proceedings of the 16th Symposium on the Geology of the Bahamas and other Carbonate Regions: San Salvador, Gerace Research Centre, p. 200–212.

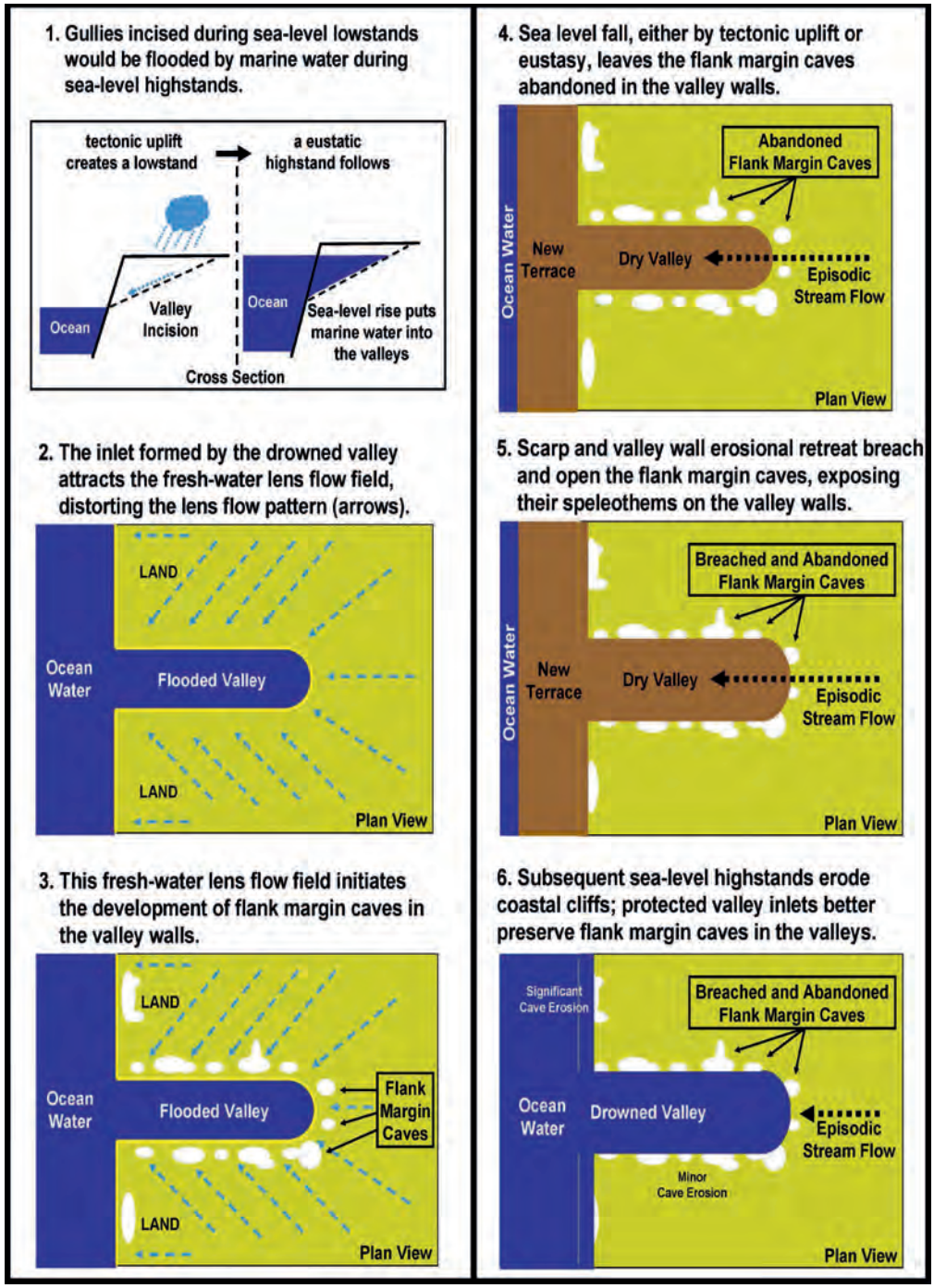

Figure 12. Six-panel cartoon demonstrating the valley-incision to valley-flooding model for developing flank margin caves in incised valleys of the Cape Range during the Miocene.

Miklavič, B., Mylroie, J.E., Jenson, .JW., Randall, R.H., Banner, J.L., and Partin, J.W., 2012, Evidence of the sea-level change since MSI 5e on Guam, tropical west Pacific: Studia Universitatis Babeş-Bolyai, Geology, Special Issue 2012, 30–32.

Mylroie, J.E., and Mylroie J. R., 2009a, Caves and Karst of the Bahamas, *in* Palmer, A.N. and Palmer, M.V., eds., Caves and Karst of the USA. National Speleological Society, Huntsville, Alabama, p. 348-353.

Mylroie, J.E., and Mylroie, J.R., 2009b, Caves as geologic indicators, Kangaroo Island, Australia: Journal of Cave and Karst Studies, v. 71, no. 1, p. 32–47.

Mylroie, J.E., 2013, Coastal karst development in carbonate rocks, *in* Lace, M.J., and Mylroie, J.E., eds., Coastal Karst Landforms: Dordrecht, Springer, Coastal Research Library 5, p. 77–109. https://doi.org/10.1007/978-94-007-5016-6 4.

Mylroie, J.E., Kambesis, P.N., Owen-Nagel, A.M., Sumrall, J.B., Larson, E.B., Mylroie, J.R., and Lace, M.J., 2015, Flank margin cave development at Cala Pi and Cala Figuera, Mallorca Island, Spain, *in* Glumac, B. and Savarese, M., eds., Proceedings of the 16th Symposium on the Geology of the Bahamas and other Carbonate Regions: San Salvador, Gerace Research Centre, p. 213–221.

Owen, A.M., 2013, Tafoni development in the Bahamas, *in* Lace, M.J., and Mylroie, J.E., eds., Coastal Karst Landforms: Dordrecht, Springer, Coastal Research Library 5, p. 177–205. https://doi.org/10.1007/978-94-007-5016-6 8.

Van de Graaff, W.J.E., Denman, P.D., and Hocking, R.M., 1976,. Emerged Pleistocene marine terraces on the Cape Range. Western Australia: Annual report of the Geological Survey Branch of the Mines Department for the year 1975, p. 62–69.

Waterstrat, W.J., Mylroie, J.E., Owen, A.M., and Mylroie, J.R., 2010, Coastal caves in Bahamian eolian calcarenites: Differentiating between sea caves and flank margin caves using quantitative morphology: Journal of Cave and Karst Studies, v. 72, p. 61–74. https://doi.org/10.4311/jcks2009es0086.

White, S., and Webb, J.A., 2015,. The influence of tectonics on flank margin cave formation on a passive continental margin: Naracoorte, Southeastern Australia: Geomorphology, v. 229, p. 58–72. https://doi.org/10.1016/j.geomorph.2014.09.003.

Whitney, B.B., and Hengesh, J.V., 2015, Geomorphological evidence for late Quaternary tectonic deformation of the Cape Region, coastal west central Australia: Geomorphology, v. 241, p. 160–174. https://doi.org/10.1016/j.geomorph.2015.04.010.

Wyrwoll, K-H., Kendrick, G.W., and Long, J.A., 1993, The geomorphology and Late Cenozoic geomorphological evolution of the Cape Range-Exmouth Gulf region, *in* Humphreys, W.F., ed., 1993, The Biogeography of Cape Range, Western Australia: Records of the Western Australian Museum, Supplement No. 45, p. 1–23

A. Rezaei, H. Karimi, and H. Zhan – The importance of understanding the hydrogeology and geochemistry of karst terrains for safely siting dams. *Journal of Cave and Karst Studies*, v. 79, no. 1, p. 48–58. DOI: 10.4311/2016ES0121

THE IMPORTANCE OF UNDERSTANDING THE HYDROGEOLOGY AND GEOCHEMISTRY OF KARST TERRAINS FOR SAFELY SITING DAMS

Abolfazl Rezaei[1,2], Haji Karimi[3,*], Hongbin Zhan[4]

Abstract: Dam site selection in karst regions is an extremely important issue in terms of dam safety and environmental impact. Groundwater in a karst aquifer near a selected dam site is deemed to be impacted greatly by the dam. This study uses the Kangir Reservoir of Iran as an example to illustrate the interrelationships of karst-groundwater condition, lithology of the dam reservoir, future climate changes, and overexploitation of water resources in the area. This study conducted a comprehensive analysis of water balance, groundwater flow, hydrochemistry, characteristics of geologic formations with respect to the quantity and quality of water, distribution of karst and evaporative formations in the catchment, and tectonic setting to highlight the importance of hydrogeological conditions on the water quality and quantity of the Kangir Reservoir. The main findings include, first, a major part of the highland karst aquifer in the Asmari Formation within the dam catchment does not drain into the dam reservoir. Instead, it leaks into the downstream Siahgel Region of the dam mainly along the Zarneh-Siahgel fault zone through the karstic Asmari Formation. Second, selecting the dam site on evaporative Gachsaran Formation causes degradation of water quality in the reservoir. The results of this study demonstrate that considering karst hydrogeological conditions is indispensable for dam site selection from the point of view of groundwater quantity and quality impacted by the dam.

Introduction

Water storage is important for economic and social development in nearly every country around the world. Taking Iran as an example, where precipitation occurs in the autumn and winter while farmers need water for irrigation in the spring and summer, groundwater is usually the primary source to meet the agricultural needs for crop irrigation. To supplement the water supply, surface water reservoirs are constructed to collect and store water during the non-irrigated season of high rainfall and river flows. Most parts of Iran have low precipitation and most streams in Iran are ephemeral, thus, groundwater plays an indispensable role for supplying water to the reservoirs, often through base flow.

In the most recent two decades, climate changes such as drought together with overexploitation of surface water and groundwater have reduced river discharge or even dried up most rivers in Iran (Motagh et al., 2008; Lehane, 2014). Such a recent negative development imposes challenges for dam site selection that is often based on past and outdated hydrological conditions, especially concerning river discharge, without enough knowledge about groundwater conditions. Indeed, it is important to revisit the interrelationship of groundwater, surface water, and site selection under the new hydrological conditions for designing better water resource management plans.

A detailed knowledge of the geology of the dam site and the future reservoir, as well as of its catchment area, is necessary before the dam site is selected; acquiring such knowledge should be vital in the siting, design, and construction of any dam (Best, 1981). Such knowledge is critically important if the site is in a karst region because of the intimate connection between surface water and groundwater in the region and the rapid pathways or channels likely to connect the surface water in the reservoir with the nearby karst groundwater (Bonacci and Rubinić, 2009; Milanović et al., 2010; van Beynen, 2011; Kazemi, 2012).

The karst groundwater boundary may be very different from the surface catchment boundary, as the groundwater flow may be through underground conduits to discharge at springs far beyond the catchment boundary (Currens, 2002; Chen et al., 2004; Rezaei et al., 2013). In addition, the boundary of a catchment area in karst terrains may occasionally or permanently change due to both natural processes and anthropogenic interventions (Bonacci et al., 2016). Dam site selection in karst is always risky, and some inadequately investigated dams have never fully filled with water or failed to retain any water (Milanović, 2000; Dokmanovic et al., 2003; Bonacci and Rubinić, 2009; Milanović et al., 2010, van Beynen, 2011). Therefore, understanding the hydrogeological conditions, especially the recharge and discharge zones of the catchment, is essential for selecting an appropriate dam site.

* Corresponding Author: haji.karimi@gmail.com, h.karimi@ilam.ac.ir.
[1] Faculty of Earth Sciences, Institute for Advanced Studies in Basic Sciences (IASBS), Zanjan 45137-66731, Iran
[2] Center for Research in Climate Change and Global Warming (CRCC), Institute for Advanced Studies in Basic Sciences (IASBS), Zanjan 45137-66731, Iran
[3] Faculty of Agriculture, Ilam University, Ilam, Iran
[4] Department of Geology and Geophysics, Texas A&M University, College Station, TX 77845, USA

Moreover, the hydrogeological conditions may affect the water quality after the construction of the dam, depending on the lithology of the reservoir rocks. For instance, if halite and gypsum rocks exist in the reservoir site, they may dissolve rapidly after the construction of the dam and eventually change the surface and groundwater geochemistry and degrade the water quality. For instance, the total dissolved solids in evaporite formations containing halite, gypsum, or anhydrite may rise two to three hundred thousand parts per million (Clark, 2015). About 95% of the Kangir Reservoir sits above the evaporate-rich Gachsaran Formation, dissolution of which will have a major impact on reservoir water quality. Sulfate concentrations in water usually equal 1000 mg/l in gypsum-karst terrains, making them inappropriate for domestic water supplies (Raeisi et al., 2013).

The dissolution of halite and gypsum beds at the reservoir site will increase the water leakage rates from the reservoir because dissolution of halite and gypsum is likely to augment its permeability (Calcano and Aizura, 1967; James and Lupton, 1978; James and Kirkpatrick, 1980; Warren et al., 1990; Dreybrodt et al., 2002; Kiyani et al., 2008; Al-Rawi et al., 2011). Weisbrod et al. (2012) reported that dissolution fissures may be created if the seepage rate increases above a threshold value, even in salt rocks that appears to be relatively homogeneous and without fractures.

The Gachsaran Formation, with high solubility (Aghanabati, 2004), crops out over approximately 20 thousand square kilometers in the south and southwest parts of Iran (Raeisi et al., 2013). Despite its obvious effects of degrading water quality of reservoirs and adjacent aquifers, they are sometimes overlooked in the site-selection process. As a case in point, the reservoir of the Upper Gotvand Dam in southwest of Iran, constructed on the Karun River with electrical conductivity of 500 μS/cm, is located above halite layers of the formation where the conductivity of water increased up to 170,000 μS/cm in the lower layers of the reservoir because of halite dissolution (Kayhan, 2015).

This study concerns the Kangir Reservoir catchment of Iran, where the construction of the Kangir Reservoir dam began in 1991 and was completed in 2013. It is an earthen dam with impervious clay core, with a 745 m length of the crest and 42 m height from the basement. The storage capacity of the Kangir Reservoir, 2.13 km^2 in area, is about 20 million cubic meters (MCM). This reservoir plays an important role in supplying water to a community of 70,000, and provides irrigation water for a cropland with an area of 2500 ha. The reason we chose the Kangir Reservoir for this study is that this reservoir was mainly designed on the basis of discharge information of the Kangir River over the past three decades, overlooking issues associated with climate change and overexploitation of water resources. At present, the Kangir River does not fill the reservoir. On the other hand, the surrounding karst groundwater was not considered as a potential source for the reservoir simply because there was not enough knowledge about the karst hydrogeology in the catchment before designing the dam. In addition, this reservoir is unique because about 95% of it is in direct contact with the marl, gypsum, and halite units in the evaporite Gachsaran Formation (Karimi and Pakzad, 2009).

The objective of this research was to find out how important the karst groundwater conditions are and how the rock types would affect the reservoir water. We employed a host of investigative tools, including water balance analysis, general flow direction, hydrochemistry, the distribution of karst and evaporite formations in the catchment, and tectonic setting to illustrate the issue from multiple angles. The final objective was to use the results of our analyses to guide future site selection in the karst terrain to meet the water-supply need and at the same time to minimize the negative water quality impact.

Study Area

The study area is located 45 km north west of Ilam city, Iran, between 45°50′ and 46°27′ longitude and 33°0.68′ and 34°4′ latitude (Fig. 1). The site is characterized as a humid climate with 667 mm average annual rainfall, 12.39 °C average annual temperature, and 1783 mm average potential evaporation (Rezaei, 2015). The watershed of the Kangir Reservoir is surrounded by highlands of Bankul (north), Manesht (east), and Sharezol (south). The Kangir River is the main surface water inflow to the reservoir, with an average long-term discharge rate of 1.53 $m^3\ s^{-1}$. Note that the average discharge rate of the river has been decreased to about 0.68 m^3/s in the last five years. The water levels in the piezometers near the river at the eastern and middle parts of the Eivan Plain are higher than the riverbed, so groundwater drains into the river. However, in recent years the river has become ephemeral during summer, since its water is diverted for agricultural purposes.

The main geologic formations of the study area are the Pabdeh marl and marl limestone, the Asmari limestone, and the Gachsaran gypsum (Aghanabati, 2004), following a decreasing order of age. The Asmari Formation, the main karstic aquifer in Zagros, covers approximately 61% of the catchment, primarily in the highlands area (Fig. 2). The evaporite Gachsaran covers about 95% of the reservoir area to an average thickness around 60 m (Karimi and Pakzad, 2009), and it negatively affects the reservoir water quality, as it mainly contains marl, gypsum, halite, and limestone. The highly soluble gypsum and halite layers can elevate the conductivity of groundwater from 1100 up to 12000 μS/cm (Raeisi et al., 2013). The Pabdeh Formation usually acts as a barrier to groundwater flow in the Zagros Mountains.

Method of Study

The investigation was carried out in two phases. The first phase studied the karst hydrogeological system; the second phase examined the influence of the evaporate Gacharan Formation on the water quality of the catchment area. In

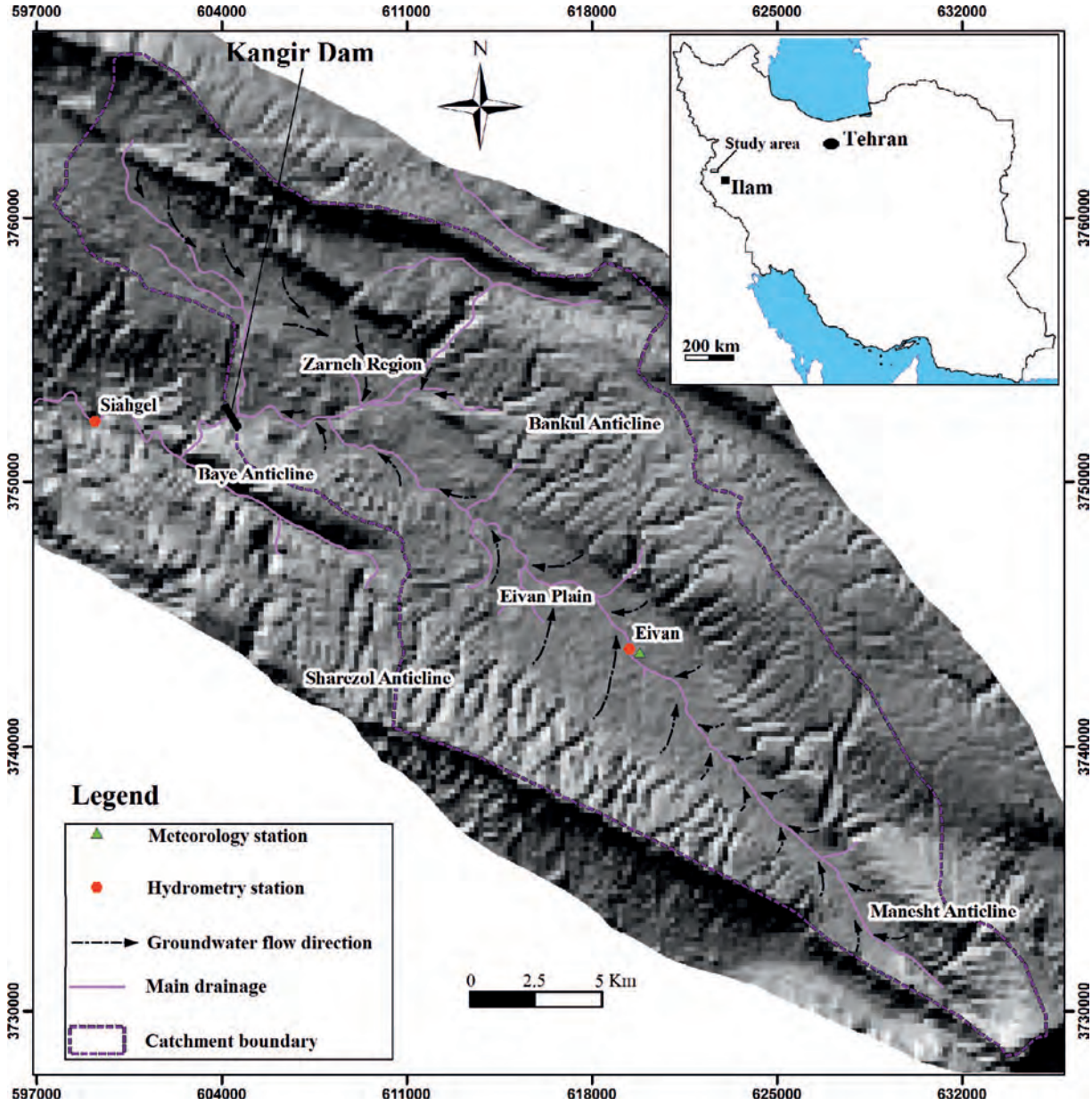

Figure 1. Location of the Kangir Dam site, the Kangir Reservoir catchment, and hydrograph stations.

addition, we predicted the impact of the GF on the quality of the reservoir water. The hydrogeological condition in the study area was studied by preparing groundwater equipotential maps, investigating the water balance, and analyzing hydrochemistry data and the tectonic setting. We acquired the discharges of springs, discharge of the Kangir River at the reservoir inlet, hydrographs at the Eivan and Siahgel hydrometric stations, and meteorological data of the study area from the Ilam Regional Water Authority (IRWA) archive. This archive contains weekly discharge data for the Kangir River at the reservoir inlet and Eivan and Siahgel hydrometric stations from January to April 2014. In addition, 15 water samples from springs, wells, and the river from the Zarneh-Siahgel fault zone area were collected and analyzed in October 2015. The discharges of the Kangir River at R2 and R3 locations in Figure 2, upstream and downstream of Sorkhejo Springs, were also measured when the Kangir River at the reservoir inlet dried up and the outlet floodgates were completely shut down. There were not enough observation wells available for preparing an adequate equipotential map, thus this map must be used with caution. We filled in the spatial gaps between the observation wells using the elevations of the static water table at production wells during the no-pumping period in the autumn and winter seasons to improve the equipotential map of the Zarneh Region as a part of the Eivan Plain. To ensure that the wells were completely recovered, we measured the water table about three months after the pumping from the aquifer was stopped. Three months

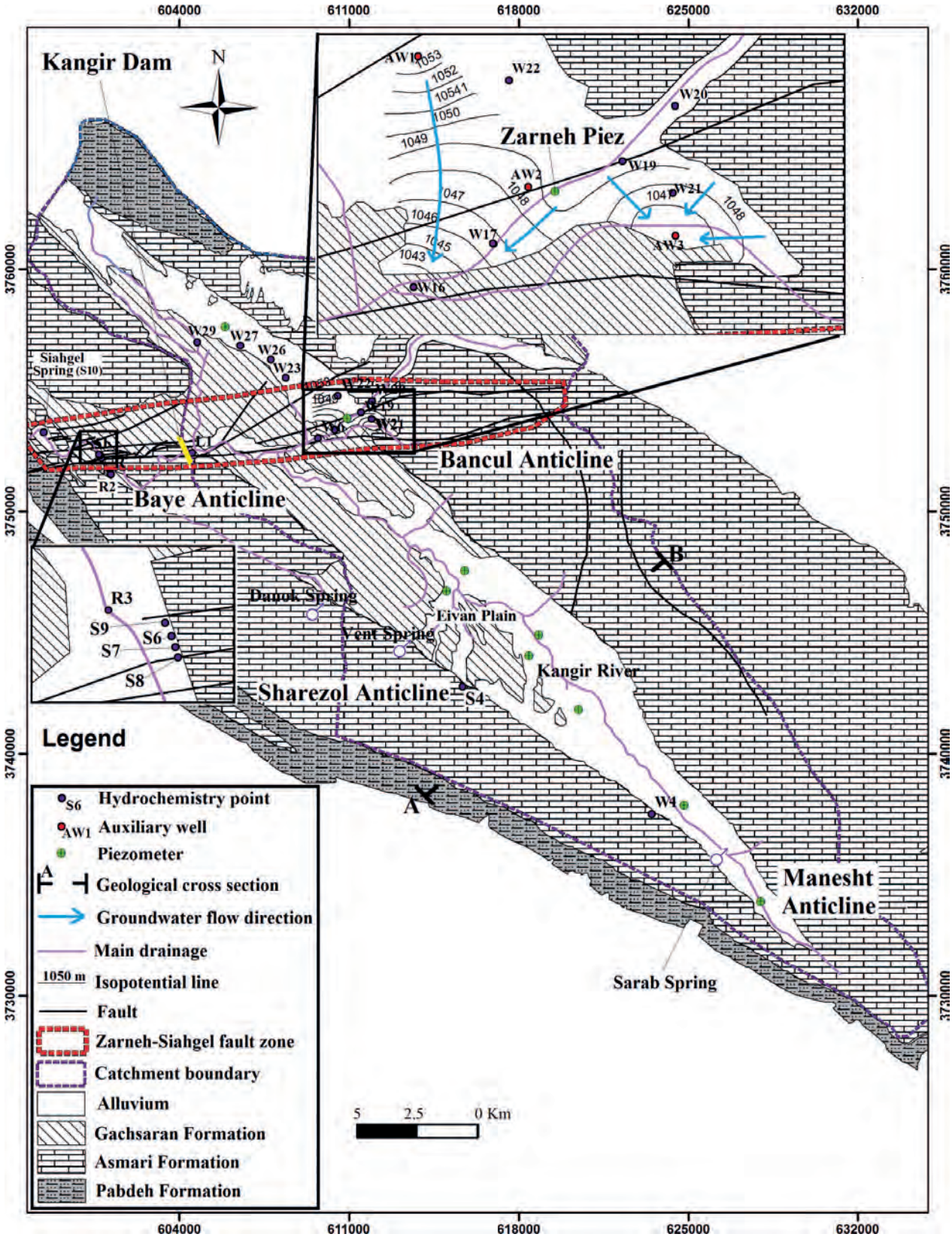

Figure 2. Hydrogeological map of the study area. Upper and lower insets show the Zarneh and Siahgel regions, respectively. AW1–AW3 are the auxiliary wells that were considered when preparing the equipotential map. The line A–B is the location of the cross-section in Figure 3.

Table 1. Groundwater budget components in the basin.

Recharge, MCM			Discharge, MCM				
Recharge from Rainfall	Agricultural Water Return	Total	Production Wells	Springs	Base Flow of Kangir River	Missing Groundwater	Total
112	1.5	113.5	9	28	27	49.5 ± 21	113.5

seems to be reasonable time since (1) the alluvium in the Zarneh Region contains coarse-grain soil according to the lithological log of the piezometers; (2) the water table rapidly responds to the recharge of precipitation since the time lag is about 1 to 2 months (Rezaei, 2015), and (3) the total pumping from the aquifer is not much in the summer. The production wells we selected were in the same aquifer as the observation wells to ensure data consistency since (1) the alluvial aquifer in the Zarneh Region is a one-layer unconfined aquifer (Rezaei, 2015); (2) the Zarneh piezometer is located somewhere between the production wells that were used to measure the water table and they have the same depth, and (3) no screens were installed in the production wells, while the screen in the piezometer is installed over the depth from the water table to the bottom.

To understand the influence of the evaporite minerals in the GF on water quality, we prepared zoning maps of electrical conductivity and sulfate and calcium ions in the Eivan Plain, as well as bivariate graphs of EC-sulfate and sulfate-calcium using the available hydrochemistry samples held by the IRWA archive for the period from 2006 to 2010. We also collected water samples in October 2015 (Table S1, presented in Supplementary Information).

The water samples were collected in clean plastic bottles and were immediately sent to the Geochemistry Lab of Novin-Rahavard, Zanjan, Iran. The water temperature, EC (by Lovibond Conductivity meter, SensoDirect Con 110) and pH (by Lovibond pH meter, SensoDirect pH 110) were measured in the field during sampling. Calcium and magnesium concentrations were determined using titration with EDTA (Eriochrom Black-T and Murexide as indicators). Sodium and potassium concentrations were estimated by flame photometry methods. Sulfate and nitrate concentrations were determined by spectrometry methods. Bicarbonate and chloride were measured using titration with H_2SO_4 (Methyl orange as indicator) and silver nitrate (potassium chromate as indicator), respectively.

GROUNDWATER BALANCE OF THE KANGIR RESERVOIR CATCHMENT

The long-term water budget of the Kangir Reservoir catchment from 1976 to 2011 reveals that about 112 MCM of total precipitation (293 MCM) recharged the groundwater, while the evapotranspiration and runoff were 160 and 21 MCM, respectively (Rezaei, 2015). These were climatologically estimated using observations like daily precipitation, temperature, evaporation, wind speed, and relative moisture of air, along with monthly discharge values of the Kangir River. Accordingly, the estimation of a long-term water budget of groundwater in the catchment indicated that about 49 MCM of groundwater drained into the surrounding regions (Table 1). This value was obtained using the long-term components of recharge and discharge in the catchment, which the average error may be associated with it (e_{mg}) was estimated to be about 43% (ranges from 23 to 63); that is, about 21.9 (ranges from 11.2 to 30.7) MCM. One can calculate the error using (Winter 1981) $e_{mg} = e_{rr} + e_{awr} + e_{pw} + e_s + e_{bf}$, where e_{rr} and e_{awr} are the error in the recharge from rainfall and the agricultural water return flow, respectively. Terms e_{pw}, e_s, and e_{bf} represent the error in the groundwater pumping of production wells, spring discharge, and the base flow of the Kangir River, respectively. The main recharge components of the groundwater system are recharge from precipitation (112 MCM) and agricultural water return flow (1.5 MCM). The main discharge components include groundwater pumping (9 MCM), spring discharge (28 MCM), and the base flow of the Kangir River (27 MCM). For practical purpose, we considered the error of 12.5 (ranges from 5 to 20) percent in the long-term groundwater recharge estimated by Rezaei (2015) in the area (Mohammadi et al., 2014). Agricultural return flow is considered to be 20 percent of the total used water with a reasonable error of 5 percent according to the range values applied in different plains of Iran (Alipour Shams-Abad, 1998; TECC, 2010; Hosseini et al., 2010; Mohammadi et al., 2014). The groundwater pumping data and springs' discharges were extracted from the archive of the IRWA. The estimation of the error associated with the groundwater pumping data in Iran is impossible, as there were no permanent flow meters on production wells and the data were only collected for a few years. From a practical point of view, we considered a 10 percent error in the withdrawal groundwater from production wells. We also considered an error of 5 percent associated with the springs discharge measurements (Kjelstrom, 1995).

The straight-line method (Chow et al., 1988) was used to determine the long-term base flow of the Kangir River at the reservoir inlet. In the absence of long-term discharge observation at the reservoir inlet, we used the relationship between the weekly discharges values at the reservoir inlet and those of the Eivan and Siahgel hydrometric stations to meet the need. This is possible because the discharge at the reservoir inlet is nearly equivalent to the average discharge of the Siahgel and Eivan stations; as can be seen on Fig. S1 (presented in Supplementary Information). Consequently, the

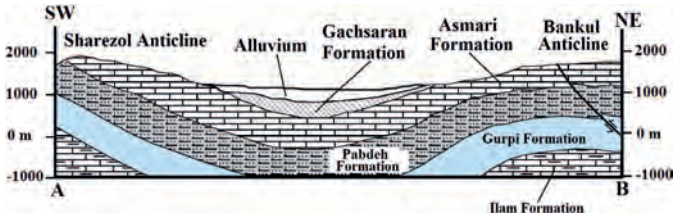

Figure 3. Schematic geological profile across the Eivan Plain; the location is shown on Figure. 2).

long-term discharge at the reservoir inlet was taken as the long-term average discharge of the Siahgel and Eivan stations. Note that because the components used in the long-term groundwater budget were average values, we were unable to calculate the long-term change in the reservoir water volume. We also considered a 17 percent error associated with the base flow estimation according to the error ranging from 12 to 22 percent (Santhi et al., 2008).

Deficit in Groundwater Budget

As mentioned above, there is a 49.5 ± 21 MCM groundwater deficit for the Kangir Reservoir catchment. None of this "missing" groundwater can rise into the northern plain of the Bankul Anticline, with an elevation of 1300 m above mean sea level, or the eastern plain of Manesht Anticline, with an elevation of 1335 m, as they are much higher than the Eivan Plain at 1070 m. In addition, the geological cross section (Fig. 3) shows that the low-permeability Pabdeh Formation in both anticlines lies structurally above the Asmari Formation contact with the alluvium of Eivan Plain. Among the surrounding regions, the southern plain of Sharezol Anticline and Siahgel Region have lower elevations (1000 m and 890 m, respectively) than the Eivan Plain, so these locations might receive the missing groundwater.

The Asmari Formation is completely missing from the southern limb of the Sharezol Anticline as outlined near the A-end in Figure 3. In addition, the geological cross section indicates that the low-permeability Pabdeh Formation crops out at a higher elevation (1600 m) than the Asmari Formation contact with the Eivan Plain alluvium (1208 m). This geometry prevents any water draining from the Eivan Plain to the southern plain of the Sharezol Anticline. Consequently, the "missing" groundwater is unlikely to end up there. Therefore, the Siahgel Region is the most likely destination of the groundwater. To test this hypothesis, the hydraulic relationship between the groundwater of the Sharezol, Baye, and Bankoul anticlines and the Siahgel Region was investigated.

Sharezol Anticline: The hydraulic relationship between the Sharezol Anticline and the Eivan Plain alluvium, from the location of Khoran Spring (S4 in Fig. 2) toward the Siahgel Region, is blocked by the low-permeability Gacharan Formation. However, along the anticline axes toward the

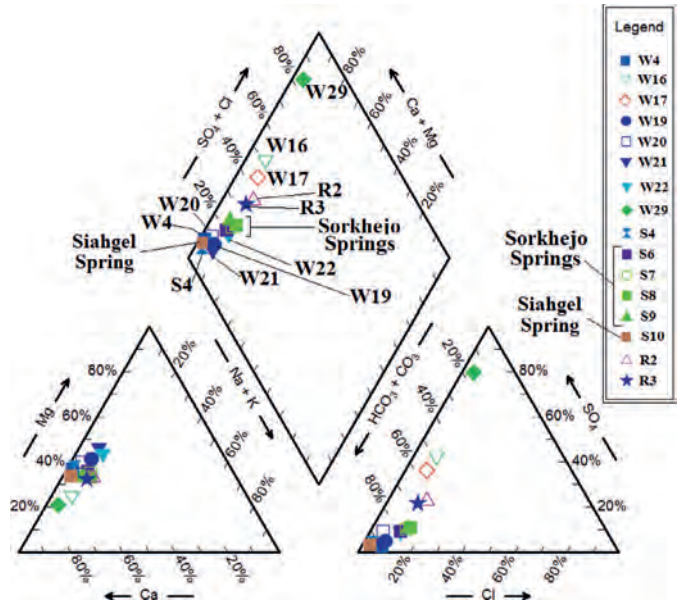

Figure 4. The Piper Diagram for the water samples of October 2015. Spring locations are shown in Figure 2.

northwest, the karstic Asmari Formation of the Sharezol Anticline is in direct contact with the Siahgel Region and has the lowest topographic elevation in the area. Furthermore, the water sample from the Siahgel Spring (presented in Fig. 2) on the Piper plot shows similar geochemical characteristics to the Khoran Spring (S4 in Fig. 4), suggesting that they may share the same source.

This hypothesis is also confirmed by our water budget calculation for the Sharezol Anticline. The Asmari Formation cropping out in that part of the Sharezol Anticline that falls within the dam catchment has an area of 65 km^2, and this area is annually recharged by about 23.6 MCM of groundwater because the recharge coefficient in this area is estimated to be about 0.5 (Rahnemaaie, 1994; Pezeshkpour, 1991; Karimi et al., 2001; Karimi et al., 2005; Ashjari and Raeisi, 2006; Kalantari et al., 2016) and the annual precipitation is 726 mm. The total discharge from karstic springs (Khoran (S4), Vent, Danok and Sarab Springs shown in Fig. 2) in this area is about 18.54 MCM. Hence, when considering the water budget estimation error (10%) associated with the karstic terrains of the Zagros Mountains (Ashjari and Raeisi, 2006), it seems that the total water produced in the Asmari Formation within the catchment discharges from the karstic springs of Khoran, Vent, Danok, and Sarab. But the groundwater produced by the rest of the Asmari Formation in the Sharezol Anticline is distributed out of the catchment and finally discharges into the Kangir River near the outlet of the Siahgel Region.

Baye and Bankul Anticlines*:* The groundwater that escapes from the Kangir Reservoir catchment drains mainly to the Sorkhejo Springs (i.e. S6 to S9) and the Kangir River along the Zarneh-Siahgel fault zone in the Siahgel Region (Fig. 2). To support this claim, we provide the following evidence.

First, there are no other springs in the Zarneh Region (upper inset in Fig. 2) structurally beneath the southern limb of the Bankul Anticline. In other words, the base level of erosion of the anticline is presumably at a lower elevation than that in the Zarneh Region and the Eivan Plain. Second, the fault zone of Zarneh-Siahgel (Fig. 2) extends from the Bankul Anticline toward the Siahgel Region. Furthermore, the groundwater level at the east end of the fault zone in the Zarneh Region has a depression cone around wells W19, W21, and AW3 (upper inset in Fig. 2); therefore, it appears that the fault zone transmits groundwater. Third, the minimum elevation of the Asmari Formation in the Baye Anticline is in direct contact with the Kangir River. This situation can easily allow the groundwater of the Baye Anticline to drain into the river as the discharge of the Kangir River increases along the Baye Anticline at the west end of the Zarneh-Siahgel fault zone (Fig. 2); the river drains the groundwater from the Baye Anticline. As a case in point, in September 2015 the river dried up just downstream of the dam, while its discharge gradually increased towards the Sorkhejo Springs. Its discharge finally reached 650 L s^{-1} downstream of the springs. Fourth, the water samples from the Sorkhejo Springs (S6 to S9) on the Piper diagram (Fig. 4) reflect similar geochemical features as those from wells W19 to W22 (see Fig. 2), located at the east end of the fault zone in the Zarneh Region.

Karimi and Pakzad (2009) reported that dye injected into the northern margin of the Kangir Reservoir emerged 4 km downstream of the dam at springs that have since dried up due to successive droughts. Furthermore, the drilling records of boreholes around the reservoir suggest that there are two different water levels in two separate aquifers in the Gachsaran and Asmari Formations, and the water level in the Asmari Formation is much lower than that in the Gachsaran (Karimi and Pakzad, 2009). Consequently, most of the karst water produced in the catchment, especially in the Bankul Anticline, does not enter the reservoir. Instead, it drains to the Sorkhejo Springs and the Kangir River in the Siahgel Region along the Zarneh-Siahgel fault zone that intercepts the Asmari Formation beneath the Gachsaran Formation. A precise calculation of the water leaking from the Bankul Anticline into the Siahgel Region is not possible; this is because an unknown amount of groundwater from the Bankul Anticline recharges the Eivan Plain, where the piezometric network is not dense enough to construct an accurate enough equipotential map to calculate the flow under the Eivan Plain.

HYDROCHEMISTRY

We used the water samples collected on October 2015 to test the "missing" water hypothesis outlined above. Then the impact of the Gachsaran Formation on water quality in the Kangir Reservoir and the Eivan Plain was investigated using not only all the available data in the IRWA archive for 2006 to 2010, but also water samples collected in October 2015. According to the water samples of October 2015 presented in the Piper plot (Fig. 4), water samples taken from wells near the Zarneh Piezometer have a conductivity range from 394 to 553 μS cm (W19 to W21). These exhibit geochemical features similar to the Sorkhejo Springs water samples (S6 to S90) that range from 671 to 745 μS cm^{-1}. A point to note is that the values of the Sorkhejo Springs are slightly higher than those of the wells. This is probably due to the effect of the Gachsaran Formation yielding higher EC values for wells penetrating it, for instance an EC value of 2450 μS cm for water sample fromW29.

Interestingly, as can be seen in Fig. 2, the spatial distribution of wells W19 to W21 and the Sorkhejo Springs spreads around the fault zone, suggesting that the fault zone might provide a pathway for the groundwater drained from the Bankul Anticline and the Zarneh Region towards the Sorkhejo Springs in the Siahgel Region, downstream from the dam. In addition, the locations of the Kangir River water samples with conductivity of about 705 μS cm^{-1} (R2 and R3, upstream and downstream of the Sorkhejo Springs, respectively) on the Piper plot are the same as those from the Sorkhejo Springs.

A notable issue is that the nitrate concentration in W20 (7.19 mg L^{-1}), measured on the southern limb of the Bankul Anticline at the east end of the Zarneh-Siahgel fault zone, lies within the range of nitrate concentrations values measured for water samples from the Sorkhejo Springs (about 6.09 to 9.26 mg L^{-1}). This evidence confirms the hypothesis that the Sorkhejo Springs drains most of the karst groundwater in the Bankul Anticline.

Another notable geochemical issue is that most of the Kangir Reservoir is in direct contact with the evaporite-rich Gachsaran Formation. Investigation of the zoning maps of EC, calcium, and sulfate (Figs. 5 a–c) along with the Piper diagram in Figure 6 indicates that the evaporate-rich GF degrades the water quality of the karstic Asmari Formation in several ways. First, it increases the values of conductivity, sulfate, and calcium (Fig. 5). Second, it converts the bicarbonate water type of the karstic Asmari Formation into sulfate and chloride water as outlined in Fig. 6. The water samples collected from the karstic Asmari Formation exhibit low conductivity and bicarbonate water type; for example, water samples from W3–W5, W7, W11, S4, and S5 on the northern limb of the Sharezol Anticline have EC of 427 to 587 μS cm, and those from W19–W22 on the southern limb of the Bankul Anticline in the Zarneh Region have EC of 394 to 553 μS cm^{-1}.

Consistent with the Gachsaran Formation distribution over the area, the highest groundwater EC value is found in the reservoir (M4 with chloride water type); this almost certainly arises from the dissolution of gypsum and salty layers in the GF. Water samples from W29 with an EC value of 2450 μS/cm and M3 with an EC value of 2412 μS cm^{-1} are characterized as sulfate-water type. This is because both are strongly affected by the dissolution of the GF (Fig. 5). The rest of the water samples lie somewhere between these two water categories of the Asmari Formation and the GF on the Piper

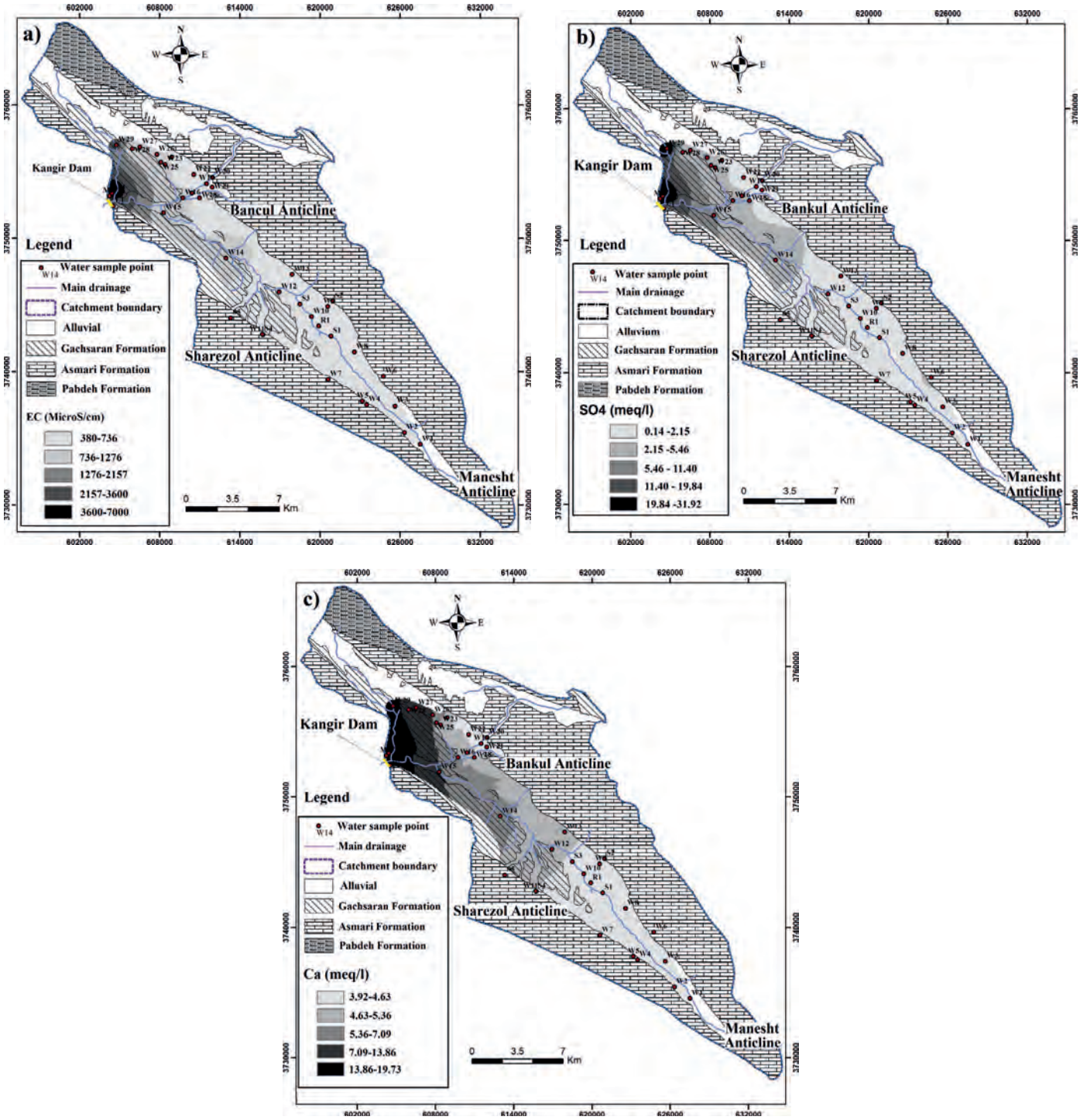

Figure 5. The zoning maps of (a) electrical conductivity, (b) sulfate, and (c) calcium cation in the Eivan Plain.

plot (Fig. 6). In general, the values of EC, chloride, sulfate, and calcium rise towards the dam, and the bicarbonate water type changes to the sulfate water type (Fig. 5).

It appears that increasing the reservoir water level further reduces the reservoir's water quality, probably because the relative contact area of the reservoir water with the GF increases. For instance, we conducted one experiment by pouring 100 ml of distilled water onto a 100 gr soil sample taken from the gypsum on the base of the reservoir. The EC value rose to 1450 µS cm^{-1} almost instantaneously and to 1950 µS/cm after two months.

Taking the above mentioned points into consideration, the Kangir Reservoir site is undesirable from a geochemical perspective. One must be aware that farmlands irrigated using

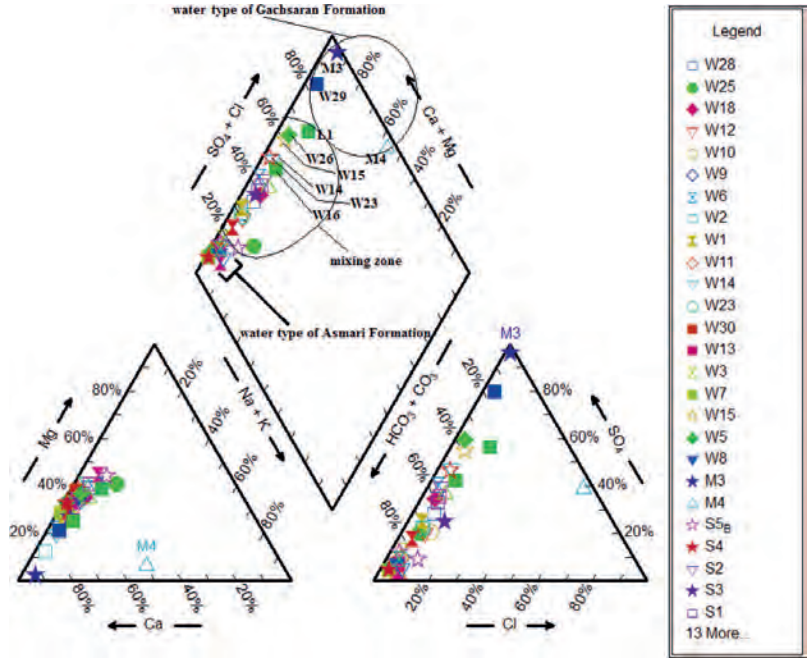

Figure 6. Piper Diagram of the water samples from the Eivan Plain. Sample locations are shown in Figure 5.

such a degraded Kangir Reservoir water can decrease agricultural productivity through a slow process of salinization and chemical deterioration of soil, and it will degrade the fresh-water resources in the area by leaking the degraded reservoir water into the relatively unpolluted groundwater and surface water.

Investigation of the bivariate curves of conductivity-sulfate and sulfate-calcium indicates that these three parameters have a linear relationship with each other (Fig. 7). This signifies that the water quality in the reservoir catchment increasingly degrades with increasing concentrations of sulfate and calcium from dissolution of gypsum in the Gachsaran Formation. As shown in Figure 7, the water samples in the GF (e.g., M4, W29, M3, W26, W15, W14, W16, and L1) represent the highest values not only for EC, but also for sulfate and calcium. As a case in point, water sample L1 (EC = 885 μS cm^{-1}) taken directly from the reservoir, clearly shows that the high quality of the Kangir River, characterized by the long-term average EC of 564 μS cm^{-1} and bicarbonate water type at the Eivan Station, will no longer exist after entering the Kangir Reservoir behind the Kangir dam. It is worth pointing out that the L1 sample with its sulfate water type was collected when the water level of the Kangir Reservoir was almost in direct contact with the river alluvium. The degradation is likely to worsen as the reservoir water level rises and widens contact with the GF.

CONCLUSION

A large portion of the Kangir Reservoir catchment's groundwater drains out of the catchment and into the surrounding regions through subsurface pathways. The higher elevation of the low-permeability Pabdeh Formation in the Bankul, Manesht, and Sharezol anticlines prevents hydraulic connection between the reservoir catchment to the surrounding plains in the north, east, and south. Groundwater escapes from the Kangir Reservoir catchment into the Siahgel Region and the Sorkhejo Springs downstream of the Kangir dam through the Zarneh-Siahgel fault zone. The evaporite minerals in the Gachsaran Formation that underlie most of the Kangir Reservoir have a negative influence on water quality in the Kangir Reservoir catchment; the highest values of conductivity, sulfate, calcium, and chloride are found in and near the reservoir itself. The Kangir dam is poorly sited in the sense that the dam can collect only a small portion (about one quarter) of all the groundwater within its catchment, and the reservoir is in direct contact with the evaporite-rich Gachsaran Formation. This factor degrades water quality in the catchment. The dam may be unstable as its foundation is on the Zarneh-Siahgel fault zone. Finally, this study indicates that hydrogeological and hydrogeochemical knowledge plays a very important role in selecting and designing the reservoir and dam sites, especially in karstic areas.

ACKNOWLEDGMENT

The authors thank the Vice Chancellor for Research at the Institute of Advanced Studies in Basic Sciences (IASBS) for supporting this hydro-geochemical analysis. We are grateful to Ilam Regional Water Authority for providing the hydrologic and hydrogeological data used in this study. The

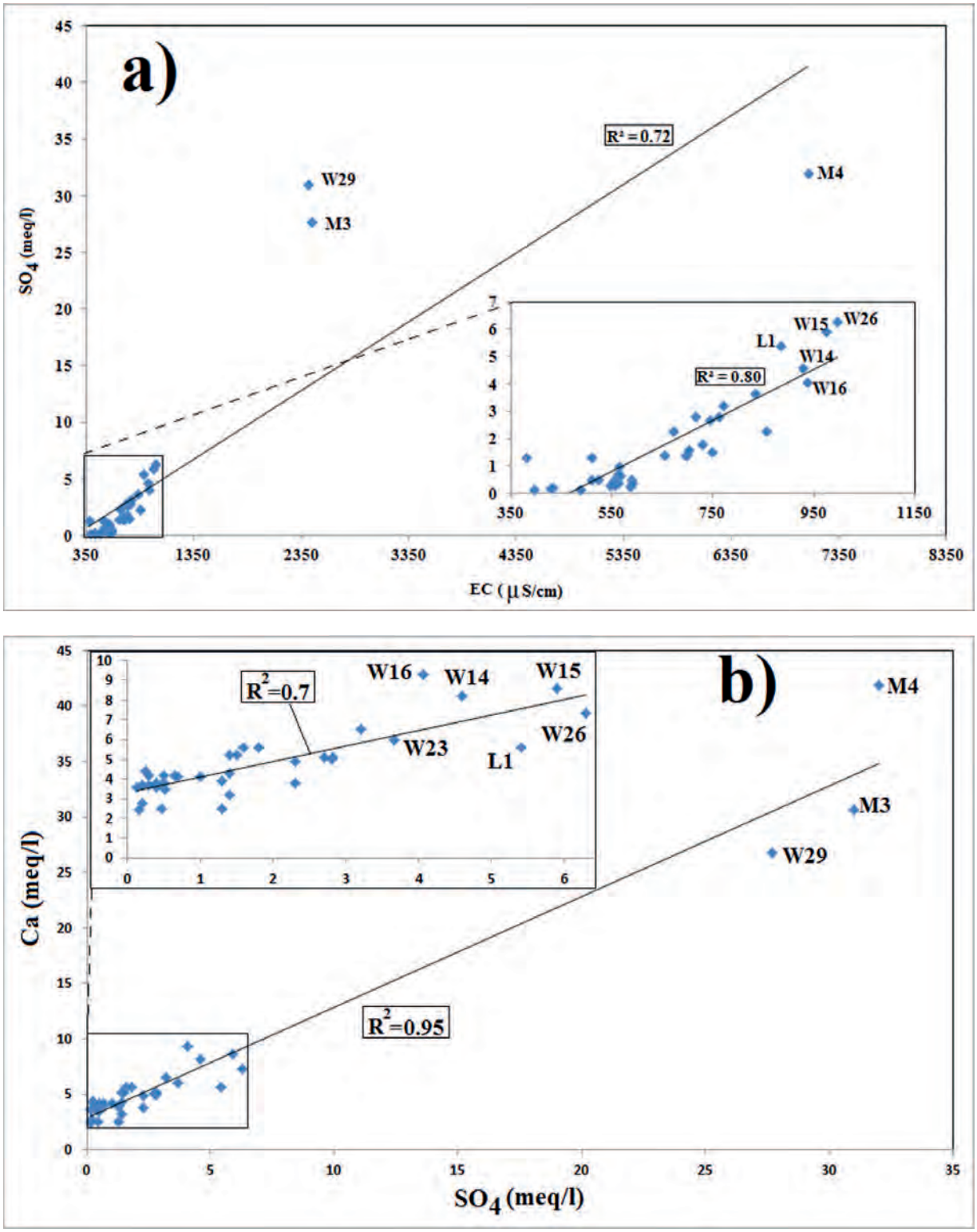

Figure 7. Bivariate graphs of (a) EC-sulfate and (b) sulfate-calcium on the Eivan Plain. Locations of labeled samples are shown in Figure 5.

constructive comments from the editor, associate editor, and the three anonymous reviewers are deeply appreciated.

REFERENCES

Aghanabati, A., 2004, Geology of Iran: Ministry of Industry and Mines, Geological Survey of Iran, (in Farsi) 576 p.

Alipour Shams-Abad, M., 1998, Evaluation of return water of irrigation to groundwater in Kavar plain by groundwater mathematical model [Ms. Thesis]: Shiraz, University of Shiraz, (in Farsi) 112 p.

Al-Rawi, O., Ghannam, Sh., and Al-Ani, H.R., 2011, Dissolution of gypseous rocks under different circumstances: Jordan Journal of Civil Engineering, v. 5, no. 3, p. 357–379.

Ashjari, J., and Raeisi, E., 2006, Influences of anticlinal structure on regional flow, Zagros, Iran: Journal of Cave and Karst Studies, v. 68, no. 3, p. 118–129.

Best, E.J., 1981, The influence of geology on the location, design and construction of water supply dams in the Canberra area: BMR Journal of Australian Geology & Geophysics, v. 6, p. 161–179.

Bonacci, O., Buzjak, N., and Roje-Bonacci, T., 2016, Changes in hydrological regime caused by human intervention in karst: the case of the Rumin Springs: Hydrological Sciences Journal, v. 61, no. 13, p. 2387–2398. https://doi.org/10.1080/02626667.2015.1111518.

Bonacci, O., and Rubinić, J., 2009, Water losses from a reservoir built in karst: the example of the Boljunčica reservoir (Istria, Croatia): Environmental Geology, v. 58, no. 2, p. 339–345. https://doi.org/10.1007/s00254-008-1599-z.

Calcano, C.E., and Aizura, P.R., 1967, Problems of dissolution of Gypsum in some dam sites: Bull. Venezuelan Soc. of Soil Mechanics and Foundation Engineering.

Chen, Jian Sheng, Li, Ling, Wang, Ji Yang, Barry, D.A., Sheng, Xue Fen, Gu, Wei Zu, Zhao, Xia, and Chen, Liang, 2004, Groundwater maintains dune landscape: Nature, v.432, no. 7016, p. 459–460. https://doi.org/10.1038/432459a.

Chow, Ven Te, Maidment, D.R., and Mays, L.W., 1988, Applied Hydrology: McGraw-Hill, Water Resources and Environmental Engineering Series, 572 p.

Clark, I., 2015, Groundwater Geochemistry and Isotopes: Boca Raton, CRC Press, Taylor & Francis Group, 456 p.

Currens, J.C., 2002, Kentucky is Karst Country! What You Should Know about Sinkholes and Springs: Lexington, Kentucky Geological Survey, Series 12, Information Circular 4, 29 p.

Dokmanovic, P., Jemcov, J., Milanović, S., and Hajdin, B., 2003, Hydrogeological risk factors of dam and reservoir construction – a case example "Bogovina": RMZ- Materials and Geoenvironment, v. 50, no. 1, p. 105–108.

Dreybrodt, W., Romanov, D., and Gabrovsek, F., 2002. Karstification below dam sites: a model of increasing leakage from reservoirs: Environmental Geology, v. 42, p. 518–524. https://doi.org/10.1007/s00254-001-0514-7.

Hosseini, A., Najafi, B., and Sadeghifar, A., 2010, Water resources balance in Feizabad-Mahvalat watershed: Basic Studies Office, Khorasan Regional Water Authority, 134 p. (in Farsi).

James, A.N., and Kirkpatrick, I.M., 1980, Design of foundations of dams containing soluble rocks and soils: Quaternary Journal of Engineering Geology and Hydrogeology, v. l3, p. 189–198. https://doi.org/10.1144/GSL.QJEG.1980.013.03.05.

James, A.N., and Lupton, A.R.R., 1978, Gypsum and anhydrite in foundations of hydraulic structures: Géotechnique, v. 28, no. 3, p. 249–272. doi: 10.1680/geot.1978.28.3.249.

Kalantari, N., Charchi, A., Mohammadi-Behzad, H.R., and Nadri, A., 2016, Bibitalkhone and Gariveh Springs paradox symbol of the Pabdeh karstic anticline in southwest Iran: Arabian Journal of Geosciences, v. 9, no. 2, p. 152–159. https://doi.org/10.1007/s12517-015-2153-4.

Karimi, H., and Pakzad, A.A., 2009, Water tightness evaluation of the Kangir dam reservoir, Ilam Province: Iran ICWR 2009 International Conference, Shahrood, Iran.

Karimi, H., Raeisi, E., and Zare, M., 2001, Determination of catchment area of aquifer bearing Tangab dam site using water balance method: Proceedings of the Second National Conference on Engineering Geology and the Environment, Tehran, 16-18 Oct 2001, v. 2, p. 755–773.

Karimi, H., Raeisi, E., and Zare, M., 2005, Physicochemical time series of karst springs as a tool to differentiate the source of spring water: Carbonates and Evaporites, v .20, no. 2, p. 138–147. https://doi.org/10.1007/BF03175457.

Kayhan Newspaper, 2015, Gotvand Dam, brine factory building (report from near and far): Tehran, Iran, http://kayhan.ir/fa/news/11429. (in Farsi)

Kazemi, Gh. A., ed., 2012, Hydrogeology – A Global Perspective: Rijeka, Croatia, InTech, 232 p. https://doi.org/10.5772/1523.

Kiyani, M., Sadrekarimi, J., and Fakhri, B., 2008, Gypsum dissolution effects on the performance of a large dam: International Journal of Engineering Transactions B: Applications, v. 21, no. 2, p. 143–150.

Kjelstrom, L.C., 1995, Methods to estimate annual mean spring discharge to the Snake River between Milner Dam and King Hill, Idaho: Boise, Idaho, U.S. Geological Survey Water-Resource Investigations Report 95-4055, 9 p.

Lehane, S., 2014, The Iranian Water Crisis: Dalkeith, Australia, Future Directions International, 11 p.

Milanović, P.T., 2000, Geological Engineering in Karst: Belgrade, Zebra Publishing, 347 p.

Milanović, S., Stevanovic, Z., and Jemcov, I., 2010, Water losses risk assessment: an example from Carpathian karst: Environmental Earth Sciences, v. 60, p. 817–827. doi: 10.1007/s12665-009-0219-x.

Mohammadi, Z., Salimi, M., and Faghih, A., 2014, Assessment of groundwater recharge in a semi-arid groundwater system using water balance equation, southern Iran: Journal of African Earth Sciences, v. 95, p. 1–8. https://doi.org/10.1016/j.jafrearsci.2014.02.006.

Motagh, M., Walter, T.R., Sharifi, M.A., Fielding, E., Schenk, A., Anderssohn, J., and Zschau, J., 2008, Land subsidence in Iran caused by widespread water reservoir overexploitation: Geophysical Research Letters, v. 35, no. 16, L16403. https://doi.org/10.1029/2008GL033814.

Pezeshkpour, P., 1991, Hydrogeological and hydrochemical evaluation of Kuh-e Gar-Barm-Firooz springs [Ms. thesis]: Shiraz, University of Shiraz. (in Farsi).

Raeisi, E., Zare, M., and Aghdam, J.A., 2013, Hydrogeology of gypsum formations in Iran: Journal of Cave and Karst Studies, v. 75, no. 1, p. 68–80. https://doi.org/10.4311/2011ES0234.

Rahnemaaie, M., 1994, Evaluation of infiltration and runoff in the karstified carbonatic rocks [Ms. thesis]: Shiraz, University of Shiraz, (in Farsi).

Rezaei, A., 2015, Investigation of decreasing trend of Kangir river discharge into Kangir dam reservoir, Ilam: Report for Research Activity of Military Service Period, Water Authority of Ilam, (in Farsi) 112 p.

Rezaei, A., Zare, M., Raeisi, E., and Ghanbari, R.N., 2013, Interaction of a freshwater lake and a karstic spring via a syncline fold: Groundwater, v. 51, p. 305–312. https://doi.org/10.1111/j.1745-6584.2012.00977.x.

Santhi, C., Allen, P. M., Muttiah, R.S., Arnold, J.G., and Tuppad, P., 2008, Regional estimation of base flow for the conterminous United States by hydrologic landscape regions: Journal of Hydrology, v. 351, no. 1, p. 139–153. https://doi.org/10.1016/j.jhydrol.2007.12.018.

TECC, 2010, Upgrading the modulation studies of water resources of Qaraqum watershed: Kalat Naderi studying region: v. 3, appendix 2, 44 p. (in Farsi).

van Beynen, Ph.E., ed., 2011, Karst Management: Dortrecht, Springer, 489 p. https://doi.org/10.1007/978-94-007-1207-2.

Warren, J.K., Havholm, K.G., Rowen, M.R., and Parsley, M., 1990, Evolution of gypsum karst formation in the Kirschberg Evaporite near Fredericksburg, Texas: Journal of Sedimentary Petrology, v. 60, p. 721–734. https://doi.org/10.1306/212F925A-2B24-11D7-8648000102C1865D.

Weisbrod, W., Alon-Mordish, C., Konen, E., and Yechieli, Y., 2012, Dynamic dissolution of halite rock during flow of dilute saline solutions: Geophysical Research Letters, v. 39, L09404, https://doi.org/10.1029/2012GL051306.

Winter, T.C., 1981, Uncertainties in estimation the water balance of lakes, Water Resources Bulletin, v. 17, no. 1, p. 82–115. https://doi.org/10.1111/j.1752-1688.1981.tb02593.x.

L.M. Boop, J.G. Wynn, G. Thompson, J.J. Fornós, and B.P. Onac – Interactions between surface conditions, the Mediterranean Sea, and cave climate within two littoral caves in Mallorca: implications for the formation of phreatic overgrowths on speleothems. *Journal of Cave and Karst Studies*, v. 79, no. 1, p. 59–72. DOI: 10.4311/2016ES0114

INTERACTIONS BETWEEN SURFACE CONDITIONS, THE MEDITERRANEAN SEA, AND CAVE CLIMATE WITHIN TWO LITTORAL CAVES IN MALLORCA: IMPLICATIONS FOR THE FORMATION OF PHREATIC OVERGROWTHS ON SPELEOTHEMS

Liana M. Boop[1]*, Jonathan G. Wynn[2], Glenn Thompson[2], Joan J. Fornós[3], and Bogdan P. Onac[2]

Abstract: Phreatic overgrowths on speleothems from Mallorca's littoral caves are valuable markers of former sea-level stands. These carbonate encrustations form as CO_2 degasses from brackish cave water that is hydrologically connected to the Mediterranean Sea. This study uses time series analysis to document relationships between surface conditions of temperature, barometric pressure, precipitation, tidal level of the Mediterranean Sea, and the coastal caves' microenvironment of temperature, partial pressure of CO_2 (pCO_2), and water level to contextualize overgrowth formation in Cova des Pas de Vallgornera (Vallgornera) and Coves del Drac (Drac). Water level in both caves was an attenuated semidiurnal function of Mediterranean Sea level with a lag of about four hours. The impact of individual rainfall events on cave water level was negligible during the study period. pCO_2 of cave air at both sites reached an annual maximum in September and decreased rapidly when surface air temperature fell below the cave air temperature (mean ~19 °C). As this threshold was reached, cooler and denser tropospheric air descended into the caves, initiating cave ventilation and displacing high-pCO_2 cave air that had accumulated. Observed pCO_2 was lower in Drac than in Vallgornera, and had small daily fluctuations because of bigger passages, fewer constrictions, and a large collapse entrance. The frequency and magnitude of pCO_2 fluctuations were higher in Vallgornera than in Drac, with both caves showing twice-daily water level maxima causing displacement of high-pCO_2 air from the cave alternating with water level minima causing tropospheric air to enter the cave via a "piston effect." A secondary control on pCO_2 variation can be attributed to variation in tropospheric barometric pressure. Thus, the geochemical conditions favorable for overgrowth formation are, in part, the result of this tidally-controlled cycle of cave-water level. The cycle causes cave-troposphere air exchange that drives CO_2 degassing, and therefore, the formation of phreatic overgrowths on speleothems.

Introduction

Mallorca's diverse Quaternary geomorphological features have made the island a world-renowned location for Quaternary sea level research (Ginés et al., 2012a). Coastal features including wave cut notches, marine terraces, fossil assemblages, and beach deposits document former sea level stands (Butzer, 1962; Butzer & Cuerda, 1962, Goy & Zazo, 1986; Hearty et al., 1986; Hearty, 1987; González-Hernández et al., 2001). The littoral caves of Mallorca host carbonate encrustations known as phreatic overgrowths on speleothems (POS) that have been used to refine the western Mediterranean Sea eustatic curve (Vesica et al., 2000; Tuccimei et al., 2006; Dorale et al., 2010; Ginés et al., 2012b). POS are robust sea level proxies because they provide precise geographic location, elevation, age, and tidal range (Ginés & Ginés, 1972; Pomar et al., 1979; Ginés & Ginés, 2007; van Hengstum et al., 2015). POS form when CO_2 degasses at the air-water interface (Pomar et al., 1976, 1979; Csoma et al., 2006; Boop et al., 2014); they are widespread in Mallorca, with over 30 identified POS paleolevels from 46 m above to 23 m below current sea level (Ginés, 2000). Some of the POS observed above the water table have been correlated with fossil marine terraces and beach deposits (Cuerda, 1975; Pomar and Cuerda, 1979). POS precipitated by former sea level stands are generally left intact within the stable cave environment, whereas beach deposits may be reworked and terraces or wave cut notches may be removed or overprinted by subsequent transgressions. In addition, encrustations that correspond to former sea level lowstands are preserved and accessible,

* Corresponding Author: liana.boop@sjcd.edu
[1] Department of Natural Sciences, San Jacinto College, 5800 Uvalde Rd., Houston, TX 77049, USA
[2] School of Geosciences, University of South Florida, 4202 E. Fowler Ave., NES 107, Tampa, FL 33620, USA
[3] Earth Sciences (Geology and Paleontology "Guillem Colom") Research Group, Department of Biology, Universitat de les Illes Balears, Cra. Valldemossa, km 7.5, 07122, Palma de Mallorca, Spain

whereas surface geomorphological evidence of lowstands is often inaccessible or destroyed by surficial processes.

Studies on the mechanisms of POS formation have focused on their distribution and mineralogy (Pomar et al., 1979; Csoma et al., 2006; Ginés et al., 2012a). However, the interactions of the subterranean environment with external forcings, including surface air temperature, precipitation, barometric pressure, tide, and sea level have not been quantified in high temporal resolution. This study uses time series analysis on data collected *in-situ* to investigate the effect that external forcings have on the subsurface air and water temperatures, partial pressure of CO_2 (pCO_2), and cave water level to address the following research questions: what are the effects of rainfall and tidal fluctuations on cave water level and to what extent is cave air CO_2 controlled by atmospheric forcings like barometric pressure, temperature, or tidal pumping?

METHODS

SITE CHARACTERISTICS

The island of Mallorca is located in the western Mediterranean and is the largest of the Balearic Islands. The geological structure of Mallorca consists of a set of northeast-southwest trending horsts and grabens formed during the middle-upper Miocene. Horsts correspond to the mountain ranges structured as a thrust and fold belt during the Alpine Orogeny, the Tramuntana range to the west and the gentler Llevant ranges in the east, and the grabens correspond to the basins, Es Pla and Migjorn among others, where horizontal upper Miocene carbonate platforms crop out (Fornós et al., 2002; Sàbat et al., 2011). This extensional event responsible for Mallorca's present day topography occurred mainly in the upper Miocene; since this event, Mallorca has remained relatively stable in terms of vertical movements (Just et al., 2011).

The climate of Mallorca is typical of the Mediterranean, with hot, dry summers and mild winters. Mean annual temperature is 16.6 °C (Guijarro, 1995), and yearly rainfall totals are highly variable, ranging from 300 mm in the central and south-eastern part to 1400 mm along the Tramuntana range (Ginés et al., 2012b). The coastal areas of Mallorca are considered low-energy environments characterized by semidiurnal microtides (< 25 cm). Tidal range, however, varies seasonally due to wind stress and changes in barometric pressure, but remains between 0 and 23 cm (García et al., 2000).

Two caves were selected for this study, both hosting modern phreatic overgrowths on speleothems at the present water table: Cova des Pas de Vallgornera (Vallgornera), located on Mallorca's southern coast near Cala Pi in the Llucmajor municipality, and Coves del Drac, on the eastern coast in the outskirts of Porto Cristo (Fig. 1). The two littoral caves are each within a horizontal distance of about 400 m of the coast and developed in upper Miocene calcarenites and limestones at less than 25 m below the surface (Ginés & Ginés, 2007; Ginés et al., 2014). Vallgornera has 74 km of mapped passage that is accessed by a single nearly-sealed entrance (Merino et al., 2014). With less than 4 km of passages (Gràcia et al., 2007), Drac is the most visited cave in Europe (Robledo & Durán, 2010). Since about 3000 tourists a day spend about an hour covering 1.2 km of the cave, their respiration likely increases the cave atmosphere pCO_2. To maintain the natural conditions of temperature, relative humidity, and CO_2 concentration, the cave is artificially ventilated, further altering the natural conditions. The study area is in the non-touristic part of the cave. Therefore, any impacts of present day tourism, including altered temperature, relative humidity, and pCO_2, are minimal at the monitoring site. However, samples collected by Boop (2014) and JJF suggest that higher pCO_2 is present in non-tourist areas of the cave, likely due to the decomposition of bat guano, passage morphology, and less efficient natural ventilation in this section of the cave.

DATA COLLECTION

This study was designed to monitor the physical and chemical conditions at the air-water interface where overgrowths precipitate. Sensors were installed in both caves for almost 16 months between December 2011 and March 2013. Sample intervals varied by parameter based on the needs of resolution, sensor memory, and the field schedule. Sensor malfunctions resulted in incomplete records.

A YSI 6920 sonde was fitted into a foam float and tethered to monitor conditions at 15 cm of depth within the water column at a fixed location. Cave-water temperature (T_w) (accuracy ± 0.15 °C; precision 0.01 °C) was measured at 3 hr intervals. Cave-water level (WL_c) was calculated at 15 min intervals using In-Situ Baro Merge software with water pressure from an In-Situ Aqua TROLL (accuracy ± 1.05 hPa; precision 0.5 hPa), and barometric pressure (p) (accuracy ± 1.5 hPa; precision 0.075 hPa) from an In-Situ Baro TROLL sensor, which also collected cave air temperature (T_c) (accuracy ± 0.1 °C; precision 0.01 °C). The accuracy of the barometric-pressure-based water level is ± 0.021 m. The mean was subtracted from WL_c to compare relative water level fluctuations. The Aqua TROLL sensors in both caves failed 11 months after their deployment.

A CO2meter.com K33-ELG logger (accuracy ± 30 ppm; precision 20 ppm) recorded hourly CO_2. The CO_2 readings were converted to partial pressure (pCO_2) using the relationship $pCO_2 = CO_{2(raw)} \times 1013/p$, where $CO_{2\ (raw)}$ is the input data and p is in-cave barometric pressure (Spötl et al., 2005).

Additional data were obtained from governmental organizations to contextualize the cave specific data. Surface temperature (T_s) (°C; 3 hr intervals) and precipitation (P) (mm; daily totals) from the Agencia Estatal de Meteorología (AEMet) weather stations Llucmajor II (Llucmajor) and Manacor-Poliesportiu (Manacor) were the closest available to Vallgornera and Drac, respectively. To determine maxima, minima, and lags during 2012, the daily averages of cave air

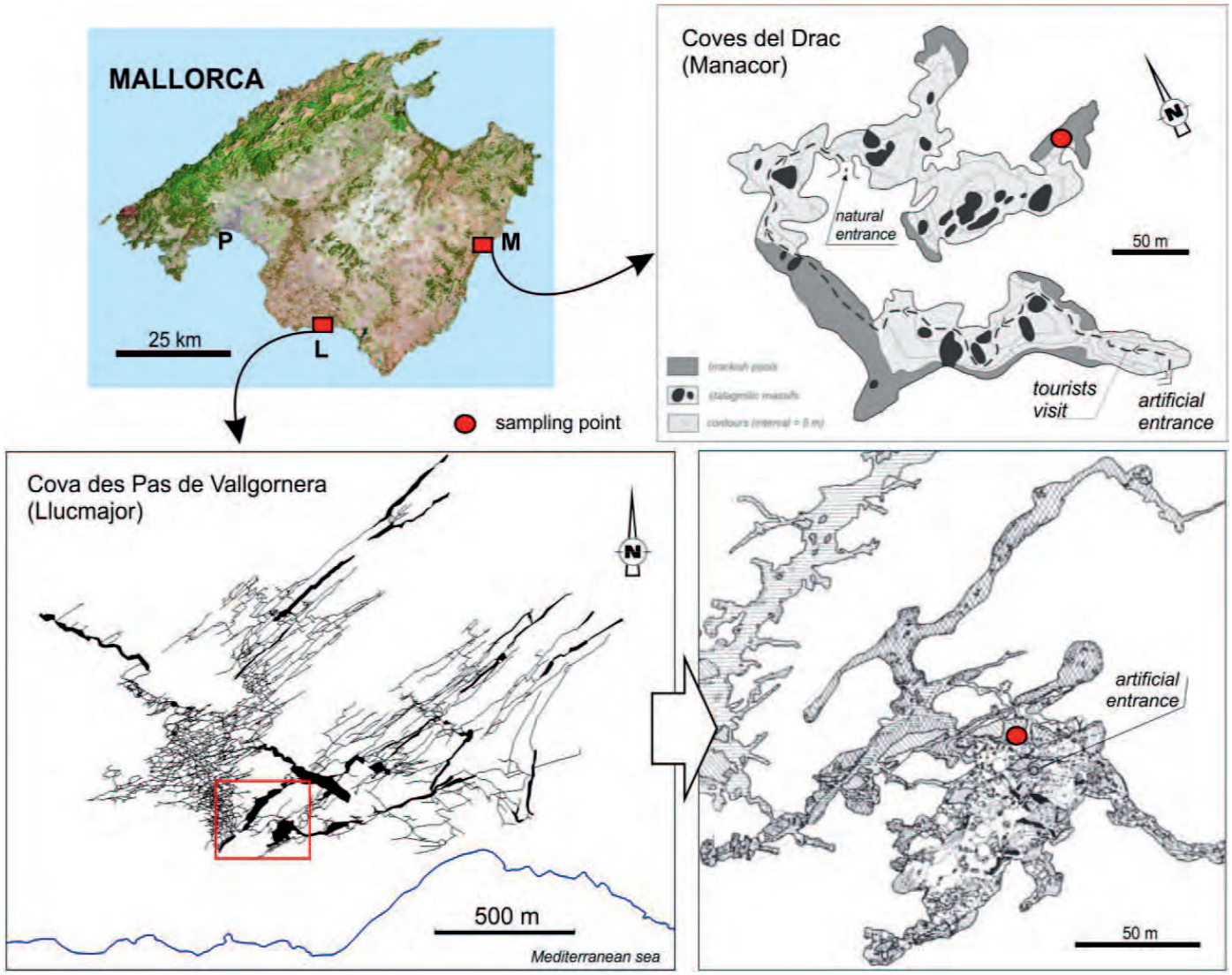

Figure 1. Map of Mallorca and caves studied. Palma Sea Level Monitoring Facility is indicated by P; Llucmajor II AEMet and the Manacor weather stations are indicated with L and M, respectively. The map of Drac is modified after Ginés and Ginés (2007) and those of Vallgornera are modified from Merino et al. (1993, 2014).

Table 1. Maxima, minima, and averages for temperature (T) and pCO_2 during 2012. The average surface temperature (T_s), cave air temperature (T_c), cave water temperature (T_w), and pCO_2 were computed for each day. This daily data was smoothed using a 7 day moving-average filter. pCO_2 averages were excluded due to missing data.

	Vallgornera				Drac			
Parameter	T_w, °C	T_c, °C	T_s, °C	pCO_2, ppm	T_w, °C	T_c, °C	T_s, °C	pCO_2, ppm
2012 Maximum	19.69	19.44	27.82	2,328	18.51	18.43	26.86	1,072
	9/12/12	10/19/12	8/11/12	9/23/12	11/19/13	12/24/12	8/11/12	8/28/12
2012 Minimum	19.23	18.99	6.05	1,007	18.45	18.31	6.34	399
	4/17/12	4/15/12	2/8/12	12/18/12	5/22/12	5/7/12	2/7/12	1/6/12
Study Average	19.4	19.2	15.6	···	18.5	18.4	15.5	···

and cave water temperatures, surface temperatures, and pCO_2 were computed, and then smoothed with a 7 day moving average filter. Finally, absolute tide gauge level (WL_P) from the Palma de Mallorca UNESCO-IOC Sea Level Station Monitoring Facility (2016) was downloaded in 15-min intervals that corresponded with the measurements of the cave-water level.

Time Series Analysis

Time series analysis was used to evaluate temporal trends in data collected at regular intervals. Analyses presented below were computed using commands in the Signal Processing Toolbox of Matlab 2013a. Frequency-domain figures are terminated below the Nyquist frequency, equal to half of the sampling frequency.

The relationship between tide gauge and cave water levels at each cave was investigated using coherency analysis. To examine controls on cave pCO_2, coherency analysis was also used to investigate barometric pressure, cave and surface temperatures, and water level in the caves. Coherency is a function of the power-spectral densities of each time series, and their cross-power spectral density. Coherency measures how well correlated two time series are as a function of frequency, with values between 0 (incoherent) and 1 (perfectly coherent). It also measures the phase angle, ψ, between these time series as a function of frequency. Thus if there is a strong coherency at a particular frequency, both time series must have significant energy at that frequency, and from ψ the time lag in hours can be determined. Magnitude-squared coherency estimates were computed using the MSCOHERE Matlab command, using a Hamming window of length 256 samples with an overlap of 128 samples.

Spectrograms are computed to investigate the temporal behavior of periodic signals. To identify high-frequency pCO_2 fluctuations, a stationary time series was created: the annual signal was removed by subtracting a 20-point (20-hr) moving average. Spectrograms were computed using the SPECTROGRAM Matlab command, a window length of 24 samples, an overlap of 12 samples, and a 2048-sample fast Fourier transform.

Results

Meteorological Data

Surface temperature and precipitation show similar patterns at both sites (Fig. 2). During the study period, mean T_s was 15.6 °C at Llucmajor and 15.5 °C at Manacor. Relative to T_s, which displays annual and daily fluctuations, cave air temperatures were nearly stable within 0.5 °C (Figs. 2A–2C). Total precipitation P differed between sites, with 485.4 mm recorded at Llucmajor (Fig. 2A) and 392.2 mm at Manacor (Fig. 2B).

Cave Air and Water Temperature

Over the study period, mean water temperature in Vallgornera was 19.4 °C, whereas mean cave air temperature was 19.2 °C (Table 1), and T_w was always greater than T_c (Fig. 2C). During 2012, maximum T_c lagged that of T_w by 37 days (Table 1). In contrast, minimum T_c lagged that of T_w by two days.

During the study, mean T_c and T_w in Drac were 18.4 and 18.5 °C, respectively, with ranges of only 0.2 and 0.15 °C, respectively (Table 1). These values are similar to spot measurements recorded in the touristic part of the cave by BPO, where temperatures would rise well above 21 °C when large groups (about 500 people) visited the cave and when forced-air ventilation was not in operation.

As in Vallgornera, T_w in Drac was always greater than T_c (Fig. 2C). The range of T_w was lower in Drac, making it difficult to determine maxima and minima and determine lag times. During 2012, the maximum T_c in Drac lagged T_s by 135 days; the same lag in Vallgornera was only 69 days (Fig. 2; Table 1). Maximum T_w in Vallgornera followed maximum T_s after 32 days. Minimum T_c and T_w in Vallgornera lag T_s by 67 and 69 days, respectively. Minimum T_c and T_w in Drac were recorded 90 and 105 days after minimum T_s, respectively.

Cave pCO_2

In both caves, peak pCO_2 occurred in August/September (Table 1, Fig. 2D). pCO_2 in Vallgornera was higher than in Drac and showed greater amplitude of variation on annual and daily scales. The time between the highest and lowest recorded pCO_2 values was 157 days in Vallgornera, and only 121 days in Drac.

There is significant surface temperature T_s – pCO_2 coherency in Vallgornera (Table 2) at a 12 hr period. The lag time of the January – April 2012 data was 4 hr, while that of the May 2012 – March 2013 was 4.8 hr. An 8 hr period is also present in the Vallgornera data; the lag is 3.9 hr in the January – April 2012 data and 3.2 hr in the May 2012 – March 2013 series. No notable T_s - pCO_2 relationship is observed in Drac (Table 2).

The cave water levels in Vallgornera and Drac are shown in Fig. 3A. WL_c – pCO_2 coherency is present in Vallgornera at the 11.6hr period (Fig. 4A, Table 2). Lead times are 4.4 hr for the January – April 2012 time series, and 2.7 hr for the July – November 2012 data (Fig. 4B). WL_c – pCO_2 coherency is also present at a 12.8 hr period with a 5 hr lead in the January – April 2012 data from Drac (Fig. 4C and D), but no cycles were identified in the July – November 2012 dataset.

Barometric pressure p – pCO_2 coherency is present at a 12.2hr period in Vallgornera, with lead times of 5.3 hr in the January – April 2012 data and 4.5 hr in the July – November 2012 dataset (Table 2). Drac p – pCO_2 coherency analysis identified an identical 12.2 hr period in the July – December 2012 series and a 12.8 hr period in the January – March 2013 data. The corresponding lead times are 9 min and 5.5 hr, respectively. A similar p – pCO_2 coherency peak is not present in the January – April 2012 data from Drac.

Table 2. Notable peaks from magnitude squared coherency analyses for surface temperature–pCO_2 (T_s–pCO_2), barometric pressure–pCO_2 (p–pCO_2), and absolute tide gauge level – cave-water level ($WL_P - WL_c$).

	Vallgonera							Drac						
Parameter	Date Range	Coherency	*f*, Hz	Period, hr	Ψ, rad	Lead, hr	Lag, hr	Date Range	Coherency	*f*, Hz	Period, hr	Ψ, rad	Lead, hr	Lag, hr
$T_s - pCO_2$														
	01–2012 –	0.91	2.32×10^{-5}	12.0	–2.10		4.0	12–2011 –						
	04–2012	0.66	3.47×10^{-5}	8.0	–3.04		3.9	04–2012						
	05–2012 –	0.32	2.32×10^{-5}	12.0	–2.53		4.8	07–2012 –	0.34	2.24×10^{-5}	12.4	0.63	1.3	
	03–2013	0.4	3.47×10^{-5}	8.0	–2.48		3.2	12–2012	0.38	2.39×10^{-5}	11.6	1.21	2.2	
								01–2013 –	0.74	1.88×10^{-5}	14.8	–3.12		7.3
								03–2013	0.35	2.46×10^{-5}	11.3	1.86	3.4	1.9
									0.35	2.60×10^{-5}	10.7	–1.11		
$p - pCO_2$														
	01–2012 –	0.97	2.28×10^{-5}	12.2	2.74	5.3		01–2012 –						
	04–2012	0.57	2.82×10^{-5}	9.8	2.47	3.9		04–2012						
		0.75	3.15×10^{-5}	8.8	2.50	3.5								
		0.87	3.47×10^{-5}	8.0	2.51	3.2								
		0.73	4.12×10^{-5}	6.7	2.18	2.3								
		0.81	4.56×10^{-5}	6.1	1.74	1.7								
		0.65	6.94×10^{-5}	4.0	1.22	0.8								
	05–2012 –	0.62	2.28×10^{-5}	12.2	2.33	4.5		07–2012 –	0.38	2.28×10^{-5}	12.2	0.008	0.1	
	03–2013	0.32	3.47×10^{-5}	8.0	2.26	2.9		12–2012	0.24		8.0	–1.71		2.2
									0.23		5.6	–2.85		2.5
								01–2013 –	0.26	1.74×10^{-5}	16.0	1.81	4.6	
								03–2013	0.28	2.17×10^{-5}	12.8	2.69	5.5	2.5
									0.24	2.50×10^{-5}	11.1	0.72	1.3	0.2
									0.23	2.82×10^{-5}	9.8	1.14	1.8	0.1
									0.37	3.91×10^{-5}	7.1	–2.23	0.8	
									0.36	5.64×10^{-5}	4.9	1.08		
									0.38	9.98×10^{-5}	2.8	–0.47		
									0.45	1.17 × 10–5	2.4	–0.15		
$WL_P - WL_c$														
	12–2011 –	0.94	1.09×10^{-5}	25.6	–1.19		4.9	12–2011 –	0.92	1.09×10^{-5}	25.6	–0.96		3.9
	11–2012	0.96	2.17×10^{-5}	12.8	–1.98		4.0	11–2012	0.96		12.8	–1.75		3.6

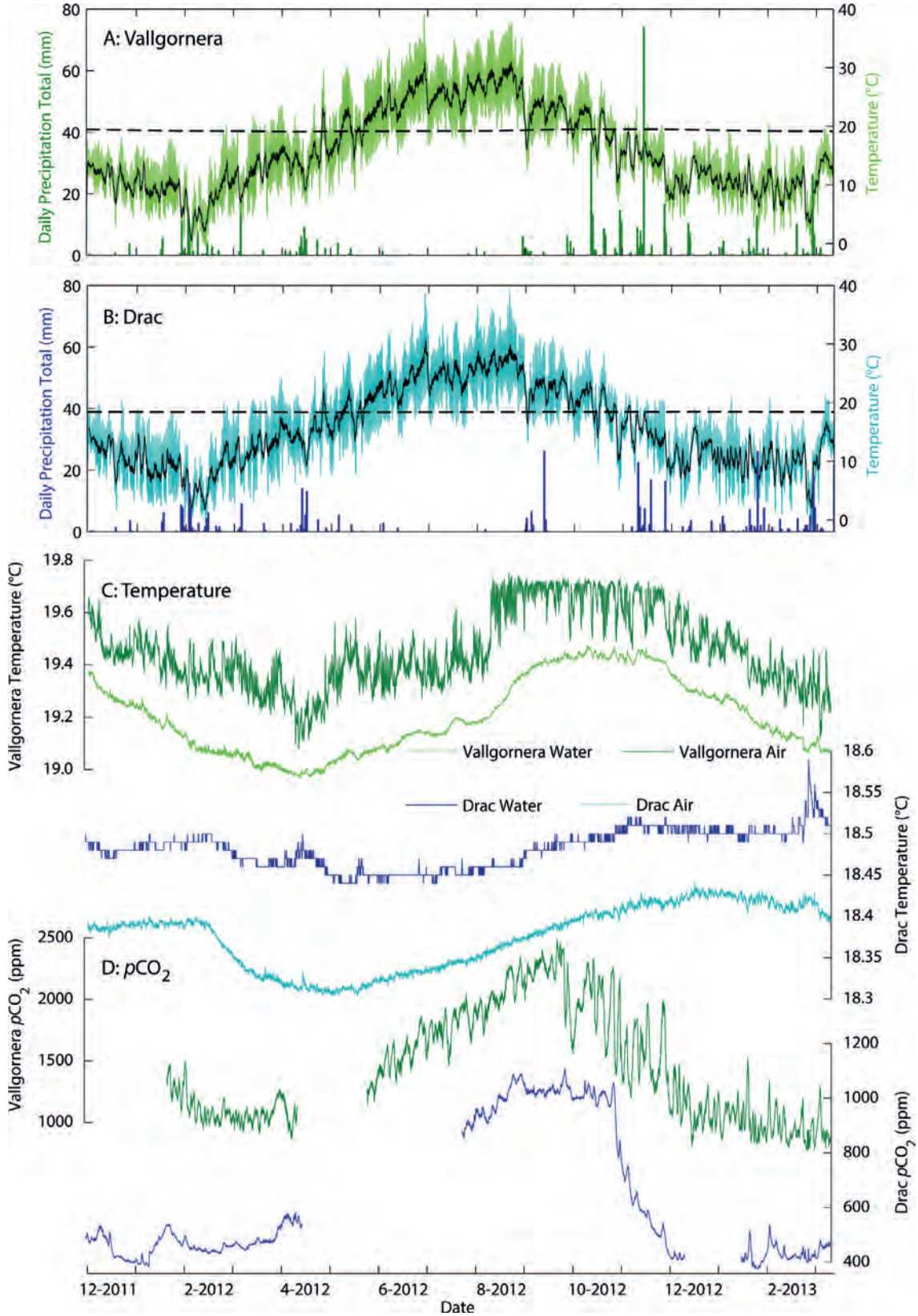

Figure 2. A) Surface temperature (T_s) and daily precipitation (P) from AEMet Llucmajor II and B) Manacor stations. Right axis: T_s (black line shows a 10-point moving average). Black dashed lines show cave air temperature (T_c) for Vallgornera (A) and Drac (B) from part C. C) Detailed cave air temperature (T_c) and water temperature (T_w) and D) cave pCO_2 (corrected for cave barometric pressure) from Vallgornera and Drac.

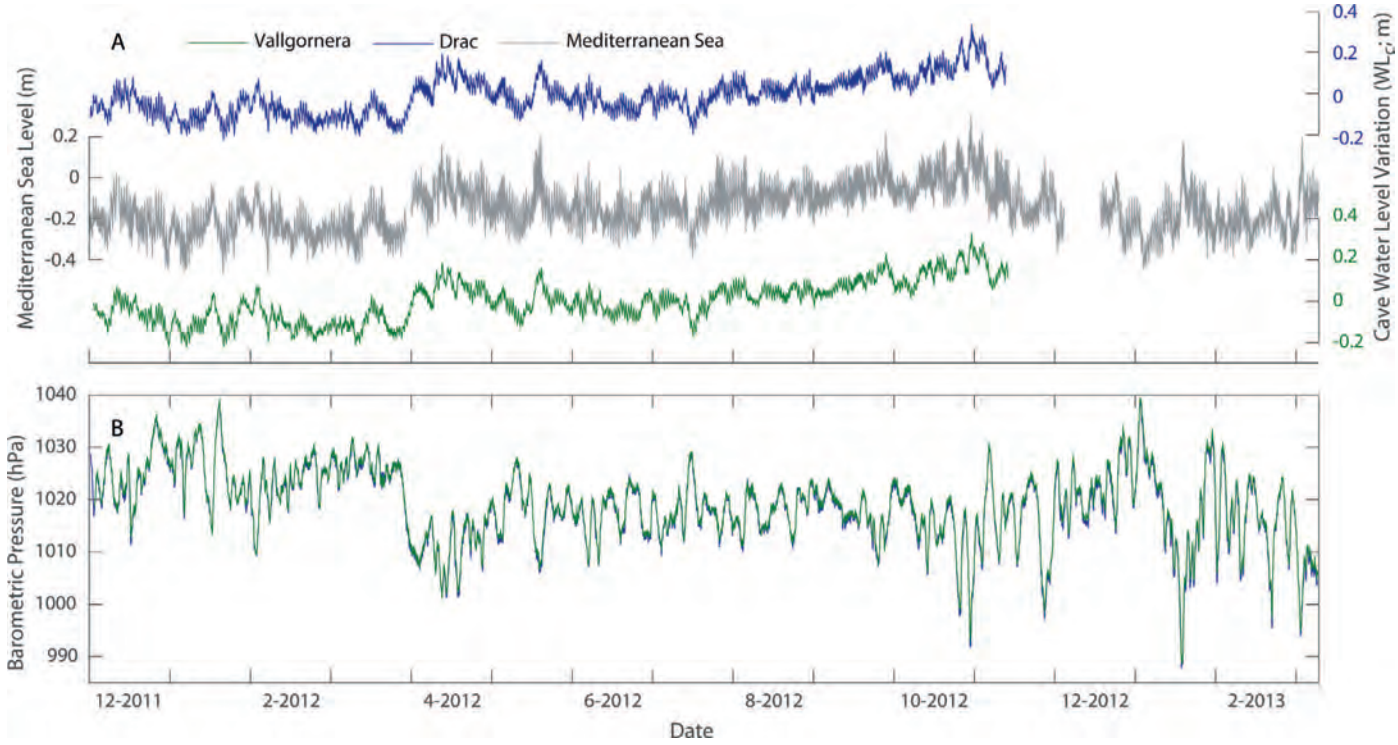

Figure 3. A) Cave water levels (WL_c) and Mediterranean Sea Level from tide gauge (WL_p). B) Barometric pressure (p).

pCO_2 records are reproduced next to the spectrograms of filtered data for both Vallgornera and Drac in Fig. 5. High-frequency pCO_2 fluctuations in Vallgornera (Fig. 5A) create spectral power at the 12-hr period in Vallgornera (Fig. 5B). In Drac, which has lower-amplitude pCO_2 fluctuations (Fig. 5C), lower spectral power exists at the 12 hr cycle at some points throughout the year (Fig. 5D).

Cave Water Level

The cave water level WL_c is similar in both caves (Fig. 3A), and both records show a similarity to the tide gauge water level WL_P. The strongest $WL_P - WL_c$ coherency peak (>0.96) in both caves corresponds to a 12.8-hr period, and the second strongest peak (>0.92) occurs at a 25.6 hr period (Fig. 6, Table 2). In Vallgornera, the 12.8-hr WL_c cycle lags WL_P by 4.0 hr, whereas the 25.8-hr cycle lags by 4.9 hr. The corresponding lag in Drac of the 12.8-hr cycle was 3.6 hr, while that of the 25.6-hr cycle was 3.9 hr.

The results from the coherency analyses indicate a period close to, but not matching the lunar day (24.8 hr). However, strong similarity between the cave (WL_c) and tide gauge (WL_P) water levels is clearly seen when the data are considered in the time domain (Fig. 7). Data from July 20 – 23, 2012 was chosen because no rainfall was recorded for > 30 days before this interval. The discrepancy between results in the frequency and time domains is a consequence of the 3-hr sample interval of the coherency analyses; the 24.8-hr lunar day signal rounds up to the closest possible frequency output (25.6 hr). The same discrepancy applies to the mixed semi-diurnal 12.4-hr cycle that is output as strong coherency at 12.8 hr.

Over the entire study period, there was strong positive linear correlation between WL_P and WL_c in both caves. In Vallgornera, the *r*-value from Pearson's correlation coefficient for WL_P and WL_c was 0.88 (slope $y = 0.82x + 1.41$, $n = 32{,}372$), while that of Drac was 0.87 (slope $y = 0.76x + 1.71$, $n = 32{,}419$). WL_P ranges 0.76 m, whereas the ranges in WL_c at Vallgornera and Drac are almost identical, 0.55 and 0.56 m, respectively (Fig. 3A). Thus, over the study period, the attenuation of WL_P is approximately 0.2 m at both sites.

Discussion

Cave Air and Water Temperatures

While it is generally accepted that cave temperature is a good approximation of the annual average surface temperature in the cave area (Wigley & Brown, 1976), over the study period, mean cave T_c and cave water T_w temperatures in both caves are approximately 3 °C greater than mean surface temperature during the same time interval. This observation could be explained by either differences in cave ventilation regimes or the heat exchange between seawater and cave atmosphere due to each cave's hydrologic connection to the Mediterranean Sea. The higher T_c and T_w in Vallgornera compared to Drac may be due to the cave's proximity to a region known to host a deep thermal reservoir (López-García & Mateos-Ruíz, 2006). Merino et al. (2011) report tempera-

tures of 27.1 °C and 23.6 °C in Cova de sa Guitarreta and Pou de Can Carro, located less than 10 km northwest of Vallgornera. Based on the presence of various hypogene features and unusual mineral assemblages, thermal basal recharge may have played a major role in the speleogenesis of Vallgornera (Ginés et al., 2009, 2014; Fornós et al., 2011; Onac et al., 2014).

pCO_2

Higher pCO_2 in Vallgornera compared to Drac may be attributed to limited ventilation in the former cave, which has a single closed entrance. A large, natural collapse entrance in Drac, as well as less-restricted cave passages, likely allows for stronger ventilation, maintaining lower pCO_2 in cave air (Ek & Gewelt, 1985; Hu et al., 2008).

In both caves, pCO_2 increases in the summer months, with the highest concentration observed at the end of the growing season. Similar findings are reported in Banner et al. (2007), Liñán et al. (2008), Faimon et al. (2012), Cowan et al. (2013), Mandić et al. (2013), and Lang et al. (2016). The pCO_2 plateau noticed in Drac between August and early November is due to this cave's particular air circulation. Annual ventilation is driven by the disparity between surface and cave temperatures during winter, when cool, relatively dense air descends into cave passages, forcing the CO_2-rich air out of the cave. Throughout the summer months, the outside temperatures exceed those inside the cave causing the ventilation to slow down or cease, allowing CO_2 to build up. Dumitru et al. (2015) confirmed this bi-directional ventilation regime in Drac by deploying radon sensors throughout the non-touristic branch of the cave, including one detector at the same site investigated in this study (Fig. 1). In Vallgornera and Drac, this exchange is sufficiently slow that rapid, high-amplitude decreases of T_c do not coincide with the seasonal decrease of pCO_2 (Fig. 2). Instead, the thermal signal is buffered between the entrances and the study sites. It is likely that the network of fractures in the overlying bedrock at Vallgornera plays a major role in the seasonal overturn, whereas in Drac, this ventilation occurs through the cave's large natural entrance.

The calculated surface temperature $T_s - pCO_2$ coherency values and corresponding lag times suggest the possibility of overnight thermal- and density-driven ventilation in Vallgornera, but there is no peak in spectral coherency at a 24 hr period (Table 2). Additionally, during the summer months when T_s consistently exceeds cave temperature T_c, thermal cave gradients could not drive ventilation and high-frequency pCO_2 variations.

pCO_2 can be controlled by cave-barometric pressure p in some caves. For example, Baldini et al. (2006) report nightly ventilation due to p minima. Cowan et al. (2013) present diurnal fluctuations that correspond to p as global atmospheric tide in caves in Texas, USA. Similarly, Benavente et al. (2011) suggest that p may drive cave-air circulation during summer, but state that their data are insufficient to support the hypothesis. $p - pCO_2$ coherency was found throughout the year in both Vallgornera and Drac in approximately 12-hr cycles (Table 2). The different lead times do not support the potential relationship identified by $p - pCO_2$ coherency values, because p should exert a constant control irrespective of surface temperature and other variables. Further, the lack of replication of $p - pCO_2$ coherency values in Drac between the January – April 2012 data and the January – March 2013

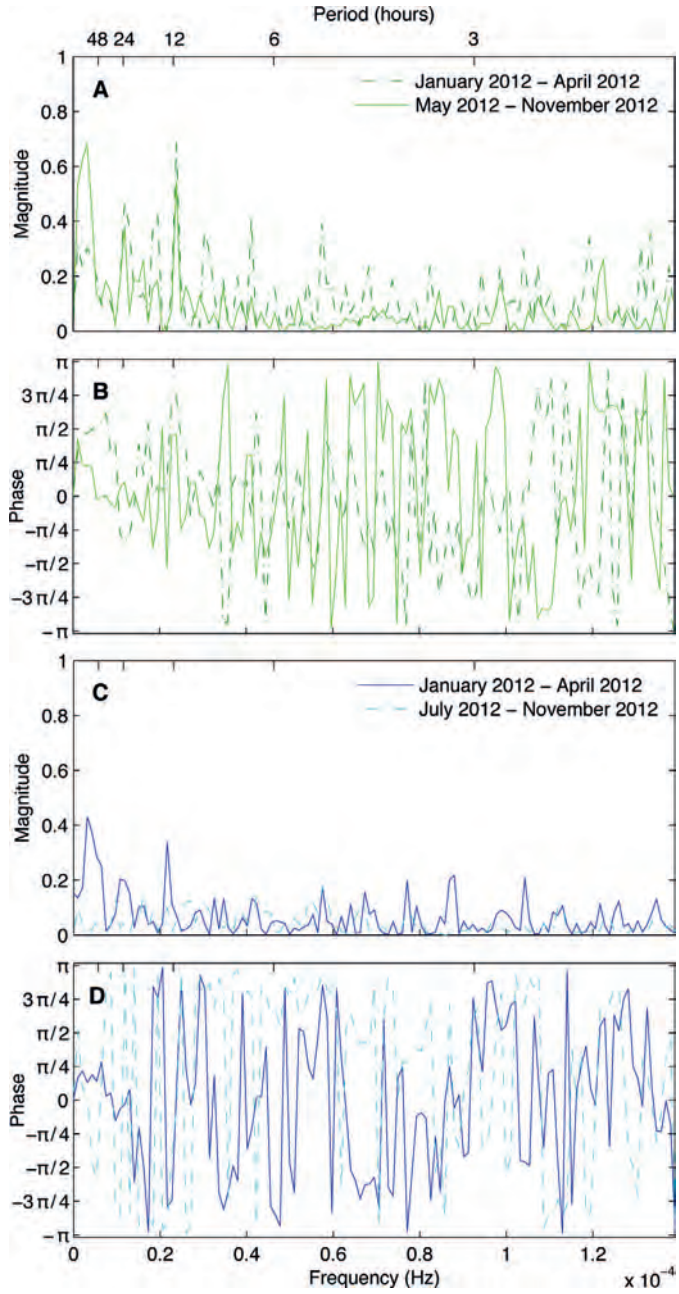

Figure 4. Cave water level $WL_C - pCO_2$ coherency for Vallgornera and Drac (A and C) and the corresponding phase angles (B and D). Top axis labels: time domain; bottom axis: frequency domain.

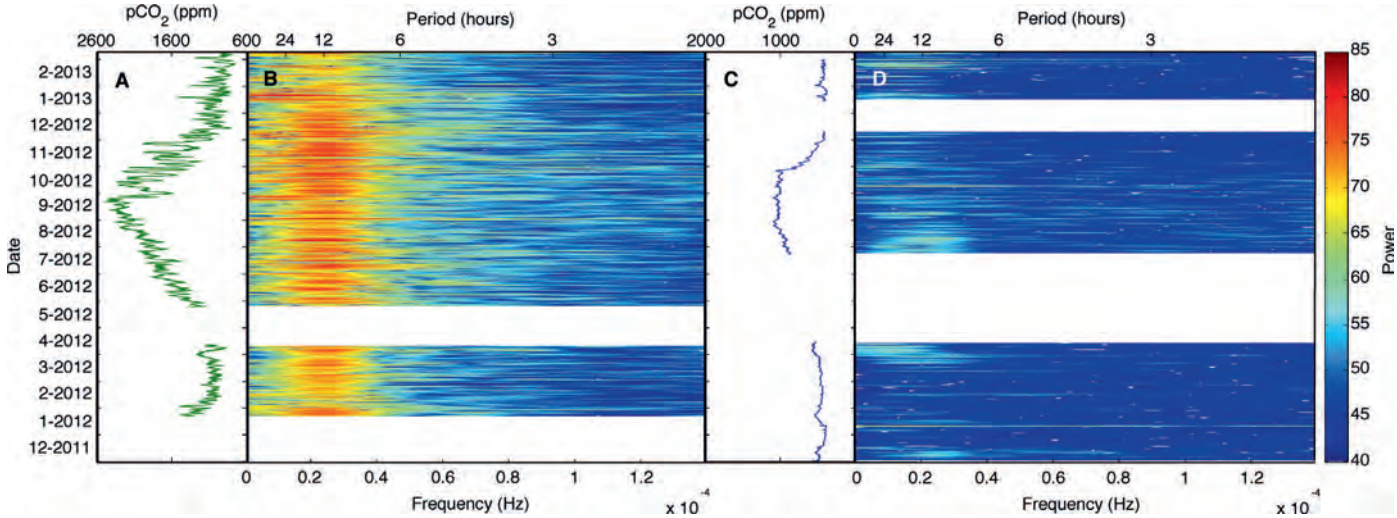

Figure 5. Vallgornera and Drac pCO_2 time series (A and C) and their spectrograms (B and D).

series indicates that further work is necessary to evaluate the control of p on pCO_2 fluctuations, at least in Drac. p – pCO_2 coherency values and consistent period and lead times in Vallgornera support the hypothesis that pCO_2 responds to p in this near closed-system cave, but it is not the primary control.

Cave water level WL_c – pCO_2 coherency values support the hypothesis that WL_c affects pCO_2 throughout the year in Vallgornera and to a lesser extent during the summer months in Drac (Fig. 4A and C, Table 2). This is reinforced by the spectral power observed at approximately 12 hr in Vallgornera (Fig. 5B). These observations suggest that the transition from low- to high-water level forces higher-pCO_2 air from the cave (Fig. 8A). Regardless of surface temperature, as the water recedes, tropospheric air sinks into the cave, with a volume equivalent to the volume reduction of seawater in the cave (a function of water level WL_c) (Fig. 8B). Significant cave temperature variation was not observed at either study site; any external thermal signal is attenuated.

In Vallgornera, a forward and reverse piston effect seems to dominate semidiurnal cave air exchange through the overlying bedrock, which is less than 20 m thick (Fig. 8). Twice-daily pCO_2 variations on the order of 300 ppm were recorded throughout the year. It is possible that in Vallgornera's extensive horizontal network of passages with limited vertical extent, the sensor recorded the movement of a boundary layer of CO_2 maintained by degassing from the water (Badino, 2009), though no data are currently available to support or refute the presence of such a boundary layer at this site.

Exchange through the entrance likely dominates in Drac (Fig. 8). In addition to maintaining lower pCO_2, Drac's large passages and few constrictions allow for cave water level driven exchange through its large entrance, which explains the lower amplitude of semidiurnal fluctuations that are only recorded during the summer months, when large-scale temperature-driven ventilation is inactive. Compared to Vallgornera, the Drac study room has greater volume, thus the amplitude of recorded pCO_2 fluctuations may be much smaller due to the homogenous cave atmosphere maintained by temperature- and density-driven convection currents. More in-depth spatial (horizontal and vertical) pCO_2 sampling is necessary to better constrain the dynamics of cave troposphere pCO_2 exchange in both caves.

CO_2 degassing from the cave water is an essential process for the formation of phreatic overgrowths on speleothems (Pomar et al., 1976, 1979; Csoma et al., 2006) and is driven by the gradient between pCO_2 in the cave water and air (Boop et al., 2014). The lower overall pCO_2 in Drac allows for periods of degassing that cause water to become supersaturated with respect to calcium carbonate, as evidenced by ephemeral rafts of calcite observed throughout the year. Conversely, relatively high pCO_2 in Vallgornera is not presently conducive to extended periods of rapid CO_2 exsolution. Thus, the conditions for supersaturation with respect to carbonate minerals and subsequent precipitation of POS are not currently satisfied (Boop et al., 2014). Based on the U/Th dates from a Vallgornera POS sample, these unfavorable geochemical conditions may have started 600 years ago (Tuccimei et al., 2009, 2010).

Cave water level

The attenuation of the tide gauge water level WL_P inside the littoral caves and the strong relationship between variation in it and the cave level WL_c, illustrated by very high coherency and robust linear correlations, further confirm that POS are excellent recorders of mean sea-level position.

Though WL_c fluctuates with a roughly 4-hr lag behind WL_P, there is limited evidence of direct Mediterranean Sea water intrusion during this tidally-driven process (Boop et al., 2014). Cave water temperatures T_w fluctuated less than 1 °C

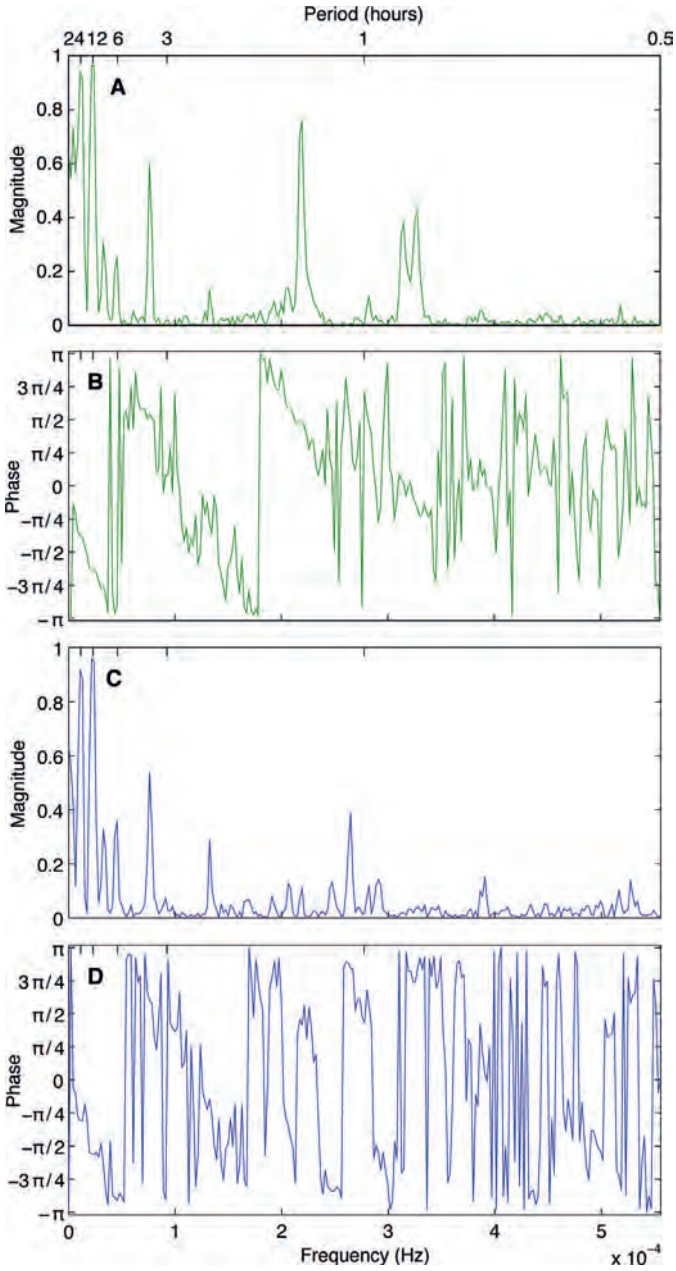

Figure 6. Vallgornera tide gauge level WL_P – cave water level WL_C coherency (A) and corresponding phase angles (B); same analyses for Drac (C and D). Top axis: time domain; bottom axis: frequency domain.

over the study period, with a higher range observed at Vallgornera than in Drac. Direct mixing with the Mediterranean Sea would introduce a strong annual period in T_w because of changes in seawater temperature. Lack of mixing is further supported by the low turbidity of the water, lack of observed currents, and the maintenance of brackish water at the surface of both study sites (Boop et al., 2014). The latter condition is likely maintained throughout the year by meteoric recharge.

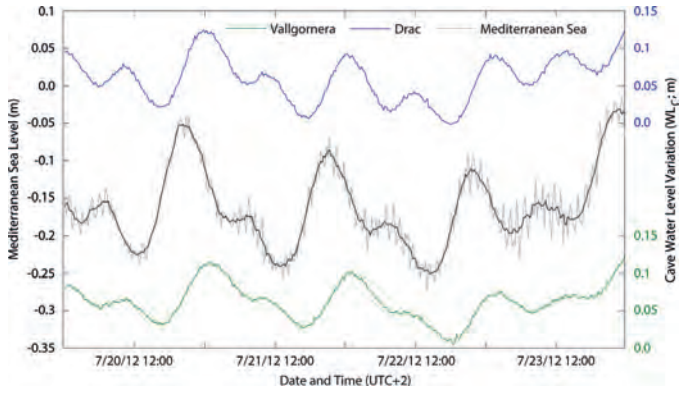

Figure 7. Expanded-scale cave water level (WL_C) variation from July 20–23, 2012, and Mediterranean Sea level (WL_P) (black line: 5-point moving average).

Time series analysis did not reveal a relationship between cave water levels and precipitation. In non-coastal areas, time series analysis can identify the effect of rainfall on karst aquifers (Padilla & Pulido-Bosch, 1995; Larocque et al., 1998; Panagopoulos & Lambrakis, 2006; Bailly-Comte et al., 2008). However, analyses based on spring discharge or piezometric head are not applicable to understand controls on water level in Mallorca's littoral caves because water level is dominantly controlled by the Mediterranean Sea level. Similarly, Kim et al. (2005) were unable to identify any effect of precipitation on coastal water levels in Korea and attribute fluctuations solely to the tidal effect using time series analysis.

CONCLUSIONS

The phreatic overgrowths on speleothems found in the littoral caves of Mallorca are valuable paleo-sea level index points. These encrustations form at the cave water table, which is, and was in the past, coincident with sea level because of the negligible hydraulic gradient between the caves and the Mediterranean Sea. The present study validates the assumption that the cave water levels fluctuate in response to the Mediterranean Sea tide by identifying an approximately 4-hr lag of WL_c behind the tide gauge level in the sea WL_P. The semidiurnal signal is preserved, though slightly attenuated, in WL_c at each study site. The primary control of WL_P masks any direct effect of P on WL_c.

The present study, Boop (2014), and Boop et al. (2014) monitored conditions relevant to the precipitation of phreatic overgrowths on speleothems. Some caves may be more likely to host the specific geochemical conditions necessary for their precipitation. These conditions are met when cave water is supersaturated with respect to carbonate minerals at times when CO_2 degasses from water into the cave atmosphere. A high concentration gradient between pCO_2 of the water and air promotes this process. Thus, faster degassing, and therefore

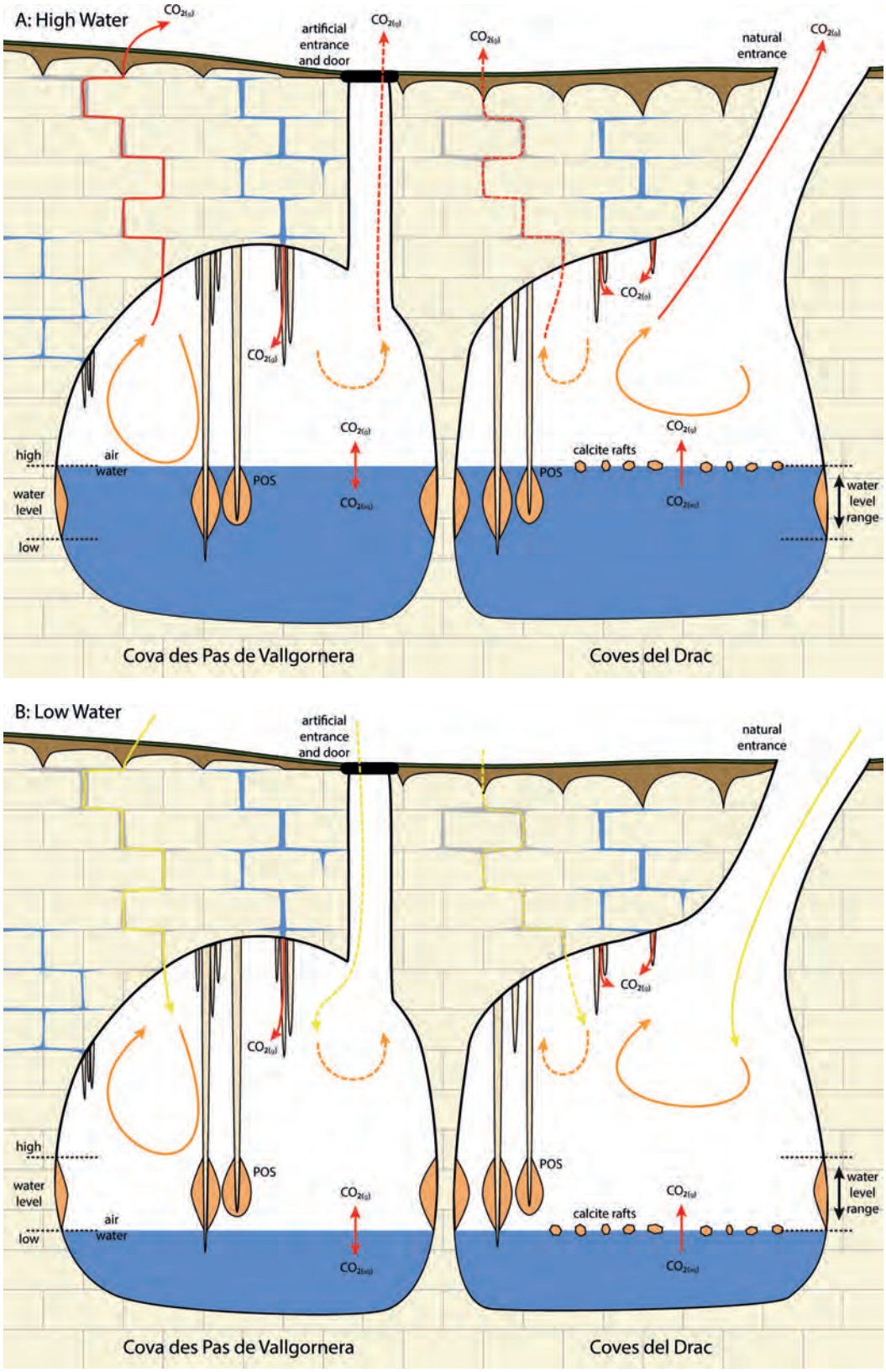

Figure 8. A simplified model of semidiurnal pCO_2 dynamics in Vallgornera (left) and Drac (right) associated with the rising (A) or receding (B) of the cave water level, which is overprinted on seasonal (winter) ventilation. Phreatic overgrowths on speleothems appear to be actively growing today in Drac but not in Vallgornera. See text for additional explanations.

solution supersaturation and possible precipitation of POS, is expected to occur with low cave air pCO_2. The annual cycle in pCO_2 is driven by cave ventilation in the winter months, when colder, denser tropospheric air sinks through the bedrock or entrances into subsurface voids, displacing cave air and reducing pCO_2. The thermal signature of this tropospheric air is quickly attenuated within the caves; cave air and cave water temperatures vary by less than 1 °C throughout the year and lag behind surface temperature by several months. pCO_2 fluctuations have larger amplitudes in Vallgornera, likely due to the overall higher pCO_2 and the constricted nature of the study site. It is likely that at both sites, rising cave water level due to barometric pressure changes and tidal pumping (Fig. 8A) forces high pCO_2 air out from the cave, driving semidiurnal tropospheric exchange throughout the year with a roughly 12-hr period. In Vallgornera, air escapes dominantly through the bedrock fissures (solid red line in Fig. 8A), whereas Drac's less-constricted passages promote displacement through its large natural entrance. When WL_c recedes (Fig. 8B), tropospheric air sinks into the cave through the bedrock in Vallgornera (solid yellow line) and primarily through the entrance in Drac. Vallgornera's nearly sealed entrance, maze-like passages, and constrictions promote the buildup of higher concentrations of pCO_2 throughout the year, restricting CO_2 degassing from the water, thus suppressing calcium carbonate supersaturation and POS precipitation. In Drac, pCO_2 is lower throughout the year, which maintains conditions for CO_2 to degas from the cave water to air; this promotes calcium carbonate supersaturation, and thus, precipitation of ephemeral rafts and POS.

ACKNOWLEDGMENTS

This material is based upon work supported by the National Science Foundation under grant AGS-1103108 to BPO and MINECO projects CGL2013-48441-P and CGL2016-79246-P (AEI/FEDER, UE) to JJF. LMB received student research grants from the National Speleological Society and the Geological Society of America. AEMet is thanked for providing the temperature and precipitation records for Llucmajor II and Manacor-Poliesportiu that were used in this study. Scott McBride (USGS Tampa) is thanked for lending two YSI 6920 sensors for this study, as well as his invaluable guidance. We are grateful to Tony Merino, Marta Rodríguez-Homar, Joaquín Ginés, and Angel Ginés for their dedication in the field. We are indebted to the administration of Coves del Drac (Porto Cristo) for granting permission to perform research in the cave. We additionally appreciate the Federació Balear d'Espeleologia and the Department de Cultura i Patrimoni del Consell de Mallorca, as well as the Direcció General de d'Espais Naturals i Biodiversitat del Govern de les Illes Balears for helping with legal permissions for our work in Vallgornera. This paper benefited from discussions at the NSF- and PAGES-sponsored workshop on *Sea-level changes into MIS 5: from observation to prediction* (award AGS-1032243 to BPO). Finally, this manuscript was greatly improved through the thoughtful suggestions of three anonymous reviewers.

REFERENCES

Badino, G., 2009, The legend of carbon dioxide heaviness: Journal of Cave and Karst Studies, v. 71, no. 1, p. 100–107.

Bailly-Comte, V., Jourde, H., Roesch, A., Pistre, S., and Batiot-Guihe, C., 2008, Time series analyses for karst/river interactions assessment: Case of the Coulazou river (southern France): Journal of Hydrology, v. 349, p. 98–114, https://doi.org/10.1016/j.jhydrol.2007.10.028.

Baldini, J.U.L., Baldini, L.M., McDermott, F., and Clipson, N., 2006, Carbon dioxide sources, sinks, and spatial variability in shallow temperate zone caves: evidence from Ballynamintra Cave, Ireland: Journal of Cave and Karst Studies, v. 68, p. 4–11.

Banner, J.L., Guilfoyle, A., James, E.W., Stern, L.A., and Musgrove, M., 2007, Seasonal variations in modern speleothem calcite growth in central Texas, U.S.A.: Journal of Sedimentary Research, v. 77, p. 615–622, https://doi.org/10.2110/jsr.2007.065.

Benavente, J., Vadillo, I., Liñan, C., Carrasco, F., and Soler, A., 2011, Ventilation effects in a karstic show cave and in its vadose environment, Nerja, Southern Spain: Carbonates and Evaporites, v. 26, 11–17, https://doi.org/10.1007/s13146-011-0050-9.

Boop, L.M., 2014, Characterization of the Depositional Environment of Phreatic Overgrowths on Speleothems in the Littoral Caves of Mallorca (Spain): a Physical, Geochemical, and Stable Isotopic Study [Ph.D. thesis]: Tampa, University of South Florida, 128 p.

Boop, L.M., Onac, B.P., Wynn, J.G., Fornós, J.J., Rodríguez-Homar, M., and Merino, A., 2014, Groundwater geochemistry observations in littoral caves of Mallorca (western Mediterranean): implications for deposition of phreatic overgrowths on speleothems: International Journal of Speleology, v. 43, no. 2, p. 193–203, https://doi.org/10.5038/1827-806X.43.2.7.

Butzer, K.W., 1962, Coastal geomorphology of Majorca: Annals of the Association of American Geographers, v. 52, no. 2, p. 191–212, https://doi.org/10.1111/j.1467-8306.1962.tb00405.x.

Butzer, K.W., and Cuerda, J., 1962, Coastal stratigraphy of southern Mallorca and its implications for Pleistocene chronology of the Mediterranean Sea: Journal of Geology, v. 70, p. 389–416, https://doi.org/10.1086/626833.

Cowan, B.D., Osborne, M.C., and Banner, J.L., 2013, Temporal variability of cave-air CO_2 in central Texas: Journal of Cave and Karst Studies, v. 75, no. 1, p. 38–50, https://doi.org/10.4311/2011ES0246.

Csoma, A.E., Goldstein, R.H., and Pomar, L., 2006, Pleistocene speleothems of Mallorca; implications for paleoclimate and carbonate diagenesis in mixing zones: Sedimentology, v. 53, p. 213–236, https://doi.org/10.1111/j.1365-3091.2005.00759.x.

Cuerda, J., 1975, Los tiempos cuaternarios en Baleares: Palma de Mallorca, Instituto de Estudios Baleáricos, 304 p.

Dorale, J.A., Onac, B.P., Fornós, J.J., Ginés, J., Ginés, A., Tuccimei, P., and Peate, D.W., 2010, Sea-level highstand 81,000 years ago in Mallorca: Science, v. 327, no. 5967, p. 860–863, https://doi.org/10.1126/science.1181725.

Dumitru, O.A., Onac, B.P., Fornós, J.J., Cosma, C., Ginés, A., Ginés, J., and Merino, A., 2015, Radon survey in caves from Mallorca Island, Spain: Science of Total Environment, v. 526, p. 196–203, https://doi.org/10.1016/j.scitotenv.2015.04.076.

Ek, C., and Gewelt, M., 1985, Carbon dioxide in cave atmospheres. New results in Belgium and comparison with some other countries: Earth Surface Processes and Landforms, v. 10, p. 173–187, https://doi.org/10.1002/esp.3290100209.

Faimon, J., Ličbinská, M., Zajíček, P., and Sracek, O., 2012, Partial pressures of CO_2 in epikarstic zone deduced from hydrogeochemistry of permanent drips, the Moravian karst, Czech Republic: Acta Carsologica, v. 41, no. 1, p. 47–57.

Fornós, J.J., Gelabert, B., Ginés, A., Ginés, J., Tuccimei, P., and Vesica, P., 2002, Phreatic overgrowths on speleothems: a useful tool in structural geology in littoral karstic landscapes. The example of eastern Mallorca (Balearic Islands): Geodinamica Acta, v. 15, p. 113–125, https://doi.org/10.1080/09853111.2002.10510745.

Fornós, J.J., Merino, A., Ginés, J., Ginés, A., and Gràcia, A., 2011, Solutional features and cave deposits related to hypogene speleogenetic processes in

a littoral cave of Mallorca Island (western Mediterranean): Carbonates and Evaporites, v. 26, p. 69–81, https://doi.org/10.1007/s13146-010-0040-3.

García M.-J., Pérez, B., Fraile, M.-A., and Millan, J.G., 2000, Sea level variability along the Spanish Coast, 1990-1999. 10th General Assembly WEGENER Project, Extended Abstract Book, San Fernando. Boletín no 3/200 del Real Observatorio de la Armada, San Fernando, España, 5 p.

Ginés, J., 2000, El karst litoral en el levante de Mallorca: una aproximación al conocimiento de sus morfogénesis y cronología [Ph.D. thesis]: Palma de Mallorca, Universitat de les Illes Balears, 595 p.

Ginés, J., Fornós, J.J., Ginés, A., Merino, A., and Gràcia, F., 2014, Geologic constraints and speleogenesis of Cova des Pas de Vallgornera, a complex coastal cave from Mallorca Island (Western Mediterranean): International Journal of Speleology, v. 43, no. 2, 105–124, https://doi.org/10.5038/1827-806X.43.2.2.

Ginés, A., and Ginés, J., 1972, Consideraciones sobre los mecanismos de fosilización de la Cova de Sa Bassa Blanca y su paralelismo con las formaciones marinas del Cuaternario, *in* Proceedings, II Congreso Nacional de Espeleología, Oviedo, Spain, p. 11–28.

Ginés, A., and Ginés, J., 2007, Eogenetic karst, glacioeustatic cave pools and anchialine environments on Mallorca Island: a discussion of coastal speleogenesis: International Journal of Speleology, v. 36, no. 2, p. 57–67, https://doi.org/10.5038/1827-806X.36.2.1.

Ginés, A., Ginés, J., Fornós, J.J., Bover, P., Gómez-Pujol, L., Gràcia, F., Merino, A., and Vicens, D., 2012a, An introduction to the Quaternary of Mallorca, *in* Ginés, A., Ginés, J., Gómez-Pujol, L., Onac, B.P., and Fornós, J.J., eds., Mallorca: A Mediterranean Benchmark for Quaternary Studies: Monografies de la Societat d'Història Natural de les Balears, v. 18, p. 13–53.

Ginés, J., Ginés, A., Fornós, J.J., Merino, A., and Gràcia, F., 2009, About the genesis of an exceptional coastal cave from Mallorca Island (western Mediterranean); the lithological control over the pattern and morphology of Cova des Pas de Vallgornera, *in* White, W.B., ed., Proceedings of the 15th International Congress of Speleology: Kerrville, Texas, v. 1, p. 481–487.

Ginés, J., Ginés, A., Fornós, J.J., Tuccimei, P., Onac, B.P., and Gràcia, F., 2012b, Phreatic overgrowths on speleothems (POS) from Mallorca, Spain: updating forty years of research, *in* Ginés, A., Ginés, J., Gómez-Pujol, L., Onac, B.P., and Fornós, J.J., eds., Mallorca: A Mediterranean Benchmark for Quaternary Studies: Monografies de la Societat d'Història Natural de les Balears, v. 18, p. 111–146.

González-Hernández, F.M., Goy, J.L., Zazo, C., and Silva, P.G., 2001, Actividad eolica—cambios del nivel del mar durante los últimos 170,000 anos (litoral de Mallorca, Islas Baleares): Cuaternario y Geomorfologia, v. 15, no. 3-4, p. 67–75.

Goy, J.L., and Zazo, C., 1986, Synthesis of the quaternary in the Almeria littoral neotectonic activity and its morphologic features, Western Betics, Spain: Tectonophysics, v. 130, no. 1-4, p. 259–270, https://doi.org/10.1016/0040-1951(86)90116-2.

Gràcia, F., Fornós, J.J., and Clamor, B., 2007, Cavitats costaneres de les Balears generades a la zona de mescal, amb importants continuacions subaquàtiques, *in* Pons, G.X., and Vicens, D., eds., Geomorfologia litoral i Quaternari, Homenatge a Joan Cuerda Barceló, Monografies de la Societat d'Història Natural de les Balears, v. 14, p. 299–352.

Guijarro, J.A., 1995, Bioclimatic aspects of karst in Mallorca: Endins, v. 20, p. 17–26.

Hearty, P.J., 1987, New data on the Pleistocene of Mallorca: Quaternary Science Reviews, v. 6, p. 245–257, https://doi.org/10.1016/0277-3791(87)90007-2.

Hearty, P.J., Miller, G.H., Stearns, C.E., and Szabo, B.J., 1986, Amino-stratigraphy of Quaternary shorelines in the Mediterranean basin: Geological Society of America Bulletin, v. 97, no. 7, p. 850–858, https://doi.org/10.1130/0016-7606(1986)97<850:AOQSIT>2.0.CO;2.

Just, J., Hübscher, C., Betzler, C., Lüdmann, T., and Reicherter, K., 2011, Erosion of continental Mediterranean due to sea-level stagnancy during the Messinian Salinity Crisis: Geo-Marine Letters, v. 31, p. 51–64. https://doi.org/10.1007/s00367-010-0213-z.

Hu, Chaoyong, Henderson, G.M., Huang, Junhua, Chen, Zhenhong, and Johnson, K.R., 2008, Report of a three-year monitoring programme at Heshang Cave, Central China: International Journal of Speleology, v. 37, no. 3, p. 143–151. https://doi.org/10.5038/1827-806X.37.3.1.

Kim, JJi-Hoon, Lee, Jeongho, Cheong, Tae-Jin, Kim, Rak-Hyeon, Koh, Dong-Chen, Ryu, Joh-Sik, and Chang, Ho-Wan, 2005, Use of time series analysis for the identification of tidal effect on groundwater in the coastal area of Kimje, Korea: Journal of Hydrology, v. 300, p. 188–198, https://doi.org/10.1016/j.jhydrol.2004.06.004.

Lang, M., Faimon, J., Godissart, J., and Ek, C., 2016, Carbon dioxide seasonality in dynamically ventilated caves: the role of advective fluxes: Theoretical and Applied Climatology, https://doi.org/10.1007/s00704-016-1858-y.

Larocque, M., Mangin, A., Razack, M., and Banton, O., 1998, Contribution of correlation and spectral analyses to the regional study of a large karst aquifer (Charente, France): Journal of Hydrology, v. 205, p. 217–231, https://doi.org/10.1016/S0022-1694(97)00155-8.

Liñán, C., Vadillo, I., and Carrasco, F., 2008, Carbon dioxide concentration in air within the Nerja Cave (Malaga, Andalusia, Spain): International Journal of Speleology, v. 37, no. 2, p. 99–106, https://doi.org/10.5038/1827-806X.37.2.2.

López-García, J.M., and Mateos-Ruíz, R.M., 2006, Control estructural de las anomalías geotérmicas y la intrusión marina en la platforma de Llucmajor y La Cubeta de Campos (Mallorca), *in* Las Aguas Subterráneas en los Paises Mediterráneos: Madrid, Instituto Geológico y Minero de España, series Hidrogeología y Aguas Subterráneas 17, p. 607–613.

Mandić, M., Mihevc, A., Leis, A., and Bronić, I.K., 2013, Concentration and stable carbon isotopic composition of CO_2 in cave air of Postojnksa jama, Slovenia: International Journal of Speleology, v. 42, no. 3, p. 279–287, https://doi.org/10.5038/1827-806X.42.3.11.

Merino, A., 1993, La Cova des Pas de Vallgornera (Llucmajor, Mallorca): Endins, v. 19, p. 17–23.

Merino, A., Mulet, A., Mulet, G., Croix, A., Kristofersson, A., Gràcia, F., Ginés, J., and Fornós, J.J., 2011, La Cova des Pas de Vallgornera (Llucmajor, Mallorca). La cavitat de major desenvolupament de les Illes Balears: Endins, v. 35, p. 147–164.

Merino, A., Mulet, A., Mulet, G., Croix, A., Kristofersson, A., Gràcia, F., and Perelló, M.A., 2014, Cova des Pas de Vallgornera (Mallorca, Spain): history of exploration and cave description: International Journal of Speleology, v. 43, no. 2, p. 95–104, https://doi.org/10.5038/1827-806X.43.2.1.

Onac, B.P., Fornós, J.J., Merino, A., Ginés, J., and Diehl, J., 2014, Linking mineral deposits to speleogenetic processes in Cova des Pas de Vallgornera (Mallorca, Spain): International Journal of Speleology, v. 43, no. 2, 143–157, https://doi.org/10.5038/1827-806X.43.2.4.

Padilla, A., and Pulido-Bosch, A., 1995, Study of hydrographs of karstic aquifers by means of correlation and cross-spectral analysis: Journal of Hydrology, v. 168, p. 73–89, https://doi.org/10.1016/0022-1694(94)02648-U.

Panagopoulos, G., and Lambrakis, N., 2006, The contribution of time series analysis to the study of the hydrodynamic characteristics of the karst systems: Application on two typical karst aquifers of Greece (Trifilia, Almyros Crete): Journal of Hydrology, v. 329, p. 368–376, https://doi.org/10.1016/j.jhydrol.2006.02.023.

Pomar, L., and Cuerda, J., 1979, Los depósitos marinos pleistocénicos en Mallorca: Acta Geológica Hispánica, v. 14, p. 505–513.

Pomar, L., Ginés, A., and Fontarnau, R., 1976, Las cristalizaciones freaticas: Endins, v. 3, p. 3–25.

Pomar, L., Ginés, A., and Ginés, J., 1979, Morfología, estructura y origen de los espeleotemas epiacuáticos: Endins, v. 5-6, p. 3–17.

Robledo, P.A., and Durán, J.J., 2010, Evolución del turismo subterráneo en las Islas Baleares y su papel en el modelo turístico, *in* Durán, J.J., and Carrasco, F., eds., Cuevas: Madrid, España Asociación de Cuevas Turísticas Españolas, patrimonio, naturaleza, cultura y turismo, p. 305–323.

Sàbat, F., Gelabert, B., Rodríguez-Perea, A., and Giménez, J., 2011, Geological structure and evolution of Mallorca: Implications for the origin of the Western Mediterranean: Tectonophysics, v. 510, p. 217–238. https://doi.org/10.1016/j.tecto.2011.07.005.

Spötl, C., Fairchild, I.J., and Tooth, A.F., 2005, Cave air control on dripwater geochemistry, Obir Caves (Austria): Implications for speleothem deposition in dynamically ventilated caves: Geochimica et Cosmochimica Acta, v. 69, no. 10, p. 2451–2468, https://doi.org/10.1016/j.gca.2004.12.009.

Tuccimei, P., Ginés, J., Delitala, M.C., Ginés, A., Gràcia, F., Fornós, J.J., and Taddeucci, A., 2006, Last interglacial sea level changes in Mallorca Island (Western Mediterranean); high precision U-series data from phreatic overgrowths on speleothems: Zeitschrift für Geomorphologie, v. 50, no. 1, p. 1–21. https://doi.org/10.1127/zfg/50/2006/1.

Tuccimei, P., Soligo, M., Fornós, J.J., Ginés, A., Ginés, J., Onac, B.P., and Villa, I.M., 2009, Precipitation of phreatic overgrowths at the water table of meteoric-marine mixing zones in coastal cave systems; a useful tool in

sea-level change reconstruction, *in* White, W.B., ed., Proceedings of the 15th International Congress of Speleology: Kerrville, Texas, v. 1, p. 554–560.

Tuccimei, P., Soligo, M., Ginés, J., Ginés, A., Fornós, J.J., Kramers, J., and Villa, I.M., 2010, Constraining Holocene sea-levels using U/Th ages of phreatic overgrowths on speleothems from coastal caves in Mallorca (western Mediterranean): Earth Surface Processes and Landforms, v. 35, no. 7, p. 782–790, https://doi.org/10.1002/esp.1955.

UNESCO-IOC, sea-level data for Palma de Mallorca, www.ioc-sealevelmonitoring.org/station.php?code=palm [accessed: April 2016].

van Hengstum, P.J., Richards, D.A., Onac, B.P., Dorale, J.A., 2015, Coastal caves and sinkholes, *in* Shennan, I., Long, A.J., and Horton, B.P., eds., Handbook for Sea-Level Research, Oxford, John Wiley & Sons, p. 83–103, https://doi.org/10.1002/9781118452547.ch6.

Vesica, P.L., Tuccimei, P., Turi, B., Fornós, J.J., Ginés, A., and Ginés, J., 2000, Late Pleistocene paleoclimates and sea-level change in the Mediterranean as inferred from stable isotope and U-series studies of overgrowths on speleothems, Mallorca, Spain: Quaternary Science Reviews, v. 19, p. 865–879, https://doi.org/10.1016/S0277-3791(99)00026-8.

Wigley, T.M.L., and Brown, M.C., 1976, The physics of caves, *in* Ford, D.T., and Cullingford, C.H.C., eds., The science of Speleology: London, Academic Press, p. 329–358.

S.U.u. Jamil, S. Zada, I. Khan, W. Sajjad, M. Rafiq, A.A. Shah, and F. Hasan – Biodegradation of polyethylene by bacterial strains isolated from Kashmir Cave, Buner, Pakistan. *Journal of Cave and Karst Studies*, v. 79, no. 1, p. 73–80. DOI: 10.4311/2015MB0133

BIODEGRADATION OF POLYETHYLENE BY BACTERIAL STRAINS ISOLATED FROM KASHMIR CAVE, BUNER, PAKISTAN

Syed Umair ullah Jamil[1,2], Sahib Zada[1], Imran Khan[1], Wasim Sajjad[1], Muhammad Rafiq[1], Aamer Ali Shah[1], Fariha Hasan[1]*

Abstract: Low density polyethylene (LDPE) is used for making common shopping bags and plastic sheets and is a significant source of environmental pollution. The present study was aimed at testing the ability of bacterial strains identified as *Serratia* sp. KC1-MRL, *Bacillus licheniformis* KC2-MRL, *Bacillus* sp. KC3-MRL and *Stenotrophomonas* sp. KC4-MRL isolated from a limestone cave to degrade polyethylene. These strains were isolated from soil of Kashmir Smast, a limestone cave in Buner, Pakistan. These strains showed antibacterial activity against *Micrococcus luteus, Klebsiella* sp., *Pseudomonas* sp., and *Staphylococcus aureus*. The pieces of LDPE plastic were incubated along with bacterial strains for a period of one month and then analyzed. Degradation was observed in terms of growth of microorganisms used in consortia, chemical changes in the composition of LDPE by fourier-transform infrared spectroscopy, and changes in physical structure of LDPE by scanning electron microscopy. Maximum growth (107×10^5 CFU mL^{-1}) at 28 °C and subsequent change in chemical and physical properties of plastic were observed in the presence of calcium and glucose. The cave soil sample had a very high concentration of calcium. The microscopy showed adherence of bacteria with lots of mechanical damage and erosion on the surface of plastic films incubated with bacterial consortia. The spectroscopy showed breakdown and formation of many compounds, as evident by the appearance and disappearance of peaks in LDPE treated with bacterial consortia as compared to the untreated control. We conclude that antibiotic-producing cave bacteria were able to bring about physical and chemical changes in LDPE pieces and degradation of LDPE was enhanced in media augmented with calcium.

Introduction

Plastics are polymers of carbon, oxygen, and hydrogen and that are synthetically derived from petrochemicals and suitable for a wide range of usage. Since plastics are artificially manufactured, they are xenobiotic compounds and they resist degradation (Kawai, 2010).

Polyethylene is one of the most commonly used commercial plastics, found in various products ranging from simple plastic bags to artificial limbs (Orhan and Büyükgüngör, 2000; Shimao, 2001). Thermal and mechanical stability and their morphologies make polymeric substances one of the most popular commodity of the modern world (Rivard et al., 1995). Plastic waste is an environmental hazard. Plastic debris poses a direct threat to wildlife. The main dangers associated with plastic objects for most species are related to entanglement and ingestion. Juvenile animals, in particular, often become entangled in plastic debris, which can result in serious injury as the animal grows, not to mention restriction of movement, preventing animals from properly feeding and, in the case of mammals, breathing (Webb et al., 2012). Due to plastic's resilience against degradation and its proliferation in industry, the issue of plastic pollution has evolved to become a threat to global ecology.

Management of plastic waste is an ever-increasing problem, and none of the current techniques of solid waste management completely alleviate all the concerns related to these recalcitrant polymers (Nkwachukwu et al., 2013). One way to deal with these polymers could be to alter the manufacturing process, and new formulations should be developed with special considerations on mechanism for their biodegradation. These alterations could include looking into factors that can aid in biodegradation like pH, temperature, chemical structure, polymeric morphology, presence or absence of certain additives, and most importantly, the type of organisms that can be involved (Gu and Gu, 2005).

Degradation of plastics is carried out by organisms that are chemoheterotrophs. Many studies have shown the presence of such bacteria in caves. Bacteria also have the ability to utilize hydrocarbons as a source of energy. Studies have shown that a variety of culturable chemoheterotrophs are present in microhabitats of caves and catacombs (De Leo et al., 2012). The microorganisms living under stressful or low nutrient habitats

* Corresponding Author: farihahasan@yahoo.com
[1] Department of Microbiology, Quaid-i-Azam University, Islamabad, 45320. Pakistan.
[2] Department of Earth and Environmental Sciences, Bahria University, Islamabad, Pakistan.

can develop the ability to use any available nutrient to survive. Studies on a bacterial strain belonging to the *Arthrobacter* genus from alpine ice showed biodegradation of phenol under various environmental conditions (Margesin et al., 2004). Bacteria present in caves are capable of carrying out a variety of biodegradative and biodeteriorative processes. Extensive studies have reported biodeteriorative effects of microorganisms in cave environment (Cuezva et al., 2012; Schabereiter-Gurtner et al., 2002).

Despite much study, the knowledge is very limited about microbial life in diverse and extreme habitats like caves. There exists much potential for isolating and studying microbes in caves that have unique and unexplored characteristics of potential commercial applicability. These studies can also be helpful in investigating evolutionary relationships of microorganisms in cave environment. Most caves are characterized as having very low nutrient availability, constant low temperature, and high humidity. Caves can either be terrestrial or aquatic. Some may be rich in specific natural minerals or have exposure to nutrient sources, and therefore, different caves will have different types of microorganisms inhabiting various ecological niches (Zada et al., 2016). Fauna, environmental factors, temperature, humidity, organic matter, and other environmental factors influence activities such as nutrient cycling, and geomicrobiological activities including the formation or alteration of cave structures (Adetutu and Ball, 2014). Cave organisms have evolved some extraordinary abilities to survive and live in this inhospitable environment.

Polyethylene makes a significant contribution to solid waste in developed countries. Management of this waste can be carried out by chemical, physical, and biological methods. Various natural microflora of soil, including bacteria and fungi, are reported to degrade low-density polyethylene (LDPE) under various physical and chemical environments. This study determines the degradation capacity of four bacterial strains isolated from Kashmir Smast, Khyber Pakhtoon Khwa, Pakistan. The bacteria isolated were previously identified and tested positive for antibiotic production in the Microbiology Research Laboratory (MRL), Department of Microbiology, Quaid-e-Azam University, Islamabad. Since antibiotic production and LDPE degradation takes place under stressed environmental conditions, it was hypothesized that bacteria positive for the first character may also be positive for the other character. For this purpose, commercially available LDPE from a shopping bag was used. Bacterial isolates *Serratia* sp. KC1-MRL, *Bacillus licheniformis* KC2-MRL, *Bacillus* sp. KC3-MRL, and *Stenotrophomonas* sp. KC4-MRL were used in consortia. The study was carried out in six different medium compositions or modifications, and their individual effects were analyzed by determining total viable cells, fourier-transform infrared spectroscopy, and scanning electron microscopy. Isolated bacteria were inoculated in mineral salt medium, and sterilized LDPE pieces were added in the flasks.

Materials and Methods

Sampling Site and Sample Collection

Soil samples were collected from Kashmir Smast (cave), Nanser, Buner, Khyber Pakhtunkhwa (Fig. 1). The Kashmir Smast is a series of natural limestone caves probably of marine origin (Khan, 2013). These caves are located in the Babozai Mountains between Mardan and Buner in northern Pakistan. The only source of water was drip water. Two soil samples were collected from wall and ground surfaces of the cave in sterile Falcon tubes under aseptic conditions. Samples were collected from the dark end of the cave about 188 m from the entrance. This cave is located far away from human access, so human intervention is negligible (Zada et al., 2016). The samples were then brought to the laboratory in an icebox and stored at 4 °C for further processing. The pH and temperature of soil was recorded as 7.2 and 25 °C.

Soil Analysis by Atomic Absorption

For the quantitative analysis of elements in the soil sample, atomic-absorption spectrophotometry was performed with a AA240FS Fast Sequential Atomic Absorption Spectrophotometer. Soil digestion was performed to prepare samples for analysis. One gram each of soil from the cave floor and control soil from outside the cave were ground separately and were then mixed in 15 mL aqua regia, heated at 15 °C, and left overnight. Then 5 mL of $HClO_4$ was added and again heated at 150 °C. The solution almost became dry before brown fumes were produced. Whatman filter paper (No. 42) was used for filtration, and the volume was made up to 50 mL using double-distilled water (Kelly et al., 2008).

Screening and Isolation of LDPE-Degrading Bacteria

Previously identified strains of *Serratia* sp. KC1-MRL, *Bacillus licheniformis* KC2-MRL, *Bacillus* sp. KC3-MRL, and *Stenotrophomonas* sp. KCMRL isolated from the cave were used in consortium to carry out biodegradation of polyethylene. Nutrient agar medium was used for isolation of bacterial strains from cave soil. The strains were isolated using standard serial dilution methods and subsequent growth on Nutrient agar plates for 48h at 37 °C. All the isolated strains were screened for polyethylene degradation. For this purpose the strains were incubated for two weeks in 120 mL of mineral salt medium (g L^{-1}): [KH_2PO_4, 2.0; K_2HPO_4, 7.0; $MgSO_4{\cdot}7H_2O$, 0.1; $ZnSO_4{\cdot}7H_2O$, 0.001; $FeSO_4{\cdot}7H_2O$, 0.01; $MnSO_4{\cdot}6H_2O$, 0.002; NH_4NO_3, 1.0; $CuSO_4{\cdot}7H_2O$, 0.0001; pH 7.2] at 37 °C with pieces of polyethylene (1 by 1 cm) (Anwar et al., 2009). Polyethylene used was pretreated by exposing it to UV light for three minutes. At the end of two weeks of incubation, viable cells were counted as CFU mL^{-1} by serial dilution. Four bacterial strains were found active in terms of growth in the medium.

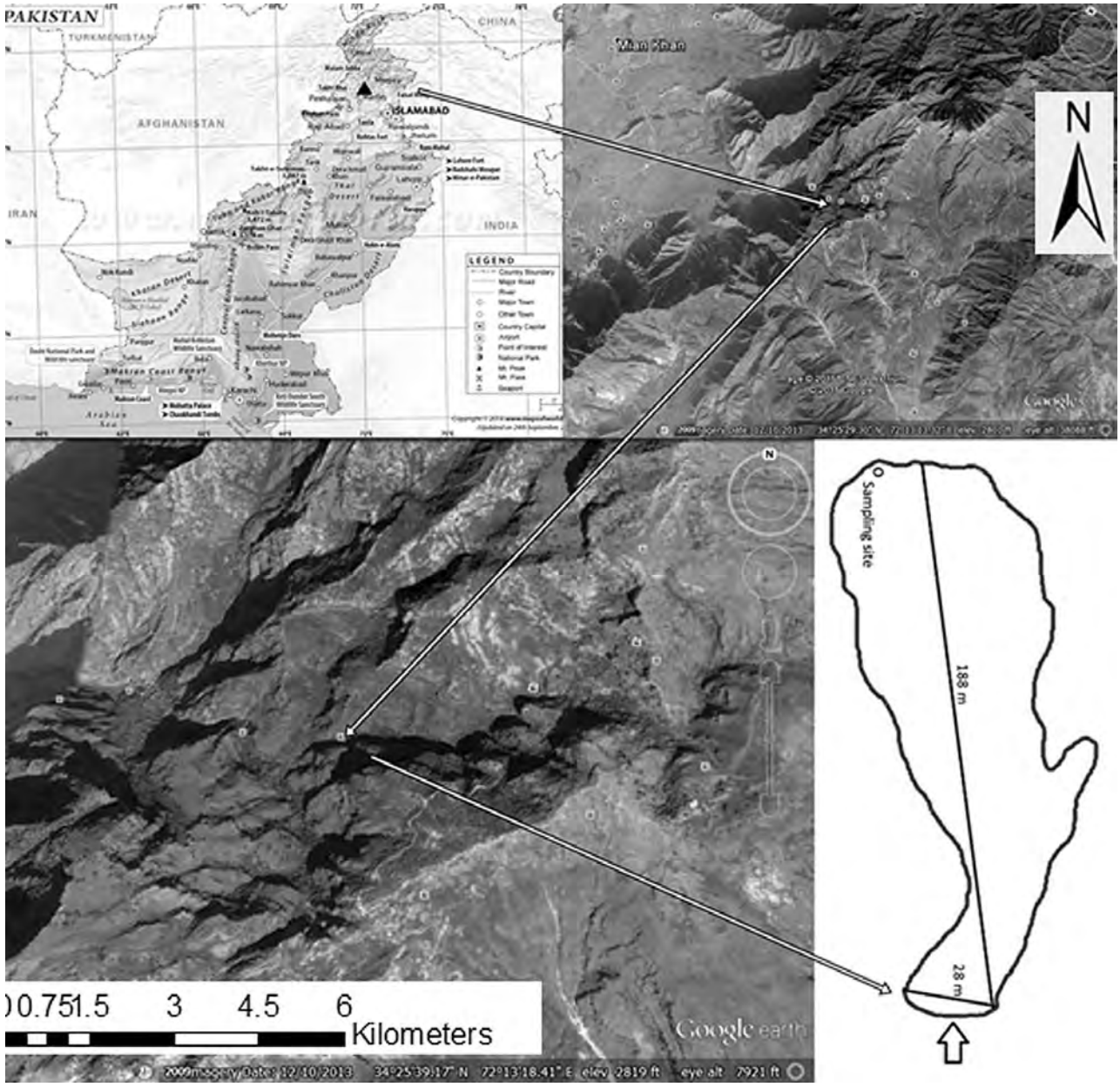

Figure 1. Location and map of Kashmir Smast (Cave), Nanseer Buner, Khyber Pakhtunkhwa, Pakistan. Sourc Zada et al. (2016).

Bacterial colonies were further purified and enriched on nutrient agar plates.

Preparation of Inoculum

About 10 mL of nutrient broth was inoculated with two or three loops of the pure culture of isolated strains. Bacterial growth was evaluated at 25 °C, 37 °C and 40 °C. Maximum growth was observed at 37 °C (O.D. at 600 nm). Consortia were developed by taking inocula from each test tube into a separate flask with 100 ml of nutrient broth. Five percent of this prepared consortia was used as inoculum for further biodegradation experiments.

Medium Preparation and Incubation

Different metabolites were used in combinations to study their effects on biodegradation of polyethylene by the cave-bacteria consortia. Glucose, yeast extract, and calcium were used as co- metabolites. About 1% w/v of glucose and yeast extract were used, whereas the concentration of calcium in the medium was maintained at 0.03% to match the natural concentration of calcium of the environment where the soil was taken.

In total six combinations of these metabolites in mineral salt medium with polyethylene pieces and bacterial consortia were incubated at 150 rpm at pH 7.2 and temperature 37 °C

Table 1. Viable Cell Count of bacterial consortium in different media compositions incubated at 37 °C.

Time (days)	MSM + PE + bacterial consortium CFU/mL ($\times 10^5$)	MSM + PE + calcium carbonate + bacterial consortium CFU/mL ($\times 10^5$)	MSM + Glucose + PE + bacterial consortium CFU/mL ($\times 10^5$)	MSM + glucose + calcium carbonate + PE + bacterial consortium CFU/mL ($\times 10^5$)	MSM + glucose + calcium carbonate + yeast extract + PE + bacterial consortium CFU/mL ($\times 10^5$)	MSM + calcium carbonate + yeast extract + PE + bacterial consortium CFU/mL ($\times 10^5$)
0	280	246	241	220	256	255
7	256	296	292	265	284	295
14	192	221	210	225	237	236
21	110	125	110	164	126	119
28	23	103	68	107	95	92

for four weeks. A negative control was set by incubating polyethylene pieces in mineral salt medium with no bacterial inoculum.

Biodegradation Analysis

Biodegradation of polyethylene was analyzed by determining CFU mL^{-1}, fourier-transform infrared spectra, and scanning electron microscope images. CFU mL^{-1} was determined after every week, whereas FTIR and SEM analysis were performed after one month of incubation. The viable cell count was done for bacterial growth determination through serial dilution and calculating CFU mL^{-1}. Test LDPE samples were compared with the untreated control samples. FTIR (Jasco FT/ IR – 620) analysis was performed to check the degradation of LDPE pieces after being mixed with the growing bacterial consortia in liquid medium. This analysis detects any change in the functional groups. Spectrum was recorded at 500-4000 wave-numbers cm^{-1} for all the LDPE samples. Surface morphology of LDPE pieces was observed by SEM (JSM 5910 Joel, Japan) to look for any change in structure or surface of LDPE piece after treating with microbial consortia. After rinsing of the LDPE pieces with autoclaved distilled water, LDPE pieces were mounted on the copper stubs with gold paint. Gold coating was carried out under vacuum by evaporation to make the samples conducting.

Results

Soil Analysis

Atomic absorption spectroscopy was performed to determine the concentration of elements in the cave soil sample (ZADA et al., 2016). Ca was 332.938 mg kg^{-1} as compared to 121.65 mg kg^{-1} in control soil, Mg was 1.2576 mg kg^{-1} in cave soil and 1.023 mg kg^{-1} in control soil. Ni 0.965 mg kg^{-1} in cave soil and 10.4 mg kg^{-1} in control soil, Cr 0.571 mg kg^{-1} in cave soil and 8.74 mg kg^{-1} in control soil, Co 0.266 mg kg^{-1} in cave soil and 0.810 mg kg^{-1} in control soil, Cu 1.824 mg kg^{-1} in cave soil and 4.7 mg kg^{-1} in control soil, Zn 12.7311 mg kg^{-1} in cave soil and 36.41 mg kg^{-1} in control soil, and Pb 1.31 mg kg^{-1} in cave soil and 8.14 mg kg^{-1} in control soil were much lower than those found in the control soil (Zada et al., 2016).

Viable Cell Count

The concentration of viable cells in CFU mL^{-1} was determined at time zero, before initial incubation, and then after every week for a period of one month (Table 1). Since polyethylene in the medium was the sole carbon source, CFU mL^{-1} is directly proportional to the ability of organisms to degrade polyethylene and use it as a carbon source. There was a consistent decrease in CFU mL^{-1} after three and four weeks of incubation. The soil from where the bacteria were isolated contained exceptionally high concentration of calcium. Considering this high amount of calcium in the native habitat

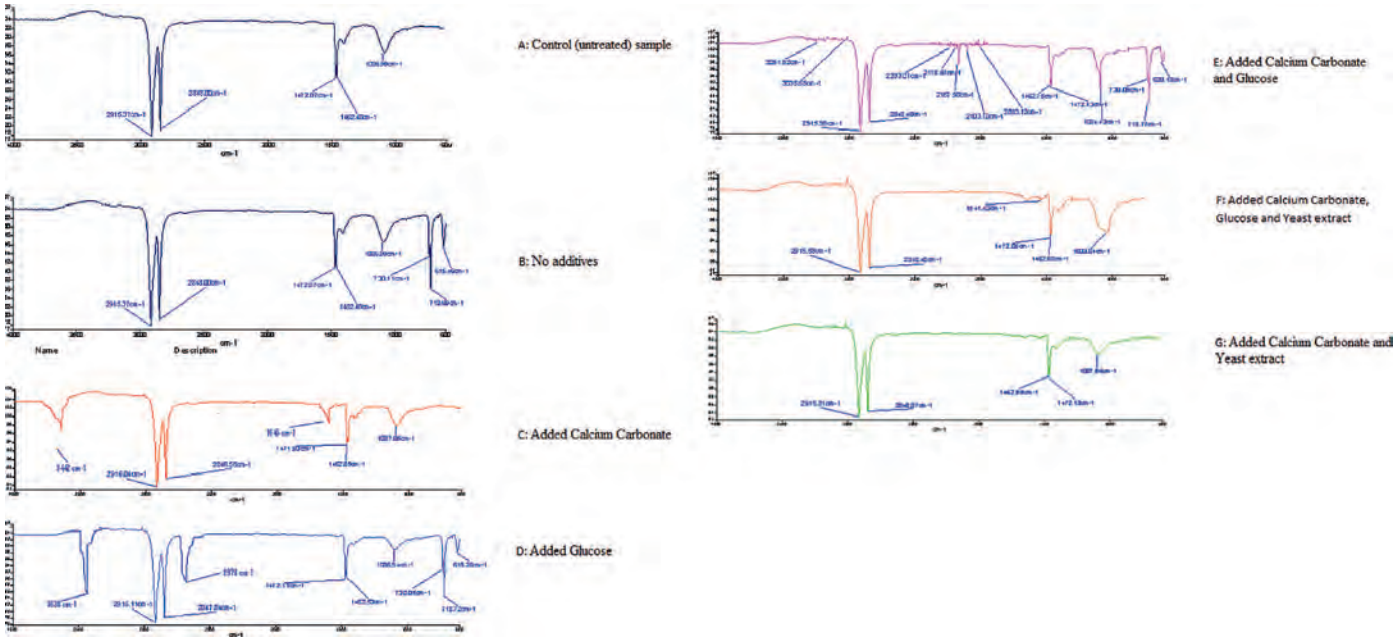

Figure 2. Fourier-transform infrared spectra from control and different media after incubation at 37 °C for one month.

of the organism, extra calcium salt was added in the medium so that the organisms experience minimum deviation from their natural environment. Medium augmented with extra calcium showed increasing values of viable cell count in the first two weeks of incubation. Increase in the values of viable cell count was also observed in the first two weeks of incubation when the medium is augmented with glucose; these higher values of CFU mL^{-1} in first two weeks were because the bacteria were provided with glucose that acted as growth activator. Additional amounts of calcium proved to be helpful for better growth of bacterial colonies.

Fourier Transform Infra-Red Spectroscopy

FTIR was carried out on LDPE films after incubation with bacterial consortia for four weeks. The peaks formed were compared with the control (Fig. 2).

LDPE in mineral salt medium containing bacterial consortia: Absorbance peaks formed at 2915 cm^{-1} and 2848 cm^{-1} suggest presence of C–H bonds. A peak of variable strength at 1472 cm^{-1} and 1462 cm^{-1} shows formation of C=C bonds. A strong peak at 1035 cm^{-1} shows formation of stretch of C–O bonds. Absorbance peaks formed at 615 cm^{-1}, 718 cm^{-1} and 730 cm^{-1} show presence of =C–H bending bonds.

LDPE in MSM containing calcium carbonate and bacterial consortia: New peaks were formed at 1645 cm^{-1} that represent formation of C=C, and a peak formed at 3442 cm^{-1} shows stretching of O-H bonds.

LDPE in MSM containing glucose and bacterial consortia: Formation of new peak at 2978 cm^{-1} shows stretching of C–H bonds and peak at 3638 cm^{-1} represents of stretching of O–H bonds.

LDPE in MSM containing calcium carbonate, glucose, and bacterial consortia: Maximum variety of peaks was observed in this film. Formation of peaks at 3251 cm^{-1} and 3032 cm^{-1} shows formation of O–H bonds. A peak at 2915 cm^{-1} and 2848 cm^{-1} represents formation of stretch of C–H bonds in the polyethylene. Peak formation at 2233 cm^{-1}, 2178 cm^{-1}, 2167 cm^{-1}, 2103 cm^{-1}, and 2013 cm^{-1} shows that new Nitrile bonds of –C ≡ N are formed. Absorbance peaks at 1462 cm^{-1} and 1472 cm^{-1} show bending of –C-H- bonds. Peak at 1084 cm^{-1} shows formation of stretch of C–O functional group. Absorbance peaks formed at 615 cm^{-1}, 718 cm^{-1}, and 730 cm^{-1} shows presence of =C-H bending bonds.

LDPE in MSM containing calcium carbonate, glucose, yeast extract, and bacterial consortia: In comparison with control, new peak was formed in this medium combination at 1033 cm^{-1} represents formation of C–O bond.

LDPE in MSM containing calcium carbonate, yeast extract and bacterial consortia: In comparison with control, anew peak was formed in this medium combination at 1033 cm^{-1} that represents formation of C-O bond.

Scanning Electron Microscopy

SEM showed adherence of bacteria that caused mechanical damage and erosion on the surface of plastic films incubated with bacterial consortia as compared to the untreated control (Fig. 3). More changes in surface topology and attachment of cells, despite the washing, were observed on the LDPE piece incubated in the presence of glucose and calcium.

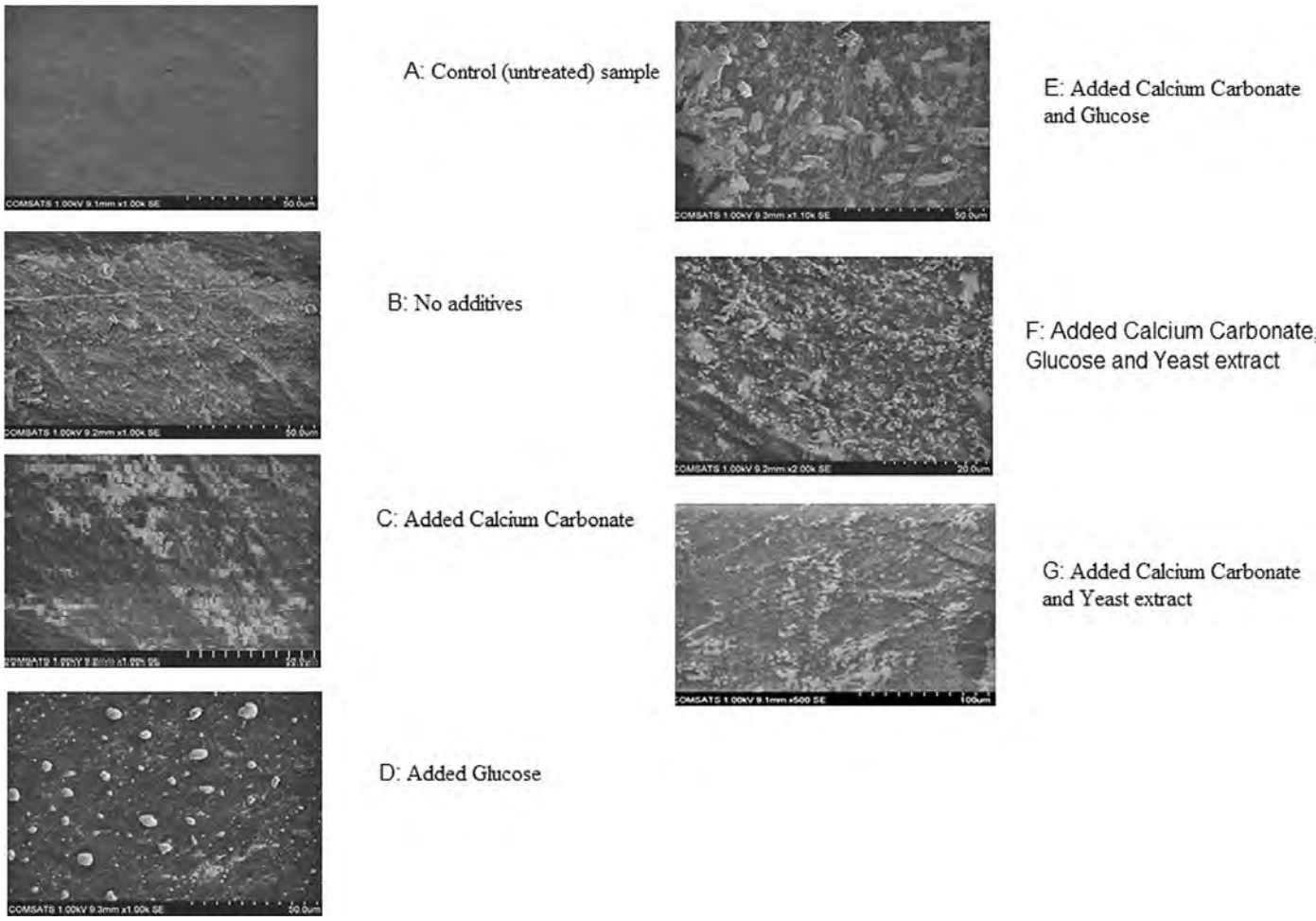

Figure. 3 A-G. Scanning electron microscopy of low-density polyethylene samples under specified treatment after incubation with bacterial consortia at 37 °C for one month.

Discussion

There is an increasing interest in investigating biodegradation of non-degradable plastics using efficient microorganisms (Bonhomme et al., 2003; Boonchan et al., 2000; Lee et al., 1991). In our present study, bacterial isolates were obtained from the soil of Kashmir Smast, which is a limestone cave in Khyber Pakhtoonkhuwa province, Pakistan. The four isolates were identified as *Serratia* sp. KC1-MRL, *Bacillus licheniformis* KC2-MRL, *Bacillus* sp. KC3-MRL, and *Stenotrophomonas* sp. KC4-MRL. These strains were used in consortia to check for the ability of these microbes to degrade polyethylene. Since both antibiotic production and polyethylene degradation occur under stressed environmental conditions, the hypothesis of the current study was that bacteria having the first property are more likely to give positive result for the other. Studies on *Brevibacillus borstelensis* 707 showed an increase in potential of polyethylene biodegradation when grown on nitrogen-limit stressed cultures (Hadad et al., 2005). It was also observed that not only nitrogen deprivation, based on the amount of KNO_3 in medium, but also carbon limitation in a mannitol-free medium alone enhanced degradation, which was also enhanced when used in combination. It was observed that mannitol-free medium supplemented with nitrogen source showed maximum biodegradation in 30 days of incubation. In the present study, it was found that bacterial consortia showed higher viable cells measured as CFU mL^{-1} when the medium was supplemented with the nitrogen source.

Loss of tensile strength of plastic after incubation with *Pseudomonas stutzeri* suggests that the bacterium is capable of degrading the polymer (Sharma and Sharma, 2004). When bacteria are grown in different media compositions along with a polymer, maximum turbidity is observed on forty-fifth day (Ciferri, 1999). The increase in growth rate in glucose, as well as in minimal medium, suggests that the bacteria were completely depending upon polyethylene film for its source of carbon in the absence of glucose. CFU mL^{-1} increased from 10^1 to 10^3 from day 15 to day 30 (Table 1). These results suggest that the bacteria growing in Lascaux Cave, France are

capable of using plastics and other resins such as glue as their sole source of carbon. Higher values of CFU mL^{-1} in the first two weeks were observed in all those media combinations in which 1% glucose w/v was added at the beginning. When the nutrients depleted, bacteria had polyethylene as the only carbon source. Addition of easily available substrate like glucose in MSM medium increases bacterial growth in initial stages of pesticide degradation (Cycoń et al., 2011). A similar effect on growth was observed when MSM media is augmented with yeast extract. The increased CFU mL^{-1} was observed in first two weeks of the experiment and then the growth decreased, which indicates depletion of glucose in the medium.

In our study, fourier-transform infrared spectral analysis was carried out to check chemical degradation of polyethylene. Low- and high-density polyethylene are made of the elements carbon and hydrogen forming chains of repeating $-CH_2-$ units (Rajandas et al., 2012). In the process of biodegradation of LDPE, enzymes catalyze a specific series of biochemical reactions that lead to various kinds of chemical conversions, such as oxidation, reduction, hydrolysis, esterification, and molecular inner conversion (Harshvardhan and Jha, 2013). Keto and ester carbonyls have been reported as major products in the presence of oxidoreductase (Karlsson and Albertsson, 1998). Analysis of FTIR showed new peaks when LDPE is treated with bacterial consortia, indicating polymer breakdown and formation of new functional groups. The results of scanning electron microscopy have shown that all those media to which calcium was added showed strong biofilm development and hence increased biodegradation. It is also evident in several studies that bacteria release various surface-active substances extracellularly, which increase the bioavailability to the polymer. Studies on *Pseudomonas* sp. AKS2 showed that the strain was capable of degradation 5 ± 1 % of initial LDPE in 45 days (Tribedi and Sil, 2013). The degradation by *Pseudomonas* depends on its capability to colonize the surface of the polymer and degrade it. Addition of calcium increases biofilm development of *Xylella fastidiosa* under *in vitro* conditions (Cruz et al., 2012). The efficient increase in formation of biofilm was observed when at least 1.0 mM $CaCl_2$ was added in the medium. There was no effect of Ca on attachment when bacteria were treated with tetracycline, indicating that Ca has a regulatory role in colonization or attachment of the cells. In another study, Ehret and Böl (2013) showed that Ca ions crosslink alginates, which is the key constituent of the extracellular polymeric material produced by the mucoid *P. aeruginosa* strain to produce biofilms. Ciferri reported a list of bacteria responsible for degradation of paints (Ciferri, 1999).

In the present study, SEM showed discoloration, spots, erosion, and cracking on the surface of polyethylene film. Modification on the surface of polyethylene after bacterial treatment was also reported by (Matsunaga and Whitney, 2000). Formation of pits and erosion on the surface of LDPE when observed through electron microscopy when incubated with *Fusarium* sp. indicating adherence and degradation of LDPE (Hasan et al., 2007).

Bacteria capable of adhering to plastic surfaces, growing, and possibly degrading it by oxidation are commonly present in soil. Microorganisms that can adhere to the surface of pre-oxidized PE are also commonly present in soil. If the pre-oxidant technology is commonly employed in the PE manufacturing process, one can expect that these plastics will be able to degrade in waste disposal sites. In the current study, structural and surface changes in PE in the form of depression, pits, and erosions were visible in SEM. Physical erosion of the surface of polyethylene observed through SEM by fungi has been reported by Bonhomme et al. (2003). Polymer treated with microorganism loses its physical strength and disintegrates on applying mild pressure. Wide spread pits and holes in polycaprolactone surface are reported by Shaw et al. (2015) after ten days of incubation with thermophilic bacterium *Ralstonia* sp. strain MRL-TL. SEM has shown that biofilms develop on the surface of polyethylene with time by PE-degrading bacteria. It is known that formation of biofilm on the surface of plastics favors adhesion of bacteria on the surface and helps them survive under low nutrient conditions and to use polyethylene as their source of carbon (Linos et al., 2000).

Conclusions

Our study indicates that antibiotic producing bacteria in consortia isolated from a limestone cave could degrade the synthetic polymer polyethylene. Maximum biodegradation was observed when the medium was augmented with calcium salt, indicating higher degradation potential of bacterial consortia when in a medium close to the natural chemical composition of their native environment. Spectroscopy and microscopy results showed certain changes in low-density polyethylene test samples as compared to a control, indicating microbial breakdown of LDPE. Further research is needed to understand the mechanism of degradation of LDPE at a molecular level. All the bacterial strains were found to viable at the end of the experiment.

Acknowledgements

We are thankful to Quaid-i-Azam University, Islamabad, for providing funds to accomplish this research.

References

Adetutu, E.M., and Ball, A.S., 2014, Microbial diversity and activity in caves: Microbiology Australia, v. 35, no. 4, p. 192–194. https://doi.org/10.1071/MA14062.

Anwar, S., Liaquat, F., Khan, Q. M., Khalid, Z. M., and Iqbal, S., 2009, Biodegradation of chlorpyrifos and its hydrolysis product 3,5,6-trichloro-2-pyridinol by *Bacillus pumilus* strain C2A1: Journal of Hazardous Materials, v. 168, no. 1, p. 400–405. https://doi.org/10.1016/j.jhazmat.2009.02.059.

Bonhomme, S., Cuer, A., Delort, A.-M, Lemaire, J., Sancelme, M., and Scott, G., 2003, Environmental biodegradation of polyethylene: Polymer Degradation and Stability, v. 81, no. 3, p. 441–452. https://doi.org/10.1016/S0141-3910(03)00129-0.

Boonchan, S., Britz, M.L., and Stanley, G.A., 2000, Degradation and mineralization of high-molecular-weight polycyclic aromatic hydrocarbons by defined fungal-bacterial cocultures: Applied and Environmental Microbiology, v. 66, no. 3, p. 1007–1019.

Ciferri, O., 1999, Microbial degradation of paintings: Applied and Environmental Microbiology, v. 65, no. 3, p. 879–885.

Cruz, L.F., Cobine, P.A., and De La Fuente, L., 2012, Calcium increases *Xylella fastidiosa* surface attachment, biofilm formation, and twitching motility: Applied and Environmental Microbiology, v. 78, no. 5, p. 1321–1331. https://doi.org/10.1128/AEM.06501-11.

Cuezva, S., Fernandez-Cortes, A., Porca, E., Pašić, L., Jurado, V., Hernandez-Marine, M., Serrano-Ortiz, P., Hermosin, B., Cañaveras, J.C., Sanchez-Moral, S., and Saiz-Jimenez, C., 2012, The biogeochemical role of Actinobacteria in Altamira Cave, Spain: FEMS Microbiology Ecology, v. 81, no. 1, p. 281–290. https://doi.org/10.1111/j.1574-6941.2012.01391.x.

Cycoń, M., Wójcik, M., and Piotrowska-Seget, Z., 2011, Biodegradation kinetics of the benzimidazole fungicide thiophanate-methyl by bacteria isolated from loamy sand soil: Biodegradation, v. 22, no. 3, p. 573–583. https://doi.org/10.1007/s10532-010-9430-4.

De Leo, F., Iero, A., Zammit, G., and Urzì, C.E., 2012, Chemoorganotrophic bacteria isolated from biodeteriorated surfaces in cave and catacombs: International Journal of Speleology, v. 41, no. 2, p. 125–136. https://doi.org/10.5038/1827-806X.41.2.1.

Ehret, A E., and Böl, M., 2013, Modelling mechanical characteristics of microbial biofilms by network theory: Journal of The Royal Society Interface, v. 10, no. 78, p. 676–687. https://doi.org/10.1098/rsif.2012.0676.

Gu, Ji-Guang, and Gu, Ji-Dong., 2005, Methods currently used in testing microbiological degradation and deterioration of a wide range of polymeric materials with various degree of degradability: a review: Journal of Polymers and the Environment, v. 13, no. 1, p. 65–74. https://doi.org/10.1007/s10924-004-1230-7.

Hadad, D., Geresh, S., and Sivan, A., 2005, Biodegradation of polyethylene by the thermophilic bacterium *Brevibacillus borstelensis*: Journal of Applied Microbiology, v. 98, no. 5, p. 1093–1100. https://doi.org/10.1111/j.1365-2672.2005.02553.x.

Harshvardhan, K., and Jha, B., 2013, Biodegradation of low-density polyethylene by marine bacteria from pelagic waters, Arabian Sea, India: Marine Pollution Bulletin, v. 77, no. 1-2, p. 100–106. https://doi.org/10.1016/j.marpolbul.2013.10.025.

Hasan, F., Shah, A.A., Hameed, A., and Ahmed, S., 2007, Synergistic effect of photo and chemical treatment on the rate of biodegradation of low density polyethylene by *Fusarium* sp. AF4: Journal of Applied Polymer Science, v. 105, no. 3, p. 1466–1470. https://doi.org/10.1002/app.26328.

Karlsson, S., and Albertsson, A.-C., 1998, Biodegradable polymers and environmental interaction: Polymer Engineering and Science, v. 38, no. 8, p. 1251–1253. https://doi.org/10.1002/pen.10294.

Kawai, F., 2010, The biochemistry and molecular biology of xenobiotic polymer degradation by microorganisms: Bioscience, Biotechnology, and Biochemistry, v. 74, no. 9, p. 1743–1759. https://doi.org/10.1271/bbb.100394.

Kelly, S.D., Hesterberg, D., and Ravel, B., 2008, Analysis of soils and minerals using X-ray absorption spectroscopy, *in* Ulery, A.L., and Drees, L.R., eds., Mineralogical Methods: Madison, Wisconsin, Soil Science Society of America, Methods of Soil Analysis series 5, p. 387–463. https://doi.org/10.2136/sssabookser5.5.c14.

Khan, M.N., 2013, The early arrival of Muslims in ancient Gandhāra study based on numismatic evidence from Kashmir Smast: Gandharan Studies, v. 7, p. 111–126.

Lee, B., Pometto, A.L. III, Fratzke, A., and Bailey, T.B., Jr., 1991, Biodegradation of degradable plastic polyethylene by *Phanerochaete* and *Streptomyces* species: Applied and Environmental Microbiology, v. 57, no. 3, p. 678–685.

Linos, A., Berekaa, M.M., Reichelt, R., Keller, U., Schmitt, J., Flemming, H.-C., Kroppenstedt, R.M., and Steinbüchel, A., 2000, Biodegradation of *cis*-1,4-polyisoprene rubbers by distinct actinomycetes: microbial strategies and detailed surface analysis: Applied and Environmental Microbiology, v. 66, no. 4, p. 1639–1645. https://doi.org/10.1128/AEM.66.4.1639-1645.2000.

Margesin, R., Schumann, P., Spröer, C., and Gounot, A.-M., 2004, *Arthrobacter psychrophenolicus* sp. nov., isolated from an alpine ice cave: International Journal of Systematic and Evolutionary Microbiology, v. 54, no. 6, p. 2067–2072. https://doi.org/10.1099/ijs.0.63124-0.

Matsunaga, M., and Whitney, P.J., 2000, Surface changes brought about by corona discharge treatment of polyethylene film and the effect on subsequent microbial colonisation: Polymer Degradation and Stability, v. 70, no. 3, p. 325–332. https://doi.org/10.1016/S0141-3910(00)00105-1.

Nkwachukwu, O.I., Chima, C.H., Ikenna, A.O., and Albert, L., 2013, Focus on potential environmental issues on plastic world towards a sustainable plastic recycling in developing countries: International Journal of Industrial Chemistry, v. 4, no. 1, p. 34–46. https://doi.org/10.1186/2228-5547-4-34.

Orhan, Y., and Büyükgüngör, H., 2000, Enhancement of biodegradability of disposable polyethylene in controlled biological soil: International Biodeterioration & Biodegradation, v. 45, no. 1-2, p. 49–55. https://doi.org/10.1016/S0964-8305(00)00048-2.

Rajandas, H., Parimannan, S., Sathasivam, K., Ravichandran, M., and Yin, Li Su, 2012, A novel FTIR-ATR spectroscopy based technique for the estimation of low-density polyethylene biodegradation: Polymer Testing, v. 31, no. 8, p. 1094–1099. https://doi.org/10.1016/j.polymertesting.2012.07.015.

Rivard, C., Moens, L., Roberts, K., Brigham, J., and Kelley, S., 1995, Starch esters as biodegradable plastics: effects of ester group chain length and degree of substitution on anaerobic biodegradation: Enzyme and Microbial Technology, v. 17, no. 9, p. 848–852. https://doi.org/10.1016/0141-0229(94)00120-G.

Schabereiter-Gurtner, C., Saiz-Jimenez, C., Piñar, G., Lubitz, W., and Rölleke, S., 2002, Altamira cave Paleolithic paintings harbor partly unknown bacterial communities: FEMS Microbiology Letters, v. 211, no. 1, p. 7–11. https://doi.org/10.1111/j.1574-6968.2002.tb11195.x.

Shah, A.A., Nawaz, A., Kanwal, L., Hasan, F., Khan, S., and Badshah, M., 2015, Degradation of poly(ε-caprolactone) by a thermophilic bacterium *Ralstonia* sp. strain MRL-TL isolated from hot spring: International Biodeterioration & Biodegradation, v. 98, p. 35–42. https://doi.org/10.1016/j.ibiod.2014.11.017.

Sharma, A., and Sharma, A., 2004, Degradation assessment of low density polythene (LDP) and polythene (PP) by an indigenous isolate of *Pseudomonas stutzeri*: Journal of Scientific and Industrial Research, v. 63, no. 3, p. 293–296.

Shimao, M., 2001, Biodegradation of plastics: Current Opinion in Biotechnology, v. 12, no. 3, p. 242–247. https://doi.org/10.1016/S0958-1669(00)00206-8.

Tribedi, P., and Sil, A.K., 2013, Low-density polyethylene degradation by *Pseudomonas* sp. AKS2 biofilm: Environmental Science and Pollution Research, v. 20, no. 6, p. 4146–4153. https://doi.org/10.1007/s11356-012-1378-y.

Webb, H.K., Arnott, J., Crawford, R.J., and Ivanova, E.P., 2012, Plastic degradation and its environmental implications with special reference to poly(ethylene terephthalate): Polymers, v. 5, no. 1, p. 1–18. https://doi.org/10.3390/polym5010001.

Zada, S., Nasem, A.A., Lee, Seong-Joo., Rafiq, M., Khan, I., Shah, A.A., and Hasan, F., 2016, Geochemical and mineralogical analysis of Kashmir Cave (SMAST), Buner, Pakistan, and isolation and characterization of bacteria having antibacterial activity: Journal of Cave and Karst Studies, v. 78, no. 2, p. 94–109. https://doi.org/10.4311/2014MB0110.

GUIDE TO AUTHORS

The *Journal of Cave and Karst Studies* is a multidisciplinary journal devoted to cave and karst research. The *Journal* is seeking original, unpublished manuscripts concerning the scientific study of caves or other karst features. Authors do not need to be members of the National Speleological Society, but preference is given to manuscripts of importance to North American speleology.

LANGUAGES: The *Journal of Cave and Karst Studies* uses American-style English as its standard language and spelling style, with the exception of allowing a second abstract in another language when room allows. In the case of proper names, the *Journal* tries to accommodate other spellings and punctuation styles. In cases where the Editor-in-Chief finds it appropriate to use non-English words outside of proper names (generally where no equivalent English word exists), the *Journal* italicizes them. However, the common abbreviations i.e., e.g., et al., and etc. should appear in roman text. Authors are encouraged to write for our combined professional and amateur readerships.

CONTENT: Each paper will contain a title with the authors' names and addresses, an abstract, and the text of the paper, including a summary or conclusions section. Acknowledgments and references follow the text.

ABSTRACTS: An abstract stating the essential points and results must accompany all articles. An abstract is a summary, not a promise of what topics are covered in the paper.

STYLE: The *Journal* consults The Chicago Manual of Style on most general style issues.

REFERENCES: In the text, references to previously published work should be followed by the relevant author's name and date (and page number, when appropriate) in parentheses. All cited references are alphabetical at the end of the manuscript with senior author's last name first, followed by date of publication, title, publisher, volume, and page numbers. Geological Society of America format should be used (see http://www.geosociety.org/pubs/geoguid5.htm). Please do not abbreviate periodical titles. Web references are acceptable when deemed appropriate. The references should follow the style of: Author (or publisher), year, Webpage title: Publisher (if a specific author is available), full URL (e.g., http://www.usgs.gov/citguide.html) and date when the web site was accessed in brackets; for example [accessed July 16, 2002]. If there are specific authors given, use their name and list the responsible organization as publisher. Because of the ephemeral nature of websites, please provide the specific date. Citations within the text should read: (Author, Year).

SUBMISSION: Effective February 2011, all manuscripts are to be submitted via Peertrack, a web-based system for online submission. The web address is http://www.edmgr.com/jcks. Instructions are provided at that address. At your first visit, you will be prompted to establish a login and password, after which you will enter information about your manuscript (e.g., authors and addresses, manuscript title, abstract, etc.). You will then enter your manuscript, tables, and figure files separately or all together as part of the manuscript. Manuscript files can be uploaded as DOC, WPD, RTF, TXT, or LaTeX. A DOC template with additional manuscript specifications may be downloaded. (Note: LaTeX files should not use any unusual style files; a LaTeX template and BiBTeX file for the *Journal* may be downloaded or obtained from the Editor-in-Chief.) Table files can be uploaded as DOC, WPD, RTF, TXT, or LaTeX files, and figure files can be uploaded as TIFF, EPS, AI, or CDR files. Alternatively, authors may submit manuscripts as PDF or HTML files, but if the manuscript is accepted for publication, the manuscript will need to be submitted as one of the accepted file types listed above. Manuscripts must be typed, double spaced, and single-sided. Manuscripts should be no longer than 6,000 words plus tables and figures, but exceptions are permitted on a case-by-case basis. Authors of accepted papers exceeding this limit may have to pay a current page charge for the extra pages unless decided otherwise by the Editor-in-Chief. Extensive supporting data will be placed on the *Journal*'s website with a paper copy placed in the NSS archives and library. The data that are used within a paper must be made available. Authors may be required to provide supporting data in a fundamental format, such as ASCII for text data or comma-delimited ASCII for tabular data.

DISCUSSIONS: Critical discussions of papers previously published in the *Journal* are welcome. Authors will be given an opportunity to reply. Discussions and replies must be limited to a maximum of 1000 words and discussions will be subject to review before publication. Discussions must be within 6 months after the original article appears.

MEASUREMENTS: All measurements will be in Systeme Internationale (metric) except when quoting historical references. Other units will be allowed where necessary if placed in parentheses and following the SI units.

FIGURES: Figures and lettering must be neat and legible. Figure captions should be on a separate sheet of paper and not within the figure. Figures should be numbered in sequence and referred to in the text by inserting (Fig. x). Most figures will be reduced, hence the lettering should be large. Photographs must be sharp and high contrast. Color will generally only be printed at author's expense.

TABLES: See http://www.caves.org/pub/journal/PDF/Tables.pdf to get guidelines for table layout.

COPYRIGHT AND AUTHOR'S RESPONSIBILITIES: It is the author's responsibility to clear any copyright or acknowledgement matters concerning text, tables, or figures used. Authors should also ensure adequate attention to sensitive or legal issues such as land owner and land manager concerns or policies.

PROCESS: All submitted manuscripts are sent out to at least two experts in the field. Reviewed manuscripts are then returned to the author for consideration of the referees' remarks and revision, where appropriate. Revised manuscripts are returned to the appropriate Associate Editor who then recommends acceptance or rejection. The Editor-in-Chief makes final decisions regarding publication. Upon acceptance, the senior author will be sent one set of PDF proofs for review. Examine the current issue for more information about the format used.

ELECTRONIC FILES: The *Journal* is printed at high resolution. Illustrations must be a minimum of 300 dpi for acceptance.

Journal of Cave and Karst Studies

Volume 79 Number 1 April 2017

***Journal of Cave and Karst Studies* Distribution**

Upon publication, electronic files (as PDFs) for each issue will be available for immediate viewing and download through the Member Portal at www.caves.org/pub/journal. For those individuals that wish to receive the *Journal* in a printed format, it is available by subscription for an additional fee. Online subscription and payment options are available on the *Journal* website.